The short-term climate variability of shallow marine environments in Central Europe during the Oligocene

Dissertation

zur Erlangung des Grades

“Doktor der Naturwissenschaften“

im Promotionsfach Geologie/Paläontologie

am Fachbereich Chemie, Pharmazie und Geowissenschaften

der Johannes Gutenberg-Universität Mainz

von

Eric Otto Walliser

geb. in Göttingen

Mainz, 2016

Dekan:

1. Berichterstatter: Not displayed for reasons of data protection

2. Berichterstatter: Not displayed for reasons of data protection

Ich erkläre hiermit, dass ich die vorliegende Arbeit selbständig verfasst und keine anderen als die angegebenen Quellen und Hilfsmittel benutzt habe.

_____

Eric Otto Walliser

(Mainz, 10. Dezember 2016)

ABSTRACT

The Oligocene epoch was the last time in the Earth history during which a unipolar glaciated world occurred. While the Northern Hemisphere remained substantially ice free, the land-ocean distribution as well as large scale circulation patterns broadly resembled the modern configuration. Atmospheric CO_2 levels fluctuated between 400 ppm and 560 ppm. Such boundary conditions resemble those predicted for the near future by numerical climate models. Therefore, the Oligocene world can serve as natural laboratory to study the possible effects of anthropogenic global warming on the climate of the next centuries. In this context, the present research project focuses on the short-term (seasonal to decadal) climate variability of Central Europe during the Oligocene, reconstructed from the sclerochronological records of fossil marine organisms, i.e., bivalves, sirenians and sharks. The result of this research were included into three manuscripts, of which two are already published in peer-reviewed journal. The third paper is currently under review in Nature Scietific Reports.

In the first paper (chapter 2-I), it was assessed whether the long-lived bivalve mollusk *Glycymeris planicostalis* from the late Rupelian deposits (ca. 30 Ma; Lower Oligocene) of the Mainz Basin (Germany) can serve as an ultra-high resolution archive of sea surface temperature (SST). Shell oxygen isotope ($\delta^{18}O_{shell}$) values indicate that the bivalves formed their shells uninterruptedly during winter and summer, providing data on the full seasonal temperature amplitude of the seawater in the Mainz Basin. Absolute SSTs were estimated using a water oxygen isotope ($\delta^{18}O_{water}$) signature of -0.9 ±0.3 ‰. This value was extrapolated from the oxygen isotope data of tooth enamel phosphate ($\delta^{18}O_{PO4}$) of coeval sea cow remains. Reconstructed temperatures ranged between 12.3 and 22.0 °C and agreed well with previous estimates. Seasonal temperature extremes varied greatly on inter-annual timescales. Averaged over 40 years, winter and summer temperatures equaled 13.6 ± 0.8 and 17.3 ± 1.2 °C, respectively, a thermal regime comparable to the modern northwestern Mediterranean realm.This study also contains an extended discussion on the advantages of using the shells of *G. planicostalis* for reconstruction of Oligocene climate conditions over other marine paleoclimate archives.

The second paper (chapter 2-II) focused on how rising atmospheric pCO_2 levels forced changes in the seasonal temperatures in Central Europe during the mid-Oligocene (ca. 31 to 25 Ma). Seasonally resolved SST were reconstructed from $\delta^{18}O$ values of fossil bivalve shells (*G.*

planicostalis, *G. obovata*, *Palliolum pictum*, *Arctica islandica* and *Isognomon maxillata sandbergeri*) and shark teeth (*Carcharias cuspidata*, *C. acutissima* and *Physogaleus latus*) collected from deposits of the Mainz and Kassel Basins (Germany). The SST estimates were then compared to numerical climate simulations computed for the Oligocene assuming an atmospheric pCO_2 rise from 400 to 560 ppm and 400 to 840 ppm (i.e., the range of variability suggested by proxy-derived data for the studied time interval). The multi-taxon $\delta^{18}O$-based reconstructions suggested a gradual increase of SST, on average, by as much as 4 °C during the Rupelian followed by 4 °C cooling during the Chattian (Upper Oligocene). Seasonal SST amplitudes increased by about 2 °C during the warmest time interval, with warming being more pronounced during summer. Climate simulations suggest that the observed warming of the upper ocean during the Rupelian required an atmospheric pCO_2 rise of at least 160 ppm (from 400 to 560 ppm).

The third paper deals with a reconstruction of atmospheric dynamics and their effect on the inter-annual climate variability of Central Europe during the mid-Oligocene. Relative annual growth increment widths of long-lived glycymerid and *Arctica islandica* specimens revealed distinct quasi-decadal growth cycles modulated on a 3 to 7 year period. These periodic changes in shell growth were most likely related to fluctuations in the availability of food and ultimately to primary productivity which in turn, were coupled to atmospheric circulation patterns and precipitation rates on land. Shell stable carbon isotope ($\delta^{13}C_{shell}$) values corroborated the link between shell growth and food availability. Numerical climate models suggested that winter surface level pressure and precipitation rate across the North Atlantic sector during the Oligocene exhibited a pattern comparable to the modern North Atlantic Oscillation (NAO). The simulated NAO index for the Oligocene show periodicities of 2.5 - 6 years, which agree with those revealed by the proxy data, yet, fluctuate on shorter wavelengths than the modern NAO (biennial and 6 - 10 year cycles). The elevated atmospheric pCO_2 concentrations and the different paleogeography likely influenced the spatial distribution of the sea level pressure patterns and at the same time, the temporal variability of the NAO precursor. This study suggest that an NAO-like variability in the North Atlantic sector was already present during the Late Paleogene, about 20 Ma earlier than formerly assumed.

Given the overall similarities between the Oligocene world and the climate scenarios predicted for the Earth during the next centuries, the results of this research give a hint of possible climate developments in Central Europe in the near future.

ZUSAMMENFASSUNG

Die oligozäne Epoche war der letzte Zeitraum in der Erdgeschichte, in dem eine unipolar vergletscherte Welt auftrat. Während die nördliche Hemisphäre weitgehend eisfrei blieb, ähnelten die Land-Ozean-Verteilung sowie großräumige atmospherischen und ozeanischen Zirkulationsmuster der modernen Konfiguration. Die atmosphärischen CO_2-Konzentrationen schwankten hingegen zwischen 400 ppm und 560 ppm. Solche Rahmenbedingungen entsprechen denen, die von numerischen Klimamodell-Projektionen für die nahe Zukunft prognostiziert werden. Daher kann die oligozäne Welt als natürliches Labor für die Erforschung der möglichen Effekte der von Menschen verursachten globalen Erwärmung auf das Klima der nächsten Jahrhunderte dienen. In diesem Zusammenhang konzentriert sich das vorliegende Forschungsprojekt auf die kurzzeitige (von saisonal bis dekadisch) Klimavariabilität in Zentraleuropa während des Oligozäns. Paläoklimabedingungen wurden anhand sklerochronologischen Rekords fossiler Organismen, nämlich Bivalven, Seekühen und Haien, rekonstruiert. Das Ergebnis dieser Forschung liegt hier in Form von drei Manuskripten vor. Bis dato wurden zwei Manuskripte bereits in anerkannten begutachteten Fachzeitschriften publiziert, während eines davon sich noch in Begutachtung befinden.

Als Erstes wurde geprüft, ob die langlebige Muschelart *Glycymeris planicostalis* aus Rupelischen Ablagerungen (ca. 30 Millionen Jahre; Unteres Oligozän) des Mainzer Beckens (Deutschland) ein geeignetes Proxy-Archiv für ultra-hoch-aufgelöste marine Oberflächenwasser-Temperaturrekonstruktionen ist (Kapitel 2-I). Die Sauerstoffisotopen-Werte ($\delta^{18}O_{shell}$) der untersuchten Schalen zeigen, dass die Muscheln ohne Unterbrechung über die Winter und Sommer-Saison ihre Schalen bildeten. Somit lieferten die $\delta^{18}O$-Werte des Schalenskarbonats Informationen über die komplette saisonale Amplitude der Wassertemperaturen im Mainzer Becken. Absolute Oberflächenwasser-Temperaturen wurden unter der Verwendung eines $\delta^{18}O_{water}$-Wert der Sauerstoffisotopie des Wassers von -0,9 ±0,3 ‰ rekonstruiert. Dieser Wert wurde aus der Phosphatssauerstoffisotopen-Signatur des fossilen Zahnschmelzes von Seekuhzähnen aus Ablagerungen gleichen Alters errechnet. Aus den fossilen Muschelschalen rekonstruierte Wassertemperaturen lagen in Bereich zwischen 12,3 und 22,0 °C und stimmten gut mit den Ergebnissen aus vorherigen Studien überein. Saisonale Temperaturextreme variierten stark von Jahr zu Jahr. Im Durchschnitt über 40 Jahre, lagen die durchschnittlichen Winter- und Sommer-

Temperaturen bei 13,6 ± 0,8 bzw.17,3 ± 1,2 °C. Diese Studie enthält auch eine ausführliche Diskussion über die Vorteile von Paläoklimarekonstruktionen mittels *G. planicostalis* Schalen gegenüber anderen marinen Archiven.

Des Weiteren wurde der Zusammenhang zwischen Fluktuationen der atmosphärischen CO_2 Konzentration und der saisonalen Temperaturschwankungen in Zentraleuropa während des mittleren Oligozäns (ca. 31 bis 25 Millionen Jahren) untersucht (Kapitel 2-II). Saisonal-aufgelöste Oberflächenwassertemperaturen wurden rekonstruiert mittels δ^{18}O-Werten fossiler Muscheln (*G. planicostalis*, *G. obovata*, *Palliolum pictum*, *Arctica islandica* und *Isognomon maxillata sandbergeri*) und Haizähne (*Carcharias cuspidata*, *C. acutissima u*nd *Physogaleus latus*) aus den Ablagerungen des Mainzer und Kasseler Beckens. Die rekonstruierten Wassertemperaturdaten wurden dann mit denen von numerischen Klimamodellen verglichen. Oligozäne Oberflächenwassertemperaturen wurden simuliert unter der Annahme eines Anstiegs des atmosphärischen pCO_2 von 400 auf 560 ppm und von 400 auf 800 ppm (d. h., der Fluktuationsbereich der proxy-basierten Abschätzungen für dieses Zeitintervall). Multispezies δ^{18}O-basierte Rekonstruktionen deuteten auf eine durchschnittliche Erwärmung des Oberflächenwassers um 4°C während des spätesten Rupelium gefolgt von einer 4°C Abkühlung im Chattium (Ober Oligozän). Saisonale Oberflächenwassertemperatur-Amplituden stiegen um etwa 2°C während des wärmsten Intervalls, wobei, die Erwärmung im Sommer stärker ausgeprägt war als im Winter. Klimamodellsimulationen zeigen, dass die Rupelische Erwärmung von einem atmosphärischen pCO_2 Anstieg von mindestens 160 ppm (von 400 zu 560 ppm) verursacht werden konnte.

Der letzte Teil dieser Arbeit beschäftigt sich mit der Rekonstruktion der von atmosphärischen Zirkulation verursachten interannuellen Klimaschwankungen in Zentral Europa während des mittleren Oligozäns. Die Untersuchung der relativen Änderungen der Schalen-Wachstumsinkremente von langlebigen Glycymeriden und *Arctica islandica* zeigten deutliche quasi-dekadische Wachstumzyklen mit einer Periode von 3 bis 7 Jahren. Periodische Änderungen im Schalenwachstum hängen hingen mit Fluktuationen in der Nahrungsverfügbarkeit (Primär Produktion) zusammen, die wiederum mit atmosphärischen Zirkulationsmustern und Niederschlagsraten gekoppelt waren. Die Kohlenstoffzusammensetzung der Schalen bestätigten den Zusammenhang zwischen Schalenwachstum und Nahrungsverfügbarkeit. Numerische Klimamodelle belegten, dass der atmosphärische Oberflächenluftdruck und Niederschlagsraten

über dem Nordatlantischen Sektor während des Oligozäns dem Muster der heutigen Nordatlantischen Oszillation (NAO) ähnelten. Der simulierte Oligozän NAO-index wies periodische Schwankungen von 2,5 bis 6 Jahren auf, die mit dem schalenbasierten Daten übereinstimmten: Allerdings entsprachen die Wellenlängen nicht denen des heutigen NAOs. Die höhe atmosphärische pCO_2 Konzentration und die unterschiedliche Paläogeographie im Oligozän sind wahrscheinlich der Grund für die von heute abweichende Variabilität des NAO-Vorläufers. Diese Studie zeigt, dass der Nordatlantische Sektor bereits während des späten Paläogens von einer NAO-ähnlichen Variabilität der atmosphärischen Zirkulationsmuster dominiert war, ca. 20 Millionen Jahren früher als bis her angenommen.

Angesichts der Ähnlichkeiten zwischen der oligozänen Welt und den vorausgesagten Klimaszenarien der Erde im Laufe der nächsten Jahrhunderten, liefern die Resultate dieser Forschungsarbeit einen Vorgeschmack auf die zukünftig möglichen Klimaentwicklungen in Zentraleuropa.

AKNOWLEDGEMENTS

Not displayed for reasons of data protection

TABLE OF CONTENTS

LIST OF FIGURES

CHAPTER 1 - INTROCUTION

CHAPTER 2 - MANUSCRIPTS

MANUSCRIPT I

MANUSCRIPT II

MANUSCRIPT III

CHAPTHER 3 - SUMMARY AND OUTLOOK

APPENDIX

LIST OF TABLES

CHAPTER 2 - MANUSCRIPTS

MANUSCRIPT I

MANUSCRIPT II

APPENDIX

Supplementary Material to MANUSCRIPT III

CHAPTER 1
INTRODUCTION

1.1. Global warming: the Oligocene as a key to future climate

Since the beginning of the industrial revolution in the 19th century, the emission of anthropogenic CO_2 has shifted the natural equilibrium of the atmospheric radiation flux, unequivocally forcing global temperature to rise. In the year 2015, atmospheric CO_2 levels have passed the 400 ppm mark (data from the Mauna Loa Observatory, Hawaii, http://www.esrl.noaa.gov/gmd/ccgg/trends/index.html) (Fig. 1), thereby pushing mean global temperatures about 1 °C above preindustrial levels (Tollefson, 2016). Particularly in the Northern Hemisphere, surface temperatures in the polar regions rose by about 2 °C during the 20th century (Hansen et al., 2010; Serreze and Barry, 2011), increasing melting and runoff rates from the Greenland ice sheet (Tedesco et al., 2013). This likely contributed to the recent weakening of the North Atlantic thermohaline circulation and the slowing of the Atlantic meridional overturning (Hansen et al., 2004; Bryden et al., 2005). Moreover, surface warming coincided with the widening of the Hadley cells and the migration of the sub-tropical jet streams toward higher latitudes (Archer and Caldeira, 2006) as well as the contraction of the Arctic polar vortex (Frauenfeld and Davies, 2003; Angell, 2006). At the same time, the main atmospheric circulation patterns of the Northern Hemisphere, the North Atlantic Oscillation, the Pacific North America pattern and the Arctic Oscillation, experienced perturbations of their internal mode (Hurrell, 1995; Hurrell and Deser, 2009).

If the emission of anthropogenic greenhouse gases is not significantly reduced in the next future, atmospheric CO_2 levels are expected to exceed 900 ppm (Stocker et al., 2013) by the year 2100 and possibly reach levels around 1800 ppm within the next 400 years (Zachos et al., 2008) (Fig. 1). By the end of the 21st century, mean global temperatures will increase by up to 4°C, thereby having severe repercussions on oceanic and atmospheric circulation patterns as well as on the seasonality and the frequency and the intensity of short-term (i.e., seasonal to decadal) climate oscillations (Dai et al., 1997; Marshall et al., 2001; Barbosa, 2009; Collins et al., 2013; Cai et al., 2014). Yet, the mode and tempo of these changes are still poorly constrained (Christensen et al., 2013), mainly because of the difficulty of climate models to reproduce sub-decadal variations in extratropical regions (Gerber et al., 2008; Xin et al., 2008; Scaife et al, 2009). Unexpected climate turnovers may have unpredictable repercussions on marine and terrestrial ecological systems, challenge settlements in coastal ecosystems and jeopardize economic hotspots (Ottersen et al.,

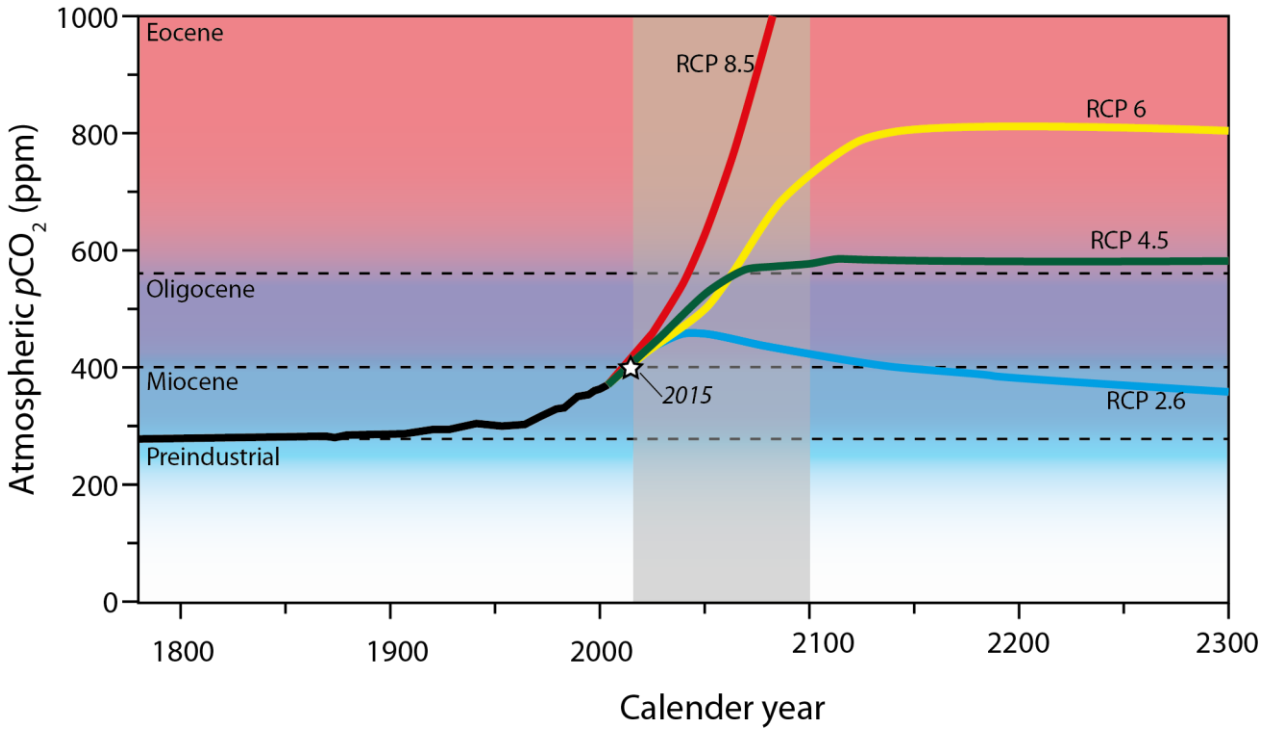

Figure 1. Atmospheric CO_2 concentrations following the four representative concentration pathways (RCPs) scenarios projected until 2300 compared to atmospheric CO_2 levels during different geological epochs of the Cenozoic. The RCP projections reflect different scenarios in which the peak of greenhouse gases emission is reached between 2010-2020 (RCP 2.6; blue line), around 2040 (RCP 4.5; green line), around 2080 (RCP 6; yellow line) and after 2100 (RCP 8.5; red line) (Modified from Meinshausen et al., 2011). The white star indicate the average value of atmospheric CO_2 concentration recorded at the Mauna Loa Observatory in Hawaii for year 2015. Atmospehric CO_2 estimates for the geological epochs come from proxy-derived data compiled by Beerling and Royer (2011).

2001; Stenseth et al., 2002; Hanewinkel et al., 2013; Da Rocha et al., 2014). Therefore, predicting short-term climate changes at mid and high latitudes is of crucial socioeconomic relevance, especially in densely populated areas such as Europe. In this context, studying the climate of geological time intervals, during which boundary conditions were similar to those predicted for the next future, can help to understand how the human-driven global warming will affect global climate in the coming centuries (Masson-Delmotte et al., 2013).

The last time in the earth history during which atmospheric CO_2 levels stabilized around modern values (between 400 and 560 ppm) was during the Oligocene Epoch (33.9 - 23-03 Ma) (Fig. 1). The Oligocene world broadly resembled the today continent-ocean distribution and most of the oceanic and atmospheric circulation patterns observed today (see Chapter 1.1). Thus, the

Oligocene world represents a valuable natural laboratory for the study of the mechanisms behind the predicted climate change.

1.2. The Oligocene icehouse world

The beginning of the Oligocene Epoch (34-23 Ma) is characterized by the most drastic climate reversal of the Cenozoic Era caused by the combination of large-scale tectonic, atmospheric and oceanographic rearrangements. According to proxy data and numerical climate models, this climate deterioration was driven by a drawdown of atmospheric CO_2 from >1200 ppm during the Eocene to 450 ± 100 ppm during Early Oligocene (Hansen et al., 2008) (Fig. 2). Although the coupling mechanisms are not yet fully understood, the atmospheric CO_2 decline was likely linked to enhanced weathering related to the uplift of the Alpine belt and the Himalaya (Raymo and Ruddiman, 1992) and the expansion of C4 grasses (Pagani et al., 2005). The resulting reduction of radiative forcing triggered global cooling, which in turn culminated in the onset of the Antarctic glaciation (Barrett, 1996). As polar ice expanded, global sea-level fell by about 50 m leaving extended continental shelf areas exposed to weathering. This further intensified the sequestration of atmospheric CO_2 (Lear et al., 2008; Cramer et al., 2011).

Major changes occurred also in the marine environments. The collision between the northward drifting Arabian plate and Eurasia (ca. 35 Ma) contributed to the closing of the eastern Tethys gateway, and so, the collapse of the Early Paleogene circum-global circulation currents (Bush, 1997; Huber and Nof, 2006; Allen and Armstrong, 2008). At the same time, the opening of Southern Ocean passages and the widening of the North Atlantic initiated new interoceanic gateways at higher latitudes. These, ultimately, gave rise to the formation large-scale circulation patterns similar to those today. In the Southern Hemisphere, the displacement of South America and Australia towards the equator and the opening of the Drake Passage and the Tasmanian Gateway initiated the Antarctic Circumpolar Current (Kennett et al., 1972; Livermore et al., 2007, Lagabrielle et al., 2009). In the Northern Hemisphere, the widening of the North Atlantic triggered the tectonic deepening of the Greenland-Norwegian sill and strengthened the Arctic deep-water flow into the Atlantic Ocean (Davies et al., 2001). As a consequence, the intensified bipolar deep water export enhanced the meridional overturning as well as the net heat transfer from the southern

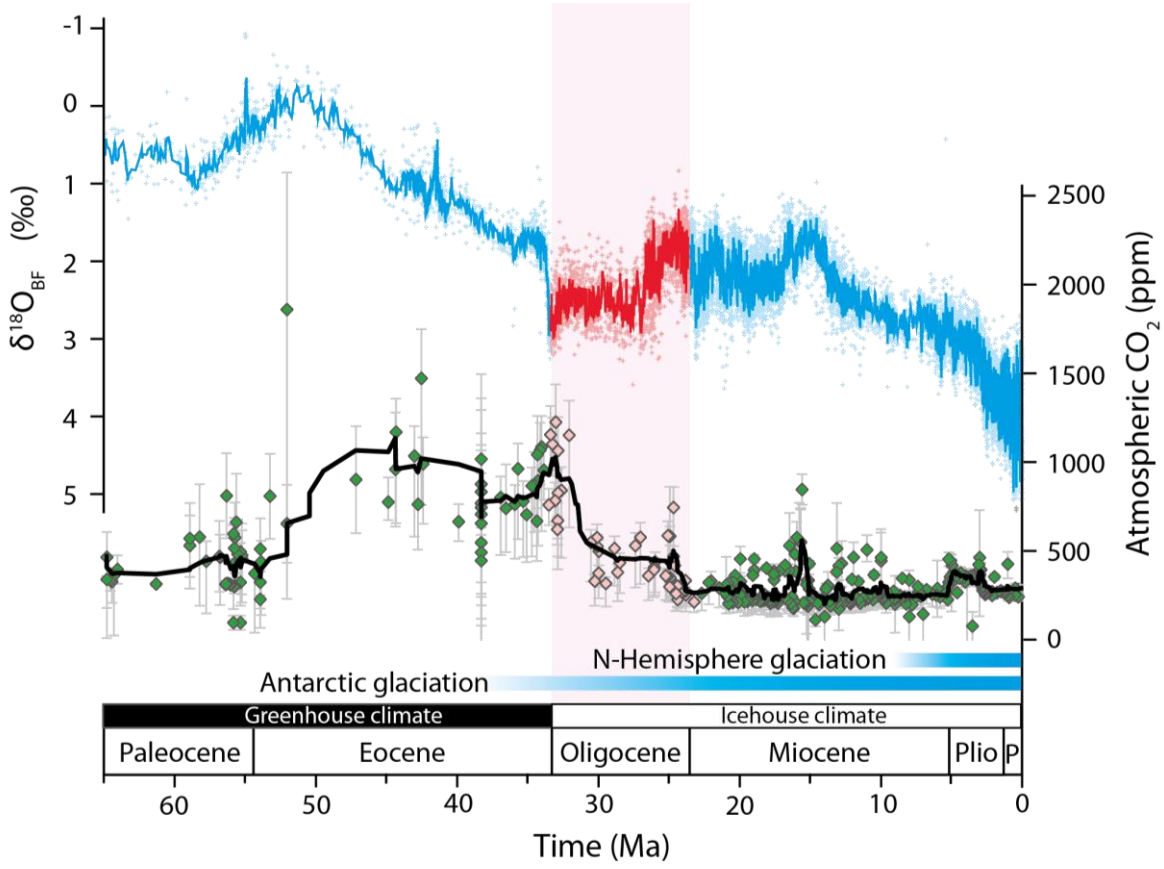

Figure 2. Trends of the isotope record of deep-sea benthic foraminiferan ($\delta^{18}O_{BF}$) and atmospheric CO_2 estimates over the Cenozoic. The $\delta^{18}O_{BF}$ data (light blue crosses; blue line: 50-data point running average) are from Zachos et al. (2001) and show a general decreasing trend over the last 60 Ma. This trend results from the combination of decreasing water temperatures and increasing $\delta^{18}O_{water}$ values related to the increasing sequestration rates of the light oxygen isotope into polar ice. Atmospheric CO_2 estimates (green squares; black line: 10-data points running average; from Beerling and Royer, 2011) generally match the $\delta^{18}O_{BF}$, showing a marked negative excursion over the Oligocene epoch (red vertical shading).

to the northern latitudes, which ultimately resulted in the onset of the present thermohaline circulation (Scher and Martin, 2008; von der Heydt and Dijkstra, 2006).

The combined effect of the atmospheric and oceanic adjustments led to profound deterioration of the Oligocene climate and to the onset of the so-called Icehouse world state[1] (Fig. 2). Thereby, global temperatures abruptly decreased affecting the deep sea as well as surface

[1.] An Icehouse world can be defined as a time of Earth history during which global climatic conditions and events are largely governed by polar ice sheet dynamics. At least seven glaciation events have been recognized from the $\delta^{18}O$ records of deep see benthic foraminifera throughout the Lower Oligocene (Oi1, Oi1a, Oi1b) and the Upper Oligocene (Oi2, Oi2a, Oi2b, Oi2c) (Miller et al., 1991; Pekar et al., 2002). These ice ages were related to an expansion of the Antarctic ice sheet, however, cooling strongly affected the Northern Hemisphere as well (van Simaeys et al., 2005; Śliwińska et al., 2010). In general, the Oligocene Icehouse is considered to be the early phase of a global cooling trend that persists until today.

environments. Proxy data show that average deep-see temperatures declined by about 2.5 - 4 °C across the Eocene/Oligocene boundary (Zachos et al., 2001; Lear et al., 2008; Liu et al., 2009). Cooling at the surface primarily affected winter temperatures that decreased about 4 °C at low latitudes (Ivany et al., 2000) as well as 10 °C in the polar regions of the Northern Hemisphere (Eldrett et al. 2009). Air temperature reconstructions based on palynological data display a similar trend across the Eurasian continent (Mosbrugger et al., 2005; Erdei et al., 2012; Utescher et al., 2015). However, cooling did not suffice to trigger a large-scale glaciation of the Northern Hemisphere, which remained substantially ice-free until atmospheric CO2 levels fell below 280 ppm around the Late Miocene and Pliocene (Shackleton et al., 1984eerling and Royer, 2011; DeConto et al., 2008). Nevertheless, ice drifted debris records from sub-Arctic seas suggest the presence of ephemeral continental ice on Greenland as early as the Late Eocene (Moran et al., 2006; Eldrett et al., 2007; Norris et al., 2014).

1.3. The studied areas and the climate of central Europe

In Central Europe, the Lower Oligocene coincides with the main phase of the uplift of the Alpine belt, and the accelerated rifting of the north-south striking intraplate graben systems across the Europe, known as the European Cenozoic Rift System (ECRIS; Dèzes et al., 2004). The German expression of the ECRIS is represented by the Rhinish Triple Junction, formed by the Upper Rhine Graben to the south, the Hesse Depression to the northeast and the Lower Rhine Graben to the northwest (Sissingh, 2003). The material investigated in this research originated from the Mainz and Kassel Basins, two small basins located in the northwestern part of the Upper Rhine Graben and the western part of the Hesse Depression, respectively. Because of the their geographical vicinity (ca. 200 km), the two basins experienced a similar depositional history, which spans from the Lower Eocene to the Lower Miocene, mostly alternating terrestrial, lacustrine and brackish successions (Grimm et al., 2011; Ritzkowski et al, 2011). However, due to the interplay of local tectonic subsidence and eustatic sea level dynamics, both basins experienced periods of extended marine ingressions from the paleo-North Sea Basin during the Oligocene. As a result, the Mainz Basin and the Kassel Basin became part of a large fully marine epicontinental sea system formed by the Upper Rhine Graben and the Hesse Depression (Sissingh, 2003; Berger et al., 2005a, b). The strongest marine ingression took place during the Lower Oligocene (Rupelian), and lasted

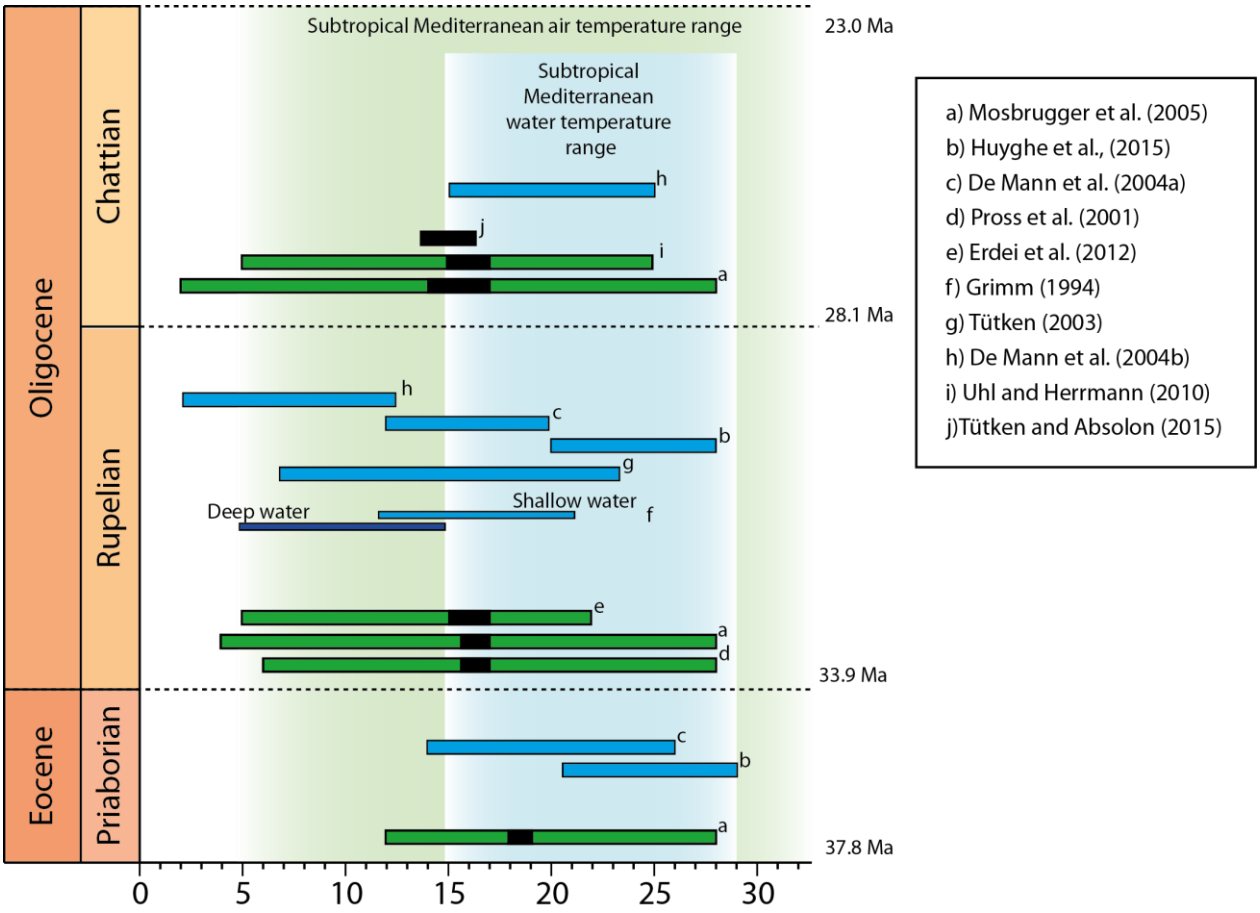

Figure 3. Air and water temperature reconstructions of Central Eurpe during the latest Eocene and Oligocene. Estimated amplitude of annual air temperatures (green bars; black bars: annual average) are based on palynological and $\delta^{18}O$ data of terrestrial and aquatic vertebrate remains (Tütken and Absolon, 2015). Data show cooling across the Eocene/Oligocene boundary, which mainly affected winter conditions, whereas average annual and summet values remained substantially unvaried. Reconstructed water temperatures reconstructions (blue bars) are less coherent and suggest warming during the Oligocene.

from sea level high stands Ru2/Ru3 (ca. 32 Ma) to Ru3/Ru4 (ca. 29.5 Ma) of Haq (1998). As a result, the North Sea Basin extended southward to the Alps and possibly connected to the Tethys via the Molasse Basin (Sissingh, 1997; Rögl, 1999). However, evidence for this southern connection is still debated (Martini 1982; Pharisat and Micklich, 1998; Picot, 2002; Grimm, 2006). This time interval is represented in the Mainz Basin by the nearshore deposits of the Alzey and Stadecken Formations (investigated here) and the basinal pelites of the Bodenheim Formation (Grimm, 1998; Grimm et al., 2000; Sissingh, 2003; Berger et al., 2005) as well as the clay and fine sands of the Rupel Clay (Ger: Rupelton) Formation in the Kassel Basin (Ritzkowski, 1967, 2005). Towards the end of the Rupelian, marine conditions ceased in the Mainz Basin, whereas they persisted in the Kassel Basin throughout the Lower Oligocene. During the Upper Oligocene (Chattian), renewed transgressions from the North Sea Basin were confined to the Kassel Basin,

where they established fully marine, shallow water conditions. Deposits representing that time are the nearshore coarse sands of the Kassel Formation (Ritzkowski, 1967, 2005), from which most of the material of this study came from.

The Oligocene Epoch represents a crucial moment for the development of the Central European climate. By the time of the early Rupelian, the Alps reached an elevation between 1 and 2 km (Kuhlemann, 2007). Together with the Pyrenean, they formed a geomorphological barrier that separated the climate in Central Europe from the Tethyan realm (Héran et al., 2010). At the same time, the North Atlantic became a major source of atmospheric moisture for the regions north of the Alps, closely resembling the modern situation (Bice et al., 2001; Kocsic et al., 2014). Yet, despite the progressive decoupling from the southern climate, environmental conditions in the German epicontinental seas remained generally warm, similar to those observed in the modern Mediterranean Sea (Pross and Schmidl, 2002; Grimm et al., 2011; Ritzkowsky et al., 2011; Grimm and Uffenorde, 2010). According to palynological data, air temperatures oscillated between 7 and 10 °C in winter, and between 26 and 28 °C in summer during the Rupelian (Pross et al, 1998, 2000; Mosbrugger et al., 2005; Erdei et al., 2012). While, slightly cooler winter temperatures (between 2 and 7 °C) have been estimated for the Chattian (Mosbrugger et al., 2005; Uhl and Hermann, 2010). These values agree with the mean air temperature reconstructions (15 ± 2 °C) of Tütken and Absolon (2015), based on the $\delta^{18}O$ values of terrestrial and aquatic vertebrate remains from the deposits of the Maar Lake Enspel in Germany (Chattian).

Information on marine water temperature is much more limited and the few available data are often contradictory (Fig. 3). Reconstructions based on the oxygen isotope composition of shark teeth (Tütken, 2003) and foraminiferan tests (Grimm et al., 1994) from the Mainz Basin yielded temperatures varying between 6 and 23 °C. These values are in general agreement with the otolith and gastropod $\delta^{18}O$-data from the Southern North Sea Basin, according to which temperature ranged between 13 and 20 °C (De Mann et al., 2004a; temperatures calculated from original $\delta^{18}O$-data using the paleotemperature equation of Grossman and Ku, 1986, with scale correction of Dettman et al., 1999; assuming a $\delta^{18}O_{water}$ value of -0.45 ‰). However, this temperature range is substantially lower than the one (20 to 28 °C) reconstructed from $\delta^{18}O$ composition of bivalve and gastropod shells from coeval strata of the Paris Basin (Huyghe et al., 2015). Unfortunately, no specific study has been carried out for the Kassel Basin. Besides some interpretation based on faunal assemblages, which vaguely suggest warm to tropical temperatures (Müller, 1996; Grimm

and Uffenorde, 2011), no quantifiable data is available from the literature. Based on the composition of benthic foraminiferan assemblages from deposits of the Southern North Sea Basin, De Mann et al. (2004b) suggested that Chattian temperatures may have been 5 to 10 °C higher than in the Rupelian, and so contradict the palynological data reported above.

1.4. Bivalve sclerochronology

The study of the shell growth patterns and the physical and chemical properties of accretionary biogenic carbonates is the core competence of sclerochronology (from Greek σκληρόσ, sklēros, 'hard'; and χρόνος, khronos, 'time'). Using a variety of different techniques, sclerochronological studies aim to reconstruct the life history traits of organisms as well as the environment in which they lived. In such studies, bivalves are often preferred over other biogenic skeletons because of their broad biogeographic distribution, their broad variety of life strategies and their extraordinary longevity.

Unlike some other organisms (e.g. corals, sponges), bivalves (Fig. 4A) do not form their shells uninterruptedly throughout their life. Shell growth formation slows or ceases at regular time intervals (usually when valves remain closed) and organic matter accumulate on the shell accretion front, forming characteristic dark lines (growth lines) (Clark, 1974; Gordon and Carriker, 1978; Checa, 2000). The timing of growth line formation spans from sub-daily to annual (e.g., Clark, 1969; Richardson et al., 1979; Wittbaard et al., 1994; Schöne et al., 2005a), and is governed by a combination of internal biological clocks (e.g., Kim et al., 1999; Schöne and Giere, 2005), physiological stress (e.g., Thompson et al., 1980; Galap et al. 1997) and environmental conditions (e.g., Fritz and Lutz, 1986; Royer et al., 2013). Annual growth lines are easily to recognize in cross-sections (Fig.4B) in the ventral margin (Fig. 4C) and the hinge plate (Fig. 4D), and can be used to subdivide the shell growth pattern into shell portions of equal duration (growth increments).

The width of growth increments reflects growth rate and is used in an analogous manner as the width of tree-rings in dendrochronological studies. During periods of favorable environmental conditions (temperature, food availability and food quality), bivalves grow their shell at faster rates than during periods of metabolic stress (Schöne, 2008). Therefore, if the range of physiological tolerance of a bivalve is known, the changes in the width of the growth increments can be used as

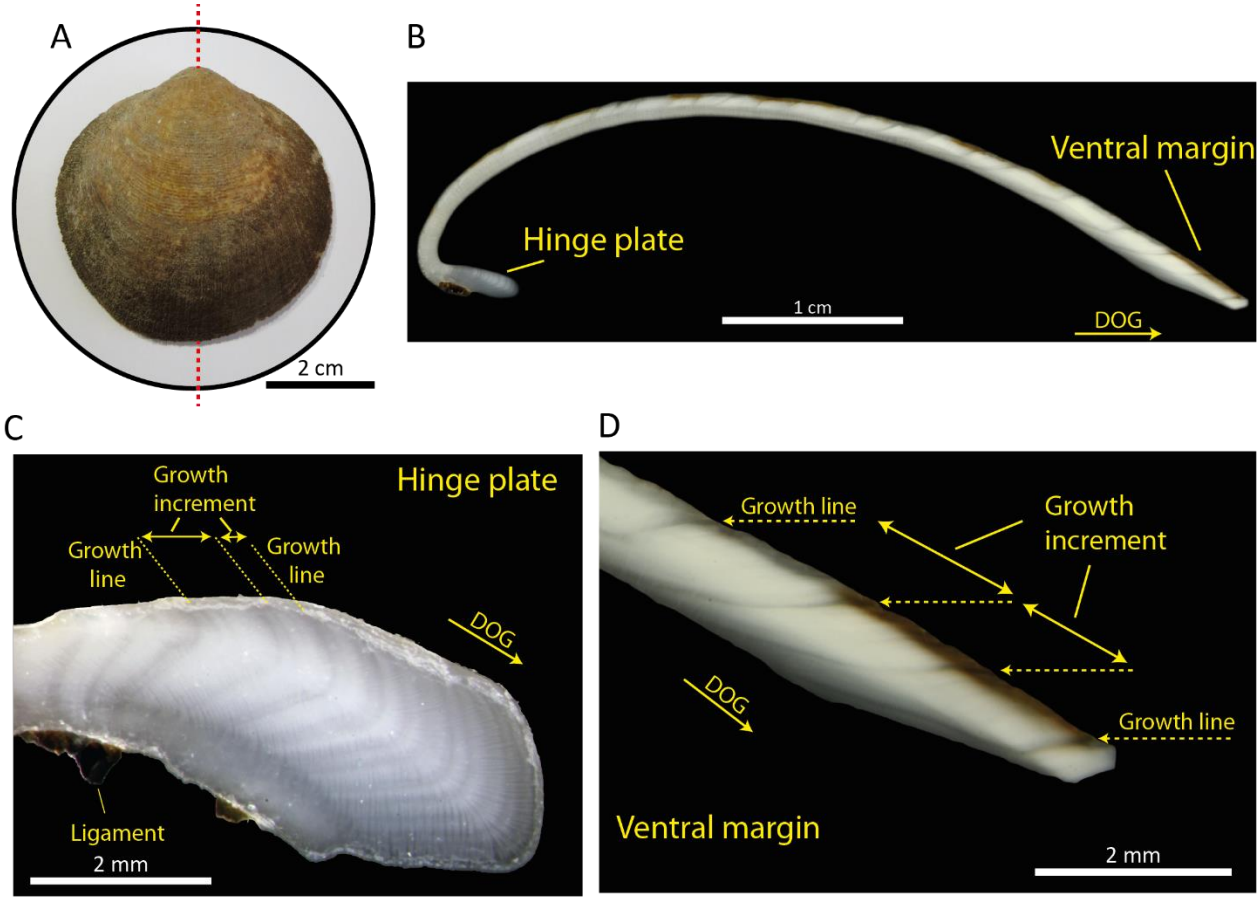

Figure 4. Life-history traits of glycymerid bivalves. (A) Photograph of a shell *Glycymeris pilosa* from Greece (live collected) showing the axis of maximum growth (red dotted line). (B) Cross section of the shell performed along the axis of maximum growth shown in (A). Growth lines and growth increments are clearly distinguishable in both the hinge plate (C) and at the ventral margin (D). DOG = Direction of growth. All figures presented here are original.

an indicator of past environmental conditions. However, shell growth rates do not solely depend on environmental parameters but also on ontogenetic age (e.g., Appeldoorn, 1983; Schöne, 2008). In fact, growth rates decrease exponentially throughout ontogeny at rates that can vary greatly between species (Wanink and Zwarts, 1993; Peharda et al., 2012; Bušelić et al., 2015) and on intraspecific levels (Jones et al., 1978; Witbaard et al., 1997, 1999; Schöne et al., 2003). However, age-trends can be estimated, e.g., using the von Bertalanffy equation (von Bertalanffy, 1938) or cubic spline fitting, and mathematically removed from raw growth increment width time-series (Schöne, 2003). Once detrended, these data provide a dimensionless measure) of environmental fluctuations that can be used to reconstruct climate phenomena over the last centuries (Lazareth et

al., 2006; Nielsen et al., 2008; Lohmann and Schöne, 2013) or even during the geological past (Ivany et al., 2011). Shells of long-lived bivalves (e.g., *Glycymeris glycymeris* or *Arctica islandica*) can provide particularly long chronologies can span decades (Ramsay et al., 2000; Strom et al., 2005; Brocas et al., 2013), centuries (Schöne et al., 2005c; Reynolds et al., 2013; Wanamaker et al., 2008), or even millennia, when chronologies of contemporaneous specimens with overlapping lifespan are combined into master chronologies (Butler et al., 2013; Holland et al., 2014).

Growth patterns also serve as a time gauge to place geochemical properties the shells into temporal context. Variation of the elemental and isotopic composition of bivalve shells can reveal valuable information about seasonal environmental variables such as water temperature and salinity (Dodd and Crisp, 1982; Williams et al., 1982; Klein et al., 1996), primary productivity (Barats et al., 2009; Goodwin et al., 2013), or water pollution (Fuge et al., 1993; Schettler et al., 1996; Liehr et al., 2005). With regard to water temperature, there have been many attempts to develop trace elements-based paleothermometers, yet empirical studies have yielded contrasting results (e.g., Hart and Blusztajn, 1998; Gillikin et al., 2005; Schöne 2008 and references therein). For instance, studies have shown that shell Sr/Ca and Mg/Ca ratios vary significantly at interspecific levels (Freitas et al., 2008) or even within the same specimen depending on crystal fabrics of the studied shell portion (Surge and Walker, 2006; Schöne et al., 2013). In addition, shell growth rate (Takesue and van Geen, 2004; Lorrain et al., 2005) and ontogenetic age (Freitas et al., 2005) can have an influence on trace element chemistry of the shells. On the contrary, the $\delta^{18}O_{shell}$ value is considered a robust paleothermometer and has been widely used in numerous paleoenvironmental studies over the last decades (e.g., Dorman and Gill, 1959; Arthur et al., 1983; Steuber, 1996). This is mainly because bivalves form their shells near isotopic equilibrium with the ambient water (Mook and Vogel, 1968; Grossman and Ku, 1986; Lécuyer et al., 2012). Unlike element-to-Calcium ratios, their $\delta^{18}O_{shell}$ signature is virtually not influenced by vital effects (e.g., Goodwin et al., 2001; Surge et al., 2001; Schöne et al., 2004). Yet, estimating paleotemperatures from the oxygen isotope value of shell carbonate can be challenging as well. In fact, the $\delta^{18}O_{shell}$ value is a dual proxy that simultaneously provides information on temperature and oxygen isotopic composition of the water ($\delta^{18}O_{water}$) from which the skeleton formed. Therefore, robust temperature estimates can only be achieved if the $\delta^{18}O_{water}$ is known, which is rarely the case for ancient environments.

1.5. The oxygen isotope signal of ancient water bodies

Estimating the $\delta^{18}O$ value of ancient marine waters is the most problematic aspect of $\delta^{18}O_{shell}$-based paleothermometry studies. In fact, choosing the wrong $\delta^{18}O_{water}$ value can lead to strong underestimation or overestimation of the actual water temperature. For example, using the empirically determined equation of Grossman and Ku (1986) a 1 ‰ change of $\delta^{18}O_{water}$ corresponds to a change of about 4.3 °C. Hence, in paleoclimate studies, $\delta^{18}O_{water}$ values have to be selected carefully, taking into account a variety of factors such as the global $\delta^{18}O$ cycle, regional hydrological dynamics and the paleogeographic position of the study area.

In general, oxygen isotopes are subject to strong kinetic fractionation when water transits between different physical states. At increasing temperature, $H_2{}^{16}O$ molecules preferentially evaporate into the atmosphere forming clouds that are always isotopically lighter than the marine water left behind. When clouds cool down, $H_2{}^{18}O$ molecules will preferentially condensate and the remaining vapor will become further enriched in the $H_2{}^{16}O$ molecules. Thus, atmospheric moisture, and so precipitation, will become progressively depleted in ^{18}O as clouds travel away from the place of evaporation. Since most of the evaporation occurs near the equator and most of the precipitation occurs at high latitudes, polar ice has very low $\delta^{18}O$ values (as low as -60 ‰) (Watanabe et al., 1999). As a consequence of this, the $\delta^{18}O$ signal of ocean waters directly depends on the global ice volume, where glacial expansion is associated with increasing ocean $\delta^{18}O$ values. Whereas the present ocean water has a mean $\delta^{18}O$ value about 0 ‰, the ocean of an ice-free world (e.g., during the Cretaceous and the Early Palogene) would have a value of -1.2 ‰ (Shackleton and Kennett, 1975). Most of the knowledge about the $\delta^{18}O_{water}$ during the Oligocene derives from the geochemical composition of foraminiferan tests. Combined $\delta^{18}O$ and Mg/Ca analyses suggest that the ocean $\delta^{18}O_{water}$ value of the unipolar glaciated Oligocene world ranged between -0.4 and -0.5 ‰ (Lear et al., 2000, 2004 Cramer et al., 2011) (Fig. 5).

Although generally indicative, such data refer to deep-sea waters and do not express the spatial and temporal $\delta^{18}O_{water}$ heterogeneity of surface waters. For instance, the present $\delta^{18}O_{water}$ values of the Atlantic Ocean range between -1.5 and +1.5 ‰ at high and low latitudes, respectively (Schmidt et al., 1999) (Fig. 6). Deviations from the average can be even greater in smaller marine basins with a restricted water exchange with the open ocean. Extraordinary high $\delta^{18}O$ (ca. 2.5 ‰) values are recorded in the highly evaporative realm of the Red Sea (Andrié and Merlivat, 1989).

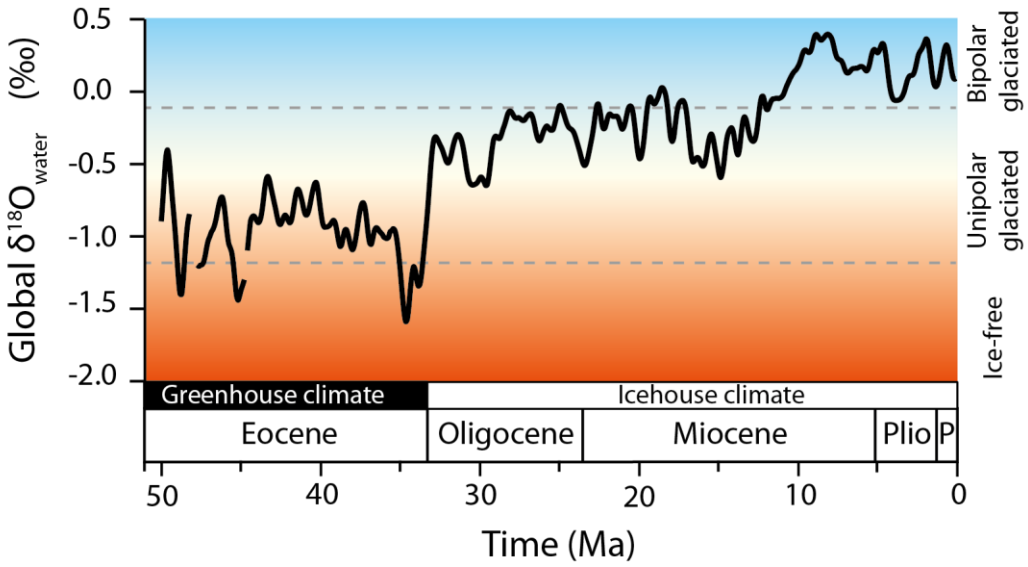

Figure 5. Estimated variation in $\delta^{18}O$ composition of sea water during the last 50 Ma (modified from Cramer et al., 2011). Horizontal dotted lined indicate the $\delta^{18}O$ levels characteristic for Ice-free (pre-Oligocene), unipolar glaciated (Oligocene to Pliocene) and bipolar glaciated (Pliocene to present) world.

Whereas, extremely low values (ca. -7 ‰) characterize the subarctic seas, such as the Hudson Bay (Granskog et al, 2011). Additionally, coastal environments usually exhibit more negative $\delta^{18}O$ values than open marine settings, because of the influence freshwater discharge from land, which is typically some per mil lighter than seawater. Since precipitation and evaporation rates oscillate seasonally, the $\delta^{18}O$ of coastal waters can strongly fluctuate during the year, especially in the upper few meters of the ocean (Stenni et al., 1995). Therefore, the reconstruction of ancient surface $\delta^{18}O_{water}$ signatures should rely on regionally sensitive and temporally highly resolved proxy archives that are able to reflect the dynamic character of shallow waters.

Most of the information on ancient surface $\delta^{18}O_{water}$ signatures comes from the oxygen isotope ratios of tooth enamel of fossil mammals (e.g., Thewissen et al., 2007; Clementz et al. 2009a; Herán et al., 2010; Kocsis et al., 2014). This is because mammals are homoeothermic (warm-blooded) animals with a constant body temperature of around 37 °C. Therefore, the $\delta^{18}O$ ratios of their skeletal bioapatite mostly depends on $\delta^{18}O$ signal of the water and the food ingested during lifetime (Kohn, 1996). In the case of fully aquatic mammals, such as sirenians and cetaceans, this value directly correlates to the marine $\delta^{18}O_{water}$ signal, which can be easily estimated using empirically determined equations (e.g., Tütken, 2003; Clementz et al., 2009b). This approach was applied in the first manuscript reported in this thesis (Chapter 2). So far, no such data were available

for the study areas. The range of $\delta^{18}O_{water}$ for the Alzey Formation was estimated from the $\delta^{18}O$ record of tooth enamel of the extinct dugong, *Halitherium schinzii*. Notably, in the last years, there have been some numerical climate model-based attempts to reproduce the $\delta^{18}O$ signal of ancient waters, however, simulations are still too coarse and struggle to replicate the complexity of the oxygen isotope cycle (e.g., Sturm et al., 2010).

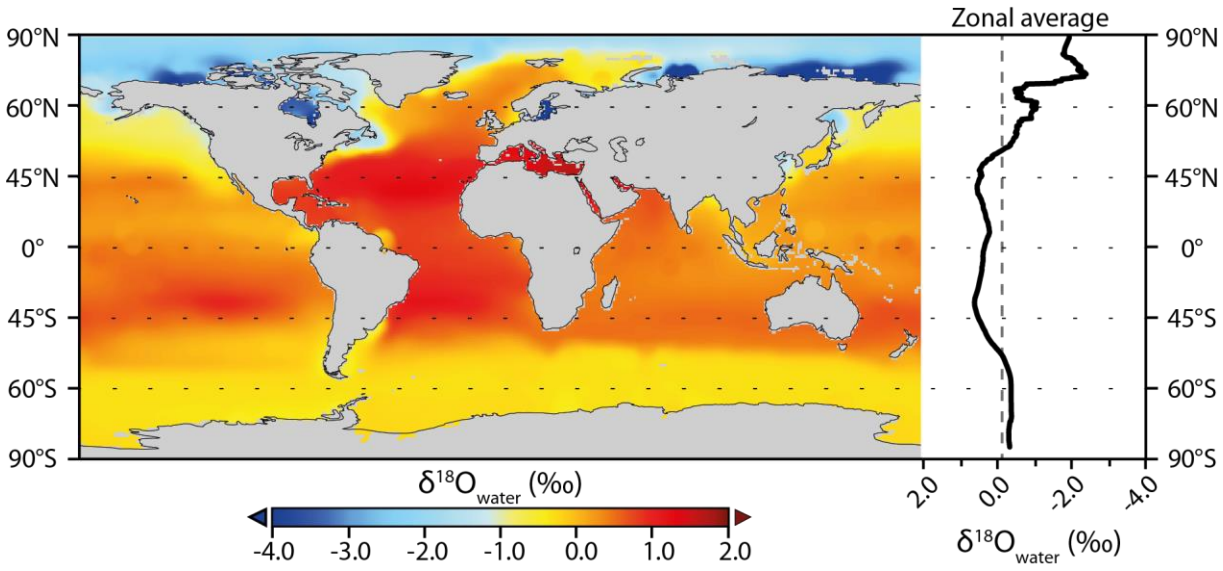

Figure 6. Present global surface distribution and zonal averages sea water $\delta^{18}O$ values (data come from Schmidt et al., 1999). Note that high $\delta^{18}O_{water}$ levels are generally recorded at equatorial and tropical latitudes, whereas polar waters display more depleted values. Highest values (up to 2.5 ‰) occurs enclosed marine basins at tropical latitudes strongly subjected to evaporation (e.g., southwestern Mediterranean and the Red Sea). Lowest values (down to -7.7 ‰) were recorded in coastal arctic regions (e.g., Hudson Bay and the Baltic Sea) that are directly exposed to enhanced glaciers runoff off. Dotted line in the left panel indicate the modern global marine $\delta^{18}O_{water}$ average value.

1.6. Aim of the research

The present (cumulative) Ph.D. thesis has been conducted within the framework of a DFG-funded research project on short-term (e.g., sub-seasonal to decadal) climate dynamics that prevailed in shallow marine settings of Central Europe during the Oligocene. The thesis consists of three manuscripts in international, peer-reviewed scientific journals that explore these climate fluctuations largely based on bivalve sclerochronological data. During the Oligocene, glycymerid bivalves were particularly thick-shelled and long-lived (up to 150 years) and inhabited the nearshore environments of epicontinental seas in the Rheinish Triple Junction. In conjunction with the large size of the shells and the extraordinary lifespan, high-resolution isotope sampling

techniques allowed to reconstruct seasonal temperatures at weekly to monthly resolution over many consecutive years. With these data it was also possible to precisely determine the timing and rate of seasonal shell formation. Furthermore, variations in annual shell growth provided information on decadal-scale climate variability. For this purpose, increment width chronologies were studied by means of spectral analysis.

In order to test the reliability of the results obtained from *Glycymeris* spp., additional $\delta^{18}O$ data were obtained from skeletons of other coeval organisms. The oxygen isotope composition of fossil sirenian teeth were used to estimate the $\delta^{18}O_{water}$ signal of the epicontinental seas in Germany. This allowed to reconstruct the regional temperature oscillations more accurately than simply using a global mean $\delta^{18}O_{water}$ value provided in the literature. Temperatures were also reconstructed from the $\delta^{18}O_{shell}$ of other bivalve species and shark teeth. This multitaxon approach allowed to test the coherency of the data as well as to recognize and correct possible biases in the estimation of seasonal seawater temperature amplitudes derived from *Glycymeris* spp. shells. In addition, the proxy data were compared to numerical climate simulations conducted for this very project by Gerrit Lohmann and Igor Niezgodzki (AWI Bremerhaven). This multidisciplinary approach permitted to investigate the global climate mechanisms and processes that gave rise to the trends observed in the proxy data.

In the present research the following key research questions were tackled:

a) Is it possible to reconstruct the full seasonal water temperature range from the oxygen isotope record of glycymerid bivalves from the Oligocene strata? Did glycymerids form their growth lines annually and if so, during which season?
b) How did seasonal surface temperatures change under different atmospheric CO_2 levels?; Can proxy data be used in combination with numerical climate models to constrain Oligocene atmospheric pCO_2 estimates?
c) Can the life-history traits of long-lived fossil bivalves (glycymerids and *Arctica islandica*) be used to reconstruct the inter-annual climate variability of Central Europe during the Oligocene? Can proxy data be combined with numerical climate models to unveil if an atmospheric circulation pattern comparable to the North Atlantic Oscillation already existed during the Late Paleogene? If yes, did the spatial distribution and the internal variability of this Oligocene NAO-like pattern differed from the modern NAO?

1.7. Overview of the research

In the next chapter, the results of this Ph.D. thesis are reported in the form of manuscripts. The first two manuscripts have already been published, the third manuscript has been submitted.

MANUSCRIPT I: Walliser, E.O., Schöne, B.R., Tütken, T., Zirkel, J., Grimm, K.I., and Pross, J., 2015. The bivalve *Glycymeris planicostalis* as a high-resolution paleoclimate archive for the Rupelian (Early Oligocene) of central Europe: Climate of the Past 11, 653–668.

This study examines the reliability of the Rupelian *G. planicostalis* as high-resolution proxy archive for seasonal sea surface temperatures (SST) of the Mainz Basin. The ultimate goal of this investigation was to explore the advantages of using the $\delta^{18}O$ of fossil glycymerid shells over other existing temperature archives such as foraminiferan tests and shark teeth.

MANUSCRIPT II: Walliser, E.O., Lohmann, G., Niezgodzki I., Tütken, T. & Schöne, B.R. 2016. Response of Central European SST to atmospheric *p*CO2 forcing during the Oligocene - a combined proxy data and numerical climate model approach. Palaeogeography, Palaeoclimatology, Palaeoecology 459, 552-569.

This study investigates the response of surface water temperatures in Central Europe to varying atmospheric pCO_2 forcing. Oxygen isotope data from bivalve shells (*Glycymeris* spp., *Isognomon* sp. etc.) and shark teeth were combined in order to reconstruct the full seasonal SST amplitudes of the Central European Epicontinental Sea (Mainz/Kassel Basisn) during selected intervals of the Oligocene. Furthermore, the proxy derived SST data were compared to surface temperatures simulated by numerical climate models to better constrain the atmospheric pCO_2 estimates provided in the literature.

MANUSCRIPT III: Walliser, E.O., Lohmann, G., Niezgodzki I. & Schöne, B.R., in review. Inter-annual climate variability in Europe during the Oligocene Icehouse. Nature Scientific Reports.

This study focused on the reconstruction of the inter-annual to decadal climate variability of Central Europe during the Oligocene. Age-detrended annual shell growth data of

Glycymeris spp. and *Arctica islandica* from Germany and Belgium were analyzed by means of spectral anaylsis. Additionally, $\delta^{13}C_{shell}$ and $\delta^{18}O_{shell}$ data were used to reconstruct the main environmental factor driving shell growth. The results where then compared to numerical climate simulations to characterize the atmospheric circulation pattern, which was governing the inter-annual climate variability of Central Europe during the Oligocene.

1.8. References

Allen, M.B., Armstrong, H.A., 2008. Arabia-Eurasia collision and the forcing of mid-Cenozoic global cooling. Palaeogeography, Palaeoclimatology, Palaeoecology 265, 52–58.

Andrié, C., Merlivat, L., 1989. Contribution des données isotopiques de deutérium, oxygène-18, hélium-3 et tritium, à l'étude de la circulation de la Mer Rouge. Oceanologica Acta 12, 165–174.

Angell, J.K., 2006. Changes in the 300-mb north circumpolar vortex, 1963–2001. Journal of Climate 19, 2984–2994.

Appeldoorn, R.S., 1983. Variation in the growth rate of *Mya arenaria* and its relationship to the environment as analyzed through principal components analysis and the ω parameter of the von Bertalanffy equation. Fishery Bulletin 81, 75–84.

Archer, C.L., Caldeira, K., 2008. Historical trends in the jet streams. Geophysical Research Letters 35, L08803.

Arthur, M.A., Williams, D.F., Jones, D.S., 1983. Seasonal temperature-salinity changes and thermocline development in the mid-Atlantic Bight as recorded by the isotopic composition of bivalves. Geology 11, 655–659.

Barbosa, S.M., 2009. Decadal variability in Europe's seasons. In: EGU General Assembly Conference,19-24 April 2009,Vienna, Austria, Abstracts 11, 5332

Barrett, P.J., 1996. Antarctic palaeoenvironment through Cenozoic times - a review. Terra Antarctica 3, 103–119.

Beerling, D.J., Royer, D.L., 2011. Convergent Cenozoic CO_2 history. Nature Geoscience 4, 418–420.

Berger, J.-P., Reichenbacher, B., Becker, D., Grimm, M., Grimm, K., Picot, L., Storni, A., Pirkenseer, C., Derer, C., Schaefer, A., 2005a. Paleogeography of the Upper Rhine Graben (URG) and the Swiss Molasse Basin (SMB) from Eocene to Pliocene. International Journal of Earth Sciences 94, 697–710.

Berger, J.-P., Reichenbacher, B., Becker, D., Grimm, M., Grimm, K., Picot, L., Storni, A., Pirkenseer, C., Schaefer, A., 2005b. Eocene-Pliocene time scale and stratigraphy of the Upper Rhine Graben (URG) and the Swiss Molasse Basin (SMB). International Journal of Earth Sciences 94, 711–731.

Bice, K.L., Scotese, C.R., Seidov, D., Barron, E.J., 2000. Quantifying the role of geographic change in Cenozoic ocean heat transport using uncoupled atmosphere and ocean models. Palaeogeography, Palaeoclimatology, Palaeoecology 161, 295–310.

Bryden, H.L., Longworth, H.R., Cunningham, S.A., 2005. Slowing of the Atlantic meridional overturning circulation at 25°N. Nature 438, 655–657.

Bušelić, I., Peharda, M., Reynolds, D.J., Butler, P.G., González, A.R., Ezgeta-Balić, D., Vilibić, I., Grbec, B., Hollyman, P., Richardson, C.A., 2015. *Glycymeris bimaculata* (Poli, 1795) - a new sclerochronological archive for the Mediterranean? Journal of Sea Research 95, 139–148.

Brocas, W.M., Reynolds, D.J., Butler, P.G., Richardson, C.A., Scourse, J.D., Ridgway, I.D., Ramsay, K., 2013. The dog cockle, *Glycymeris glycymeris* (L.), a new annually-resolved sclerochronological archive for the Irish Sea. Palaeogeography, Palaeoclimatology, Palaeoecology 373, 133–140.

Bush, A.B.G., 1997. Numerical simulation of the Cretaceous Tethys circumglobal current. Science 275, 807–810.

Cai, W., Borlace, S., Lengaigne, M., van Rensch, P., Collins, M., Vecchi, G., Timmermann, A., Santoso, A., McPhaden, M.J., Wu, L., England, M.H., Wang, G., Guilyardi, E., Jin, F.-F., 2014. Increasing frequency of extreme El Niño events due to greenhouse warming. Nature Climate Change 4, 111–116.

Checa, A., 2000. A new model for periostracum and shell formation in Unionidae (Bivalvia, Mollusca). Tissue & cell 32, 405–16.

Christensen, J.H., K. Krishna Kumar, et al., 2013: Climate phenomena and their relevance for future regional climate change. In: Stocker, T.F., Qin, D., et al., (Eds.), Climate Change 2013: The Physical Science Basis. Contribution of Working Group I to the Fifth Assessment Report of the Intergovernmental Panel on Climate Change. Cambridge University Press, Cambridge, United Kingdom and New York, NY, USA, pp. 1217-1308.

Clark, G.R., 1969. Daily growth lines in the bivalve faminly pectinidae. In: Abstract and Programs of the Annual Meeting of the Geological Society of America 1, 34.

Clark, G.R., 1974. Growth lines in invertebrate skeletons. Annual Review of Earth and Planetary Sciences 2, 77–99.

Clementz, M.T., Sewall, J.O., 2009a. Latitudinal gradients in greenhouse seawater $\delta^{18}O$: evidence from Eocene sirenian tooth enamel. Science 332, 455–458.

Clementz, M.T., Sorbi, S., Domning, D.P., 2009b. Evidence of Cenozoic environmental and ecological change from stable isotope analysis of sirenian remains from the Tethys-Mediterranean region. Geology 37, 307–310.

Collins, M., Knutti, et al., 2013: Long-term climate change: projections, commitments and irreversibility. In: Stocker, T.F., Qin, D., et al., (Eds.), Climate Change 2013: The Physical Science Basis. Contribution of Working Group I to the Fifth Assessment Report of the Intergovernmental Panel on Climate Change. Cambridge University Press, Cambridge, United Kingdom and New York, NY, USA, pp. 1029–1136.

Cramer, B.S., Miller, K.G., Barrett, P.J., Wright, J.D., 2011. Late Cretaceous-Neogene trends in deep ocean temperature and continental ice volume: reconciling records of benthic foraminiferal geochemistry ($\delta^{18}O$ and Mg/Ca) with sea level history. Journal of Geophysical Research 116, 1–23.

Dai, A., Fung, I.Y., Del Genio, A.D., 1997. Surface observed global land precipitation variations during 1900-88. Journal of Climate 10, 2943–2962.

Da Rocha, J.-M., Gutiérrez, M.-J., Villasante, S., 2014. Economic effects of global warming under stock growth uncertainty: the European sardine fishery. Regional Environmental Change 14, 195–205.

Davies, R., Cartwright, J., Pike, J., Line, C., 2001. Early Oligocene initiation of North Atlantic deep water formation. Nature 410, 917–20.

De Man, E., Ivany, L.C., Vandenberghe, N., 2004a. Stable oxygen isotope record of the Eocene-Oligocene transition in the southern North Sea Basin: positioning the Oi-1 event. Netherlands Journal of Geosciences 83, 193–197.

De Man, E., Van Simaeys, S., 2004b. Late Oligocene warming event in the southern North Sea Basin: Benthic foraminifera as paleotemperature proxies. Netherlands Journal of Geosciences 83, 227–239.

Dettman, D.L., Reische, A.K., Lohmann, K.C., 1999. Controls on the stable isotope composition of seasonal growth bands in aragonitic fresh-water bivalves (unionidae). Geochimica et Cosmochimica Acta 63, 1049–1057.

Dèzes, P., Schmid, S.M., Ziegler, P.A., 2004. Evolution of the European Cenozoic Rift System: interaction of the Alpine and Pyrenean orogens with their foreland lithosphere. Tectonophysics 389, 1–33.

Dodd, J.R., Crisp, E.L., 1982. Non-linear variation with salinity of Sr/Ca and Mg/Ca ratios in water and aragonitic bivalve shells and implications for paleosalinity studies. Palaeogeography, Palaeoclimatology, Palaeoecology 38, 45–56.

Dorman, F.H., Gill, E.D., 1959. Oxygen isotope paleotemperature determinations of Australian Cainozoic fossils. Science 130, 1576–1576.

Eldrett, J.S., Harding, I.C., Wilson, P. A, Butler, E., Roberts, A.P., 2007. Continental ice in Greenland during the Eocene and Oligocene. Nature 446, 176–179.

Eldrett, J.S., Greenwood, D.R., Harding, I.C., Huber, M., 2009. Increased seasonality through the Eocene to Oligocene transition in northern high latitudes. Nature 459, 969–73.

Erdei, B., Utescher, T., Hably, L., Tamás, J., Roth-Nebelsick, A., Grein, M., 2012. Early Oligocene continental climate of the Palaeogene Basin (Hungary and Slovenia) and the surrounding Area. Turkish Journal of Earth Sciences 21, 153–186.

Frauenfeld, O.W., Davis, R.E., 2003. Northern Hemisphere circumpolar vortex trends and climate change implications. Journal of Geophysical Research 108, 4423.

Freitas, P.S., Clarke, L.J., Kennedy, H.A., Richardson, C.A., Abrantes, F., 2005. Mg/Ca, Sr/Ca, and stable-isotope ($\delta^{18}O$ and $\delta^{13}C$) ratio profiles from the fan mussel *Pinna nobilis*: seasonal records and temperature relationships. Geochemistry, Geophysics, Geosystems 6, Q04D14.

Freitas, P.S., Clarke, L.J., Kennedy, H.A., Richardson, C.A., 2008. Inter- and intra-specimen variability masks reliable temperature control on shell Mg/Ca ratios in laboratory- and field-cultured *Mytilus edulis* and *Pecten maximus* (bivalvia). Biogeosciences 5, 1245–1258.

Fritz, L.W., Lutz., R.A., 1986. Environmental perturbations reflected in internal shell growth patterns of *Corbicula fluminea* (Mollusca: Bivalvia). Veliger 28, 401–417.

Fuge, R., Palmer, T.J., Pearce, N.J.G., Perkins, W.T., 1993. Minor and trace element chemistry of modern shells: a laser ablation inductively coupled plasma mass spectrometry study. Applied Geochemistry 8, 111–116.

Galap, C., Leboulenger, F., Grillot, J.-P., 1997. Seasonal variations in biochemical constituents during the reproductive cycle of the female dog cockle *Glycymeris glycymeris*. Marine Biology 129, 625–634.

Gerber, E.P., Polvani, L.M., Ancukiewicz, D., 2008. Annular mode time scales in the Intergovernmental Panel on Climate Change Fourth Assessment Report models. Geophysical Research Letters 35, L22707.

Gillikin, D.P., Lorrain, A., Navez, J., Taylor, J.W., André, L., Keppens, E., Baeyens, W., Dehairs, F., 2005. Strong biological controls on Sr/Ca ratios in aragonitic marine bivalve shells. Geochemistry, Geophysics, Geosystems 6, Q05009.

Goodwin, D.H., Flessa, K.W., Schöne, B.R., Dettman, D.L., 2001. Cross-calibration of daily growth increments, stable isotope variation, and temperature in the Gulf of California bivalve mollusk *Chione cortezi*: implications for paleoenvironmental analysis. PALAIOS 16, 387–398.

Goodwin, D.H., Gillikin, D.P., Roopnarine, P.D., 2013. Preliminary evaluation of potential stable isotope and trace element productivity proxies in the oyster *Crassostrea gigas*. Palaeogeography, Palaeoclimatology, Palaeoecology 373, 88–97.

Gordon, J., Carriker, M.R., 1978. Growth lines in a bivalve mollusk: subdaily patterns and dissolution of the shell. Science 202, 519–521.

Granskog, M.A., Kuzyk, Z.Z.A., Azetsu-Scott, K., Macdonald, R.W., 2011. Distributions of runoff, sea-ice melt and brine using $\delta^{18}O$ and salinity data - a new view on freshwater cycling in Hudson Bay. Journal of Marine Systems 88, 362–374.

Grimm, K.I., 1994. Paläoökologie, Paläogeographie und Stratigraphie im Mainzer Becken, im Oberrheingraben, in der Hessischen Senke und in der Leipziger Bucht während des Mittleren Rupeltons (Fischschiefer/Rupelium/Unteroligozän). Mitteilungen Pollichia 81, 7–193.

Grimm, K.I., 1998. Correlation of Rupelian coastal and basin facies in the Mainz Basin (Oligocene, Germany). Neues Jahrbuch für Geologie und Paläontologie Monatshefte 3, 146–156.

Grimm, K.I., 2006. Meeresverbindungen im Rupelium Mitteleuropas – Paläobiogeographische Untersuchungen anhand von Foraminiferen. Geologisches Jahrbuch Hessen 133, 19–27.

Grimm, K.I., Grimm, M.C., Schindler, T., 2000. Lithostratigraphische Gliederung im Rupelium/Chattium des Mainzer Beckens, Deutschland. Neues Jahrbuch für Geologie und Paläontologie Abhandlungen 218, 343–397.

Grimm, K.I., Uffenorde, H., 2010. Erster Nachweis von *Miogypsina*, einer Großforaminifere aus der Kassel-Formation (Ober-Oligozän, Nordhessen). Geoloighes Jahrbuch Hesse 136, 59–64.

Grimm, K.I., Grimm, M., Radtke, G., Kadolsky, D., Schäfer, P., Franzen, J.L., Schindler, T., Hottenrott Martin, 2011. Mainzer Becken. In: Deutsche Stratigraphische Kommission (Eds.), Stratigraphie von Deutschland IX. Tertiär, Teil 1. SDGG 75, 133–209.

Grossman, E.L., Ku, T.-L., 1986. Oxygen and carbon isotope fractionation in biogenic aragonite: temperature effects. Chemical Geology: Isotope Geoscience Section 59, 59–74.

Hanewinkel, M., Cullmann, D. A., Schelhaas, M.-J., Nabuurs, G.-J., Zimmermann, N.E., 2012. Climate change may cause severe loss in the economic value of European forest land. Nature Climate Change 3, 203–207.

Hansen, B., Østerhus, S., Quadfasel, D., Turrell, W., 2004. Already the day after tomorrow? Science 305, 953–954.

Hansen, J., Sato, M., Kharecha, P., Beerling, D., Berner, R., Masson-Delmotte, V., Pagani, M., Raymo, M., Royer, D.L., Zachos, J.C., 2008. Target atmospheric CO_2: where should humanity aim? The Open Atmospheric Science Journal 2, 217–231.

Hansen, J., Ruedy, R., Sato, M., Lo, K., 2010. Global surface temperature change. Review of Geophysics 48, RG4004.

Haq, B.U., Hardenbol, J., Vail, P.R., 1988. Mesozoic and Cenozoic chronostratigraphy and cycles of sea-level change, in: Wilgus, C.K., Hasting, B.S., Posamentier, H., Van Wagoner, J., Ross, C.K., Kendall, C.G.S.C. (Eds.), Sea-Level Changes. Society of Economic Paleontologists and Mineralogists (SEPM) Special Publication 42, 71–108.

Héran, M.-A., Lécuyer, C., Legendre, S., 2010. Cenozoic long-term terrestrial climatic evolution in Germany tracked by $\delta^{18}O$ of rodent tooth phosphate. Palaeogeography, Palaeoclimatology, Palaeoecology 285, 331–342.

Hart, S.R., 1998. Clams as recorders of ocean ridge volcanism and hydrothermal vent field activity. Science 280, 883–886.

Holland, H.A., Schone, B.R., Lipowsky, C., Esper, J., 2014. Decadal climate variability of the North Sea during the last millennium reconstructed from bivalve shells (*Arctica islandica*). The Holocene 24, 771–786.

Huber, M., Nof, D., 2006. The ocean circulation in the Southern Hemisphere and its climatic impacts in the Eocene. Palaeogeography, Palaeoclimatology, Palaeoecology 231, 9–28.

Hurrell, J.W., 1995. Decadal trends in the North Atlantic Oscillation: regional temperatures and precipitation. Science 269, 676–9.

Hurrell, J.W., Deser, C., 2009. North Atlantic climate variability: the role of the North Atlantic Oscillation. Journal of Marine Systems 78, 28–41.

Huyghe, D., Lartaud, F., Emmanuel, L., Merle, D., Renard, M., 2015. Palaeogene climate evolution in the Paris Basin from oxygen stable isotope ($\delta^{18}O$) compositions of marine molluscs. Journal of the Geological Society 172, 576–587.

Ivany, L.C., Patterson, W.P., Lohmann, K.C., 2000. Cooler winters as a possible cause of mass extinctions at the Eocene/Oligocene boundary. Nature 407, 887–890.

Ivany, L.C., Brey, T., Huber, M., Buick, D.P., Schöne, B.R., 2011. El Niño in the Eocene greenhouse recorded by fossil bivalves and wood from Antarctica. Geophysical Research Letters 38, L16709.

Jones, D.S., Thompson, I., Ambrose, W., 1978. Age and growth rate determinations for the Atlantic surf clam *Spisula solidissima* (Bivalvia: Mactracea), based on internal growth lines in shell cross-sections. Marine Biology 47, 63–70.

Kennett, J.P., Burns, R.E., Andrews, J.E., Churkin, M. jr, Davies, T.A., Dumitrica, P., Edwards, A.R., Galehouse, J.S., Packham, G.H., van der Lingen, G.J., 1972. Australian-Antarctic continental drift, palaeocirculation changes and Oligocene deep-sea erosion. Nature Physical Science 239, 51–55.

Kim, W.S., Huh, H.T., Lee, J.H., Rumohr, H., Koh, C.H., 1999. Endogenous circatidal rhythm in the Manila clam *Ruditapes philippinarum* (Bivalvia: Veneridae). Marine Biology 134, 107–112.

Klein, R.T., Lohmann, K.C., Thayer, C.W., 1996. Bivalve skeletons record sea-surface temperature and $\delta^{18}O$ via Mg/Ca and $^{18}O/^{16}O$ ratios. Geology 24, 415.

Kocsis, L., Ozsvart, P., Becker, D., Ziegler, R., Scherler, L., Codrea, V., 2014. Orogeny forced terrestrial climate variation during the late Eocene-early Oligocene in Europe. Geology 42, 727–730.

Kohn, M.J., 1996. Predicting animal $\delta^{18}O$: accounting for diet and physiological adaptation. Geochimica et Cosmochimica Acta 60, 4811–4829.

Kuhlemann, J., 2007. Paleogeographic and paleotopographic evolution of the Swiss and Eastern Alps since the Oligocene. Global and Planetary Change 58, 224–236.

Lagabrielle, Y., Goddéris, Y., Donnadieu, Y., Malavieille, J., Suarez, M., 2009. The tectonic history of Drake Passage and its possible impacts on global climate. Earth and Planetary Science Letters 279, 197–211.

Lazareth, C.E., Lasne, G., Ortlieb, L., 2006. Growth anomalies in *Protothaca thaca* (Mollusca, Veneridae) shells as markers of ENSO conditions. Climate Research 30, 263–269.

Lear, C.H., Elderfield, H., Wilson, P. A, 2000. Cenozoic deep-sea temperatures and global ice volumes from Mg/Ca in benthic foraminiferal calcite. Science 287, 269–272.

Lear, C.H., Rosenthal, Y., Coxall, H.K., Wilson, P.A., 2004. Late Eocene to early Miocene ice sheet dynamics and the global carbon cycle. Paleoceanography 19, 1–11.

Lear, C.H., Bailey, T.R., Pearson, P.N., Coxall, H.K., Rosenthal, Y., 2008. Cooling and ice growth across the Eocene-Oligocene transition. Geology 36, 251.

Lécuyer, C., Hutzler, A., Amiot, R., Daux, V., Grosheny, D., Otero, O., Martineau, F., Fourel, F., Balter, V., Reynard, B., 2012. Carbon and oxygen isotope fractionations between aragonite and calcite of shells from modern molluscs. Chemical Geology 332-333, 92–101.

Liehr, G.A., Zettler, M.L., Leipe, T., Witt, G., 2005. The ocean quahog *Arctica islandica* L.: a bioindicator for contaminated sediments. Marine Biology 147, 671–679.

Liu, Z., Pagani, M., Zinniker, D., DeConto, R., Huber, M., Brinkhuis, H., Shah, S.R., Leckie, R.M., Pearson, A., 2009. Global cooling during the Eocene-Oligocene climate transition. Science 323, 1187–1190.

Livermore, R., Hillenbrand, C.-D., Meredith, M., Eagles, G., 2007. Drake Passage and Cenozoic climate: an open and shut case? Geochemistry, Geophysics, Geosystems 8, Q01005.

Lorrain, A., Gillikin, D.P., Paulet, Y.M., Chauvaud, L., Le Mercier, A., Navez, J., André, L., 2005. Strong kinetic effects on Sr/Ca ratios in the calcitic bivalve *Pecten maximus*. Geology 33, 965–968.

Marshall, J., Kushnir, Y., Battisti, D., Chang, P., Czaja, A., Dickson, R., Hurrell, J.W., McCartney, M., Saravanan, R., Visbeck, M., 2001. North Atlantic climate variability: phenomena, impacts and mechanisms. Internation Journal of Climatology 21, 1863–1898.

Martini, E., 1982. Bestandsaufnahme des Nannoplankton im "prä-aquitanen" Tertiär des Mainzer Beckens. Mainzer geowissenschaftliche Mitteilungen 10, 29–36.

Masson-Delmotte, V.M., Schulz, M., et al., 2013. Information from paleoclimate archives. In: Stocker, T.F., Qin, D., et al (Eds.), Climate Change 2013: The Physical Science Basis. Contribution of Working Group I to the Fifth Assessment Report of the Intergovernmental Panel on Climate Change. Cambridge University Press, Cambridge, United Kingdom and New York, NY, USA, pp. 383-464.

Meinshausen, M., Smith, S.J., Calvin, K., Daniel, J.S., Kainuma, M.L.T., Lamarque, J., Matsumoto, K., Montzka, S.A., Raper, S.C.B., Riahi, K., Thomson, A., Velders, G.J.M., van Vuuren, D.P.P., 2011. The RCP greenhouse gas concentrations and their extensions from 1765 to 2300. Climatic Change 109, 213–241.

Miller, K.G., Wright, J.D., Fairbanks, R.G., 1991. Unlocking the ice house: Oligocene-Miocene oxygen isotopes, eustasy, and margin erosion. Journal of Geophysical Research: Solid Earth 96, 6829–6848.

Moran, K., Backman, J., et al., 2006. The Cenozoic palaeoenvironment of the Arctic Ocean. Nature 441, 601–605.

Mosbrugger, V., Utescher, T., Dilcher, D.L., 2005. Cenozoic continental climatic evolution of Central Europe. Proceedings of the National Academy of Sciences 102, 14964–14969.

Mook, W.G., Vogel, J.C., 1968. Isotopic equilibrium between shells and their environment. Science 159, 874–875.

Müller, A., 1996. Die Ichthyofauna des Oberoligozäns der Hessischen Senke (Raum Kassel, Deutschland). Leipziger Geowissenschaften 2, 31–115.

Nielsen, J.K., Helama, S., Schöne, B., 2008. Shell growth history of geoduck clam (*Panopea abrupta*) in Parry Passage, British Columbia, Canada: temporal variation in annuli and the Pacific Decadal Oscillation. Journal of Oceanography 64, 951–960.

Norris, R.D., Wilson, P.A., et al., 2014. Expedition 342 summary. In: Norris, R.D., Wilson, P.A., Blum, P., and the Expedition 342 Scientists, Proceedings of the Integrated Ocean Drilling Program (IODP) 342, 1–149.

Ottersen, G., Planque, B., Belgrano, A., Post, E., Reid, P., Stenseth, N., 2001. Ecological effects of the North Atlantic Oscillation. Oecologia 128, 1–14.

Pagani, M., Zachos, J.C., Freeman, K.H., Tipple, B., Bohaty, S., 2005. Marked decline in atmospheric carbon dioxide concentrations during the Paleogene. Science 309, 600–603.

Peharda, M., Crnčević, M., Bušelić, I., Richardson, C.A., Ezgeta-Balić, D., 2012. Growth and longevity of *Glycymeris nummaria* (Linnaeus, 1758) from the Eastern Adriatic, Croatia. Journal of Shellfish Research 31, 947–950.

Pekar, S.F., Christie-Blick, N., Kominz, M. a., Miller, K.G., 2002. Calibration between eustatic estimates from backstripping and oxygen isotopic records for the Oligocene. Geology 30, 903–906.

Pharisat, A., Micklich, N., 1998. Oligocene fishes in the western Paratethys of the Rhine Valley Rift System. Italian Journal of Zoology 65, 163–168.

Picot, L., 2002. Le Paléogène des synclinaux du Jura et de la bordure sud-rhénane: paléontologie (Ostracodes), paléoécologie, biostratigraphie, paléogéographie. Geofocus 5, 1–240.

Pross, J., Bruch, A., Kvaček, Z., 1998. Paläoklima-Rekonstruktionen für den Mittleren Rupelton (Unter-Oligozän) des Mainzer Beckens auf der Basis mikro-und makrobotanischer Befunde. Mainzer geowissenschaftliche Mitteilungen 27, 79–92.

Pross, J., Bruch, A., Mosbrugger, V., Kvacek, Z., 2000. Paleogene pollen and spores as a tool for quantitative paleoclimate reconstructions: the Rupelian (Oligocene) of Central Europe. Proceedings of the Ninth International Palynological Congress, Texas, USA, 1996, 23–28 June 1996, American Association of Stratigraphic Palynologists Foundation, pp. 299–310.

Pross, J., Schmiedl, G., 2002. Early Oligocene dinoflagellate cysts from the Upper Rhine Graben (SW Germany): paleoenvironmental and paleoclimatic implications. Marine Micropaleontology 45, 1–24.

Ramsay, K., Kaiser, M., Richardson, C., Veale, L., Brand, A., 2000. Can shell scars on dog cockles (*Glycymeris glycymeris* L.) be used as an indicator of fishing disturbance? Journal of Sea Research 43, 167–176.

Raymo, M.E., Ruddiman, W.F., 1992. Tectonic forcing of late Cenozoic climate. Nature 359, 117–122.

Reynolds, D.J., Butler, P.G., Williams, S.M., Scourse, J.D., Richardson, C.A., Wanamaker Jr., A.D., Austin, W.E.N., Cage, A.G., Sayer, M.D.J., 2013. A multiproxy reconstruction of Hebridean (NW Scotland) spring sea surface temperatures between AD 1805 and 2010. Palaeogeography, Palaeoclimatology, Palaeoecology 386, 275–285.

Richardson, C.A., Crisp, D.J., Runham, D.W., 1979. Tidally deposited growth bands in the shell of the common cockle, *Cerastoderma edule* (L.). Malacologia 18, 277–290.

Ritzkowski, S., 1967. Mittel-Oligozän, Ober-Oligozän und die Grenze Rupel/Chatt im nördlichen Hessen. Neues Jahrbuch für Geologie und Paläontologie Abhandlungen 127, 293–336.

Ritzkowski, S., 2005. Das Tertiär der Hessischen Senke in der Stratigraphischen Tabelle von Deutschland 2002. Newsletters on Stratigraphie 41, 339–346.

Ritzkowski, S., Grimm, M.C., Hottenrott, M., 2011. Niederhessische Tertiärsenke. In: Deutsche Stratigraphische Kommission (Eds.), Stratigraphie von Deutschland IX. Tertiär, Teil 1. SDGG 75, pp. 303–375.

Rögl, F., 1999. Mediterranean and Paratethys. Facts and hypotheses of an Oligocene to Miocene paleogeography (short overview). Geologica Carpathica 50, 339–349.

Royer, C., Thébault, J., Chauvaud, L., Olivier, F., 2013. Structural analysis and paleoenvironmental potential of dog cockle shells (*Glycymeris glycymeris*) in Brittany, northwest France. Palaeogeography, Palaeoclimatology, Palaeoecology 373, 123–132.

Scaife, A.A., Kucharski, F., et al., 2009. The CLIVAR C20C project: selected twentieth century climate events. Climate Dynamics 33, 603–614.

Scher, H.D., Martin, E.E., 2008. Oligocene deep water export from the North Atlantic and the development of the Antarctic Circumpolar Current examined with neodymium isotopes. Paleoceanography 23, PA1205.

Schettler, G., Pearce, N.J.G., 1996. Metal pollution recorded in extinct *Dreissena polymorpha* communities, Lake Breitling, Havel Lakes system, Germany: a laser ablation inductively coupled plasma mass spectrometry study. Hydrobiologia 317, 1–11.

Schmidt, G.A., Bigg, G.R., Rohling, E.J., 1999. "Global Seawater Oxygen-18 Database - v1.21" http://data.giss.nasa.gov/o18data/. (Checked at: 30.04.2016)

Schöne, B.R., 2008. The curse of physiology - challenges and opportunities in the interpretation of geochemical data from mollusk shells. Geo-Marine Letters 28, 269–285.

Schöne, B.R., Tanabe, K., Dettman, D.L., Sato, S., 2003. Environmental controls on shell growth rates and $\delta^{18}O$ of the shallow-marine bivalve mollusk *Phacosoma japonicum* in Japan. Marine Biology 142, 473–485.

Schöne, B.R., Freyre Castro, A.D., Fiebig, J., Houk, S.D., Oschmann, W., Kröncke, I., 2004. Sea surface water temperatures over the period 1884–1983 reconstructed from oxygen isotope ratios of a bivalve mollusk shell (*Arctica islandica*, southern North Sea). Palaeogeography, Palaeoclimatology, Palaeoecology 212, 215–232.

Schöne, B.R., Houk, S.D., Freyre Castro, a. D., Fiebig, J., Oschmann, W., Kroncke, I., Dreyer, W., Gosselck, F., 2005a. Daily growth rates in shells of *Arctica islandica*: assessing sub-seasonal environmental controls on a long-lived bivalve mollusk. Palaios 20, 78–92.

Schöne, B.R., Giere, O., 2005b. Growth increments and stable isotope variation in shells of the deep-sea hydrothermal vent bivalve mollusk *Bathymodiolus brevior* from the North Fiji Basin, Pacific Ocean. Deep-Sea Research Part I: Oceanographic Research Papers 52, 1896–1910.

Schöne, B.R., Fiebig, J., Pfeiffer, M., Gleβ, R., Hickson, J., Johnson, A.L.A., Dreyer, W., Oschmann, W., 2005c. Climate records from a bivalved Methuselah (*Arctica islandica*, Mollusca; Iceland). Palaeogeography, Palaeoclimatology, Palaeoecology 228, 130–148.

Schöne, B.R., Radermacher, P., Zhang, Z., Jacob, D.E., 2013. Crystal fabrics and element impurities (Sr/Ca, Mg/Ca, and Ba/Ca) in shells of *Arctica islandica* - implications for paleoclimate reconstructions. Palaeogeography, Palaeoclimatology, Palaeoecology 373, 50–59.

Serreze, M.C., Barry, R.G., 2011. Processes and impacts of Arctic amplification: a research synthesis. Global and Planetary Change 77, 85–96.

Shackleton, N.J., Kennett, J.P., 1975. Paleotemperature history of the Cenozoic and the initiation of Antarctic glaciation: oxygen and carbon isotope analyses in DSDP Sites 277, 279 and 281. In: Kennett, J. P., Houtz, R. E., et al., (Eds.) Initial reports of the deep sea drilling project, 29, U.S. Government Printing Office, pp. 743–755.

Sissingh, W., 1997. Tectonostratigraphy of the North Alpine Foreland Basin: correlation of Tertiary depositional cycles and orogenic phases. Tectonophysics 282, 223–256.

Sissingh, W., 2003. Tertiary paleogeographic and tectonostratigraphic evolution of the Rhenish Triple Junction. Palaeogeography, Palaeoclimatology, Palaeoecology 196, 229–263.

Śliwińska, K.K., Clausen, O.R., Heilmann-Clausen, C., 2010. A mid-Oligocene cooling (Oi-2b) reflected in the dinoflagellate record and in depositional sequence architecture. An integrated study from the eastern North Sea Basin. Marine and Petroleum Geology 27, 1424–1430.

Stenni, B., Nichetto, P., Bregant, D., Scarazzato, P., Longinelli, A., 1995. The $\delta^{18}O$ signal of the northward flow of Mediterranean waters in the Adriatic Sea. Oceanologica Acta 18, 319–328.

Stenseth, N.C., Mysterud, A., Ottersen, G., Hurrell, J.W., Chan, K.-S., Lima, M., 2002. Ecological effects of climate fluctuations. Science 297, 1292–6.

Steuber, T., 1996. Stable isotope sclerochronology of rudist bivalves: growth rates and Late Cretaceous seasonality. Geology 24, 315.

Stocker, T.F., Qin, D., et al., 2013: Technical summary. In: Stocker, T.F., Qin, D., et al (Eds.), Climate Change 2013: The Physical Science Basis. Contribution of Working Group I to the Fifth Assessment Report of the Intergovernmental Panel on Climate Change. Cambridge University Press, Cambridge, United Kingdom and New York, NY, USA, pp. 33-115.

Strom, A., Francis, R.C., Mantua, N.J., Miles, E.L., Peterson, D.L., 2005. Preserving low-frequency climate signals in growth records of geoduck clams (*Panopea abrupta*). Palaeogeography, Palaeoclimatology, Palaeoecology 228, 167–178.

Sturm, C., Zhang, Q., Noone, D., 2010. An introduction to stable water isotopes in climate models: benefits of forward proxy modelling for paleoclimatology. Climate of the Past 5, 115–129.

Surge, D., Lohmann, K.C., Dettman, D.L., 2001. Controls on isotopic chemistry of the American oyster, *Crassostrea virginica*: implications for growth patterns. Palaeogeography, Palaeoclimatology, Palaeoecology 172, 283–296.

Surge, D., Walker, K.J., 2006. Geochemical variation in microstructural shell layers of the southern quahog (*Mercenaria campechiensis*): implications for reconstructing seasonality. Palaeogeography, Palaeoclimatology, Palaeoecology 237, 182–190.

Takesue, R.K., van Geen, A., 2004. Mg/Ca, Sr/Ca, and stable isotopes in modern and Holocene *Protothaca staminea* shells from a northern California coastal upwelling region. Geochimica et Cosmochimica Acta 68, 3845–3861.

Thewissen, J.G.M., Cooper, L.N., Clementz, M.T., Bajpai, S., Tiwari, B.N., 2007. Whales originated from aquatic artiodactyls in the Eocene epoch of India. Nature 450, 1190–4.

Thompson, I., Jones, D.S., Dreibelbis, D., 1980. Annual internal growth banding and life history of the ocean quahog *Arctica islandica* (Mollusca: Bivalvia). Marine Biology 57, 25–34.

Tollefson, J., 2016. 2015 breaks heat record. Nature 529, 450.

Tütken, T., 2003. Die Bedeutung der Knochenfrühdiagenese für die Erhaltungsfähigkeit in vivo erworbener Element- und Isotopenzusammensetzungen in fossilen Knochen. Doctoral thesis, Eberhard-Karls-Universität Tübingen, pp. 331.

Tütken, T., Absolon, J., 2015. Late Oligocene ambient temperatures reconstructed by stable isotope analysis of terrestrial and aquatic vertebrate fossils of Enspel, Germany. Palaeobiodiversity and Palaeoenvironments 95, 17–31.

Uhl, D., Herrmann, M., 2010. Palaeoclimate estimates for the Late Oligocene taphoflora of Enspel (Westerwald, West Germany) based on palaeobotanical proxies. Palaeobiodiversity and Palaeoenvironments 90, 39–47.

Utescher, T., Bondarenko, O.V., Mosbrugger, V., 2015. The Cenozoic cooling - continental signals from the Atlantic and Pacific side of Eurasia. Earth and Planetary Science Letters 415, 121–133.

Van Simaeys, S., Brinkhuis, H., Pross, J., Williams, G.L., Zachos, J.C., 2005. Arctic dinoflagellate migrations mark the strongest Oligocene glaciations. Geology 33, 709–712.

von Bertalanffy, L., 1938. A quantitative theory of organic growth. Human Biology 10, 181–213.

von der Heydt, A., Dijkstra, H.A., 2006. Effect of ocean gateways on the global ocean circulation in the late Oligocene and early Miocene. Paleoceanography 21, 1–18.

Xin, X.-G., Zhou, T.-J., Yu, R.-C., 2008. The Arctic Oscillation in coupled climate models. Chinese Journal of Geophysics 51, 223–239.

Wanink, J.H., Zwarts, L., 1993. Environmental effects of the growth rate of intertidal invertebrates and some implications for foraging waders. Netherlands Journal of Sea Research 31, 407–418.

Watanabe, O., Kamiyama, K., Motoyama, H., Fujii, Y., Shoji, H., Satow, K., 1999. The paleoclimate record in the ice core at Dome Fuji station, East Antarctica. Annals of Glaciology 29, 176–178.

Williams, D.F., Arthur, M.A., Jones, D.S., Healy-Williams, N., 1982. Seasonality and mean annual sea surface temperatures from isotopic and sclerochronological records. Nature 296, 432–434.

Witbaard, R., Franken, R., Visser, B., 1997. Growth of juvenile *Arctica islandica* under experimental conditions. Helgoländer Meeresuntersuchungen 51, 417–431.

Witbaard, R., Duineveld, G.C.A, de Wilde, P.A.W.J., 1999. Geographical differences in growth rates of *Arctica islandica* (Mollusc: Bivalvia) from the North Sea and adjacent waters. Journal of the Marine Biological Association in the United Kingdom 79, 907–915.

Zachos, J.C., Dickens, G.R., Zeebe, R.E., 2008. An early Cenozoic perspective on greenhouse warming and carbon-cycle dynamics. Nature 451, 279–283.

Zachos, J.C., Pagani, M., Sloan, L., Thomas, E., Billups, K., 2001. Trends, rhythms, and aberrations in global climate 65 Ma to present. Science (New York, N.Y.) 292, 686–693.

CHAPTER 2 MANUSCRIPTS

MANUSCRIPT I

The bivalve *Glycymeris planicostalis* as a high-resolution paleoclimate archive for the Rupelian (Early Oligocene) of central Europe

Published in Climate of the Past

E. O. Walliser[1], B. R. Schöne[1], T. Tütken[1], J. Zirkel[1,*], K. I. Grimm[1] and J. Pross[2]

[1] Institute of Geosciences, University of Mainz, Johann-Joachim-Becher-Weg 21, 55128 Mainz, Germany

[2] Paleoenvironmental Dynamics Group, Institute of Earth Sciences, University of Heidelberg, Im Neuenheimer Feld 234, 69120 Heidelberg, Germany

* now at: Institute of Geosciences, University of Frankfurt, Altenhöferallee 1, 60438 Frankfurt am Main, Germany

Contribution:

Concept: EOW, BRS

Writing: EOW, BRS

Oxygen isotope analysis EOW (bivalves), TT and JZ (sirenian)

Stratigraphy and regional geology: EOW, KG, JP, BRS

Walliser, E. O., Schöne, B. R., Tütken, T., Zirkel, J., and Pross, J., 2015. The bivalve *Glycymeris planicostalis* as a high-resolution paleoclimate archive for the Rupelian (Early Oligocene) of central Europe. Climate of the Past, 11, 653-668.

Abstract

Current global warming is likely to result in a unipolar glaciated world with unpredictable repercussions on atmospheric and oceanic circulation patterns. These changes are expected to affect seasonal extremes and the year-to-year variability of seasonality. To better constrain the mode and tempo of the anticipated changes, climatologists require ultra-high-resolution proxy data of time intervals in the past, e.g. the Oligocene, during which boundary conditions were similar to those predicted for the near future. In the present paper, we assess if such information can be obtained from shells of the long-lived bivalve mollusk *Glycymeris planicostalis* from the late Rupelian of the Mainz Basin, Germany. Our results indicate that the studied shells are pristinely preserved and provide an excellent archive to reconstruct changes of sea surface temperature on seasonal to inter-annual time scales. Shells of *G. planicostalis* grew uninterruptedly during winter and summer and therefore recorded the full seasonal temperature amplitude that prevailed in the Mainz Basin ~30 Ma ago. Absolute sea surface temperature data were reconstructed from $\delta^{18}O_{shell}$ values assuming a $\delta^{18}O_{water}$ signature that was extrapolated from coeval sirenian tooth enamel. Reconstructed values range between 12.3 °C and 22.0 °C and agree well with previous estimates based on planktonic foraminifera and shark teeth. However, temperatures during seasonal extremes vary greatly on inter-annual time scales. Mathematically re-sampled (i.e., corrected for uneven number of samples per annual increment) winter and summer temperatures averaged over 40 annual increments of three specimens equal 13.6 ± 0.8 °C and 17.3 ± 1.2 °C, respectively. Such high-resolution paleoclimate information can be highly relevant for numerical climate studies aiming to predict possible future climates in a unipolar glaciated or, ultimately, polar ice-free world.

1. Introduction

Current CO_2-induced global warming is likely to result in a unipolar glaciated world ultimately followed by one without polar ice caps (e.g. Raper and Braithwaite, 2006). In light of these predicted boundary conditions, climate is expected to change profoundly, particularly at higher latitudes. According to numerical climate models, reduced meridional gradients will lead to substantial changes in atmospheric and oceanic circulation patterns (e.g., Cai & Chu, 1998; Hansen et al., 2004), thereby affecting seasonality as well as the frequency and intensity of decadal climate oscillations (e.g. Marshall et al., 2001; Solomon et al., 2007). In turn, this will alter surface temperature patterns, storm intensities and precipitation rates (Hurrell, 1995; Dai et al., 1997; Barbosa, 2009), all of which present a major challenge to densely populated coastal areas and coastal ecosystems, particularly in Europe (Ottersen et al., 2001; Stenseth et al., 2002).

To date, the mode and tempo of the environmental change anticipated for the near future have remained poorly constrained (e.g., Vellinga and Wood, 2002; Hátún et al., 2005). This applies specifically to time scales of human perception, i.e., seasonal extremes and inter-annual variability. A promising avenue toward a better understanding of future climates is to investigate the short-term climate variability of time intervals in the past during which boundary conditions were similar to those predicted for the coming millennia. The last time a unipolar glaciated world occurred in Earth history was during the early Oligocene when atmospheric CO_2 levels were slightly higher than today (Zachos et al., 2008) and the paleogeographic configuration on a global scale was at least broadly similar to the present-day situation (Lefebvre et al., 2013). Thus, the Oligocene world can serve as a natural laboratory for studying the possible effects of anthropogenic global warming. As yet, however, the Oligocene has remained a relatively poorly studied epoch of Earth history, which is at least partially attributed to the stratigraphic incompleteness of many Oligocene successions. In particular, shallow-water sequences of Oligocene age are often compromised by unconformities resulting from strong, glacially induced eustatic sea-level fluctuations (e.g., Miller et al., 2005; Pälike et al., 2006).

The epicontinental sedimentary archives from the Oligocene of Central Europe, notably the Rhenish triple junction system (e.g., Sissingh, 2003), can play a prime role in elucidating the short-term (i.e., seasonal to inter-annual) climate dynamics during that time. The significance of Oligocene sediments from the Rhenish triple junction system was first stressed by Beyrich (1854),

whose work on strata from the Mainz and Kassel Basins ultimately led to the coinage of the term "Oligocene". These shallow marine successions exhibit much higher sedimentation rates and generally contain more macrofossils than their open marine counterparts. Moreover, the shallow water depth and the low water-mass inertia as compared to the open ocean make them particularly sensitive to short-term paleoclimatic and paleoceanographic change. Furthermore, these strata contain well-preserved shells of long-lived bivalves (*Glycymeris planicostalis*, Lamarck 1819). Modern *Glycymeris* spp. have recently been identified as promising tools for ultra-high-resolution climate reconstructions (Brocas et al., 2013; Royer et al., 2013; Bušelić et al., 2014). This genus occurs worldwide in subtidal settings and lives infaunally in sandy and gravelly sediments (Ansell and Trueman, 1967; Thomas, 1978). Their fossil history dates back to the Aptian (Gillet, 1924; Casey, 1961) and despite some evolutionary innovations acquired during the early Cenozoic, their fundamental bauplan has remained largely unvaried until today (Thomas, 1975).

Bivalve shells serve as reliable recorders of ambient environmental conditions (e.g., Wanamaker et al., 2011). The production of shell material occurs on a periodic basis resulting in the formation of distinct growth lines that separate the growth pattern into time slices of equal duration, so-called growth increments. These growth patterns serve as a calendar which can be used to place each shell portion and each geochemical data point in a precise temporal context. Some bivalve species live for decades to several centuries and can therefore provide uninterrupted records of seasonality such as the genera *Glycymeris* (Ramsay et al., 2000; Brocas et al., 2013), *Arctica* (e.g. Ropes, 1985; Butler et al., 2013) and *Panopea* (e.g., Strom et al., 2004; Black et al., 2008).

In the present study, we have analyzed the ontogenetically young shell portions of three *G. planicostalis* specimens from the upper Rupelian of the Mainz Basin, SW Germany, with regard to their oxygen isotopic composition in order to assess their potential as 'deep-time' archives of paleoseasonality. Such data are currently not available. In particular, we focused on elucidating (i) whether the shells are sufficiently well preserved to permit reconstruction of water temperatures from shell oxygen isotope data; (ii) what the timing and rate of seasonal shell growth of these specimens were; and (iii) how the seasonal $\delta^{18}O_{shell}$-derived water temperatures compare to existing temperature proxy data from that region. In order to assess the oxygen isotope composition of the local seawater ($\delta^{18}O_{water}$) in the Mainz Basin during the Rupelian we measured the phosphate

oxygen isotope composition ($\delta^{18}O_{PO4}$) of the enamel of seven teeth of the sea cow *Halitherium schinzii* from the same formation as the *G. planicostalis* shells. The $\delta^{18}O_{PO4}$ value has been successfully exploited as a $\delta^{18}O_{water}$ proxy by many authors (e.g. Clementz and Koch, 2001; Clementz et al., 2006; Thewissen et al., 2007; Clementz and Sewall, 2009). Hence, this study lays the groundwork for future ultra-high resolution paleoclimate reconstructions for the Oligocene.

2. Material and methods

2.1. Study area

The Mainz Basin is located near the northwestern margin of the Upper Rhine Graben. Its formation dates back to the middle Eocene and is related to the taphrogenesis of the European Cenozoic rift system (Dèzes et al., 2004; Ritzkowski, 2005; Grimm et al., 2011) (Fig. 1). Its sedimentary succession, which was mainly deposited in shallow marine and brackish settings, covers a time interval of ca. 20 Ma, from the Lutetian (~49.5 Ma) to the early Burdigalian (~18.5 Ma). During the late Rupelian (i.e., late Early Oligocene; 34.9 - 28.4 Ma; Gradstein et al., 2004), central Europe experienced a period of extended marine transgressions due to local tectonic subsidence and eustatic sea level rise. As a consequence, the Mainz Basin became part of a marine strait that extended from the paleo-North Sea Basin to the southernmost Upper Rhine Graben (Picot, 2002; Sissingh, 2003; Berger et al., 2005a). A possible southern connection with the western Molasse Basin has been controversially debated (Martini, 1982; Picot, 2002; Berger et al., 2005a, 2005b; Grimm, 2006).

According to Berger et al. (2005b), marine conditions in the Mainz Basin lasted for about 2.5 Ma from the sea-level high stand Ru2/Ru3 (~32 Ma) to Ru3/Ru4 (~29.5 Ma) of Haq et al. (1988). Nearshore deposits representing that time comprise coarse-grained (sand to gravel) siliciclastics of the Alzey Formation (from which the studied fossil material was collected - see below) and the overlaying Stadecken Formation. Contemporaneously deposited basinal sediments (pelites) belong to the Bodenheim Formation (Grimm et al., 2000; Sissingh, 2003; Berger et al., 2005b). Age control for the marine strata of the Mainz Basin is mainly based on calcareous

nanoplankton (Martini and Müller, 1971; Martini, 1982), dinoflagellate cysts (e.g., Pross, 1997), and, to a lesser extent, benthic foraminifera (Grimm, 1998, 2002). With regard to the nanoplankton zonation, the Alzey and Bodenheim Formations comprise the upper part of nanoplankton zone NP23 and the lower part of nanoplankton zone NP24 (Grimm, 1994; Pross and Schmiedl, 2002; Berger et al., 2005b).

Paleoenvironmental reconstructions of the Alzey Formation are based on palynological and faunal data indicating an overall warm climate comparable to modern subtropical climate zones of the Mediterranean (Grimm et al., 2011). Reconstructed mean annual air temperature in the hinterland fluctuated between ~16 and ~17°C, and mean annual precipitation was between 1000 and 1250 mm per year (Pross et al., 1998; Pross et al., 2000). The Mainz Basin experienced repeated alternations between drier and wetter conditions during the deposition of the Alzey Formation, which caused fluctuations in surface water salinity levels (remaining within the range of normal marine conditions) and the episodic formation of water-mass stratifications (Pross 2001; Pross and Schmiedl, 2002). Temperature estimates of the seawater have been derived from the $\delta^{18}O$ values of shark teeth and foraminiferan tests. These estimates yielded values of 6.9 to 23.3 °C for shallow-water settings (Tütken, 2003) and 5.9 to 14.9 °C for bottom waters (maximum depth: 150 m; Grimm, 1994; Grimm et al., 2011).

2.2. Material

The studied shell material was collected by Prof. Jürgen Boy during the 1970s and 1980s and has been stored at the Paleontological collection of the Institute of Geosciences in Mainz. Samples originate from the outcrop 'Trift' near Weinheim, the stratotype of the Alzey Formation (Grimm et al., 2000) (Fig. 1). Additional information about the precise stratigraphic position of the sampled layer is not available. The outcrop is ~8 m thick and ~40 m wide; it consists of fossiliferous middle to coarse sands and fine gravels. Numerical dating with strontium isotope ($^{87}Sr/^{86}Sr$) stratigraphy of a well-preserved bivalve shell from the outcrop yielded an age of 30.1 ± 0.1 Ma (Grimm et al.,

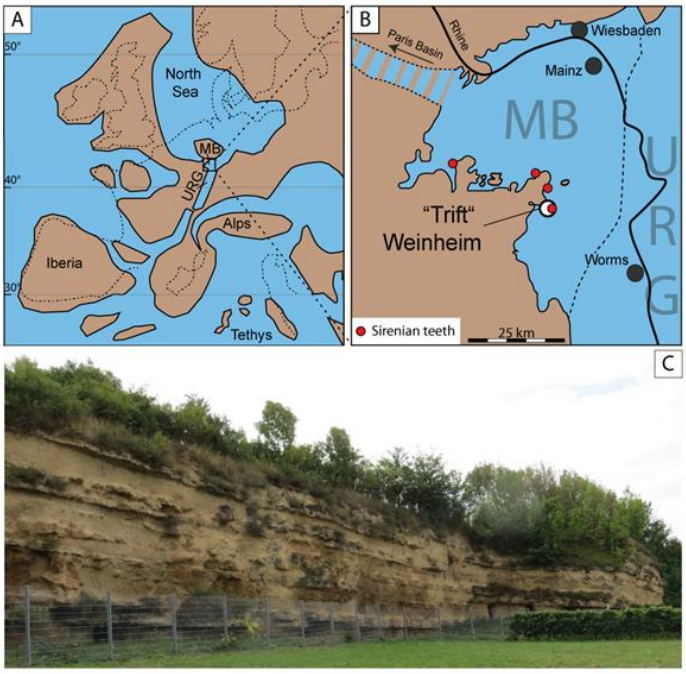

Figure 1. Map showing the paleogeography during the Rupelian stage and the sample locality in the Mainz Basin. (A) Position of the Mainz Basin (MB) in Central Europe. URG = Upper Rhine Graben. Emerged land areas are shown in brown and marine environments in blue. Modified from Spiegel et al. (2007). (B) Sample locality of the shells (outcrop 'Trift' near Weinheim; white dot) and sea cow teeth (red dots). The presence of a western gateway (dashed area) connecting the Mainz Basin to the Paris Basin is unclear. Dashed line denotes the tectonic boundary between the MB and URG. Modified after Grimm et al. (2011). (C) Photograph of the outcrop "Trift" near Weinheim, type locality of the Alzey Formation from which the bivalves were collected.

2003). The outcrop exhibits a highly diverse and fully marine benthic fauna dominated by bivalves, gastropods and scaphopods that dwelled in shallow subtidal waters. Furthermore, corals were found suggesting limited seasonal salinity changes. Water-depth estimates, which are based on sedimentological features (Grimm et al., 2003) and ichnofossils (Schindler et al., 2005), range from ~30 to ~40 m. The sea cow teeth originated from four localities located along the southwestern paleo-coastline of the Mainz Basin (Fig. 1; Table 1), and were stored at the Paleontological collection of the Institute of Geosciences and the collection of the Museum of Natural History Mainz (in german: Landessammlung für Naturkunde Rheinland-Pfalz).

2.3. Methods

From the *Glycymeris planicostalis* specimens collected at the outcrop "Trift", three large valves (~8 cm in height) that visually appeared well-preserved were selected for further investigations. These valves were labeled (MB-Wht-2, MB-Wht-4 and MB-Wht-7), mounted on Plexiglas cubes with GlueTec Multipower plastic welder and coated with WIKO metal epoxy resin to avoid fracture during cross-sectioning. From each valve, two ca. 3 mm-thick slabs were cut perpendicular to the growth lines and along the axis of maximum growth from the umbo to the commissure using a low-speed precision saw (Buehler Isomet 1000; at 200 rpm) equipped with a wafering-thin (0.4 mm),

diamond coated blade. Both shell slabs were glued to glass slides with the mirroring sides facing up, ground on glass plates (320, 800, 1200 grit SiC powder) and polished with 1 µm Al_2O_3 powder. After each preparation step, the samples were ultrasonically rinsed in deionized water.

One polished slab of each specimen was firstly used for diagenetic screening. For this purpose, a set of different methods was employed including cathodoluminescence petrography, Raman spectroscopy and immersion of the shell slabs in Feigl solution. The presence of Mn^{2+} (>10-20 ppm) in calcium carbonates produces an orange cathodoluminescence (Machel et al., 1991) and is typically regarded as an indicator of diagenetic neomorphism (Grossman et al., 1996; Flügel, 2004) because biogenic aragonite is non-cathodoluminescent (Major, 1991). Like modern *Glycymeris* spp., shells of fossil representatives of this genus consisted of aragonite, which is prone to change to calcite during diagenesis. Raman spectroscopy can yield detailed and spatially highly resolved information on the type of polymorphs of $CaCO_3$. Likewise, the Feigl test can distinguish between aragonite and calcite (Feigl, 1958). Feigl solution stains aragonite black and calcite pale grey. After diagenesis screening, the shell slabs were ground and polished again, and prepared for sclerochronological studies and subsequent scanning electron microscopic (SEM) analyses. For this purpose, polished cross-sections were immersed in Mutvei's solution for 40 min under constant stirring at 37 - 40°C (Schöne et al., 2005a). After the staining process, the samples were gently rinsed in deionized water, air-dried and then photographed with a digital camera (Canon EOS 600D) mounted to a binocular microscope (Wild Heerbrugg M8). Growth increments were counted and their width measured with the image processing software Panopea (© Peinl & Schöne). Subsequently, samples were sputter-coated with a 2 nm thick gold layer and viewed under a scanning electron microscope (LOT Quantum Design Phenom Pro, 2nd generation) in order to describe the prevailing microstructures and identify possible neomorphic minerals that may have formed during diagenesis (Fig. 2).

The other polished slab of each specimen was used for the analysis of oxygen isotope values ($\delta^{18}O_{shell}$). Prior to the analysis, the outer ca. 0.5 to 1 mm thick chalky rim of the shell surfaces was physically removed (Fig. 2A-C). Then, 675 individual carbonate powder samples were micromilled from the outer shell layer (ventral margin) of the three specimens (316, 193 and 166 samples from specimens MB-Wht-2, MB-Wht-4 and MB-Wht-7, respectively) using a Rexim Minimo dental drill mounted to a stereomicroscope and equipped with a cylindrical, diamond-coated bit (1 mm

diameter; Komet/Gebr. Brasseler GmbH & Co. KG, model no. 835 104 010). Sampling was performed in the ontogenetically youngest part of the shells. Individual milling steps contoured the shell growth patterns and measured between 100 and 200 µm in width. Carbonate powder samples weighing between 50 and 120 µg were reacted with 100 % phosphoric acid in He-flushed borosilicate exetainers at 72 °C. The resulting CO_2 was measured with a GasBench II-coupled Thermo Finnigan MAT 253 gas source isotope ratio mass spectrometer in continuous flow mode at the Institute of Geosciences of the University of Mainz. Oxygen isotope values are reported in δ-notation and given as parts per mil (‰). Data were calibrated against a NBS-19 calibrated IVA Carrara marble ($\delta^{18}O$ = -1.91 ‰). On average, replicated internal precision (1σ) and accuracy (1σ) were better than 0.05‰, respectively.

If the bivalves formed their shell in oxygen isotopic equilibrium with the ambient water, the $\delta^{18}O_{shell}$ values can provide information on water temperature during growth (Epstein et al., 1953). For aragonitic shells, the paleothermometry equation of Grossman and Ku (1986) with a scale correction of -0.27‰ (see Dettman et al., 1999) is typically employed:

$$T_{\delta^{18}O}(°C) = 20.60 - 4.34 \cdot (\delta^{18}O_{shell} - (\delta^{18}O_{water} - 0.27)) \quad (1)$$

where $\delta^{18}O_{shell}$ is measured relative to VPDB and $\delta^{18}O_{water}$ relative to VSMOW. To compute reliable temperatures from $\delta^{18}O_{shell}$ values also requires knowledge of the $\delta^{18}O_{water}$ value during shell formation. This value was reconstructed from $\delta^{18}O_{PO4}$ values of tooth enamel of sea cows, i.e., homoeothermic marine mammals, from the same stratigraphic level. The average $T_{\delta 18O}$ error was calculated by combining the average precision errors of the mass spectrometric analyses of bivalve shells and sirenian teeth (error propagation method). This resulted in an average $T_{\delta 18O}$ error of ± 0.4 °C. An additional source of uncertainty is represented by the standard deviation of the reconstructed average $\delta^{18}O_{water}$ values (± 0.3 ‰). The integration of both values results in a combined temperature error of ± 1.3 °C.

2.4. Sea cow teeth

The oxygen isotope composition of tooth enamel from marine vertebrates can provide information on the $\delta^{18}O_{water}$ value of ambient seawater (e.g. Lécuyer et al., 1996; Clementz and Koch, 2001;

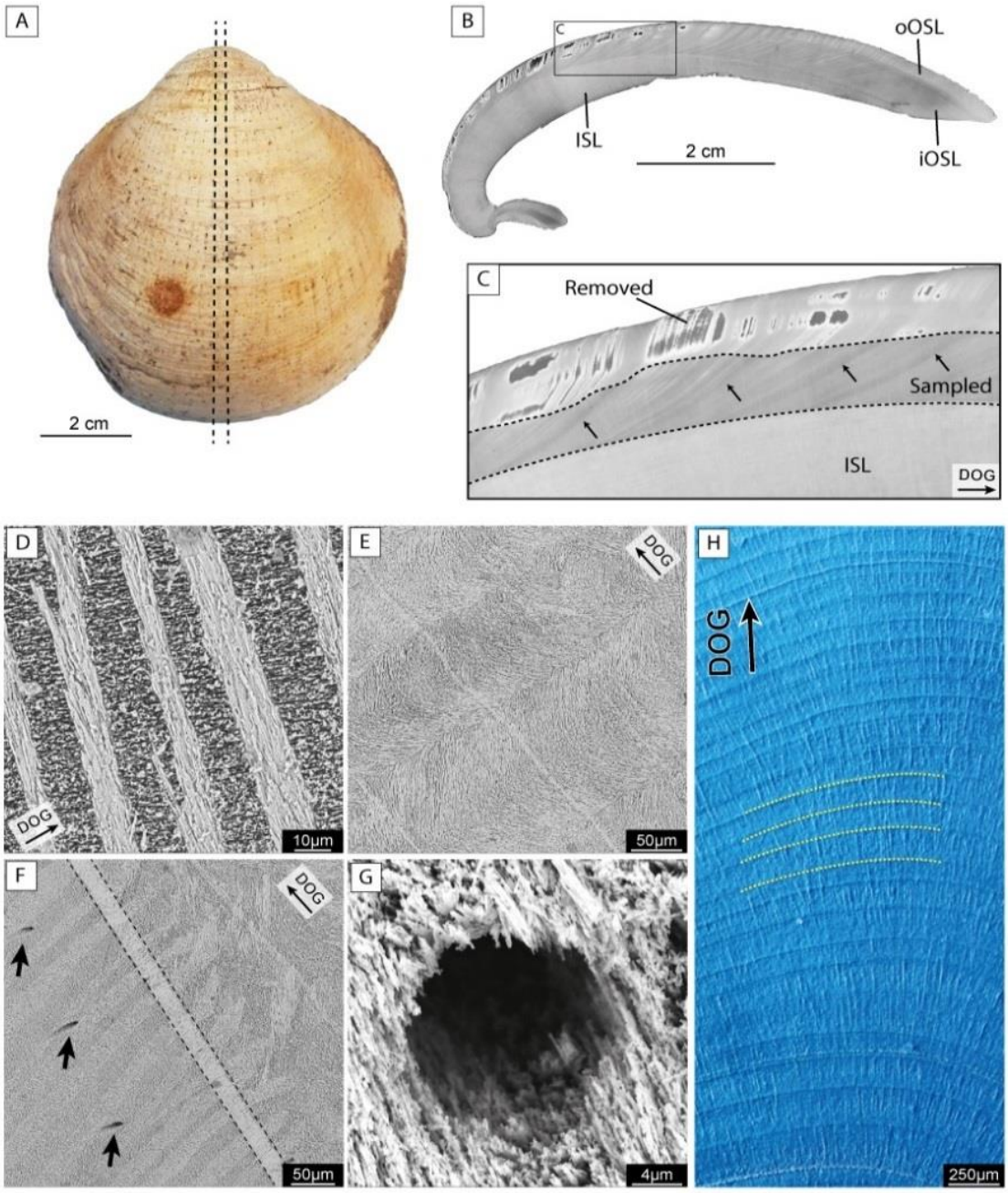

Figure 2. Macroscopic and microscopic views of the studied shell material (*Glycymeris planicostalis*) from the early Oligocene of the Mainz Basin. (A) Left valve. Dotted lines = cutting axis. (B) Outer and inner portions of the outer shell layer (oOSL, iOSL) as well as the inner shell layer (ISL) are clearly visible in the umbo-ventral margin cross-section (dotted line in A) of specimen EOW-MB-Wht-7. (C) Carbonate powder was collected from the outer shell layer after removing the outer chalky shell portions. Arrows point to annual growth lines. (D-G) SEM images show the extraordinary preservation state of the studied shell material. Primary microstructures are still present. (D) Outer crossed-lamellar layer, (E) inner complex crossed-lamellar layer and (F) transition zone between outer and inner shell layer (dotted lines). Arrows point to tubule openings. (G) Detailed view of a tubule. The lack of diagenetic fillings inside the cavity further supports the absence of any significant diagenetic overprint. (H) Distinct growth lines (yellow dotted lines) are visible in the hinge plate of Mutvei-stained cross-sections. DOG=direction of growth.

Clementz et al., 2006; Clementz and Sewall, 2009). Therefore, we measured the phosphate oxygen isotope composition ($\delta^{18}O_{PO4}$) of the enamel from seven sirenian teeth of *Halitherium schinzii* recovered from the deposits of the Alzey Formation.

The surface of the teeth was physically cleaned and then sampled with a hand-held dental drill. Five teeth, which were large enough, were sampled twice, one sample at top and another one at the bottom of the crown. A fraction of each enamel powder sample was then treated with 2 % NaOCl and 0.18 mL of 0.1 molar acetic acid to remove organics and potential diagenetic carbonates, respectively. Subsequently, ca. 4 mg of each pretreated sample were converted into silver phosphate (Ag_3PO_4) following the method of O´Neil et al. (1994) with modifications of Dettman et al. (2001) and Tütken et al. (2006). Triplicates of 500 µg of each Ag_3PO_4 sample were analyzed with a Thermo Fisher Delta Plus XL mass spectrometer coupled to a TC-EA, at the University of Tübingen, Germany. Measured values were normalized to calibrated in-house standards, Tu-1 and Tu-2 (Vennemann et al., 2002) and reported in δ-notation versus VSMOW. Replicate (n = 6) analyses of NBS 120c (pretreated as the samples) yielded a $\delta^{18}O_{PO4}$ value of 21.6 ± 0.13 ‰ which agrees well with the value of 21.7 ‰ reported by Lécuyer et al. (1993) and subsequently confirmed by many other laboratories (summarized in the appendix of Chenery et al., 2010). The $\delta^{18}O_{PO4}$ values of the *H. schinzii* teeth of the Mainz Basin were converted into $\delta^{18}O_{water}$ values using the equation determined for modern sirenians by Tütken (2003):

$$\delta^{18}O_{water} = \frac{\delta^{18}O_{PO_4} - 20.23}{0.86} \qquad (2)$$

where $\delta^{18}O_{water}$ and $\delta^{18}O_{PO4}$ are given relative to VSMOW. We used the equation of Tütken (2003) instead the one proposed by Lécuyer et al. (1996), because the calibration of Eq. 2 is based on more sea cow specimens and covers a 3-times larger range of measured ambient $\delta^{18}O_{water}$ values. However, $\delta^{18}O_{water}$ values reconstructed using both equations yielded similar values that are statistically invariant (Tütken, 2003: -0.9 ± 0.3 ‰; Lécuyer et al., 1996: -0.6 ± ca. 0.8 ‰).

In order to assess the possibility of diagenetic alteration of the enamel oxygen isotope composition, the carbonate ($\delta^{18}O_{CO3}$) and the phosphate ($\delta^{18}O_{PO4}$) group of the enamel were plotted against each other and compared to a compilation of $\delta^{18}O_{CO3}$ vs. $\delta^{18}O_{PO4}$ pairs from extant

mammals published by Pellegrini et al. (2011). The $\delta^{18}O_{CO3}$ values were determined in the remaining fraction of the pretreated *H. schinzii* enamel powders. About 800 µg of each enamel powder sample were analyzed with a Thermo Finnigan MAT 253 gas source isotope ratio mass spectrometer in continuous flow mode equipped with a GasBench II at the University of Mainz. The $\delta^{18}O_{CO3}$ values were measured against VPDB and normalized to a NBS-18 and NBS-19 calibrated Laaser marble (-5.21 ‰; replicated precision, 1σ, better than 0.1 ‰). Afterward, the results were converted to the SMOW scale using the equation of Coplen et al. (1983):

$$\delta^{18}O_{SMOW} = 1.03091 \cdot \delta^{18}O_{PDB} + 30.91 . \quad (3)$$

2.5. Mathematical re-sampling of intra-annual isotope data

In bivalves, shell growth rate declines during ontogeny resulting in increasingly narrow annual growth increments with increasing lifespan (Jones and Quitmyer, 1996). Since the isotope samples were taken at approximately equidistant intervals (100 to 200 µm), the number of samples per year decreases through lifetime and the time represented by each carbonate sample (= time-averaging) increases in ontogenetically older shell portions. To compensate for that bias and make the isotope samples from different ontogenetic years comparable to each other, the number of $\delta^{18}O_{shell}$ values per year was mathematically equalized by a re-sampling technique similar to that described in Schöne et al. (2004) and Hallmann et al. (2011). Following previous work (e.g. Schöne and Fiebig, 2008; Wanamaker et al., 2011), we fitted the isotope data of each annual increment with a 7-point cubic spline using the software Analyseries 1.1 (Paillard et al., 1996) and re-sampled each intra-annual curve so that the same number of isotope values were available for each annual increment, i.e., seven $\delta^{18}O_{shell}$´ values. This re-sampling method slightly deviated from previous approaches (Schöne et al., 2004; Hallmann et al., 2011), because it was impossible to determine seasonal growth curves from microgrowth patterns. Hence, the $\delta^{18}O_{shell}$´ values within a given year most likely represented different amounts of time, but the first, second, third etc. $\delta^{18}O_{shell}$´ values of different years represented same amounts of time.

3. Results

3.1. Preservation of material

According to a set of different diagenesis screening tests outlined above, the studied shells of *Glycymeris planicostalis* from the Rupelian of the Mainz Basin consist of aragonite and were remarkably well preserved. This even applies to the chalky rims of the shells, i.e., the shell portions that were only pale blue stained by Mutvei's solution and lost almost all organics during taphonomy. Orange cathodoluminescence was only emitted from very few isolated spots, i.e., cracks containing neomorphic mineral phases. Most other portions of the shells were dark blue to non-luminescent. Moreover, both reflected light microscope and electron microscope analyses revealed the same shell microstructures that occur in modern representatives of this genus, i.e., crossed-lamellar structures (Fig. 2D-F). Alternately, the 1st order lamellae appear dark and bright because the higher order-lamellae are arranged in a fence-like manner and stand perpendicular to each other (compare Füllenbach et al., 2014). Furthermore, both shell layers are perforated by numerous hollow microtubuli (Fig. 2G), especially in the juvenile portion of the shells. On rare occasions, these tubuli (ca. 10 µm in diameter) are filled with pyrite crystals or iron oxides. Like the bivalves, the studied sirenian teeth are well preserved (Fig. 3). The $\delta^{18}O_{CO3}$ vs. $\delta^{18}O_{PO4}$ pairs of the seven specimens plot well within the 95% prediction intervals of modern and other well-preserved fossil mammal enamel data compiled by Pellegrini

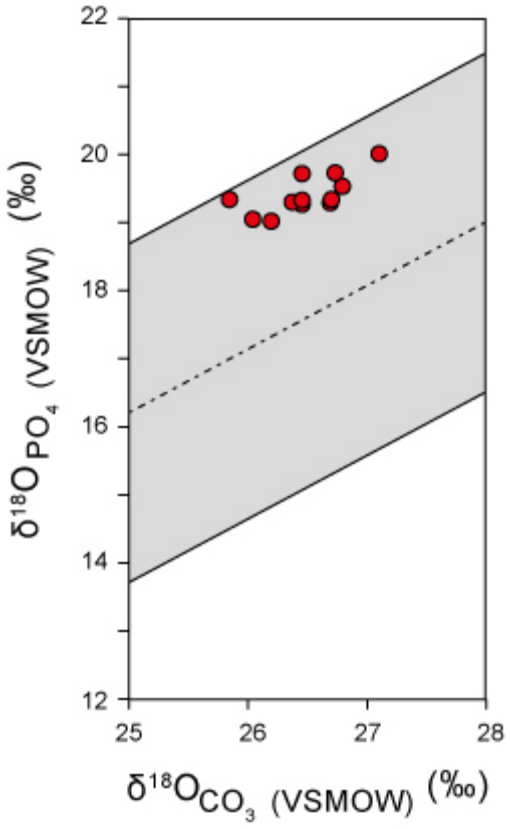

Figure 3. Cross-plot of mammal tooth enamel $\delta^{18}O_{PO4}$ and $\delta^{18}O_{CO3}$ pairs (dashed line = average; grey area = 95 % prediction intervals) compiled by Pellegrini et al. (2011) with respective data from the seven Oligocene sirenian teeth of the present study (red filled circles). Sea cow isotope data plot within the 95% prediction intervals suggesting that diagenesis has not affected the isotope composition of the phosphate group.

et al. (2011) (Table 1; Fig. 3). Digenetic alteration of tooth enamel would in the first place have affected the carbonate-bound oxygen (Iacumin et al., 1996) and resulted in $\delta^{18}O_{CO3}$ vs. $\delta^{18}O_{PO4}$ pairs plotting farther away from the regression line depicted in Pellegrini et al. (2011).

Given the excellent preservation, $\delta^{18}O_{water}$ values were computed from $\delta^{18}O_{PO4}$ values of the enamel using equation 2. On average, the $\delta^{18}O_{water}$ value of the ambient seawater was -0.9 ± 0.3 ‰ (1σ).

Table 1. Enamel $\delta^{18}O_{PO4}$ and $\delta^{18}O_{CO3}$ values (VSMOW) of the sea cow teeth from the Alzey Formation deposits of the Mainz Basin and $\delta^{18}O_{water}$ values calculated from the sea cow enamel $\delta^{18}O_{PO4}$ values. See text for details.

Sample ID	Sample Locality	$\delta^{18}O_{PO4}$ [‰]	$\delta^{18}O_{CO3}$ [‰]	$\delta^{18}O_{water}$ [‰]
Trai 01-1	Traisen	19.36	25.79	-1.01
Trai 01-2	Traisen	19.04	26.14	-1.38
Eck 01-1	Eckelsheim	19.29	26.40	-1.09
Eck 01-2	Eckelsheim	19.74	26.40	-0.57
Wein 01-1	Weinheim	19.31	26.63	-1.07
Wein 01-2	Weinheim	19.36	26.64	-1.01
PW 2008/5017-LS-2-1	Alzey-Weinheim	19.32	26.31	-1.06
PW 2008/5017-LS-2-2	Alzey-Weinheim	19.55	26.74	-0.79
PW 2008/5017-LS-1B	Alzey-Weinheim	20.03	27.05	-0.23
PW 2008/5017-LS-1A	Alzey-Weinheim	19.35	26.40	-1.02
STS-BE 62-1	Eckelsheim	19.07	25.98	-1.35
PW 2005/5042-LS-1	Wendelsheim	19.75	26.67	-0.56
Average ± 1σ		19.43 ± 0.29	26.43 ± 0.35	-0.9 ± 0.3
Min		19.04	25.79	-1.38
Max		20.03	27.05	-0.23

3.2. Bivalve sclerochronology: $\delta^{18}O_{shell}$ and reconstructed water temperatures

The studied fossil *G. planicostalis* specimens show distinct growth lines in the ventral margin and the hinge plate of Mutvei-stained cross-sections (Fig. 2H). These lines were previously identified as periodic annual features (Berthou et al., 1986; Royer et al., 2013; Bušelić et al., 2014) separating the growth pattern in annual time slices, i.e., annual growth increments. The annual growth lines are more distinctly developed and hence easier to discern in the hinge plate than in the ventral margin. Based on annual increment counts, it was possible to determine the ontogenetic ages of the specimens. Specimens MB-Wht-2, MB-Wht-4 and MB-Wht-7 reached life spans of 77, 84 and 67 years, respectively.

Oxygen isotope curves of all three specimens exhibit distinct seasonal oscillations (16, 14 and 10 cycles in specimens MB-Wht-2, -4, and -7, respectively) with the annual growth lines occurring shortly after the most negative $\delta^{18}O_{shell}$ values of each cycle (Fig. 4; see Supplements). In other words, the full seasonal amplitudes are preserved in the shells including winter and summer values. The annual growth line formation occurred in late summer/early fall.

The shells grew faster during the first half of the year than after summer. This is well reflected in the seasonal temperature curve based on the averaged $\delta^{18}O_{shell}$´ values of all 40 measured annual increments (Fig. 5). There are more data points in shell portions formed during spring than in shell portions formed during fall (Fig. 5). Accordingly, the reconstructed temperature curve is right-skewed.

The average annual $\delta^{18}O_{shell}$ values and seasonal $\delta^{18}O_{shell}$ ranges are fairly similar among the three studied specimens (Table 2). Seasonal extremes fluctuate between -1.48 ‰ (summer value) and 0.75 ‰ (winter value) in specimen MB-Wht-2, between -1.16 ‰ and 0.67 ‰ in specimen MB-Wht-4, and between -1.19 ‰ and 0.60 ‰ in specimen MB-Wht-7. Using the reconstructed $\delta^{18}O_{water}$ value, this translates into total temperature ($T_{\delta 18O}$) ranges of 9.7 °C, 7.6 °C and 7.8 °C in specimens MB-Wht-2, MB-Wht-4 and MB-Wht-7, respectively. Taking the resampled values of the 40 seasonal cycles of all three specimens, the average annual temperature is 15.4 ± 0.7 °C (1σ), and the seasonal temperature range equals 3.7 °C with average minimum (winter) values of 13.6 ± 0.8 °C (1σ) and average maximum (summer) values of 17.3 ± 1.2 °C (1σ).

Noteworthy, the seasonal amplitudes vary through time. In some years, the seasonal $T_{\delta 18O}$ range was less than 2 °C (Fig. 4).

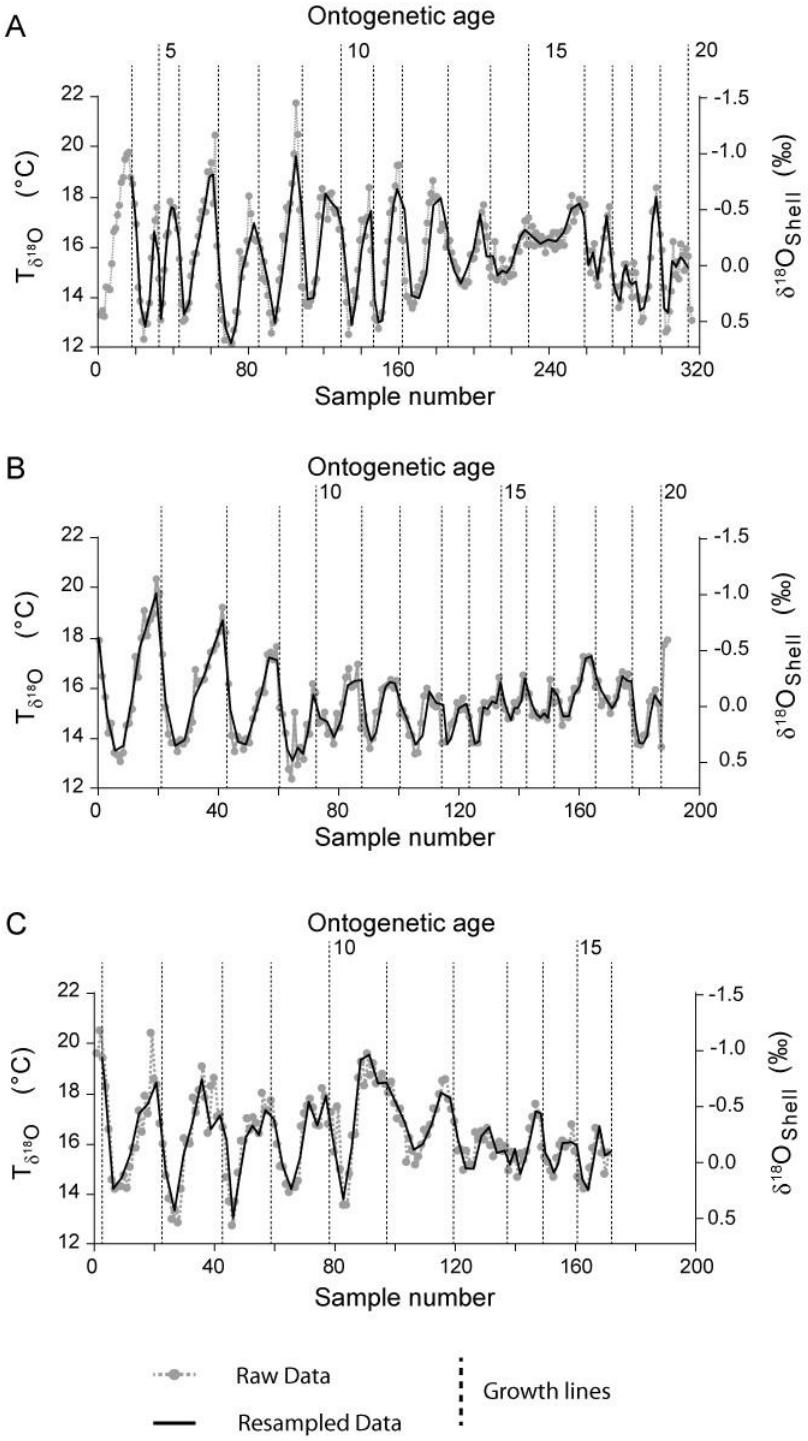

Figure 4. Raw (grey) and re-sampled (black) $\delta^{18}O_{shell}$ values for each of the three *Glycymeris planicostalis* shells analyzed in this study (A = MB-Wht-2; B = MB-Wht-4; C = MB-Wht-7). Vertical dotted bars represent annual growth lines. Temperatures were calculated using Eq. 2 with a $\delta^{18}O_{water}$ value reconstructed from $\delta^{18}O_{PO4}$ values of sea cow tooth enamel (see text for description).

Table 2. Oxygen isotope values ($\delta^{18}O$ vs. VPDB) of the three *Glycymeris planicostalis* shells analyzed in this study. The table lists seasonal extremes ($\delta^{18}O_{min}$ and $\delta^{18}O_{max}$) as well as average summer ($\delta^{18}O'_{summer}$; re-sampled values; explanation see text).

Sample ID	**$\delta^{18}O_{min}$ [‰]**	**$\delta^{18}O'_{summer} \pm 1\sigma$ [‰]**	**$\delta^{18}O_{max}$ [‰]**	**$\delta^{18}O'_{winter} \pm 1\sigma$ [‰]**	**$\delta^{18}O_{mean} \pm 1\sigma$ [‰]**
MB-Wht-2	-1.48	-0.66 ± 0.21	0.75	0.38 ± 0.23	-0.12 ± 0.13
MB-Wht-4	-1.16	-0.40 ± 0.31	0.67	0.28 ± 0.14	-0.03 ± 0.13
MB-Wht-7	-1.19	-0.61 ± 0.23	0.60	0.24 ± 0.19	-0.20 ± 0.16

4. Discussion

As demonstrated by this study, shells of *Glycymeris planicostalis* provide an excellent archive to reconstruct climate dynamics - in particular changes of sea surface temperature - during the Oligocene on subseasonal to inter-annual time-scales. Shells of the studied species grew during both the coldest and warmest periods of the year and therefore contain information on the full seasonal temperature amplitude over a coherent time interval of several years that prevailed in the Mainz Basin ~30 Ma ago. Furthermore, the shells are pristinely preserved and their $\delta^{18}O_{shell}$ values can potentially reflect changes of ambient water temperature.

4.1. Preservation

According to diagenetic screening the studied *G. planicostalis* shells are well preserved. The shells consist of pristine aragonite. Furthermore, SEM analysis revealed original delicate shell microstructures including the typical skeletal feature of glycymerids, i.e., microtubuli. These cylindrical cavities perforate the inner and outer shell layers and are filled with organics during the lifetime of the animal (e.g., Waller, 1980; Crippa, 2013). The diagenetic loss of organic material leaves behind hollow cavities that potentially can be filled with neomorphic mineral phases.

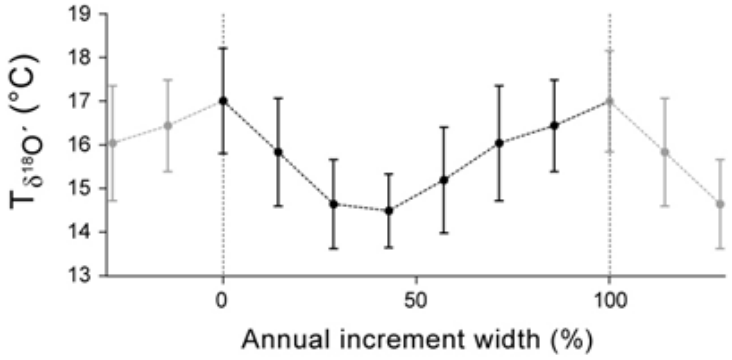

Figure 5. Average seasonal temperature changes (black dots, ±1σ) based on mathematically re-sampled shell oxygen isotope values ($\delta^{18}O_{shell}$´ values; see text for explanation) of 40 annual increments measured in three specimens of *Glycymeris planicostalis*.

However, the microtubuli of the studied specimens were typically hollow and only rarely contained pyrite. Pyrite crystals can even occur in shells of living bivalves and are possibly related to the bacterial degradation of organic matter (Clark and Lutz, 1980).

In fact, the recovery of pristinely preserved fossil glycymerids has been reported from many other localities and geological time intervals (e.g., Tsuboi and Hirata, 1935; Crippa, 2013). Since *Glycymeris* spp. dwell in sandy to fine gravelly habitats, shells of this genus are usually embedded in coarse grained and highly porous sediments. In such type of host rock and stratigraphic age, one would not expect aragonitic shell preservation, particularly if the burial depth is shallow (few tens of meters) and the sediment is still unconsolidated as this is the case with the weakly cemented sandstones of the Alzey Formation. Under surface conditions, aragonite is metastable and slowly turns into the more stable polymorph of $CaCO_3$, i.e., calcite (Boettcher and Wyllie, 1967). This conversion into calcite can be expedited when a fluid is present (Putnis and Putnis, 2007) and when temperature is increased (Dasgupta, 1963). The resistance of glycymerid shells against diagenetic alteration likely resulted from low organic content and the dense crossed-lamellar microstructure (Taylor and Layman, 1972).

4.2. Timing and rate of shell growth

Pristine preservation is a major prerequisite for the reconstruction of environmental variables from geochemical properties of the shells including ambient water temperature from $\delta^{18}O_{shell}$ values. According to shell oxygen isotope data the studied shells grew during winter and summer. Similar findings on shell growth during seasonal extremes were recently reported for modern *Glycymeris bimaculata* from Croatia (Bušelić et al., 2014). The only difference is that the Oligocene shells formed annual growth lines in late summer/early fall, whereas the period of extremely slow or no shell growth in specimens from Croatia occurs during spring. On the contrary, modern *G. glycymeris* from the North Atlantic form annual growth breaks in winter (Berthou et al., 1986; Royer et al., 2013). These findings suggest that the timing and rate of shell growth can vary greatly

Table 3. Dentine and enamel $\delta^{18}O_{PO4}$ values (VSMOW) of shark teeth recovered from the early Oligocene deposits of the Mainz Basin (Tütken, 2003). Values have been converted to temperature ($T_{\delta 18OPO4}$) using the paleothermometry equation by Longinelli and Nutti (1973) assuming $\delta^{18}O_{water}$ = -0.9 ‰.

Sample ID	Genus	$\delta^{18}O_{PO4}$ [‰]	$T_{\delta 18OPO4}$ [°C]
FD HAI MB 2	*Carcharias* sp.	22.9	9.1
FZ HAI MB 2	*Carcharias* sp.	22.8	9.5
FZ HAI MB 3	*Carcharias* sp.	19.6	23.3
FD HAI MB 4	*Carcharias* sp.	21.0	17.2
FZ HAI MB 4	*Carcharias* sp.	21.5	15.1
FZ HAI MB 8	*Carcharias* sp.	20.1	21.1
FZ HAI MB 9	*Carcharias* sp.	21.0	17.2
FZ HAI MB 10	*Carcharias* sp.	23.4	6.9
Average ± 1σ		21.5 ± 1.3	14.9 ± 5.9
Min		19.6	6.9
Max		23.4	23.3

among different species of the same genus and most likely even among specimens of the same species alive at different localities (e.g., Ansell, 1968; Jones & Quitmyer, 1996). A number of explanations have been proposed to explain the reason for periodic cessation of shell growth. Temperature stress seems to limit shell growth in many bivalves. Above and below a taxon-specific water temperature range, biomineralization ceases and results in the formation of winter or summer growth lines (Jones and Quitmyer, 1996) or even both (Schöne et al., 2002). For example, *Mercenaria mercenaria* stops shell growth above 31 °C and below 9 °C (Ansell 1968). Following this explanation, modern *G. glycymeris* from the North Atlantic forms winter lines when temperatures fall below the tolerance limit of this species, as suggested by Royer et al. (2013). In some taxa, annual growth line formation can also be linked to the reproductive cycle. For example, *Phacosoma japonicum* from Japan not only forms winter lines, but also slows down shell growth regularly during June and July, i.e., during the peak spawning phase (Sato, 1995). Instead of biomineralizing shell, the energy is then allocated to the formation of eggs and sperms. Spawning breaks may be limited to species lacking specific tissues for energy (lipids) storage. Modern *G. glycymeris* from the North Atlantic, for example, belongs to this group of bivalves and reportedly spawns once or twice per year between spring and fall (Galap et al. 1997). In the Mediterranean Sea, *G. nummaria* spawns in July and August, followed by a sudden decrease of the condition index in late summer/fall (Crnčević et al., 2013). However, it has remained unresolved whether modern *Glycymeris* spp. can only form shell during periods of sexual inactivity. Existing studies on seasonal shell growth of this genus were based on juvenile specimens or juvenile portions of adult specimens (Peharda et al., 2012; Bušelić et al., 2014; Royer et al., 2013). Therefore, it is difficult to draw conclusions on how the reproductive cycle affects seasonal growth in (modern) *Glycymeris* spp. It is not possible to determine whether growth line formation of *G. planicostalis* was governed by reproduction or other environmental factors. At least the annual growth lines in the studied specimens from the Oligocene are unrelated to seasonal temperature extremes because the lines do not fall together with the most negative and positive oxygen isotope-derived water temperatures (Fig. 4).

Shell growth rates of the studied bivalves from the early Oligocene of the Mainz Basin also varied during the main growing season. For example, shell production was faster during spring and summer than during fall and winter. This finding has implications for geochemical sampling

strategies. In order to obtain reliable information on the actual seasonal temperature spread, a higher sampling resolution has to be applied in slow-growing shell portions.

4.3. Temperatures of the Mainz Basin during the Rupelian

Only few temperature estimates of the Mainz Basin and adjacent regions during the Rupelian are currently available. For example, sediments of the Alzey Formation contain a diverse warm-water fauna including marine fish, mammals and crocodiles as well as terrestrial turtles. Based on this fossil assemblage, subtropical climate conditions - similar to the modern southeastern Mediterranean - were inferred for the Mainz Basin (Grimm et al., 2003, 2011). Furthermore, macroflora and palynological data from the Bodenheim Formation yielded winter and summer air temperatures of 7.1 - 10.2 °C and 25.7 - 28.1 °C, respectively (Pross et al., 1998; Pross et al., 2000). These estimates compare well with those obtained from fossil floras of other contemporaneous localities in Central Europe (Mosbrugger et al., 2005; Erdei et al., 2012).

Knowledge on water temperatures of the Mainz Basin comes from oxygen isotope compositions of biogenic skeletons. Tütken (2003) reported $\delta^{18}O_{PO4}$ values of shark teeth that correspond to absolute temperatures between 6.9 °C and 23.3 °C (temperatures recalculated assuming a $\delta^{18}O_{water}$ value of -0.9 ‰; Table 3), using the thermometry equation of Longinelli and Nuti (1973). Grimm (1994) reported oxygen isotope data of planktonic and benthic foraminifera that can be converted into absolute temperatures using the paleothermometry equation by Anderson and Arthur (1983) and a $\delta^{18}O_{water}$ value of -0.9 ‰. Based on this calculation, sea surface temperatures of the Mainz Basin fluctuated between 11.7 °C and 21.3 °C (Table 4), whereas bottom water (up to 150 m depth; Grimm et al., 2011) temperatures were as cold as 5.9 °C to 14.9 °C during the Rupelian. Similar surface water temperatures were reconstructed from bivalve shells in the present study (12.3 °C and 22.0 °C), although the lowest temperatures are ~5 °C higher than those obtained from shark teeth (Fig. 6). Leaving aside the fact that it is rather unlikely that the studied bivalves, sharks and foraminifera lived during the exact same time interval, a direct comparison of temperature extremes derived from the different marine archives seems problematic for a variety of reasons:

(i) The temporal resolution provided by foraminifera is much higher than that of bivalves. Foraminiferan tests can grow within a few weeks (Bé et al., 1981). Thus, each specimen recorded environmental conditions during a very short time interval of the year. On the opposite, each sample taken from the bivalve shells represents, on average, about two weeks to one month worth of growth. Foraminifera samples analyzed so far may not necessarily have grown when the most extreme seasonal temperatures occurred. Accordingly, actual winter temperatures may have been slightly colder and summers slightly warmer than suggested by the $\delta^{18}O$ values of foraminifera.

(ii) Seasonal temperature extremes given by sharks may not represent the actual temperatures where the bivalves lived. Being highly mobile, nektonic organisms, the sharks may have foraged temporarily in the shallowest waters near the coast and at other times dived to the very bottom of the sea. In addition to vertical movements, they may have travelled large distances such as modern sharks (e.g., Domeier and Nasby-Lucas, 2008). Lowest temperatures recorded by sharks may thus represent conditions below the thermocline or settings much further north instead of winter temperatures in the Mainz Basin. In turn, those teeth that provided temperature estimates of 22 °C may actually have been formed while the animals lived in warmer waters farther south or near the coast.

(iii) Actual sea surface temperatures during both winter and summer may have been underestimated by the planktonic foraminifera (and sharks while they resided in shallowest, coastal waters), because the assumed average $\delta^{18}O_{water}$ value did not reflect the actual isotope signature of the water. Planktonic foraminifera lived in the upper few meters of the water column in a narrow, shallow epicontinental sea. In such a habitat, seasonally varying riverine freshwater influx, precipitation and evaporation rates likely resulted in seasonal changes of the $\delta^{18}O_{water}$ value. Increased evaporation during summer may have shifted the $\delta^{18}O_{water}$ value toward more positive values resulting in lower than actual reconstructed water temperatures near sea surface. In contrast, higher precipitation rates during winter may have shifted the $\delta^{18}O_{water}$ value toward more negative values so that the oxygen isotope-derived temperatures appeared colder than they actually were. Indications for a seasonally varying $\delta^{18}O_{water}$ value come, to some extent, from sirenian teeth. Like their extant relatives, sea cows lived in the upper ten meters of the ocean and near the coast (Louise Chilvers et al., 2004). Thus, they have recorded the isotope signature of the near-coastal surface water in which the planktonic foraminifera (*Globigerina* sp.) lived.

Reconstructed $\delta^{18}O_{water}$ values fluctuated between -0.2 ‰ and -1.4 ‰. If the latter value reflected conditions during winter and the former during summer, actual seasonal temperatures in the upper few meters of the Mainz Basin reconstructed from foraminifera ranged between ca. 11 °C and 27 °C.

(iv) Bivalve shell-based temperature estimates cannot be compared directly to those of planktonic foraminifera even if the fluctuating $\delta^{18}O_{water}$ values in the upper few meters of the ocean were precisely known. At ca. 30 - 40 m water depth, bivalves likely experienced a smaller seasonal temperature range than organisms in the upper few meters of the sea.

The benthic faunal associations of the Mainz Basin have been interpreted as reflecting paleoclimate conditions similar to those of the modern southeastern Mediterranean Sea (Grimm et al., 2003, 2011). However, temperature estimates derived from *G. planicostalis* shells suggest

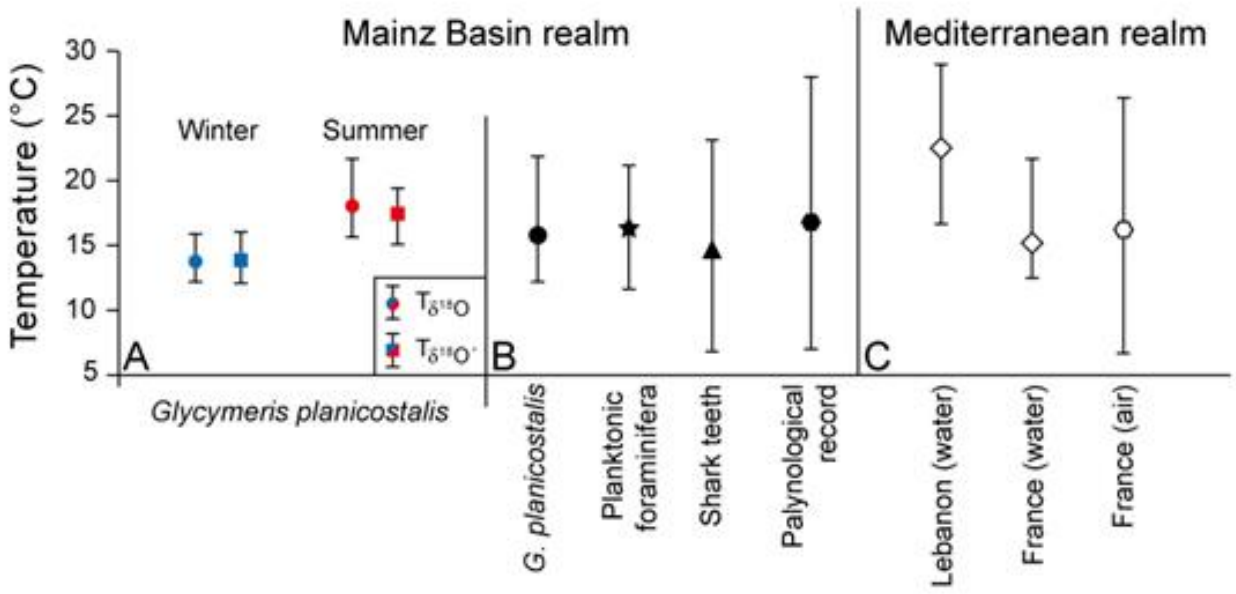

Figure 6. Seasonal temperature ranges. (A) Comparison between raw (circles) and mathematically re-sampled (squares) summer (red) and winter (blue) temperature data based on shell oxygen isotope data of three fossil *Glycymeris planicostalis* shells. Whereas mathematical re-sampling did not greatly affect average values and winter ranges, the summer temperature range of re-sampled data is truncated. (B) Comparison of the reconstructed temperature data based on $\delta^{18}O_{shell}$ values of the three studied bivalve shells (filled black circle) and previously published temperature data based on planktonic foraminifera (Grimm, 1994), shark teeth (Tütken, 2003) and palynological associations (Pross et al., 2000). (C) Seawater temperatures off Lebanon and southern France at 35 m depth (Abboud-Abi Saab et al., 2004) and air temperatures in southern France (GHCN Monthly Dataset; Lawrimore et al., 2011).

lower water temperatures. According to hydrographical studies from coastal regions in the northwestern Mediterranean (France) and southeastern Mediterranean (Lebanon), the temperature in 30 to 40 m water depth is still influenced by surface conditions (Abboud-Abi Saab et al., 2004). At 35 m water depth, the temperatures off Lebanon ranged between 16.9 °C and 29.1 °C with an annual average of 22.5 ± 4.1°C (1σ), whereas the coastal waters off France ranged between 12.3 °C and 21.8 °C with an annual average of 15.2 ± 2.2 °C (1σ). Temperatures recorded by *G. planicostalis* lay well within these ranges which would suggest that water temperatures were more similar to regions in the northwestern Mediterranean than those from subtropical areas. However, the mean annual precipitation in the area of Marseille (Mediterranean coast of southern France) equals 751 ± 172 mm (Harris et al., 2014), which is considerably lower than 1000-1250 mm/a reconstructed precipitation rates for the hinterland of the Mainz Basin (Pross et al., 1998, 2000). A possible explanation for the high precipitation rates in Central Europe during the Oligocene has been provided by Pross and Schmiedl (2002). The deposition of the Alzey Formation and its basinal counterparts, the Bodenheim Formation, took place during sea-level highstands, which could have increased the moisture concentration in the atmosphere, and so, intensified rainfalls. Such linkage between sea level rise and precipitation has recently been postulated for the early Holocene intensification of the Australian-Indonesian monsoon rainfall (Griffiths et al., 2009).

4.4. Advantages of using shells of *Glycymeris planicostalis* for reconstruction of Oligocene climate conditions

The studied specimens of *G. planicostalis* offer a number of advantages over existing marine paleoclimate archives. As sessile organisms, bivalves record the water properties at a specific locality and depth throughout their lifetimes. Since their shells grew almost year-round, each isotope sample can be assigned to a particular season. If preservation permits, daily microgrowth increments can be employed to temporally contextualize the seasonal shell growth to the nearest week or so (e.g. Schöne et al., 2005b). Such an internal calendar is missing in foraminifera.

The studied *G. planicostalis* specimens lived for several decades and recorded seasonal temperature changes over the course of many consecutive years. This is a clear advantage over other climate archives that only provide very short temporal snapshots of unknown timing within the year such as foraminifera or shark teeth, or few consecutive years, such as fish otoliths.

Analogously to bivalve shells, they form growth lines, and their oxygen isotope composition can be used for seasonal paleotemperature reconstructions, for example, at the Eocene/Oligocene boundary (Ivany et al., 2000). Although fish otoliths are very common components of marine nektonic microfossil assemblages, their reduced size makes them difficult to sample, and analyses of their chemical composition usually cover only short time intervals.

Long proxy records offer the possibility to examine variability of winter and summer temperatures over the course of several years. Future studies should generate $\delta^{18}O_{shell}$ time-series of *G. planicostalis* that are long enough to permit spectral analyses. These data should then be combined with numerical climate models for that time. Furthermore, $\delta^{18}O_{shell}$ chronologies should also be compared to increment widths in order to identify potential influences of temperature on shell growth rates.

Table 4. Oxygen isotope values ($\delta^{18}O$ vs. VPDB) of foraminiferal tests from the Bodenheim Formation (Kriegsfeld 5 and Bodenheim 65 well) reported by Grimm (1994). $\delta^{18}O_{Glob}$ is *Globigerina* sp. (planktonic foraminifera); $\delta^{18}O_{Bol}$ is *Bolivina* sp. (benthonic foraminifera). Values have been converted to temperature ($T\delta^{18}O_{Glob}$, $T\delta^{18}O_{Bol}$) using the equation by Anderson and Arthur (1983) assuming $\delta^{18}O_w = -0.9$ ‰.

Kriegsfeld 5 Depth [m]	**$\delta^{18}O_{Glob}$ [‰]**	**$T\delta^{18}O_{Glob}$ [°C]**	**Bodenheim 65 Depth [m]**	**$\delta^{18}O_{Bol}$ [‰]**	**$T\delta^{18}O_{Bol}$ [°C]**
15	-1.8	18.7	21.5	1.5	5.9
23	-2.4	21.3	70	-0.9	14.9
25	-0.1	11.7	80	1.0	7.6
28	-1.3	16.5	85	1.1	7.3
30	-2.0	19.5	90	0.7	8.7
32	-0.7	14.1	95	-0.03	11.4
34	-0.8	14.5	99	0.7	8.7
Average ± 1σ	2.75 ± 0.81	16.6 ± 3.4	Average	0.6 ± 0.8	9.5 ± 2.9
Min	-2.4	11.7	Min	-0.9	5.9
Max	-0.1	21.3	Max	1.5	14.9

The $\delta^{18}O_{water}$ value at 30 - 40 m water depth was most probably much less variable than near the sea surface. Seasonal changes in freshwater influx into the Mainz Basin likely did not have any significant effect on the isotope signature of the water in which the bivalves lived. In fact, modern *G. glycymeris* from the North Atlantic is most prolific in water with stable salinity of 34 - 35 PSU (Rombouts et al., 2012). If the same preference is true for the Oligocene relatives of this genus, water temperatures can be reconstructed with smaller error bars from oxygen isotope values of the bivalve shells than from skeletal hard parts of nektonic and planktonic organisms. Evidently, absolute temperature estimates from $\delta^{18}O$ values require knowledge of the oxygen isotope composition of the ambient water, which is rarely available for fossil environments. In the present study, the $\delta^{18}O_{water}$ value was reconstructed from the tooth enamel of sea cows from the same stratigraphic level. Although the bivalves and the sea cows did most certainly not live during the exact same time and the sphere of action of the sea cows was the upper ten meters of the ocean, the average $\delta^{18}O_{PO4}$ value of the sirenian teeth serves as a reasonable estimate of the Rupelian $\delta^{18}O_{water}$ value (-0.9 ‰) of the Mainz Basin. A similar value (-1 ‰) was also assumed by Grimm (1994). For comparison, the $\delta^{18}O_{water}$ of the open ocean was -0.5 ‰ at that time (Lear et al., 2000). To test the temperature estimates obtained from $\delta^{18}O_{shell}$ values and circumvent uncertainties related to the precise $\delta^{18}O_{water}$ signature during shell formation, future studies should explore other potential temperature proxies such as Sr/Ca and Δ_{47} values (Eagle et al., 2013).

5. Summary and conclusions

Shells of *Glycymeris planicostalis* serve as excellent recorders of sea surface temperatures in the Mainz Basin during the Rupelian stage. Since the shells were preserved as pristine aragonite, the $\delta^{18}O_{shell}$ values can be used to reconstruct ambient water temperature. The $\delta^{18}O_{water}$ value for the temperature calculation was reconstructed using tooth enamel $\delta^{18}O_{PO4}$ values of the sea cow *Halitherium schinzii* from the same strata. Although the exact oxygen isotope signature of the water is not known, it is highly likely to assume that the $\delta^{18}O_{water}$ value in 30 - 40 m water depth, in which *G. planicostalis* lived, remained largely invariant through time. Attributed to its notable longevity, shells of this species can be used to study seasonal temperature changes over several consecutive

years, even up to decades. As shown in the present study, summer and winter temperatures varied greatly from year to year. As yet, such data are hardly available from any other paleoclimate archive of the Oligocene. Such information can be highly relevant for numerical climate studies aiming to predict possible future climates in a unipolar glaciated or polar ice-free world.

Acknowledgements

Not displayed for reasons of data protection

References

Abboud-Abi Saab, M., Romano, J.-C., Bensoussan, N. Fakhri, M., 2004. Suivis temporels comparés de la structure thermique d'eaux côtières libanaises (Batroun) et françaises (Marseille) entre juin 1999 et octobre 2002. Comptes Rendus Geoscience 336, 1379–1390.

Anderson, T.F., Arthur, M.A., 1983. Stable isotopes of oxygen and carbon and their application to sedimentologic and paleoenvironmental problems. Society of Economic Paleontologists and Mineralogists (SEPM) Short Course 10, 1–151.

Ansell, A.D., 1968 The rate of growth of the hard clam *Mercenaria mercenaria* (L) throughout the geogrpahical range. Journal du Conseil Permanent Internatinal pour l'Exploration de la Mer 31, 364–409, 1968.

Ansell, A.D., Trueman, E.R., 1967. Observations on burrowing in *Glycymeris glycymeris* (L.) (Bivalvia, Arcacea). Journal of Experimental Marine Biology and Ecology 1, 65–75.

Barbosa, S.M., 2009. Decadal variability in Europe's seasons. In: EGU General Assembly Conference,19-24 April 2009, Vienna, Austria, Abstracts 11, 5332

Bé, A.W.H., Caron, D.A. Anderson, O.R., 1981. Effects of feeding frequency on life processes of the planktonic foraminifer *Globigerinoides sacculifer* in laboratory culture. Journal of Marine Ecologist Association of the United Kingdom 61, 257–277.

Berger, J.-P., Reichenbacher, B., Becker, D., Grimm, M., Grimm, K., Picot, L., Storni, A., Pirkenseer, C., Derer, C., Schaefer, A., 2005a. Paleogeography of the Upper Rhine Graben (URG) and the Swiss Molasse Basin (SMB) from Eocene to Pliocene. International Journal of Earth Sciences 94, 697–710.

Berger, J.-P., Reichenbacher, B., Becker, D., Grimm, M., Grimm, K., Picot, L., Storni, A., Pirkenseer, C., Schaefer, A., 2005b. Eocene-Pliocene time scale and stratigraphy of the Upper Rhine Graben (URG) and the Swiss Molasse Basin (SMB). International Journal of Earth Sciences 94, 711–731.

Berthou, P., Blanchard, M., Noel, P. Vergnaud-Grazzini, C., 1986. The analysis of stable isotopes of the shell applied to the determination of the age of four bivalves of the "Normano-Breton" gulf, Western Channel. International Council for the Exploration of the Sea, Shellfish Commitee, Copenhagen, Denmark, Annual Report, 1986/K:16, 1–13.

Beyrich, E., 1854. Über die Stellung der hessischen Tertiärbildungen. Bericht über die zur Bekanntmachung geeigneten Verhandlungen der Königlich Preußischen Akademie der Wissenschaften zu Berlin, Germany, 640–666.

Black, B.A., Gillespie, D.C., MacLellan, S.E., Hand, C.M., 2008. Establishing highly accurate production-age data using the tree-ring technique of crossdating: a case study for Pacific geoduck *(Panopea abrupta*). Canadian Journal of Fisheries and Aquatic Sciences 65, 2572–2578.

Boettcher, A.L., Wyllie, P.J., 1967. Revision of the calcite-aragonite transition, with the location of a triple point between calcite I, calcite II and aragonite. Nature, 213, 792–793.

Brocas, W.M., Reynolds, D.J., Butler, P.G., Richardson, C.A., Scourse, J.D., Ridgway, I.D., Ramsay, K., 2013. The dog cockle, *Glycymeris glycymeris* (L.), a new annually-resolved sclerochronological archive for the Irish Sea. Palaeogeography, Palaeoclimatology, Palaeoecology 373, 133–140.

Bušelić, I., Peharda, M., Reynolds, D.J., Butler, P.G., González, A.R., Ezgeta-Balić, D., Vilibić, I., Grbec, B., Hollyman, P., Richardson, C.A., 2015. *Glycymeris bimaculata* (Poli, 1795) – a new sclerochronological archive for the Mediterranean? Journal of Sea Research 95, 139–148.

Butler, P.G., Wanamaker, A.D., Scourse, J.D., Richardson, C.A., Reynolds, D.J., 2013. Variability of marine climate on the North Icelandic Shelf in a 1357-year proxy archive based on growth increments in the bivalve *Arctica islandica*. Palaeogeography, Palaeoclimatology, Palaeoecology 373, 141–151, 2013.

Cai, W., Chu, P.C., 1998. Oceanic responses to gradual transitions of equator-to-pole. Quarterly Journal of the Royal Meteorological Society 124, 2817–2828, 1998.

Casey, R., 1961. The stratigraphycal palaeontology of the Lower Greensand. Palaeontology, 3, 487–621.

Chenery, C., Müldner, G., Evans, J., Eckardt, H., Lewis, M., 2010. Strontium and stable isotope evidence for diet and mobility in Roman Gloucester, UK. Journal of Archaeological Science 37, 150–163, 2010.

Clark, G.R., Lutz, R.A., 1980. Pyritization in the shells of living bivalves. Geology, 8, 268–271.

Clementz, M.T., Koch, P.L., 2001. Differentiating aquatic mammal habitat and foraging ecology with stable isotopes in tooth enamel. Oecologia 129, 461–472.

Clementz, M.T., Sewall, J.O., 2009. Latitudinal gradients in greenhouse seawater $\delta^{18}O$: evidence from Eocene sirenian tooth enamel. Science 332, 455–458.

Clementz, M.T., Goswami, A., Gingerich, P.D., Koch, P.L., 2006. Isotopic records from early whales and sea cows: contrasting patterns of ecological transition. Journal of Vertebrate Paleontology 26, 355–370.

Coplen, T.B., Kendall, C., Hopple, J., 1983: Comparison of stable isotope reference samples. Nature 302, 236–238.

Crippa, G., 2013. The shell ultrastructure of the genus *Glycymeris* DA COSTA, 1778: a comparison between fossil and recent specimens. Rivista Italiana di Paleontologia e Sedimentologia 119, 387–399.

Crnčević, M., Peharda, M., Ezgeta-Balić, D., Pećarević, M., 2012: Reproductivecycle *of Glycymeris nummaria* (Mollusca: Bivalvia) from Mali Ston Bay, Adriatic Sea, Croatia. Scientia Marina 77, 293–300.

Dai, A., Fung, I.Y., Del Genio, A.D., 1997. Surface observed global land precipitation variations during 1900-88. Journal of Climate 10, 2943–2962.

Dasgupta, D.R., 1963. The oriented transformation of aragonite into calcite. Mineralogical Magazine 33, 924–928.

Dettman, D.L., Reische, A.K., Lohmann, K.C., 1999. Controls on the stable isotope composition of seasonal growth bands in aragonitic fresh-water bivalves (unionidae). Geochimica et Cosmochimica Acta 63, 1049–1057.

Dettman, D.L., Kohn, M.J., Quade, J., Ryerson, F.J., Ojha, T.P., Hamidullah, S., 2001. Seasonal stable isotope evidence for a strong Asian monsoon throughout the past 10.7 m.y.. Geology 29, 31–34.

Dèzes, P., Schmid, S.M., Ziegler, P.A., 2004. Evolution of the European Cenozoic Rift System: interaction of the Alpine and Pyrenean orogens with their foreland lithosphere. Tectonophysics 389, 1–33.

Domeier, M., Nasby-Lucas, N., 2008. Migration patterns of white sharks *Carcharodon carcharias* tagged at Guadalupe Island, Mexico, and identification of an eastern Pacific shared offshore foraging area. Marine Ecology Progess Series 370, 221–237.

Eagle, R.A., Eiler, J.M., Tripati, A.K., Ries, J.B., Freitas, P.S., Hiebenthal, C., Wanamaker Jr., A.D., Taviani, M., Elliot, M., Marenssi, S., Nakamura, K., Ramirez, P., Roy, K., 2013. The influence of temperature and seawater carbonate saturation state on ^{13}C-^{18}O bond ordering in bivalve mollusks. Biogeosciences 10, 4591-4606.

Epstein, S., Buchsbaum, R., Lowenstam, H., Urey, H., 1953. Revisited carbonate-water isotopic temperature scale. Bulletin of the American Meteorological Society 64, 1315–1326.

Erdei, B., Utescher, T., Hably, L., Tamás, J., Roth-Nebelsick, A., Grein, M., 2012. Early Oligocene continental climate of the Palaeogene Basin (Hungary and Slovenia) and the surrounding Area. Turkish Journal of Earth Sciences 21, 153–186.

Feigl, F., 1958. Spot tests in inorganic analysis. Fifth Enlarged and Revisited English Edition, Elsevier, Amsterdam, Netherland.

Flügel, E., 2004. Microfacies of carbonate rocks: analysis, interpretation and application, Springer, Berlin, Germany, 2004.

Füllenbach, C.S., Schöne, B.R., Branscheid, R., 2014. Microstructures in shells of the freshwater gastropod *Viviparus viviparus*: a potential sensor for temperature change? Acta Biomaterialia 1, 3911–3921.

Galap, C., Leboulenger, F., Grillot, J.-P., 1997. Seasonal variations in biochemical constituents during the reproductive cycle of the female dog cockle *Glycymeris glycymeris*. Marine Biology 129, 625–634.

Gillet, S., 1924. Études sur les Lamellibranches néocomiens. Mémoires de la Société géologique de France 1, 1–324.

Gradstein, F.M., Ogg, J.G., Smith, A.G., 2004. A geologic time scale 2004. Cambridge University Press, Cambridge, United Kingdom and New York, NY, USA.

Griffiths, M.L., Drysdale, R.N., Gagan, M.K., Zhao, J.-X., Ayliffe, L.K., Hellstrom, J.C., Hantoro, W.S., Frisia, S., Feng, Y.-X., Cartwright, I., Pierre, E.S., Fischer, M.J., Suwargadi, B.W., 2009. Increasing Australian-Indonesian monsoon rainfall linked to early Holocene sea-level rise. Nature Geoscience 2, 636–639.

Grimm, K.I., 1994. Paläoökologie, Paläogeographie und Stratigraphie im Mainzer Becken, im Oberrheingraben, in der Hessischen Senke und in der Leipziger Bucht während des Mittleren Rupeltons (Fischschiefer/Rupelium/Unteroligozän). Mitteilungen Pollichia, 81, 7–193.

Grimm, K.I., 1998. Correlation of Rupelian coastal and basin facies in the Mainz Basin (Oligocene, Germany). Neues Jahrbuch für Geologie und Paläontologie Monatshefte 3, 146–156.

Grimm, K.I., 2002. Foraminiferal zonation of early Oligocene deposits (Selztal Group, Latdorfian, Rupelian) in the Mainz Basin, Germany. Journal of Micropalaeontology 21, 67–74.

Grimm, K.I., 2006. Meeresverbindungen im Rupelium Mitteleuropas – Paläobiogeographische Untersuchungen anhand von Foraminiferen. Geologisches Jahrbuch Hessen 133, 19–27.

Grimm, K.I., Grimm, M.C., Schindler, T., 2000. Lithostratigraphische Gliederung im Rupelium/Chattium des Mainzer Beckens, Deutschland. Neues Jahrbuch für Geologie und Paläontologie Abhandlungen 218, 343–397.

Grimm, K.I., Grimm, M.C., Neuffer, Lutz, H., 2003. Die fossilen Wirbellosendes Mainzer Tertiärbeckens Teil 1-1 Geologischer Führer durch das Mainzer Tertiärbecken. Mainzer Naturwissenschaftliches Archiv, Beihefte 26, 1–158.

Grimm, K.I., Grimm, M., Radtke, G., Kadolsky, D., Schäfer, P., Franzen, J.L., Schindler, T., Hottenrott Martin, 2011. Mainzer Becken. In: Deutsche Stratigraphische Kommission (Eds.), Stratigraphie von Deutschland IX. Tertiär, Teil 1. SDGG 75, 133–209.

Grossman, E.L., Ku, T.-L., 1986. Oxygen and carbon isotope fractionation in biogenic aragonite: temperature effects. Chemical Geology: Isotope Geoscience Section 59, 59–74.

Grossman, E.L., Mii, H.-Zhang, C., Yancey, T.E., 1996. Chemical variation in Pennsylvanian brachiopod shells - diagenetic, taxonomic, microstructural, and seasonal effects, Journal of Sedimentology 66, 1011–1022.

Hallmann, N., Schöne, B.R., Irvine, G.V, Burchell, M., Cokelet, E.D., Hilton, M.R., 2011. An improved understanding of the Alaska Coastal Current: the application of a bivalve growth-temperature model to reconstruct freshwater-influenced paleoenvironments. Palaios 26, 346–363.

Hansen, B., Østerhus, S., Quadfasel, D., Turrell, W., 2004. Already the day after tomorrow? Science 305, 953–954.

Haq, B.U., Hardenbol, J., Vail, P.R., 1988. Mesozoic and Cenozoic chronostratigraphy and cycles of sea-level change, in: Wilgus, C.K., Hasting, B.S., Posamentier, H., Van Wagoner, J., Ross, C.K., Kendall, C.G.S.C. (Eds.), Sea-Level Changes. Society of Economic Paleontologists and Mineralogists (SEPM) Special Publication 42, 71–108.

Harris, I., Jones, P.D., Osborn, T.J., Lister, D.H., 2014. Updated high-resolution grids of monthly climatic observations - the CRU TS3.10 Dataset. Interational Journal of Climatology 34, 623–642.

Hátún, H., Sandø, A.B., Drange, H., Hansen, B., Valdimarsson, H., 2005. Influence of the Atlantic subpolar gyre on the thermohaline circulation. Science 309, 1841–1844.

Hurrell, J.W., 1995. Decadal trends in the North Atlantic Oscillation: regional temperatures and precipitation. Science 269, 676–9.

Iacumin, P., Bocherens, H., Mariotti, A., Longinelli, A., 1996. Oxygen isotope analyses of co-existing carbonate and phosphate in biogenic apatite: a way to monitor diagenetic alteration of bone phosphate? Earth and Planetary Science Letters 142, 1–6.

Ivany, L.C., Patterson, W.P., Lohmann, K.C., 2000. Cooler winters as a possible cause of mass extinctions at the Eocene/Oligocene boundary. Nature 407, 887–890.

Jones, D.S., Quitmyer, I.R., 1996. Marking time with bivalve shells: oxygen isotopes and season of annualincrement formation. Palaios 11, 340–346.

Lawrimore, J.H., Menne, M.J., Gleason, B.E., Williams, C.N., Wuertz, D.B., Vose, R.S., Rennie, J., 2011. An overview of the Global Historical Climatology Network 25 monthly mean temperature data set, version 3. Journal of Geophysical Research 116, D19121.

Lear, C.H., Elderfield, H., Wilson, P. A, 2000. Cenozoic deep-sea temperatures and global ice volumes from Mg/Ca in benthic foraminiferal calcite. Science 287, 269–272.

Lécuyer, C., Grandjean, P., O'Neil, J.R., Cappetta, H., Martineau, F., 1993. Thermal excursions in the ocean at the Cretaceous - Tertiary boundary (northern Morocco): $\delta^{18}O$ record of phosphatic fish debris. Palaeogeography, Palaeoclimatology, Palaeoecology 105, 235–243.

Lécuyer, C., Grandjean, P., Paris, F., Robardet, M., Robineau, D., 1996. Deciphering "temperature" and "salinity" from biogenic phosphates: the $\delta^{18}O$ of coexisting fishes and mammals of the Middle Miocene sea of western France. Palaeogeography, Palaeoclimatology, Palaeoecology 126, 61–74.

Lefebvre, V., Donnadieu, Y., Goddéris, Y., Fluteau, F., Hubert-Théou, L., 2013. Was the Antarctic glaciation delayed by a high degassing rate during the early Cenozoic? Earth and Planetary Science Letters 372, 203–211.

Longinelli, A., Nuti, S., 1973. Revisited phosphate-water isotopic temperature scale. Earth and Planetary Science Letters 19, 373–376.

Louise Chilvers, B., Delean, S., Gales, N.J., Holley, D.K., Lawler, I.R., Marsh, H., Preen, A.R., 2004. Diving behaviour of dugongs, *Dugong dugon*. Journal of Experimental Marine Biology and Ecology 304, 203–224.

Machel, H.G., Mason, R.A., Mariano, A.N., Mucci, A., 1991. Causes and emission of luminescence in calcite and dolomite. In: Barker, C.E., Kopp, O.C., (Eds.): Luminescence microscopy and spectroscopy: qualitative and quantitative applications. Society of Economic Paleontologists and Mineralogists (SEPM) Short Course, Tulsa, Oklahoma, USA, 25, pp. 9–173.

Major, R.P., 1991. Cathodoluminescence in post-Miocene carbonates. In: Barker, C.E., Kopp, O.C., (Eds.): Luminescence microscopy and spectroscopy: qualitative and quantitative applications. Society of Economic Paleontologists and Mineralogists (SEPM) Short Course, Tulsa, Oklahoma, USA, 25, 149–155.

Marshall, J., Kushnir, Y., Battisti, D., Chang, P., Czaja, A., Dickson, R., Hurrell, J. W., McCartney, M., Saravanan, R., Visbeck, M., 2001. North Atlantic climate variability: phenomena, impacts and mechanisms. International Journal of Climatology 21, 1863–1898.

Martini, E., 1982. Bestandsaufnahme des Nannoplankton im "prä-aquitanen" Tertiär des Mainzer Beckens. Mainzer geowissenschaftliche Mitteilungen 10, 29–36.

Martini, E., Müller, C., 1971. Das marine Alttertiär in Deutschland und seine Einordnung in die Standard Nannoplankton Zonen. Erdol und Kohle 24, 381–384.

Miller, K.G., Kominz, M.A., Browning, J.V, Wright, J.D., Mountain, G.S., Katz, M.E., Sugarman, P.J., Cramer, B.S., Christie-Blick, N., Pekar, S.F., 2005. The Phanerozoic record of global sea-level change. Science 310, 1293–1298.

Mosbrugger, V., Utescher, T., Dilcher, D.L., 2005. Cenozoic continental climatic evolution of Central Europe. Proceedings of the National Academy of Sciences 102, 14964–14969.

O´Neil, J.R., Roe, L.J., Reinhard, E., Blakes, R.E., 1994. A rapid and precise method of oxygen isotope analysis of biogenic phosphate. Israel Journal of Earth Science 43, 203–212.

Ottersen, G., Planque, B., Belgrano, A., Post, E., Reid, P., Stenseth, N., 2001. Ecological effects of the North Atlantic Oscillation. Oecologia 128, 1–14.

Paillard, D., Labeyrie, L., Yiou, P., 1996. Macintosh program performs time-series analysis. Eos Transaction of the American Geophysical Union 77, 379.

Pälike, H., Norris, R.D., Herrle, J.O., Wilson, P.A., Coxall, H.K., Lear, C.H., Shackleton, N.J., Tripati, A.K., Wade, B.S., 2006. The heartbeat of the Oligocene climate system. Science 314, 1894–1898.

Peharda, M., Crnčević, M., Bušelić, I., Richardson, C.A., Ezgeta-Balić, D., 2012. Growth and longevity of *Glycymeris nummaria* (Linnaeus, 1758) from the Eastern Adriatic, Croatia. Journal of Shellfish Research 31, 947–950.

Pellegrini, M., Lee-Thorp, J.A., Donahue, R.E., 2011. Exploring the variation of the $\delta^{18}O_p$ and $\delta^{18}O_c$ relationship in enamel increments. Palaeogeography, Palaeoclimatology, Palaeoecology 310, 71–83, 2011.

Picot, L., 2002. Le Paléogène des synclinaux du Jura et de la bordure sud-rhénane: paléontologie (Ostracodes), paléoécologie, biostratigraphie, paléogéographie. Geofocus 5, 1–240.

Pross, J., 1997. Aquatische Palynomorphe im Rupel des Mainzer Beckens (Oligozän, Südwestdeutschland): Paläoökologie, Biostratigraphie und Taxonomie. Tübinger Mikropaläontologische Mitteilungen 15, 1-181.

Pross, J., 2001. Paleo-oxygenation in Tertiary epeiric seas: evidence from dinoflagellate cysts. Palaeogeography, Palaeoclimatology, Palaeoecology 166, 369–381.

Pross, J., Schmiedl, G., 2002. Early Oligocene dinoflagellate cysts from the Upper Rhine Graben (SW Germany): paleoenvironmental and paleoclimatic implications. Marine Micropaleontology 45, 1–24.

Pross, J., Bruch, A., Mosbrugger, V., Kvacek, Z., 2000. Paleogene pollen and spores as a tool for quantitative paleoclimate reconstructions: the Rupelian (Oligocene) of Central Europe. Proceedings of the Ninth International Palynological Congress, Texas, USA, 1996, 23–28 June 1996, American Association of Stratigraphic Palynologists Foundation, pp. 299–310.

Pross, J., Bruch, A., Kvaček, Z., 1998. Paläoklima-Rekonstruktionen für den Mittleren Rupelton (Unter-Oligozän) des Mainzer Beckens auf der Basis mikro-und makrobotanischer Befunde. Mainzer Geowissenschafliche Mitteilungen 27, 79–92.

Putnis, A., Putnis, C.V., 2007. The mechanism of reequilibration of solids in the presence of a fluid phase. Journal of Solid State Chemistry 180, 1783–1786.

Ramsay, K., Kaiser, M., Richardson, C., Veale, L., Brand, A., 2000. Can shell scars on dog cockles (*Glycymeris glycymeris* L.) be used as an indicator of fishing disturbance? Journal of Sea Research 43, 167–176.

Raper, S.C.B., Braithwaite, R.J., 2006. Low sea level rise projections from mountain glaciers and icecaps under global warming. Nature 439, 311–313.

Ritzkowski, S., 2005. Das Tertiär der Hessischen Senke in der Stratigraphischen Tabelle von Deutschland 2002. Newsletters on Stratigraphy 41, 339–346.

Rombouts, I., Beaugrand, G., Dauvin, J.-C., 2012. Potential changes in benthic macrofaunal distributions from the English Channel simulated under climate change scenarios. Estuarine and Coastal Shelf Science 99, 153–161.

Ropes, J.W., 1985. Modern methods used to age oceanic bivalves. Nautilus 99, 53–57.

Royer, C., Thébault, J., Chauvaud, L., Olivier, F., 2013. Structural analysis and paleoenvironmental potential of dog cockle shells (*Glycymeris glycymeris*) in Brittany, northwest France. Palaeogeography, Palaeoclimatology, Palaeoecology 373, 123–132.

Sato, S., 1995. Spawning periodicity and shell microgrowth patterns of the venerid bivalve *Phacosoma japonicum* (Reeve, 1850). Veliger 38, 61–72.

Schindler, T., Poschmann, M., Wuttke, M., 2005. Chondrichthyan feeding depressions in a subtidal coastal environment from the Mainz Basin (Oligocene, SW Germany), Neues Jahrbuch für Geologie und Paläontologie, Abhandlungen 237, 29–39.

Schöne, B.R., Goodwin, D.H., Flessa, K.W., Dettman, D.L., Roopnarine, P.D., 2002. Sclerochronology and growth of the bivalve mollusks *Chione* (*Chionista*) *fluctifraga* and *C.* (*Chionista*) *cortezi* in the northern Gulf of California, Mexico. Veliger 45, 45–54.

Schöne, B.R., Freyre Castro, A.D., Fiebig, J., Houk, S.D., Oschmann, W., Kröncke, I., 2004. Sea surface water temperatures over the period 1884-1983 reconstructed from oxygen isotope ratios of a bivalve mollusk shell (*Arctica islandica*, southern North Sea). Palaeogeography, Palaeoclimatology, Palaeoecology 212, 215–232.

Schöne, B.R., Dunca, E., Fiebig, J., Pfeiffer, M., 2005a. Mutvei's solution: an ideal agent for resolving microgrowth structures of biogenic carbonates. Palaeogeography, Palaeoclimatology, Palaeoecology 228, 149–166.

Schöne, B.R., Houk, S.D., Freyre Castro, A.D., Fiebig, J., Oschmann, W., Kroncke, I., Dreyer, W., Gosselck, F., 2005b. Daily growth rates in shells of *Arctica islandica*: assessing sub-seasonal environmental controls on a long-lived bivalve mollusk. Palaios 20, 78–92.

Schöne, B.R., Fiebig, J., 2008. Seasonality in the North Sea during the Allerød and Late Medieval Climate Optimum using bivalve sclerochronology. International Journal of Earth Science 98, 83–98.

Sissingh, W., 2003. Tertiary paleogeographic and tectonostratigraphic evolution of the Rhenish Triple Junction. Palaeogeography, Palaeoclimatology, Palaeoecology 196, 229–263.

Solomon, S., Qin, D., Manning, M., Chen, Z., Marquis, M., Averyt, K.B., Tignor, M., Miller, H.L., 2007. Contribution of Working Group I to the Fourth Assessment Report of the Intergovernmental Panel on Climate Change, 2007, Cambridge University Press, Cambridge, UK and New York, NY, USA, 996 pp.

Spiegel, C., Kuhlemann, J., Frisch, W., 2007. Tracing sediment pathways by zircon fission track analysis: Oligocene marine connections in Central Europe. International Journal of Earth Science 96, 363–374.

Stenseth, N.C., Mysterud, A., Ottersen, G., Hurrell, J.W., Chan, K.-S., Lima, M., 2002. Ecological effects of climate fluctuations. Science 297, 1292–1296.

Strom, A., Francis, R.C., Mantua, N.J, Miles, E.L., Peterson, D.L., 2004. North Pacific climate recorded in growth rings of geoduck clams: a new tool for paleoenvironmental reconstruction, Geophysical Research Letters 31, L06206.

Taylor, J.D., Layman, M., 1972. The mechanical properties of bivalve (Mollusca) shell structures. Palaeontology 15, 73–87.

Thewissen, J.G.M., Cooper, L.N., Clementz, M.T., Bajpai, S., Tiwari, B.N., 2007. Whales originated from aquatic artiodactyls in the Eocene epoch of India. Nature 450, 1190–1194.

Thomas, R.D.K., 1975. Functional morphology, ecology, and evolutionary conservatism in the Glycymerididae (Bivalvia). Palaeontology 18, 217–254.

Thomas, R.D.K., 1978. Shell form and the ecological range of living and extinct Arcoida. Paleobiology 4, 181–194.

Tsuboi, C., Hirata, M., 1935. Arrangement of micro-crystals of calcium carbonate in some fossil shells, *Glycymeris yessoensis* SOWERBY. Bulletin of the Earthquake Research Institute of Tokio 13, 660–664.

Tütken, T., 2003. Die Bedeutung der Knochenfrühdiagenese für die Erhaltungsfähigkeit in vivo erworbener Element- und Isotopenzusammensetzungen in fossilen Knochen. Doctoral thesis, Eberhard-Karls-Universität Tübingen, pp. 331.

Tütken, T., Vennemann, T.W., Janz, H., Heizmann, E.P.J., 2006. Palaeoenvironment and palaeoclimate of the Middle Miocene lake in the Steinheim basin, SW Germany: a

reconstruction from C, O, and Sr isotopes of fossil remains. Palaeogeography, Palaeoclimatology, Palaeoecology 241, 457–491.

Vellinga, M., Wood, R.A., 2002. Global climatic impact of a collapse of the Atlantic thermohaline circulation. Climatic Changes 54, 251–267.

Vennemann, T.W., Fricke, H.C., Blake, R.E., Neil, J.R.O., Colman, A., 2002. Oxygen isotope analysis of phosphates: a comparison of techniques for analysis of Ag_3PO_4. Chemical Geology 185, 321–336.

Waller, T.R., 1980. Scanning electron microscopy of shell and mantle in the order Arcoida (Mollusca: Bivalvia). Smithsonian Contributions to Zoology 313, 1–58.

Wanamaker Jr., A.D., Kreutz, K.J., Schöne, B.R., Introne, D.S., 2011. Gulf of Maine shells reveal changes in seawater temperature seasonality during the medieval climate anomaly and the Little Ice Age. Palaeogeography, Palaeoclimatology, Palaeoecology 302, 43–51.

Zachos, J.C., Dickens, G.R., Zeebe, R.E., 2008. An early Cenozoic perspective on greenhouse warming and carbon-cycle dynamics. Nature 451, 279–283.

MANUSCRIPT II

Response of Central European SST to atmospheric pCO_2 forcing during the Oligocene - a combined proxy data and numerical climate model approach

Published in Palaeogeography, Palaeoclimatology, Palaeoecology

Walliser, E.O.[1], Lohmann, G.[2], Niezgodzki I.[2, 3], Tütken, T.[1] & Schöne, B.R.[1]

[1] Institute of Geosciences, University of Mainz, Johann-Joachim-Becher-Weg 21, 55128 Mainz, Germany

[2] Alfred Wegener Institute Helmholtz Centre for Polar and Marine Research, Am Alten Hafen 26, 27568 Bremerhaven, Germany

[3] ING PAN - Institute Of Geological Sciences Polish Academy of Sciences, Research Center in Kraków, Senacka 1, 31-002, Kraków, Poland

Contribution:

Concept: EOW, BRS

Writing: EOW, BRS

Oxygen isotope analysis EOW (bivalves), TT (sharks)

Numerical climate models: GL, IN

Walliser, E.O., Lohmann, G., Niezgodzki, I., Tütken, T., Schöne, B.R., 2016. Response of Central European SST to atmospheric pCO_2 forcing during the Oligocene - a combined proxy data and numerical climate model approach. Palaeogeography, Palaeoclimatology, Palaeoecology 459, 552–569.

Abstract

CO_2-induced global warming will affect seasonal to decadal temperature patterns. Expected changes will be particularly strong in extratropical regions where temperatures will increase at faster rates than at lower latitudes. Despite that, it is still poorly constrained how precisely short-term climate dynamics will change in a generally warmer world, particularly in nearshore surface waters in the extratropics, i.e., the ecologically most productive regions of the ocean on which many human societies depend. Specifically, a detailed knowledge of the relationship between pCO_2 and seasonal SST is crucial to understand interactions between the ocean and the atmosphere. In the present investigation, we have studied for the first time how rising atmospheric pCO_2 levels forced surface temperature changes in Central Europe (paleolatitude ~45 °N) during the mid-Oligocene (from ca. 31 to 25 Ma), a time interval of Earth history during which global conditions were comparable to those predicted for the next few centuries. For this purpose, we computed numerical climate models for the Oligocene (winter, summer, annual average) assuming an atmospheric carbon dioxide rise from 400 to 560 ppm (current level to two times pre-industrial levels, PAL) and from 400 to 840 ppm (= three times PAL), respectively. These models were compared to seasonally resolved sea surface temperatures (SST) reconstructed from $\delta^{18}O$ values of fossil bivalve shells (*Glycymeris planicostalis, G. obovata, Palliolum pictum, Arctica islandica* and *Isognomon maxillata sandbergeri*) and shark teeth (*Carcharias cuspidata, C. acutissima* and *Physogaleus latus*) collected from the shallow water deposits of the Mainz and Kassel Basins (Germany). Multi-taxon oxygen isotope-based reconstructions suggest a gradual rise of temperatures in surface waters (upper 30 to 40 m), on average, by as much as 4 °C during the Rupelian stage followed by a 4 °C cooling during the Chattian stage. Seasonal temperature amplitudes increased by ca. 2 °C during the warmest time interval of the Rupelian stage, with warming being more pronounced during summer (5 °C) than during winter (3 °C). According to numerical climate simulations, the warming of surface waters during the early Oligocene required a CO_2 increase by at least 160 ppm, i.e., 400 ppm to 560 ppm. Given that atmospheric carbon dioxide levels predicted for the near future will likely exceed this value significantly, the Early Oligocene warming gives a hint of the possible future climate in Central Europe under elevated CO_2 levels.

Keywords

Sea surface temperature; oxygen isotopes; sclerochronology; bivalve shell; shark tooth; global warming.

Research highlights

(1) Oligocene SST was estimated from $\delta^{18}O$ of bivalve shells and shark teeth.

(2) 4 °C SST warming during the Rupelian, 4 °C cooling during the Chattian stage.

(3) Seasonal amplitudes increased from 9 to 11 °C during the late Rupelian stage.

(4) Late Rupelian warming required pCO_2 increase by at least 160 ppm.

1. Introduction

Unabated CO_2 emissions will result in atmospheric concentrations of this greenhouse gas of over 900 ppm by the end of the current century (Collins et al., 2013) and up to 1,800 ppm 300 years later (Zachos et al., 2008). In this scenario, surface temperatures are expected to increase significantly, specifically at higher latitudes, causing polar ice to melt and eventually disappear (e.g., Körper et al., 2013). Reduced meridional temperature gradients will lead to substantially different circulation patterns (e.g., Cai and Chu, 1998; Hansen et al., 2004) with major repercussions on seasonal to multi-annual climate dynamics (e.g., Marshall et al., 2001; Solomon et al., 2007), i.e., within the time-scales of human perception.

Despite the relevance for human societies and the global economy, it is still not well constrained how short-term climate variability will change in a generally warmer world (e.g., Collins et al., 2010). For example, will summers become hotter and winters colder, and how much for a given atmospheric pCO_2? How will seasonal temperature amplitudes change in nearshore surface waters? These settings are the ecologically most productive regions of the ocean on which many human societies depend, and they are particularly sensitive to short-term climate fluctuations, because of their low water-mass inertia and shallow water depth. Such questions can be addressed by studying past climates during which boundary conditions were broadly similar to those today and predicted for the near future. For this purpose, the Oligocene epoch serves as a suitable candidate. The distribution of land and sea was comparable to the present-day situation (e.g., Scotese et al., 1988; Rögl, 1999). During the early Oligocene, CO_2 levels and surface temperatures were slightly higher than in modern times (Hendriks and Pagani, 2008; Cramer et al., 2011). Although this time interval could help us to obtain a better perspective on future, anthropogenically forced climates, our knowledge on seasonality during the Oligocene and its relationship with pCO_2 is extremely limited.

Atmospheric pCO_2 levels of the Oligocene have been inferred from $\delta^{13}C$ values of sedimentary biomarkers such as algal alkenones (e.g., Pagani et al., 2005; Hendriks and Pagani, 2008; Zhang et al., 2013), boron isotopes of foraminiferan tests (e.g., Pearson et al., 2009; Raitzsch and Hönisch, 2013) and stomatal density of fossil leaves (e.g., Retallack, 2001; Roth-Nebelsick et al., 2012). Based on data recorded in these archives, atmospheric pCO_2 oscillated between ca. 200 and ca. 1000 ppm. However, these reconstructions come with large uncertainties (Royer and

Beerling, 2011). Likewise, numerical modeling does not provide more precise estimates and suggests that atmospheric pCO_2 may have fluctuated between ca. 300 ppm and ca. 800 ppm, i.e., the threshold of the northern and southern hemisphere polar glaciations, respectively (DeConto and Pollard, 2003; Pollard and DeConto, 2005; DeConto et al., 2008).

The great majority of existing Oligocene temperature reconstructions are based on geochemical records preserved in biogenic archives of the deep sea. For example, the $\delta^{18}O$ signature of deep-sea benthic foraminifera ($\delta^{18}O_{BF}$) has been used to track long-term climate trends (e.g. Miller et al., 1991; Zachos et al., 2001; Pekar et al., 2002; Wade and Pälike, 2004; Pälike et al., 2006). Information on how temperature fluctuated on shorter time-scales is largely limited to air temperatures. According to Pross et al. (1998, 2000), seasonal air temperatures in Central Europe during the late Rupelian oscillated between 7 and 10 °C in winter, and 26 and 28 °C in summer. These values agree well with the air temperature data (5 to 26 °C; average: 16 - 17 °C) provided by Mosbrugger et al. (2005) and Erdei et al. (2012). However, seasonally resolved temperature data from surface ocean waters is virtually absent. The $\delta^{18}O$ values of shark teeth (Tütken, 2003) and foraminiferan tests (Grimm, 1994) yield temperature ranges of 12 to 22 °C in surface waters, and 6 to 15 °C in settings below the thermocline (ca. 150 m; Grimm et al., 2011). More recently, Walliser et al. (2015) demonstrated for the first time that $\delta^{18}O$ values of well-preserved bivalve shells from the Rhenish triple junction (Central European epicontinental seaway) can provide subseasonally resolved records of temperature that prevailed in surface waters at mid-latitudes during the Early Oligocene. Up until now, has not been resolved how seasonal temperatures in surface waters evolved during the Oligocene.

Inspired by the proof-of-concept study by Walliser et al. (2015), we investigated how seasonal sea surface temperatures (SST) in central Europe changed during selected time slices of the Rupelian and Chattian stages. Reconstructions were based on $\delta^{18}O$ values of well-preserved shells of five different bivalve species (*Glycymeris planicostalis, G. obovata, Arctica islandica, Isognomon maxillata sandbergeri* and *Palliolum pictum*), together with information on their growth patterns, as well as shark teeth. Fossils came from shallow marine sediments of the Rhenish triple junction, i.e., the Mainz and Kassel Basins. Furthermore, numerical climate models were computed to estimate how winter, summer and average Oligocene SST change when atmospheric pCO_2 increases from 400 ppm to 560 ppm (= 2 x PAL, preindustrial atmospheric level) and 840 ppm (3 x PAL), respectively. These data were then compared to proxy-based SST reconstructions

in order to further constrain Oligocene atmospheric pCO_2 levels. A detailed knowledge of the relationship between pCO_2 and seasonal SST is crucial to understand interactions between the ocean and the atmosphere.

2. Geological setting, material and methods

2.1. Geological setting

The Mainz Basin and the Kassel Basin are located at the northwestern margin of the Upper Rhine Graben and the central part of the Hesse Depression (Fig. 1A), respectively. Their formation is associated with the taphrogenesis of the European Cenozoic Rift System (Sissingh, 2003; Dèzes et al., 2004). Due to their geographical vicinity and the absence of major tectonic boundaries between them, the two basins experienced similar sedimentary histories which encompass marine, brackish and terrestrial deposits covering a time interval of ca. 20 Ma (Lower Eocene to Early Miocene; Grimm et al., 2011; Ritzkowski et al., 2011). During the Oligocene, repeated marine transgressions occurred from the north (Berger et al., 2005a, b) which were caused by local subsidence and eustatic sea level rise (Fig. 1B-D). As a consequence, the Mainz Basin and Kassel Basin became part of an intracontinental marine strait that extended from the paleo-North Sea to the Alpine Belt (Picot, 2002; Berger et al., 2005a) (Fig. 1B). The largest marine ingression took place during the upper Rupelian stage (Fig. 1C), i.e., between sea-level high stand Ru2/Ru3 (~32 Ma) and Ru3/Ru4 (~29.5 Ma) of Haq et al. (1988). It possibly resulted in a (temporary) connection of the southern Upper Rhine Graben (URG) system with the western Molasse Basin (Martini 1982; Picot, 2002; Berger et al., 2005a, b; Grimm, 2006). In the Mainz Basin, this marine phase is represented by nearshore, coarse-grained siliciclastic deposits of the Alzey Formation and coeval basinal pelites of the Bodenheim Formation as well as the overlying clays and fine sands of the Stadecken Formation (Grimm et al., 2000; Berger et al., 2005b; Grimm et al., 2011). The studied bivalve shells originate from sediments of the Alzey Formation and the Stadecken Formation (Albig Bank) (Figs. 1D and 2).

Age control of the nearshore strata of the Alzey Formation is mainly based on the correlation with basinal pelites of the Bodenheim Formation (Grimm et al., 2000). Age control of the latter is largely based on calcareous nanoplankton (Martini and Müller, 1971; Grimm et al.,

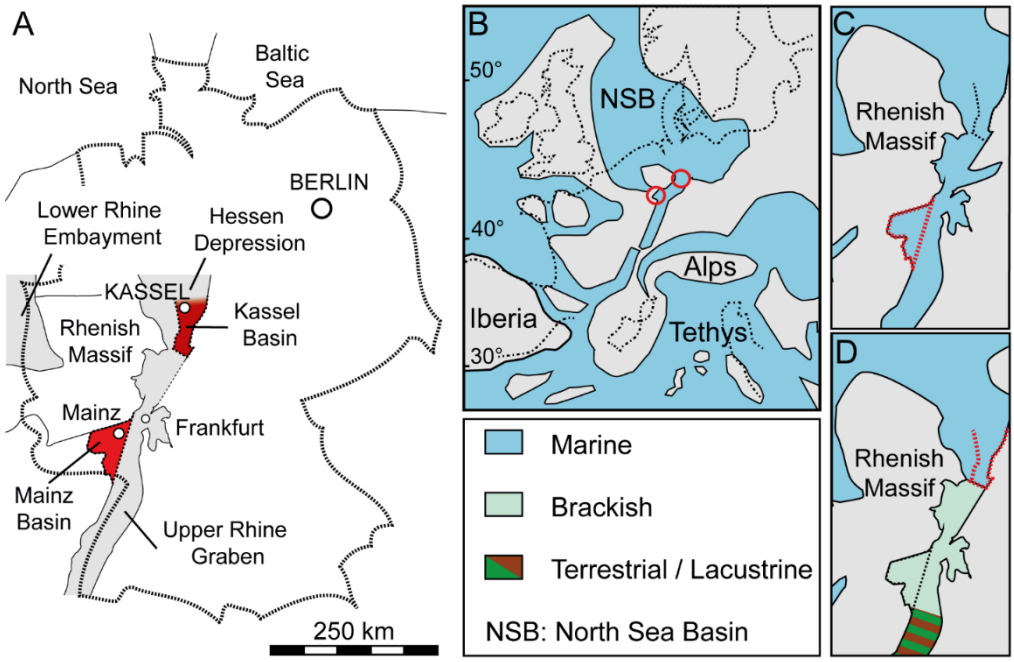

Figure 1. Map showing the position of the Mainz Basin and the Kassel Basin in Germany and their stratigraphic and paleogeographic position during the Oligocence. (A) The Mainz Basin and the Kassel Basin are marked in red, whereas the grey shadow represents the extension of the Rhenish Triple Junction formed by the Upper Rhine Graben, the Hesse Depression and the Lower Rhine Embayment (modified after Sissingh, 2003). (B) Paleogeographic position of the Mainz and Kassel Basins in Central Europe during the Oligocene (red circles). (C and D) Distribution of the prevailing lithofacies within the studied areas (C: Rupelian; D: Chattian).

2005), dinoflagellate cysts (Pross, 2001; Grimm et al., 2005) and to a lesser extent, benthic foraminifera (Grimm, 1998, 2002) (Fig. 2). With regard to the nanoplankton zonation, the Alzey Formation comprises the upper part of NP23 and the lower part of NP24 (Grimm, 1994; Berger et al., 2005b). Furthermore, the presence of the benthic foraminiferan, *Turrilina alsatica* in the lowermost deposits of the Bodenheim Formation (Grimm et al., 2000, 2011) places the onset of fully marine sedimentation in the Mainz Basin within the benthic foraminifera zone NSR 7b (Hardenbol et al., 1998) (Fig. 2). Thus, the lower boundary of the Alzey Formation falls about in the middle of the nanoplankton zone NP23 (Grimm et al., 2011). Based on benthic foraminiferan associations, the Alzey Formation can be subdivided into a lower *Planorbulina difformis* - *Cibicides lobatus* Abundance Zone (here referred to as lower Alzey Formation) belonging to NP23, and an upper Miliolid Abundance Zone (here referred to as upper Alzey Formation) which comprises the upper part of NP23 and the lower part of NP24 (Grimm, 1998; Grimm, 2002).

Numerical $^{87}Sr/^{86}Sr$ dating performed on a well-preserved bivalve shell collected from the Miliolid Zone yielded an age of 30.1 ± 0.1 Ma (Grimm et al., 2003).

The overlying deposits of the Stadecken Formation belong exclusively to the nanoplankton zone NP24 (Martini and Müller, 1971; Grimm et al., 2005, 2011) and are capped by a wide-spread tempestite horizon (the so-called Albig Bank) which comprises the lower part of the *Chara microcera* zone (Grimm et al., 2000). The upper boundary of the Stadecken Formation is delimited by the onset of the brackish facies of the overlying Sulzheim Formation (Grimm et al., 2005) which comprises in its lowermost part the fossil mammal assemblages belonging to the Paleogene mammal zone MP24 (Bahlo, 1976; Bahlo and Neuffer, 1978; Bahlo and Tobien, 1982). Accordingly, the deposition of the Albig Bank probably occurred during a relatively short (several hundred thousand years) time interval after the onset of the *Chara microcera* zone and before the onset of MP25 (Fig. 2).

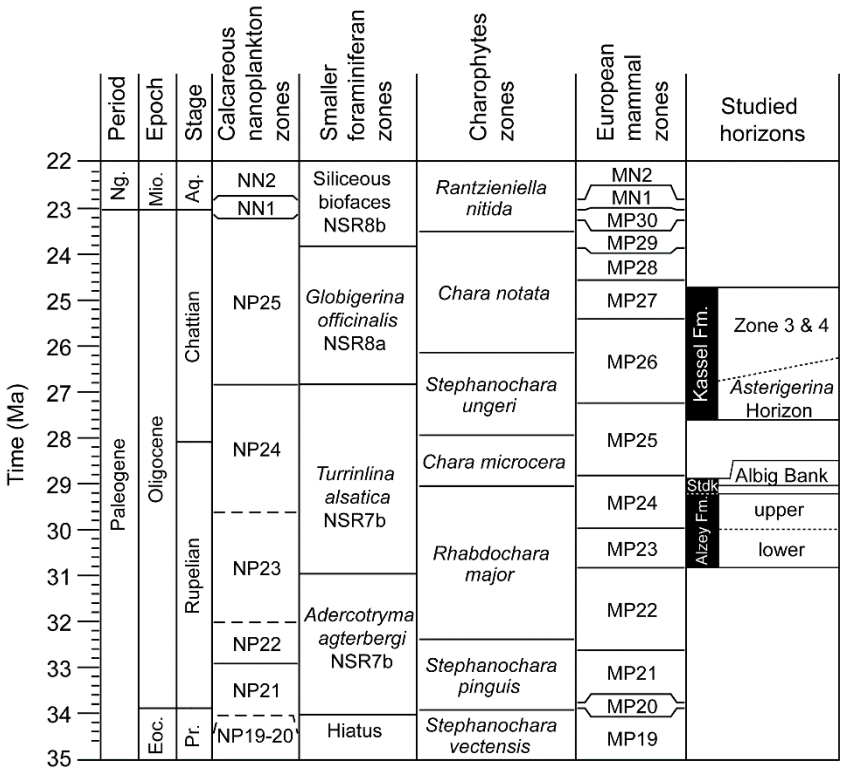

Figure 2. (B) Age model applied in this study (Gradstein et al., 2012) and the stratigraphic position of the studied horizons. Startigraphic chart was produced using TSCreator software (available at: http://www.tscreator.org). Smaller foraminiferan zonation was from Hardenbol et al. (1998) and Grimm (2002). Stdk = Stadecken Formation.

Table 1. Oxygen isotope values (raw: δ^{18}Oshell; re-sampled: $\delta^{18}O_{R\text{-}shell}$; explanation see text) of the bivalve shells analyzed in this study (* = data from Walliser et al., 2015).

Sample ID	Species	Sample locality	Stratigraphy	# full years	# δ^{18}O samples	$\delta^{18}O_{shell}$ min [‰]	$\delta^{18}O_{shell}$ max [‰]	$\delta^{18}O_{shell}$ average ± 1σ [‰]	$\delta^{18}O_{R\text{-}shell}$ min [‰]	$\delta^{18}O_{R\text{-}shell}$ max [‰]	$\delta^{18}O_{R\text{-}shell}$ average ± 1σ [‰]
2009-KS6-D36L	*Glycymeris obovata*	Kassel Wilhelmshöhe	Kassel Formation	7	60	-1.72	1.78	0.20 ± 0.91	-1.31	1.59	0.19 ± 0.82
2009-KS6-D17L	*Glycymeris obovata*	Kassel Wilhelmshöhe	Kassel Formation	11	250	-1.41	2.00	0.52 ± 0.84	-1.25	1.90	0.51 ± 0.77
H1282.1	*Glycymeris obovata*	Brandkopf at Ahne River Valley	Kassel Formation	5	57	-1.50	2.06	0.01 ± 1.01	-1.39	1.64	0.00 ± 0.93
EOW-Iso-Spi-F1X	*Isognomon maxillata sandbergeri*	Sommersee near Spiesheim	Stadecken Formation	-	43	-1.82	-0.10	-0.72 ± 0.40	-	-	-
EOW-Iso-Sul-F1X	*Isognomon maxillata sandbergeri*	Sulzheim	Stadecken Formation	-	38	-1.73	-0.38	-1.09 ± 0.33	-	-	-
EOW-Gly-Alb-1	*Glycymeris planicostalis*	Sommersee near Spiesheim	Stadecken Formation	4	51	-2.79	0.83	-1.07 ± 0.95	-2.46	0.62	-0.91 ± 0.78
EOW-Gly-Alb-2a	*Glycymeris planicostalis*	Sommersee near Spiesheim	Stadecken Formation	2	60	-2.69	0.27	-1.21 ± 0.78	-2.30	-0.14	-1.29 ± 0.73
EOW-Gly-Alb-3	*Glycymeris planicostalis*	Sommersee near Spiesheim	Stadecken Formation	4	44	-3.28	0.47	-1.44 ± 1.08	-3.10	0.36	-1.46 ± 1.01
EOW-Gly-BH-9	*Glycymeris planicostalis*	10 Km NW of Bodenheim	Stadecken Formation	4	42	-3.00	0.58	-0.85 ± 0.91	-2.33	0.45	-0.87 ± 0.82
EOW-Iso-Wht-F1X	*Isognomon maxillata sandbergeri*	"Trift" near Weinheim	Upper Alzey Formation	-	14	-1.39	-0.04	-0.81 ± 0.45	-	-	-
MB-Wht-7*	*Glycymeris planicostalis*	"Trift" near Weinheim	Upper Alzey Formation	10	166	-1-19	0.75	-0.12 ± 0.13	-1.00	0.49	0.00 ± 0.28
MB-Wht-4*	*Glycymeris planicostalis*	"Trift" near Weinheim	Upper Alzey Formation	14	193	-1.16	0.67	-0.03 ± 0.13	-0.98	0.54	-0.20 ± 0.33
MB-Wht-2*	*Glycymeris planicostalis*	"Trift" near Weinheim	Upper Alzey Formation	16	316	-1.48	0.60	-0.20 ± 0.19	-1.01	0.73	-0.08 ±0.38
EOW-Pec-Wöl-F2X	*Palliolum pictum*	Sand pit Müller & Schmidt near Wöllstein	Lower Alzey Formation	1	43	-1.34	0.64	-0.60 ± 0.58	-1.06	0.37	-0.50 ± 0.54
EOW-Iso-Wöl-F1X	*Isognomon maxilata sandbergeri*	Sand pit Müller & Schmidt near Wöllstein	Lower Alzey Formation	-	36	-0.92	0.16	-0.37 ± 0.25	-	-	-
EOW-Arc-Zeil-F1X	*Arctica islandica*	"Zeilstück" near Weinheim	Lower Alzey Formation	1	9	0.79	1.12	0.95 ± 0.13	0.81	1.06	0.94 ± 0.10

Throughout the Chattian stage and early portions of the Miocene, marine ingressions occurred from the paleo-North Sea into the European Cenozoic Rift System (Sissingh, 2003; Ritzkowski et al., 2011). However, marine ingressions were limited to the Hessen Depression and did not reach the URG, where the cessation of fully marine conditions made way for a brackish facies (Fig. 1D) (e.g. Martini 1982; Berger et al., 2005a, b). After the Rupelian/Chattian eustatic sea level drop (Ru4/Ch1; Hardenbol et al., 1998), renewed transgressions from the North Sea Basin entered the Kassel Basin, establishing fully marine conditions that persisted until the latest Chattian (Fig. 1D). Nearshore deposits representing that time comprise the fine sands of the Kassel Formation which correspond to the local stratigraphic stage of the Eochattian (Ritzkowski, 2005). Age control for the marine strata of this formation is mainly based on nanoplankton (Roth, 1970; Martini & Müller, 1971) and benthic foraminifera (Kümmerle 1963; Ritzkowski, 1967). The Kassel Formation encompasses the upper part of NP24 and the lower part of NP25 (Roth, 1970; Martini & Müller, 1971; Ritzkowski et al., 2011).

The NP24/NP25 boundary falls within the German Eochattian substage, between the pectinid units A and B of the Chattian stratotype section at Doberg near Bünde, Germany (Anderson, 1961). The basal unit of the Chattian stratoptype (unit A) is characterized by the bloom of the benthic foraminiferan, *Asterigerinoides guerichi* (Indans, 1965). This horizon (regarded in the literature as "*Asterigerina* Horizon") is also recognized in the Kassel Basin (e.g. Ritzkowski, 2011) and the southern and eastern North Sea Basins (e.g., Van Simaeys et al., 2004; De Man et al., 2010, Śliwińska et al., 2010). Within the Kassel Basin, the *Asterigerina* Horizon corresponds to the deposits of the subunits of the Kassel Formation, zones 1 and 2, as defined by Kümmerle (1963; see also Ritzkowski, 1965). The overlying zone 3 is characterized by the absence of *A. guerichi* and the occurrence of large shell beds which are nearly absent in the other strata (Kümmerle 1963; Ritzkowsi, 1965; 1967). Therefore, the stratigraphic position of the studied Chattian shells can be confidently taken as zone 3 (Fig. 2).

According to De Man et al. (2004), the zone 3 of Kümmerle (1963) is equivalent to the upper part of the biozone X (biofacies 20) of the southern North Sea Basin. According to Vandenberghe et al. (2004), this level corresponds to the second Chattian sequence of Hardenbol et al. (1998), is equivalent to the Chattian B, and falls within the lower part of NP25 (Van Simaeys et al., 2004; De Man et al., 2010). Absolute age dating of biozone X in the southern North Sea Basin revealed ages of 26.1 ± 0.4 and 26.9 ± 0.4 Ma (De Man et al., 2010). These ages agree well with the $^{87}Sr/^{86}Sr$

date of 25.5 ± 0.5 Ma yielded by one shell from Kassel Wilhelmshöhe (unpublished data of the senior author; calculated using the regression curves LOWESS version 5, 26 March 2013, revised version of McArthur et al., 2001). The strata are younger than the *Asterigerina* Horizon which was dated to 26.2 ± 0.5 Ma in northern Germany (Gramann et al., 1980) (Fig. 2).

2.2. Shell Material

In this study, fossil bivalve shells of *G. planicostalis, G. obovata*, *A. islandica, I. maxillata sandbergeri*, and *P. pictum* and teeth of sand tiger sharks, *Carcharias cuspidata*, *C. acutissima* and *Physogaleus latus* from nearshore deposits of the Mainz and Kassel Basins were analyzed (Table 1). These taxa were chosen because their modern representatives commonly inhabit nearshore shallow waters where prevailing environmental conditions are comparable to those of the Mainz and Kassel Basin during the Oligocene. The modern geographical distribution as well as water temperature, salinity and depth ranges for each taxon are listed in Table 2.

Table 2. Estimated ecological ranges (geographical distribution, temperature, salinity and water depth) of the modern representatives of the investigated fossil taxa. Data were compiled from: (a) = Huber (2010); (b) = Siung (1980); (c) = Hall (1985); (d) = Carpenter and Niem (1998); (e) = Gilles (1972); (f) = Nerot et al., (2012); (g) = Crnčević et al. (2013); (h) = Schöne (2013); (i) = Dijkstra et al. (2009); (j) = Dijkstra (2013); (k) = Compagno (2001); (*) = data from the Ocean Biogeographic Information System (OBIS) of the Intergovernmental Oceanographic Commission of UNESCO (available at: http://www.iobis.org; accessed: July 19th, 2016).

Taxon	Distribution	Temperature	Salinity	Water depth
Isognomon	Tropics to subtropical regionsof both hemispheres [a]	25 - 35 °C [b, c]	14 - 36 psu [b]	Littoral to sublittoral, usually not deeper than 20 m [d]
Glycymeris	Tropics to sub-polar regions of both hemispheres [a]	4 - 27 °C [*]	17 - 35 psu [e]	4 - 200 m [f, g]
Arctica islandica	Mid-latitudes and boreal North Atlantic [h]	1 - 16 °C [h]	22 - 35 psu [h]	4 - 500 m [h]
Palliolum	Tropics and boreal North Atlantic [i]	3 - 24 °C [*]	33 - 36 psu [*]	sublittoral to bathyal [i, j]
Carcharias taurus (Sand tiger shark)	Equator to mid-latitudes of both hemispheres [k]	4 - 26 °C [*]	33 - 37 psu [k, *]	Inshore coastal waters 1 - 150 m usually 15 - 25 m [k]

One *G. obovata* specimen (ID: H1282.1) and the shark teeth from the Kassel Basin were kindly provided by Dr. Cornelia Kurz, Museum of Natural History, Kassel (Germany). All remaining shell samples came from the paleontological collection of the Institute of Geosciences, University of Mainz (Germany). Furthermore, 38 teeth of *Carcharias* spp. were obtained from collections of the Museum of Natural History, Mainz and the Institute of Geosciences, University of Mainz (for details see Table 1).

2.3. Shell preparation

In order to optimize the sampling for the oxygen isotope analysis, the specimens underwent different preparation procedures depending on the morphological characteristics of the shells. The large, thick-shelled *Glycymeris* spp. and *A. islandica* specimens were mounted on Plexiglas cubes with Gluetec Multipower plastic welder and coated along the axis of maximum growth with a WIKO metal epoxy resin, to avoid breakage during sectioning. From the axial zone, two 3 mm-thick slabs were cut using a low-speed (225 rpm) precision saw (Buehler Isomet 1000) equipped with a 0.4 mm diamond-coated blade (Fig. 3A). Both slabs were glued to glass slides with the mirroring sides facing up, ground on glass plates (320, 800, 1200 grit SiC powder) and polished with 1 µm Al_2O_3 powder. After each preparation step, samples were ultrasonically rinsed in deionized water. Subsequently, carbonate powder was taken from the outer layer in the ontogenetically younger shell portion (Fig. 3B). Powder samples from the thin-shelled *P. pictum* specimen were taken from the outer shell surface (Fig. 3C). To avoid sampling of potentially diagenetically altered shell material, several hundred µm of the outer shell surface were physically removed prior to the actual sampling. Carbonate powder was obtained from the central plica by drilling (Fig. 3D). *I. maxillata sandbergeri* specimens consisted of large umbonal fragments (aragonite), whereas the main valve was only partially preserved (Fig. 4A). Therefore, the collection of powder samples for stable isotope analysis was performed in the hinge plate. For this purpose, the hinge plates were ground down until ligament pits were evenly reduced (Fig. 4B). The resulting surface was then polished and subsequently sampled by drilling for oxygen isotope analysis (Fig. 4C).

For all studied shells, powder samples (50-120 µg) were obtained with a Rexim Minimo dental drill mounted to a stereomicroscope and equipped with a 300 µm diameter conical bit

(drilling) or a 1 mm diameter cylindrical diamond coated bit (milling) (Gebr. Brasseler GmbH & Co. KG, model numbers H52 104 003 and 835 104 010).

To ensure that the seasonal extremes were properly sampled, the required sampling resolution was identified in test series during which the spatial sampling resolution was gradually increased. The optimal sampling resolution was attained as soon as a more detailed sampling did not result in higher or lower $\delta^{18}O$ values.

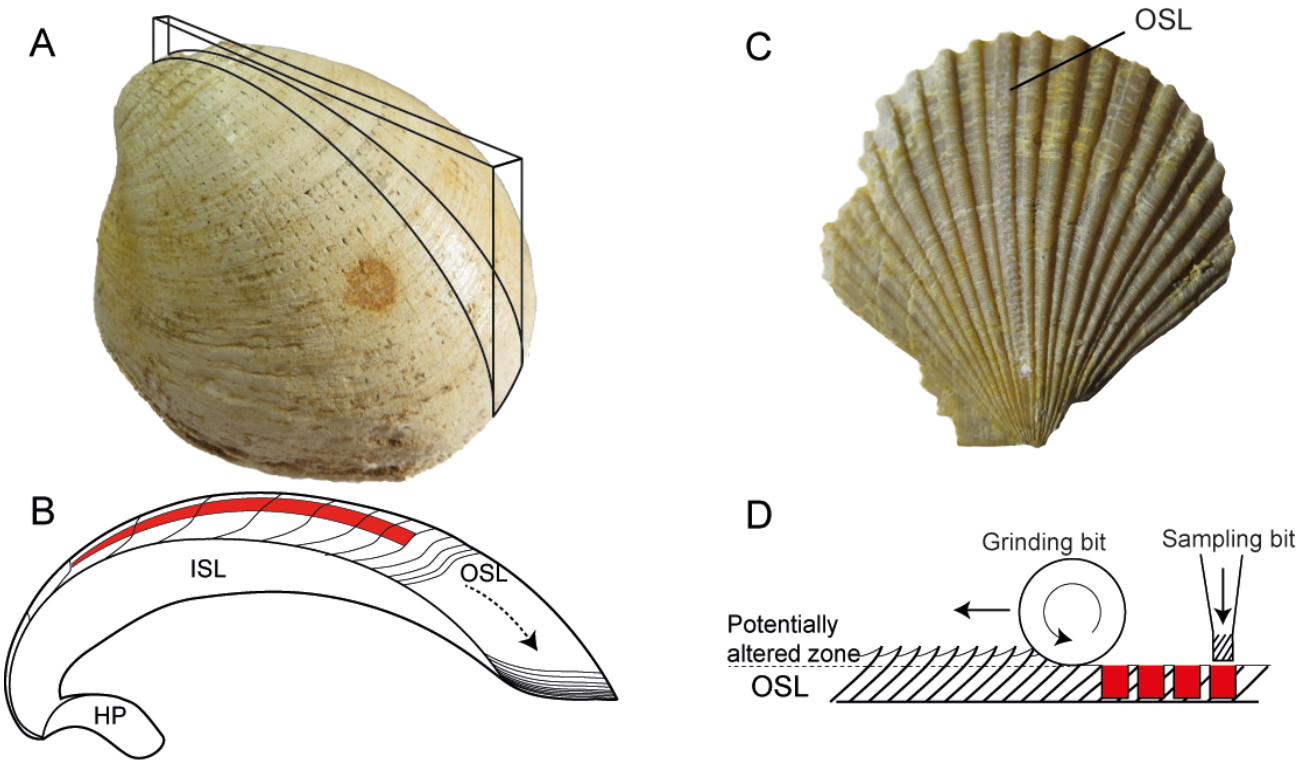

Figure 3. Preparation of *Glycymeris* spp., *Arctica islandica* and *Palliolum pictum* shells. (A) Valves of *Glycymeris spp.* and *A. islandica* (not shown in the figure) were cut along the axis of maximum growth, and carbonate powder samples were collected (by drilling and milling) from the outer shell layer (B). (C) In *P. pictum*, powder samples were drilled from the outer shell surface by drilling (D) after physical removal of the outermost shell surface. Red = sampled shell portion; ISL = inner shell layer; OSL = outer shell layer; HP = hinge plate.

2.4. Diagenesis screening of the bivalve shells and shark teeth

All fossil bivalve shells were tested with a set of different techniques (cathodoluminescence, Raman spectroscopy, immersion in Feigl´s solution, scanning electron microscopy) for possible diagenetic overprint that could have altered the pristine oxygen isotope signals. If the criteria defined in Walliser et al. (2015) were met, the studied material was considered well-preserved and suitable for further geochemical analysis. The phosphate of enamel apatite as in shark teeth is particularly resistant against diagenetic alteration and thus considered suitable for oxygen isotope studies (e.g., Vennemann et al., 2001; Fisher et al., 2013). Tooth material from the Mainz and Kassel Basins did not reveal any macroscopic differences with respect to the state of preservation. Furthermore, scanning electron microscopy analyses of selected samples confirmed the pristine preservation of the tooth enamel and dentine microstructures.

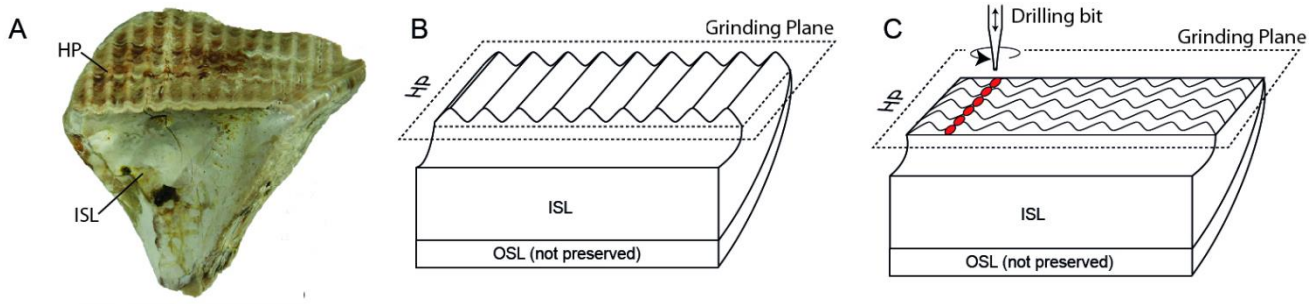

Figure 4. Preparation of *Isognomon maxillata sandbergeri* shells. (A) Studied specimens consisted of large umbonal fragments. (B) Ligament areas were ground parallel to the plane of the hinge line. (C) Afterward, carbonate powder samples were collected by drilling from the hinge plate. Red: sampled shell portion; ISL = inner shell layer; OSL = outer shell layer; HP = hinge plate.

2.5. $\delta^{18}O_{shell}$ data

For oxygen isotope analysis, shell powder samples (n = 1422, Table 1) were dissolved with concentrated phosphoric acid in helium-flushed borosilicate glass exetainers at 72 °C (2 h reaction time) and the liberated CO_2 gas processed in a Thermo Finnigan MAT 253 continuous flow - isotope ratio mass spectrometer coupled to a GasBench II (Institute of Geosciences, University of Mainz). Isotope data were calibrated against an NBS-19 calibrated Carrara marble ($\delta^{13}C = 2.01$ ‰;

$\delta^{18}O$ = -1.91 ‰; distributed by IVA-Analysentechnik e.K., Germany). On average, accuracy (external reproducibility) and internal precision (1σ) of $\delta^{13}C$ and $\delta^{18}O$ values were better than 0.05 ‰ and 0.05 ‰, respectively. The results are expressed in δ-notation and given as parts per mil (‰) with respect to the Vienna Pee Dee belemnite (VPDB) standard.

The $\delta^{18}O$ values of shell aragonite were not adjusted for differences in acid fractionation factors of aragonite and calcite. Using the acid fractionation factors of Kim et al. (2007) for a reaction temperature of 72 °C, actual $\delta^{18}O$ values of aragonite would be 0.38 ‰ more negative than reported here. However, this correction was not applied, because we used paleotemperature equations (Grossman and Ku, 1986; Royer et al., 2013) that assumed no differences in acid fractionation factors for the two $CaCO_3$ polymorphs. These equations do not consider temperature-induced changes of the acid fractionation factors. Grossman and Ku (1986) reacted their carbonate samples at 50 and 60 °C and, accordingly, their $\delta^{18}O$ values of aragonite would require a correction by only -0.34 ‰ and -0.36 ‰, respectively (using acid fractionation factors from Kim et al, 2007). In order to compute temperatures with the equation of Grossman & Ku (1986), $\delta^{18}O$ values of aragonite processed at 72 °C would therefore require a correction of -0.02 to -0.04 ‰. Since this difference is smaller than the precision uncertainty of the mass spectrometer (see below), our data were not adjusted.

Since bivalves form their shell near oxygen isotopic equilibrium with the ambient water (e.g., Mook, 1971), shell $\delta^{18}O$ values can be used to reconstruct ancient water temperature in which the animals grew. The literature provides several paleothermometry equations which were empirically developed for different polymorphs of $CaCO_3$ (Epstein et al., 1953; Grossman and Ku, 1986; Dettman et al., 1999) and different bivalve species (e.g., Royer et al., 2013). For *Glycymeris* spp. we applied the paleothermoetry equation by Royer et al. (2013) which was specifically developed for modern *G. glycymeris* using environmental data and live-collected bivalves from the Bay of Brest:

$$T_{\delta 18O}\,(°C) = 18.11 - 2.66 \times (\delta^{18}O_{shell} - \delta^{18}O_{water}). \qquad (1)$$

For *I. maxillata sandbergeri* and *A. islandica* shells, we employed the temperature equation of Grossman and Ku (1986) corrected for different scales (Dettman et al., 1999):

$$T_{\delta 18O}\ (°C)\ =\ 20.6 -\ 4.34\ \times\ (\delta^{18}O_{shell} - (\delta^{18}O_{water}\ -\ 0.27)).\qquad (2)$$

This equation was developed for biogenic aragonite and has been successfully applied in previous studies of both genera (e.g., Hendry et al., 2001; Schöne et al., 2004).

For calcitic shells, such as *P. pictum*, the paleothermometry equation of Anderson and Arthur (1983) was used:

$$T_{\delta 18O}\ (°C)\ =\ 16.0 - 4.14\ \times\ (\delta^{18}O_{shell} - \delta^{18}O_{water}) + 0.13\ \times\ (\delta^{18}O_{shell} - \delta^{18}O_{water})^2 \qquad (3)$$

In all equations, $\delta^{18}O_{shell}$ values were given relative to VPDB and $\delta^{18}O_{water}$ relative to VSMOW. Reliable temperature estimates require knowledge of the $\delta^{18}O_{water}$ signature during shell formation. For the Rupelian stage of the Mainz Basin, Walliser et al. (2015) provided a value of -0.9 ± 0.3 ‰ (1σ) based on the $\delta^{18}O_{PO4}$ composition of sirenian teeth. Here, we used the same value for the Chattian Kassel Basin. According to Walliser et al. (2015), the uncertainty of the reconstructed temperature equals ± 1.3 °C (combined error of the average precision of the mass spectrometric analysis and the standard deviation of the $\delta^{18}O_{water}$ value).

2.6. Mathematical re-sampling of $\delta^{18}O_{shell}$ curves

Shell powder samples were collected at equidistant intervals. In case of drilling, the spacing between individual drill holes remained unchanged, and in case of milling, each milling step covered the same spatial distance. However, since shell growth rates change during different seasons and through life, the time represented by each sample greatly varies. Typically, faster shell growth occurs at optimal growth temperatures and food supply, for example, during spring, and slower growth during the cold season. Furthermore, in mature bivalves, the growth rate is significantly reduced (Jones and Quitmyer, 1996) and the time-averaging of each sample is much

larger than during youth. Thus, ontogenetically older shell portions tend to have truncated $\delta^{18}O_{shell}$ amplitudes. To reduce such biases, the measured $\delta^{18}O_{shell}$ records of *Glycymeris* spp., *A. islandica* and *P. pictum* were mathematically re-sampled (Schöne and Fiebig, 2008; Hallmann et al. 2011), so that seven data points ($\delta^{18}O_{R\text{-}shell}$) were available for each annual increment. The 1st, 2nd … nth value of one year represented the same amount of time as the respective value of another year. This enabled a direct comparison of $\delta^{18}O_{shell}$ values between years. The re-sampled oxygen isotope curves ($\delta^{18}O_{R\text{-}shell}$) slightly differ from those of the raw data (Figs. 5-7). As shown by previous works, the choice of seven points is a fair compromise between the need for data conformity and the preservation of the original $\delta^{18}O_{shell}$ signal (e.g., Schöne and Fiebig, 2008; Wanamaker et al., 2011).

Since *I. maxillata sandbergeri* did not reveal distinct growth patterns, it was not possible to cross-match $\delta^{18}O_{shell}$ data with periodic growth lines and increments. Furthermore, because no anchor point was available for the seasonal arrangement of the $\delta^{18}O_{shell}$ values, no mathematical re-sampling could be performed (Fig. 8).

2.7. $\delta^{18}O_{PO4}$ data of shark teeth

The oxygen isotope composition of the phosphate phase ($\delta^{18}O_{PO4}$) of the enameloid of shark teeth (n = 68; Table 3) was used to reconstruct water temperatures (Fig. 9). For this purpose, the shark teeth were ultrasonically rinsed in de-ionized water. Then, the tooth surface was physically cleaned and the enameloid sampled using a hand-held dental drill. About 10 mg of enameloid powder was immersed in 2 % NaOCl for 45 minutes and subsequently in 0.1 molar suprapure acetic acid for 10 minutes to remove organics and diagenetic carbonate, respectively. Afterward, the powder was rinsed in MilliQ water. An aliquot of 4 mg of air-dried powder was dissolved in 0.8 ml 2 M HF overnight. The supernatant solution with the dissolved phosphate ions was transferred to a new safe-lock centrifuge vessel leaving the CaF_2 residue behind. After neutralization with 25 vol % NH_4OH solution, 0.8 ml of 2 N $AgNO_3$ solution was added to precipitate silver phosphate (Ag_3PO_4) using the rapid precipitation method of Tütken et al. (2006).

The $\delta^{18}O_{PO4}$ value of the rinsed and air-dried Ag_3PO_4 of each sample was determined in triplicate (500 µg aliquots) using a Finnigan™ Thermal Conversion Elemental Analyzer (TC/EA)

for pyrolysis at 1450 °C. The TC/EA was coupled to an Elementar Analysensysteme GmbH Isoprime 100 isotope ratio mass spectrometer at the Institute of Geosciences, University of Mainz. Some samples from the Kassel Basin were processed in a TC/EA coupled to a Thermo Fisher Delta Plus XL isotope ratio mass spectrometer at the Department of Geochemistry, University of Tübingen (Table 3). Measured $\delta^{18}O_{PO4}$ values are reported relative to VSMOW and were normalized offline to calibrated in-house silver phosphate standards, Tu-1 and Tu-2 (Vennemann et al., 2002) at Tübingen and a silver phosphate standard (P/N IVA33802207, batch no. 180097, distributed by IVA-Analysentechnik e.K., Germany) with a certified value of 21.7 ‰ at Mainz. For quality control, two different apatite standards were prepared in the same manner as the samples and analyzed during the same runs, namely HAP, a synthetic hydroxyapatite from Merck, and the international phosphate reference material NBS 120c. The $\delta^{18}O_{PO4}$ values for the HAP were 17.2 ± 0.2 ‰ (n = 13) and for the NBS 120c 22.1 ± 0.5 ‰ (n = 17). Both values are close to the long-term expected value for HAP of 17.0 ‰ and the consensus value for NBS 120c of 21.7 ‰ (Lécuyer et al., 1993; see also Chenery et al., 2010). The precision of $\delta^{18}O_{PO4}$ analyses of the samples was better than ± 0.3 ‰. The $\delta^{18}O_{PO4}$ were then used for the reconstruction of ambient water temperatures that prevailed during the growth of the teeth. For bio-apatite, the revised paleothermometry equation of Longinelli and Nuti (1973) was used:

$$T_{\delta PO4}\,(°C) \;=\; 111.4 - 4.3 \ast (\delta^{18}O_{PO4} - \delta^{18}O_{Water}), \qquad (4)$$

where $\delta^{18}O_{PO4}$ and $\delta^{18}O_{water}$ are given relative to VSMOW. Taking into account the $\delta^{18}O_{water}$ value of -0.9 ± 0.3 ‰ of Walliser et al. (2015), the resulting water temperatures are given with an average error of about 1.3 °C.

2.8. Numerical climate simulations

Model simulations were performed with the Earth System model COSMOS for pre-industrial (Wei et al., 2012) and Oligocene conditions. The model configuration includes the atmosphere component ECHAM5 at T31 resolution (~3.75°) with nineteen vertical layers (Roeckner et al.,

2006), complemented by a land-surface scheme including dynamical vegetation (Brovkin et al., 2009). The ocean component MPI-OM, including the dynamics of sea ice formulated using viscous-plastic rheology, has an average horizontal resolution of 3 º x 1.8 ° with 40 uneven vertical layers (Marsland et al., 2003). The performance of this climate model has been evaluated for the Holocene (Wei and Lohmann, 2012; Lohmann et al., 2013), the last millennium (Jungclaus et al., 2006), glacial millennial-scale variability (Gong et al., 2013; Weber et al., 2014; Zhang et al., 2014), and warm climates in the Miocene (Knorr and Lohmann, 2014) and Pliocene (Stepanek and Lohmann, 2012).

For the Late Oligocene (Chattian, 26 Ma) simulations we employed the paleogeography compiled by Markwick (2007) who created paleogeographies representing periods of Earth history with different paleoshorelines. Based on this paleogeography we have set up the boundary conditions necessary to run the model (cf. Stepanek and Lohmann, 2012) which include the set-up of the hydrological discharge model (Hagemann and Dümenil, 1997), orography-related parameters for the gravity wave drag parametrization (Lott and Miller, 1997), glacier mask, concentration of greenhouse gases in the atmosphere and orbital parameters. The paleogeographic model of Marckwick (2007) assumes an unipolar glaciated world for the Oligocene with an ice sheet on Antarctica reaching 2000 m above sea level. The absence of large glaciations of the Northern Hemisphere is in agreement with other models and proxy-based reconstructions provided in more recent studies (e.g., DeConto et al., 2008; Liu et al., 2009; Scotese, 2014). Orbital parameters were set to the present-day values. The solar constant was reduced by 0.4 % compared to present-day and is equal to 1361.5 W/m^2. We prescribed the ice sheet on Antarctica, whereas on the Northern Hemisphere the ice sheet was considered absent. In order to test the regional climate sensitivity of the Oligocene in Central Europe, we simulated the seasonal and annual change in surface temperatures for three atmospheric carbon dioxide scenarios, namely 400 ppm, 2 x PAL, and 3 x PAL (PAL - preindustrial atmospheric level of 280 ppm). The concentrations of CH_4 and N_2O were set to preindustrial values (650 ppb and 270 ppb, respectively).

All simulations were integrated for 500 model years. The coupled atmosphere-ocean configuration with working hydrological discharge model was run for the last 350 years in the case of the 400 ppm experiment and for the last ~250 years in the case of the 2 x PAL (560 ppm) and 3

x PAL (840 ppm) experiments (Fig. 10). The analysis is based on a climatology (long-term average) calculated from the last 100 years of simulations.

3. Results

A summary of oxygen isotope data of bivalve shells and shark teeth (and temperatures reconstructed therefrom) are given in Tables 1 and 3, respectively.

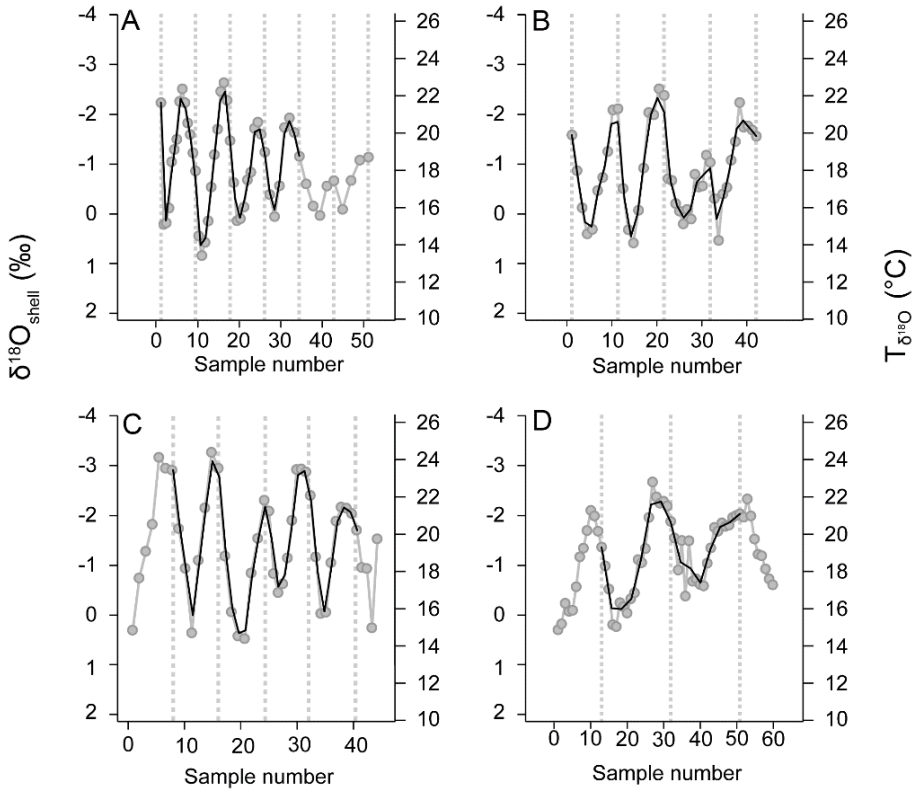

Figure 5. Raw (grey) and re-sampled (black) $\delta^{18}O_{shell}$ values of the studied *Glycymeris planicostalis* specimens from the Stadecken Formation. (A) EOW-Gly-Alb-1, (B) EOW-Gly-BH-9, (C) EOW-Gly-Alb-3, (D) EOW-Gly-Alb-2a. Dotted vertical bars represent annual growth lines. Temperatures were calculated using equation 1, assuming a $\delta^{18}O_{water}$ value = -0.9 ‰ (see text for reasons).

3.1. Bivalve shell data

A combined analysis of shell growth patterns and $\delta^{18}O_{shell}$ values was used to identify the seasonal timing of shell growth in the studied specimens, specifically when shell formation ceased and annual growth lines formed. For instance, *G. planicostalis* (Fig. 5) and *G. obovata* (Fig. 6) formed distinct growth lines shortly after the summer temperature maximum. However, one specimen of *G. obovata* from the Kassel Basin formed annual growth lines in spring (Fig. 6B). Whereas in *P. pictu*m the major growth line was associated with the highest $\delta^{18}O_{shell}$ value indicating winter, annual growth lines of *A. islandica* occurred when $\delta^{18}O_{shell}$ values were at minimum, suggesting that the majority of shell material was formed during the cold season when water temperatures dropped below ca. 12 °C (Fig. 7A and B). Although distinct growth lines were not recognized in shells of *I. maxillata sandbergeri*, the generally low isotope values (i.e., high temperatures) suggested that this species grew mostly during summer (Fig. 7C, D and 8).

By combining the $\delta^{18}O_{shell}$ records of different species (Table 1), it was possible to reconstruct the full seasonal temperature amplitude in surface waters during each of the four studied time intervals. Seasonal temperature bounds during deposition of the

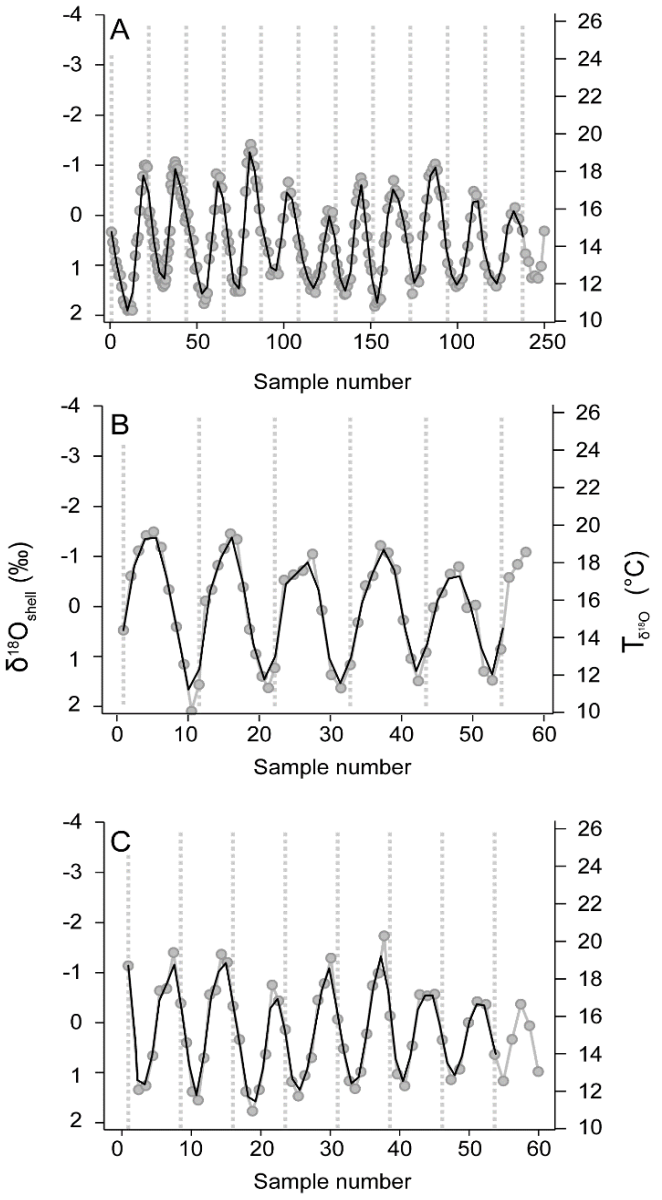

Figure 6. Raw (grey) and re-sampled (black) $\delta^{18}O_{shell}$ values of the studied *Glycymeris obovata* specimens from the Kassel Formation. (A) 2009-KS6-D17L, (B) H1282.1, (C) 2009-KS6-D36L. Dotted vertical bars in B to E represent annual growth lines. Temperatures were calculated using Eq. (1), assuming a $\delta^{18}O_{water}$ value = -0.9‰ (see text for reasons).

lower Alzey Formation are given by *P. pictum*, *A. islandica* and *I. maxillata sandbergeri*. *A. islandica* showed only minor seasonal $\delta^{18}O_{R\text{-}shell}$ variations of ca. 0.2 ‰ and an annual average of 0.94 ± 0.10 ‰ (11.4 ± 0.4 °C; ± 1σ; Fig. 7A). The convex shape of the curve of the reconstructed temperatures suggests that shell growth occurred mainly during winter months. Similar winter temperatures were reconstructed from $\delta^{18}O_{R\text{-}shell}$ values of *P. pictum* (0.37 ‰, 11.0 °C; Fig. 7B). Warmest temperatures ranged between 16.7 °C (-1.06 ‰) and 17.1 ± 1.1 °C (-0.37 ± 0.25 ‰; ±1σ;

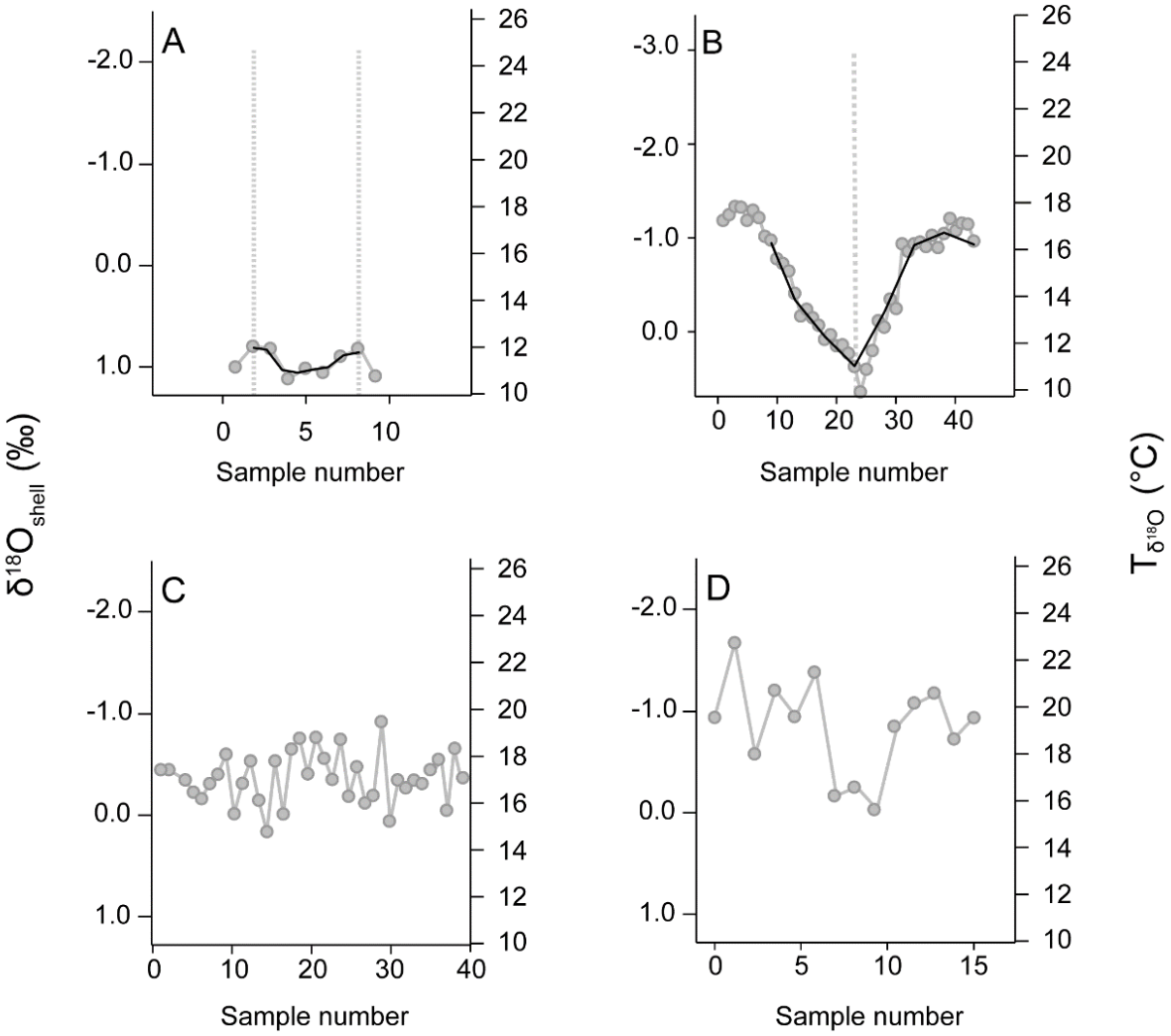

Figure7. Raw (grey) and re-sampled (black; only for A and B) $\delta^{18}O_{shell}$ values of the studied *Arctica islandica* (A), *Palliolum pictum* (B) and *Isognomon maxillata sandbergeri* (C and D) specimens from the lower (A-C) and upper (D) Alzey Formation. (A) EOW-Arc-Zeil-F1X, (B) EOW-Pec-Wöl-F2X, (C) EOW-Iso-Wöl-F1X, (D) EOW-Wht-F1X. Dotted bars in A and B represent annual growth lines. Temperatures of specimens depicted in A, C and D were calculated using equation 2, whereas those of B were calculated with equation 3, assuming a $\delta^{18}O_{water}$ value = -0.9 ‰ (see text for reasons).

Fig. 7C) as suggested by oxygen isotope data of *P. pictum* and *I. maxillata sandbergeri*, respectively.

From the lower to the upper Alzey Formation, warmest temperatures increased by ca. 2 °C as indicated by a lower average $\delta^{18}O_{shell}$ value in *I. maxillata sandbergeri*: -0.81 ± 0.45 ‰ (19.0 ± 2.0 °C; ± 1σ; Fig. 7D). Similar summer temperatures were reconstructed from the oxygen isotope values of *I. maxillata sandbergeri* from the Stadecken Formation, i.e., on average, -0.89 ± 0.41 ‰ (19.4 ± 1.8 °C; ± 1σ; Fig. 8).

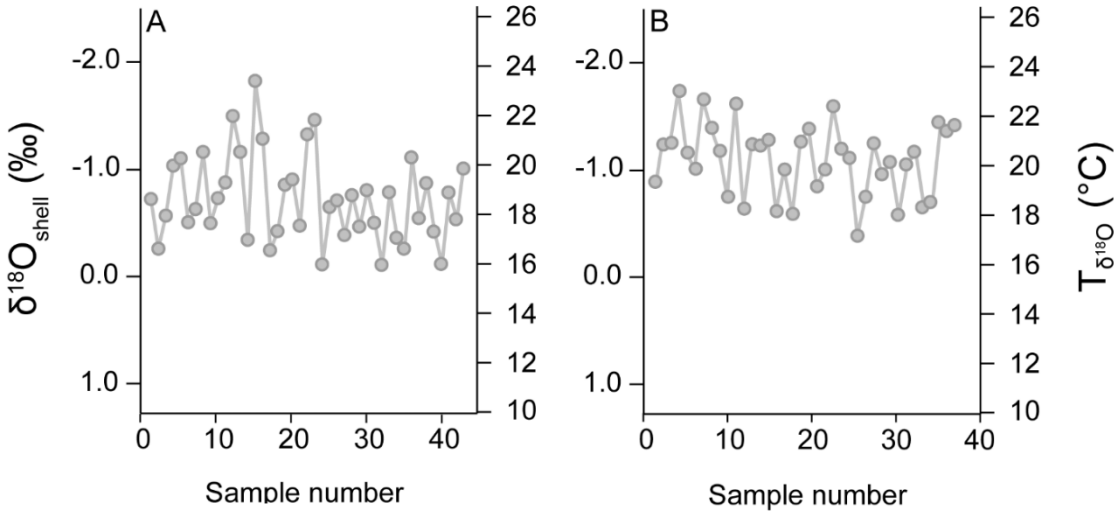

Figure 8. Raw $\delta^{18}O_{shell}$ values of the Isognomon maxillata sandbergeri specimens EOW-Iso-Spi-F1X (A) and EOW-Iso-Sul-F1X (B) from the Stadecken Formation. Temperatures were calculated using equation 2, assuming a $\delta^{18}O_{water}$ value = -0.9 ‰ (see text for reasons).

The seasonal oxygen isotope amplitudes of the four studied *G. planicostalis* shells from the Stadecken Formation (Mainz Basin; Fig. 5) agreed well with each other (Table 1). On average, the seasonal $\delta^{18}O_{R\text{-}shell}$ range was 2.30 ± 0.56 ‰ (corresponding to a seasonal temperature range of 6.1 ±1.5 °C) with minimum and maximum values of -2.26 ± 0.43 (21.7 ± 1.1 °C; average ± 1σ) and 0.04 ± 0.35 (14.1 ± 0.9 °C), respectively. The annual average was -1.15 ± 0.90 ‰ (18.8 ± 2.4 °C). The $\delta^{18}O_{R\text{-}shell}$ values of *G. obovata* from the Kassel Formation were in general ca. 1.40 ‰ more positive (average value ± σ: 0.30 ± 0.85 ‰; Fig. 6) than those of *G. planicostalis* from the

Stadecken Formation. Accordingly, the bivalves from the Kassel Basin grew in colder water. On average, annual temperatures oscillated between a winter and a summer average value of 12.0 ± 0.9 °C (1.40 ± 0.35 ‰; ± 1σ) and 17.8 ± 1.1 °C (-0.77 ± 0.42 ‰; ± 1σ), respectively.

All studied bivalves passed a set of different diagenesis screening tests and were preserved in nearly original condition. Except for *I. maxillata sandbergeri*, the studied species did not reveal signs of post-mortem transport, i.e., no significant surface abrasion or damaged edges. In the case of some glycymerid specimens, both valves were present. Shells of *I. maxillata sandbergeri*, however, occurred exclusively as fragments.

3.2. Shark teeth data

The temperatures reconstructed from the $\delta^{18}O_{PO4}$ value of the shark teeth exhibited a much broader range (up to 12 °C) than those estimated from bivalve shell $\delta^{18}O$ (Fig. 9). The lowest temperatures were similar in all studied strata, i.e., 5 °C. Conversely, the warmest values changed substantially through time and followed the same general trend given by $\delta^{18}O_{shell}$ values. From the lower Alzey Formation to the Stadecken Formation, the warmest temperatures increased from 17.0 °C to 22.4 °C, and subsequently dropped to 21.1 °C in the Kassel Formation.

3.3. Numerical climate simulations

According to our simulations, surface temperatures increase under elevated atmospheric pCO_2, but to different magnitudes according to locality and time interval represented. In both scenarios (Fig. 10), i.e., increase to 2 x PAL and 3 x PAL, temperature anomalies increase with latitude, with the Arctic regions warming, on average, by up to 4 °C (2 X PAL, Fig. 10D) and 12 °C (3 X PAL; Fig. 10G), according to the simulated time interval. At the seasonal scale, winter temperatures are more sensitive to rising pCO_2, showing anomalies of up to 10 °C (2 X PAL; Fig. 10E) and 18 °C (3 X PAL; Fig. 10H) around Greenland.

Numerical climate models further suggest that (summer and winter) surface temperatures in Central Europe increase by 2 to 3 °C when pCO_2 rises from 400 ppm to 2 x PAL (Fig. 10C and E) and by 8 to 10 °C when levels increase to 3 x PAL (Fig. 10F and H). The first scenario seems more plausible because the temperature rise is closer to that indicated by the proxy data.

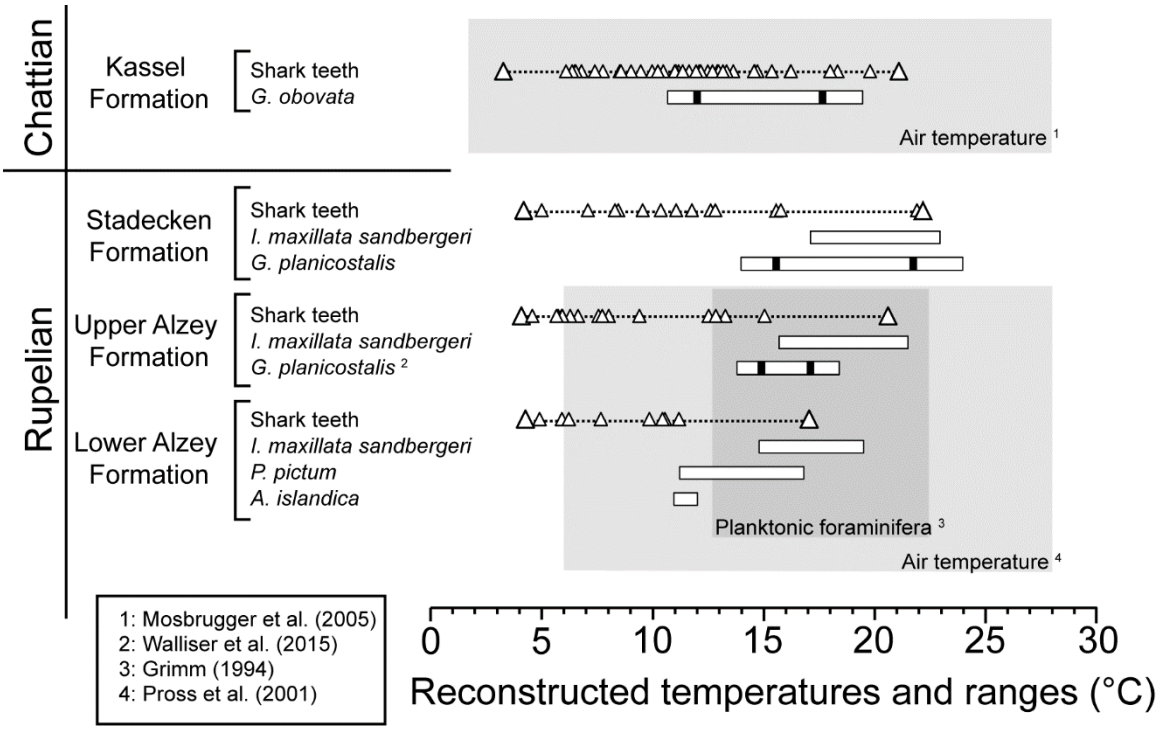

Figure 9. Oxygen isotope-based temperature ranges of the studied bivalves (horizontal bars) and shark teeth (triangles connected with dotted line). For *Glycymeris* spp. the average winter and summer temperatures are indicated in black. Reconstructed values fit well into previous air temperatures from palynological proxies (light grey; Pross et al., 2001; Mosbrugger et al., 2005) and SST derived from $\delta^{18}O$ values of planktonic foraminiferan tests (dark grey; Grimm, 1994). Both bivalve shells and shark teeth-derived temperatures show a warming trend toward the Stadecken Formation and a subsequent cooling toward the Kassel Formation that was not discernable from the other proxy records.

4. Discussion

The present study is the first to show how seasonal temperatures changed in an extratropical shallow marine setting of Central Europe (paleolatitude ~45 °N) during the Oligocene epoch.

Multi-taxon (bivalves) oxygen isotope-based reconstructions suggest a gradual rise of temperatures in surface waters (upper 30 to 40 m), on average, by as much as 4 °C during the Rupelian stage, i.e., from the lower Alzey to the Stadecken Formation, followed by a 4 °C cooling during the Chattian stage represented by the Kassel Formation. In all studied time intervals, $\delta^{18}O_{shell}$-based seasonal temperature amplitudes in the upper 30 to 40 m of the water column were similar and equaled ca. 9.0 ± 1.2 °C. However, seasonal temperature amplitudes increased by ca. 2 °C during the warmest time interval of the Rupelian stage, i.e., the Stadecken Formation.

Highest temperatures reconstructed from $\delta^{18}O_{PO4}$ of shark teeth closely resembled that of shell-based estimates and showed similar trends through time, i.e., a gradual warming in surface waters during the Rupelian stage followed by cooling during the Chattian stage. However, lowest temperatures reconstructed from shark teeth were significantly lower than winter temperatures estimated from bivalve shells and remained virtually unchanged through time. This is likely because sharks often dwelled in deeper bottom water below the thermocline.

According to numerical climate simulations, the 4 °C warming of surface waters during the early Oligocene required an atmospheric pCO_2 increase by at least 160 ppm, i.e., 400 ppm to 560 ppm. Given that atmospheric carbon dioxide levels predicted for the near future will likely exceed this value significantly, the Early Oligocene warming gives a hint of the possible future climate in Central Europe under elevated pCO_2 levels.

4.1. Reliability of $\delta^{18}O$-based paleotemperature estimates from bivalve shells and shark teeth

Obtaining reliable paleotemperature estimates from $\delta^{18}O$ values of fossil materials can represent a very challenging task. An indispensable prerequisite for such reconstructions is the use of pristinely preserved materials. Specifically when aragonite is studied, a detailed crystallographic analysis is required to ensure that this metastable $CaCO_3$ polymorph did not locally turn into calcite. In addition, neomorphic mineral phases such as secondary calcite may have precipitated in cavities from percolating pore waters. In the present study, various different tests were applied to preclude materials that were affected by diagenetic overprint.

Furthermore, reliable $\delta^{18}O$-based temperature estimates require that the biominerals have formed at or near oxygen isotopic equilibrium with the ambient environment. Except for very a few species (Gillikin et al., 2005; Hallmann et al., 2008; Yan et al., 2012), typically deep burrowers, all hitherto studied bivalves including modern relatives of the studied bivalves such *A. islandica*, glycymerids, pectinids and pteriids fulfill this requirement (Weidman et al., 1994; Royer et al., 2013; Chauvaud et al., 2005; Lécuyer et al., 2012). All fish, including sharks, mineralize their enameloid also in isotopic equilibrium with the ambient medium, enabling water temperature reconstructions (Kolodny et al, 1983: Vennemann et al., 2001).

Another essential aspect for reliable stable oxygen isotope-based temperature reconstructions is knowledge of the $\delta^{18}O$ signature of the water in which the bivalves and sharks lived during formation of their hard parts. For example, the $\delta^{18}O_{water}$ value changes through time depending on global ice volume (e.g., Lear et al., 2000). Smaller amounts of polar ice will shift the ocean $\delta^{18}O$ signature toward lower values and vice versa. In a polar ice-free world, the average $\delta^{18}O_{water}$ value will be close to -1.2 ‰ (Shackleton and Kennett, 1975). According to a recent study by Cramer et al. (2011) using coupled Mg/Ca and $\delta^{18}O$ data of benthic

Table 3. Ranges of the enamel $\delta^{18}O_{PO4}$ values (VSMOW) of the shark teeth from the Alzey Formation and the Stadecken Formation (Mainz Basin), as well as the Kassel Formation (Kassel Basin). Water temperatures were calculated from $\delta^{18}O_{PO4}$ values using the paleotemperature equation of Longinelli and Nuti (1973) assuming a $\delta^{18}O_{PO4}$ of -0.9 ‰ (Walliser et al., 2015).

Stratigraphy	Species	# of teeth	Sampled localities	$\delta^{18}O_{PO4}$ min [‰]	$\delta^{18}O_{PO4}$ max [‰]	$\delta^{18}O_{PO4}$ average ± 1σ [‰]	T $\delta^{18}O_{PO4}$ min [°C]	T $\delta^{18}O_{PO4}$ max [°C]	T $\delta^{18}O_{PO4}$ average ± 1σ [°C]
Kassel Formation	*Carcharias cuspidata* *C. acutissima* *Physogaleus latus*	30	Brandkopf at the Ahne River Valley, Kaufungen, Glimmerode, Kassel Wilhelmshöhe,	20.1	24.1	22.2 ± 0.9	4.1	21.1	12.1 ± 3.8
Stadecken Formation	*Carcharias cuspidata* *C. acutissima*	11	Stadecken, Heimersheim	19.8	23.8	22.3 ± 1.0	5.2	22.4	11.5 ± 4.5
Upper Alzey Foramtion	*Carcharias cuspidata* *C. acutissima*	17	Sand pit near Flonheim, "Trift"/Neumühle near Weinheim	20.2	23.8	22.8 ± 1.0	5.1	20.6	9.6 ± 4.2
Lower Alzey Formation	*Carcharias cuspidata* *C. acutissima*	10	Sand pit Müller & Schmidt near Wöllstein	21.1	23.8	22.8 ± 0.8	5.2	17.0	9.4 ± 3.5

foraminifera, the $\delta^{18}O_{water}$ value of the deep ocean fluctuated between -0.33 and -0.04 ‰ during the time slices of the Oligocene studied here. In contemporaneous surface waters of the Central European epicontinental seaway, this value was slightly more negative (-0.9 ± 0.3 ‰) as recently shown by Walliser et al. (2015) based on tooth enamel of sea cows of the Mainz Basin. Given the paleogeographic proximity of the two study regions (ca. 200 km apart), this figure also serves as a reasonable estimate for surface waters of the Kassel Basin. Furthermore, considering the results of Cramer et al. (2011), the average $\delta^{18}O_{water}$ value remained nearly invariant (± 0.15 ‰) over the stratigraphic levels of the present study. To reflect this small variability, we have added 0.15 ‰ to the 1σ uncertainty. Accordingly, $\delta^{18}O$-derived temperature estimates come with an error of ± 1.7 °C (= ± 0.45 ‰) instead of ± 1.3 °C (= ± 0.3 ‰).

Even if it was desirable to provide quantitative estimates, relative changes of temperature were of primary importance in the current study (Figs. 9 and 11). Such data can be provided without knowing the exact $\delta^{18}O_{water}$ signature during the time of biomineral formation as long as this value remained relatively stable over time. In fact, palynological data show that mean annual precipitation rates in Central Europe did not significantly change during the course of the Oligocene, but remained at around 1200 mm/a (Pross, 1998, 2000, Mosbrugger et al., 2005; Erdei et al., 2012). Furthermore, paleogeographical reconstructions do not show significant changes in the paleocoastline of the Mainz Basin between the Alzey and the Stadecken Formation (Grimm et al., 2003). Thus, it is likely that the local hydrological cycles and river discharge into the epicontinental sea remained fairly stable during the late Rupelian stage, and therefore that $\delta^{18}O$ of seawater was likewise stable.

Independently from the local hydrological balance, a change of the ambient $\delta^{18}O_{water}$ signature to more negative values could have been achieved through a negative shift of the oxygen isotope composition of the meteoric water. Kocsis et al. (2014) showed that during the Eocene-Oligocene transition (35 to 31 Ma), the source of Central European atmospheric moisture migrated from the Tethys to the North Atlantic. Thereby, the $\delta^{18}O$ signature of meteoric water in Central Europe decreased by about 2.2 ‰. However, according to longer records which encompass the stratigraphic range of the present study (30 to 25 Ma), the meteoric water $\delta^{18}O$ values remained more or less stable or even moved towards more positive values (Héran et al., 2010) after the

Eocene-Oligocene boundary. More positive meteoric water $\delta^{18}O$ values would imply that the warming was even greater than estimated in this study.

On much shorter time-scales, the upper few meters of the sea surface, specifically at settings near the coast often experience seasonal changes of the $\delta^{18}O_{water}$ value. This is likely reflected in the large spread of sirenian tooth-based $\delta^{18}O_{water}$ estimates provided by Walliser et al. (2015). $\delta^{18}O_{water}$ values of -0.2 ‰ may indicate times during which strong evaporation occurred in hot summer, whereas values of -1.4 ‰ characterized the upper few meters of the sea in rainy winters. Thus, summer temperatures reconstructed from $\delta^{18}O$ values of shells and teeth of organisms that lived near the sea surface such as *I. maxillata sandbergeri* and sharks may thus underestimate actual temperatures by ca. 2 °C.

Variations of freshwater discharge rates from land can also affect the $\delta^{18}O_{water}$ signature of the habitat of the bivalves, especially in settings close to river outlets. However, several lines of evidence suggest that this not the case for the studied localities. For instance, the investigated localities are located several hundreds of meters (e.g., locality Alzey "Trift") or even kilometers (e.g., Kassel Wilhelmshöhe) away from the reconstructed Oligocene paleo-coastlines (e.g., Ritzkowsky, 1965; Grimm et al., 2000). Therefore, the influence of riverine freshwater on the $\delta^{18}O_{water}$ signature of the sea is virtually absent, particularly at 30-40 m water depth (e.g., Stenni et al., 1995; Walliser et al., 2015). Furthermore, the general orientation of clastic transport suggests the presence of strong water currents along the coastlines of the Mainz Basin originating from the southern Upper Rhine Graben (Sissingh, 2003). This is in line with the presence of Alpine detritus of Cretaceous age in nearshore deposits of the Alzey Formation (Picot, 2002; Spiegel et al., 2007) which otherwise consists of reworked material from the local rocky shores formed by Permian (Rotliegend) rhyolites and sedimentary rocks (Grimm et al., 2011). Such near coastal currents likely acted as a buffer for occasional freshwater pulses preventing the formation of (temporary) brackish environments. Stable salinity levels are also suggested by the highly diverse fully marine benthic faunal associations which contain organisms with restricted tolerance to salinity oscillations such as corals (Grimm and Grimm, 2005; Schindler et al., 2009).

In the present study, both long-term and seasonal variations of $\delta^{18}O_{water}$ values were not taken into consideration. Instead, all past water temperatures were computed with a $\delta^{18}O_{water}$ value of -0.9 ± 0.4 ‰. This conservative approach may yield lower long-term and seasonal temperature

amplitudes than actually existed and provides a minimum estimate of the temperature variability in Central Europe during the Oligocene.

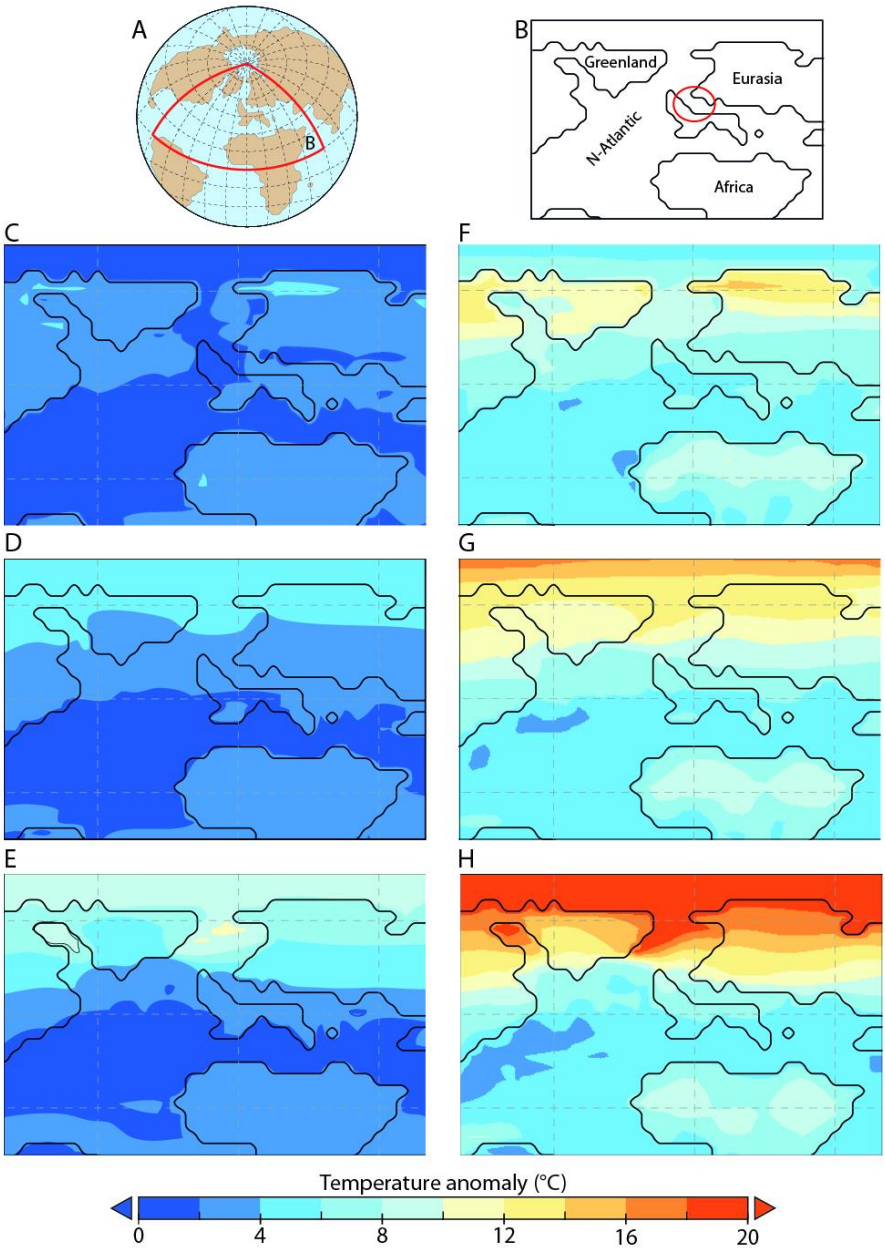

Figure 10. Modelled surface temperatures for the Oligocene world. (A) Paleogeographic distribution of land and ocean adopted in the model and (B) an enlargement showing the area of study (red circle) in this context. Simulations of summer (C, F), annual (D, G) and winter (E, H) near surface temperature anomalies (relative to present) during the Oligocene for the area shown in (B) (land: black outline). Simulated anomalies indicate a general SST warming of 3-4 °C for an atmospheric pCO_2 rise from 400 ppm to 2 x PAL (C-E), and 6-8 °C for an increase from 400 ppm to 3 x PAL (F-H).

4.2. Multi-taxon approach to estimating seasonal temperature amplitudes

As demonstrated by the results of this study, the combined use of different species with overlapping habitats and different growing seasons can provide more robust data on seasonal amplitudes than a single species. For example, *P. pictum* ceased growing shell during the coldest part of the year and stopped recording environmental conditions. The annual growth lines coincided with the maximum $\delta^{18}O_{shell}$ values (Fig. 7B), but the actual winter temperatures in surface waters probably reached lower values than those computed from shell oxygen isotopes. Therefore, this species is not suitable for the reconstruction of winter temperatures. Presumably, the same applies to *I. maxillata sandbergeri*. However, the growth patterns *of I. maxillata sandbergeri* were very difficult to interpret, and it remains unclear during which season the shells were formed since no annual growth line was identified. At least, modern representatives of *P. pictum* and *I. maxillata sandbergeri*, i.e., most pectinids and pteriids tend to produce annual growth lines during the cold season (e.g., Chauvaud et al., 1998; Hendry et al., 2001; Owen et al., 2002). In contrast, the studied shells of *Glycymeris* spp. were growing uninterruptedly during the coldest and warmest part of the year. Like modern representatives of these genera (e.g., Bušelić et al., 2014), their $\delta^{18}O_{shell}$ curves show distinct inflection points which are not associated with the annual growth lines (Figs. 5 and 6). The interpretation of the data from the *Artica islandica* is somewhat more difficult. Annual growth lines coincided with the highest recorded temperatures, suggesting that shell accretion occurred only during the winter months. However, studies on modern *A. islandica* showed that this species typically grows its shell over most part of the year forming growth lines during fall (see Schöne, 2013 for a review). Thereby, annual shell formation rates are not constant throughout the growing season. Because of this, oxygen isotope curves usually display an asymmetric saw-tooth shaped pattern with the minimum $\delta^{18}O_{shell}$ (maximum $T_{\delta 18O}$) values occurring shortly before the annual growth lines (Schöne et al., 2005). Therefore, unless a very high-resolution sampling technique (milling) is applied, the summer $\delta^{18}O_{shell}$ signals may remain undetected. Likely, this is the case of this study where the *A. islandica* shell was sampled using a lower-resolution technique (drilling).

The isotope data of shark teeth are more difficult to interpret. Like *Glycymeris* spp. and *A. islandica*, shark teeth can potentially provide faithful estimates of seasonal temperature extremes, because they grow at nearly any time of the year. However, the formation of a shark

tooth is completed within a few weeks, and a single tooth therefore only provides environmental data for a very short time interval of the year. A large number of coeval teeth is thus required to obtain a statistically significant representation of the most extreme water temperatures that prevailed in a given time interval of the past. The interpretation of shark teeth $\delta^{18}O$ is further complicated by the fact that these animals are highly mobile. They migrate vertically in the water column and can travel long distances (e.g., Domeier and Nasby-Lucas, 2008). The most positive $\delta^{18}O_{PO4}$ values translate into a temperature of ca. 4 or 5 °C which is 7 to 10 °C colder than the minimum temperatures reconstructed here from bivalves (ca. 11 to 14 °C) (Fig. 9). Even temperatures in deeper (sub-thermocline) waters nearby were slightly warmer. According to $\delta^{18}O$ values of benthic foraminiferan tests from the Bodenheim Formation, i.e., the basinal counterpart of the Alzey Formation (ca. 150 m water depth; Grimm et al., 2011), temperatures did not fall below ca. 6-7 °C ($\delta^{18}O_{BF}$ values from Grimm, 1994; recalculated with the paleothermometry equation by Anderson and Arthur, 1983, assuming a $\delta^{18}O_{water}$ of -0.9 ‰). Therefore, when the teeth with highest $\delta^{18}O_{PO4}$ values formed, the sharks most likely resided in cold bottom water further north. Temperatures reconstructed from the most positive $\delta^{18}O_{PO4}$ values of shark teeth are therefore not suitable to estimate winter temperatures in surface waters of the Mainz and Kassel Basins. It should be noted that minimum temperatures estimated from $\delta^{18}O_{PO4}$ of shark teeth barely changed through time. Presumably, this finding does not indicate bottom water temperatures remained invariant throughout the Oligocene, but more likely a preference of the sharks for a certain temperature regime in winter.

The lowest $\delta^{18}O_{PO4}$ values of shark teeth ($T_{\delta 18O}$ = 17 to 22 °C) likely reflect times during which these animals foraged in very shallow waters of the Mainz Basin during summer. Since ocean gateways to the south probably did not exist (Berger et al., 2005a, b; Grimm, 2006) or were only temporarily available (Martini 1982; Picot, 2002), the sharks could not reach warmer waters in the Western Paratethys without taking the detour through the Atlantic. However, this seems unlikely, because the studied sharks, *Carcharias* and *Physogaleus*, like their modern relatives, presumably had a relatively small range of action (e.g., Otway and Ellis, 2011) and did not travel excessive distances as some modern sharks do, e.g., *Carcharodon carcharias* (Bonfil et al., 2005). Presumably, the studied sharks largely stayed in the Central European epicontinental seaway. Summer temperatures estimated from shark teeth (17 to 22 °C) compared well to $T_{\delta 18O}$ of coeval

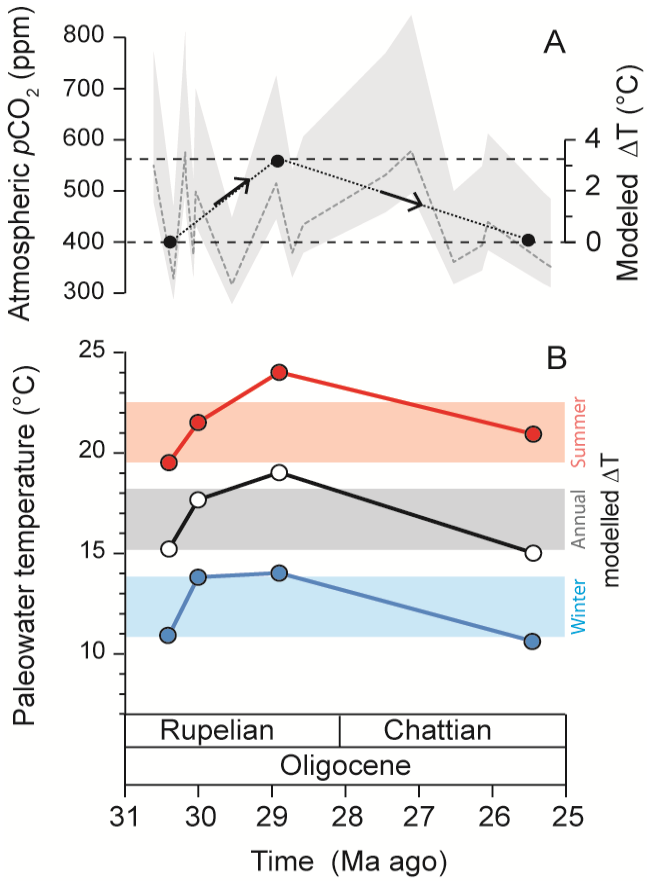

Figure 11. (A) Long-term variability of proxy-derived atmospheric pCO_2 concentrations (Beerling and Royer, 2011) and (B) the seasonal SST ranges reconstructed in this study. (A) The proxy-based atmospheric pCO_2 levels (grey dotted lines) and their uncertainties (grey envelopes) are compared to atmospheric pCO_2 (horizontal dashed lines) derived from the proxy-validated models for the investigated stratigraphic intervals (black dots). The scale to the right indicates the simulated temperature anomaly (ΔT) resulting from a 160 ppm increase of carbon dioxide (from 400 ppm to 2 x PAL), for the area indicated by the red circle in Figure 9B; black dotted lines indicates the inferred change in pCO_2 of the Oligocene atmosphere. (B) The modelled winter (blue shading), summer (red shading) and annual (grey shading) ranges of ΔT are compared to the reconstructed winter (blue dots), summer (red dots) and annual (white dots) changes in water temperatures during the studied time intervals. The SST values are a synthesis of both the bivalve shells and shark teeth temperatures (Fig. 9).

I. maxillata sandbergeri (19 to 23 °C) and planktonic foraminifera (22 °C; Grimm, 1994) from the Mainz Basin.

As sessile organisms, the bivalves recorded environmental conditions at the same water depth through lifetime. However, different species are adapted to different water depth, and after death the shells may have been displaced from the original habitat. A detailed analysis of the facies is thus needed to determine if and how much post-mortem transport of the shells has occurred. The pteriid, *I. maxillata sandbergeri* lived on rocky shores near the coast, attached by byssal threads to a hard substrate (typically Permian rhyolites in the case of the Mainz Basin; e.g., Rousse et al., 2012), and recorded conditions in the uppermost portion of the ocean through lifetime. Modern *Isognomon* spp. are mainly distributed in littoral to sublittoral tropical waters (Huber, 2010), typically at depths less than 20 m (e.g., Carpenter and Niem, 1998). Highest summer temperatures recovered from oxygen isotopes of *I. maxillata sandbergeri* (19 to 23 °C) were only slightly lower than the upper temperature tolerance of modern *I. alatus* (Trueman and Lowe, 1971; Siung, 1980; Hall, 1985). During major storm events (or

after death), the valves of *I. maxillata sandbergeri* were detached from the substrate and transported into deeper water where they became part of a death assemblage with glycymerids or *P. pictum*.

In contrast to *I. maxillata sandbergeri* which exclusively occurred as fragments, shells of *A. islandica*, *Glycymeris* spp. and even the fragile *P. pictum* were preserved intact, sometimes both valves of a specimen, without signs of surface abrasion. Most likely, these shells did not experience significant displacement from their original habitat. The water depth at which they dwelled likely did not change significantly through time. Based on a detailed facies analysis (Grimm et al., 2003; Schindler et al., 2005), the water depth during which the sediments of the Alzey Formation (locality "Trift") were deposited ranged between 30 and 40 m. During the following time interval, represented by the Stadecken Formation, the depth became slightly shallower Grimm et al. (2000, 2003, 2011). With respect to the Kassel Basin, Ritzkowski et al. (2011) suggested that the sediments of the Kassel Formation were deposited slightly above or at the storm-weather wave base which in small epeiric basins lay at ca. 30 ± 10 m (cf. Immenhauser, 2009). *A. islandica* exhibited only minor seasonal temperature changes of 1.1 °C which is comparable to the range of temperature variation recorded in the shells of modern *A. islandica* living below the seasonal thermocline (Schöne et al., 2005). It is likely that this species lived very close to the (seasonal) thermocline and experienced, therefore, winter temperatures (ca. 11 to 12 °C) over most time of the year. In contrast, *P. pictum* lived above the seasonal thermocline and experienced both seasonal extremes. Summer temperatures (16.4 °C) reconstructed from this species compared well with the lowest temperatures estimated from coeval *I. maxillata sandbergeri* (14.8 °C), whereas the coldest reconstructed temperature (11 °C) overlapped with those of *A. islandica*. This suggest that the scallop was inhabiting deeper waters than *I. maxillata sandbergeri*, but still living in shallower environments than *A. islandica*. The two studied *Glycymeris* species showed very distinct and very similar seasonal temperature oscillations (on average, 5.9 ± 1.3 °C; ± 1σ), with summer extremes (*G. planicostalis*: 21.7 ± 1.1 °C; *G. obovata*: 17.8 ± 1.1 °C; ± 1σ) close to those provided by shark teeth and *I. maxillata sandbergeri* (Fig. 9).

The temperature trends during the four studied time intervals reflected in the different organisms were remarkably similar (Fig. 9). Summer temperature estimated from shark teeth and *I. maxillata sandbergeri* compared well to that recorded by *P. pictum* and glycymerids. Likewise, winter temperatures and average annual temperatures estimated from glycymerids and *A. islandica*

changed by a similar, but somewhat smaller amount during the studied time interval (Fig. 11). Given the strong correspondence of temperature trends among different species from slightly different habitats, these trends most certainly reflect actual changes in water temperature rather than changes in biological or other environmental factors.

As shown here, by using different species (and different organism groups) it was possible to cross-verify the temperature trends through time. The combination of $T_{\delta 18O}$ data sets from species that mineralized their hard tissues during slightly different times of the year helped to constrain seasonal temperature amplitudes and compensate for biases related to species-specific life-history traits. Furthermore, the close agreement of winter temperatures estimated from shells of A. *islandica*, *Glycymeris* spp. and *P. pictum* as well as very similar summer temperatures obtained from shark teeth, *Glycymeris* spp., *P. pictum* and *I. maxillata sandbergeri* provides strong support the view that these biominerals were formed in oxygen isotopic equilibrium with the ambient water.

In a wider paleogeographical context, results of this study agree with those described from adjacent marine settings. For example, similar SST trends have been reconstructed from $\delta^{18}O$ of shallow-marine bivalves from Oligocene strata of the Paris Basin (Huyghe et al., 2015). Although this record does not include data for the Chattian stage, it clearly shows increasing water temperatures during the early Oligocene. The common trends in the two records corroborate the hypothesis that the observed SST changes areas are not merely a local phenomenon, but rather a regional climate signal. Interestingly, such warming trends do not occur in deeper settings of the ocean. According to benthic foraminifera, temperatures in the deep sea remained nearly invariant throughout the Oligocene (Zachos et al., 2008; Cramer et al., 2011). In order to interpret the discrepant temperature trends in shallow waters and the deep sea and examine if a warming of surface waters also occurred elsewhere requires future studies of shallow marine deposits in other parts of the world.

4.3. Numerical simulations of CO_2 levels

Existing pCO_2 reconstructions for the studied time interval suggest an increase from to 400 to merely 520 ppm during the middle and latest Rupelian (Henderiks and Pagani, 2008; Fig. 11A).

Our new proxy data in conjunction with the new numerical simulation, however, suggests a stronger increase of pCO_2 levels by at least 160 ppm (400 ppm to 2 x PAL) during that time interval (Fig. 11A). In fact, the proxy-derived temperatures exceed those predicted by the new models by up to 2 °C (Fig. 11B). One possibility for this discrepancy is that the actual pCO_2 rise was even larger than 160 ppm, but certainly less than 440 ppm (= increase from 400 ppm to 3 x PAL). An alternative explanation is that the regional climate sensitivity, i.e., the environmental feedback to atmospheric pCO_2 forcing in Central Europe was higher than assumed by the model. In fact, our model is already on the high end of Earth system sensitivity (4.1 °C for a doubling of pCO_2; compare Stepanek and Lohmann, 2012, and Haywood et al., 2013) as compared to several other models participating in PlioMip (Haywood et al., 2013).

The large-scale response of the Earth system depends on the climate sensitivity in the model. Every doubling of pCO_2 will increase global temperatures by about 3-4 °C (Hansen et al., 2008; Solomon et al., 2007). In general, the Earth system sensitivity of our models is higher than the climate sensitivity of 3 - 4 °C (PALAEOSENSE, 2012). Furthermore, the response to changes in radiative forcing can be regionally strongly different (Boer and Yu, 2003), with especial influences from the land-sea distribution and non-linear effects like sea ice. Our climate simulation is admittedly coarse and the regional details might be difficult to simulate, especially when dealing with very narrow gateways (in our case, there is no southern gateway). We suspect however, that the large-scale features are well captured. Interestingly, we detect a large Arctic polar amplification (Fig. 10) which is consistent with model results dealing with global warming scenarios in the next century (Stocker et al., 2013).

5. Summary and conclusions

Seasonal SST that prevailed during the middle Rupelian stage to the middle Chattian stage (ca. from 31 to 25 Ma) in surface waters of the Central European epicontinental seaway were reconstructed from oxygen isotope data of bivalve shell carbonate and shark teeth enamel. The multispecies approach (five bivalve species and three shark species with different growing seasons) provided a robust data set for the reconstruction of paleoseasonality. Our findings revealed for the

first time a 4 °C warming during the late Rupelian (ca. 29 Ma), with the warming being more pronounced during summer (5 °C) than during winter (3 °C). According to new climate models, the observed late Rupelian warming can be explained by an atmospheric pCO_2 rise of at least 160 ppm (from 400 to 560 ppm). Such an increase exceeds the rise suggested by existing pCO_2 estimates, but still lies within the uncertainty ranges of proxy-derived pCO_2 reconstructions for that time interval.

The present study showed how seasonally resolved SST estimates from fossils can be used to validate the reliability of numerical paleoclimate simulations. In turn, numerical climate models can help to place such regional data in a broader context to address climate changes on a global scale. Furthermore, the projected atmospheric pCO_2 increase reported in this study compares well with pCO_2 predicted for the next centuries. Given the overall similarity with the modern world (primarily in terms of paleogeography), the mid-Oligocene interval can serve as a natural laboratory to study the possible effects of human-driven global warming.

6. Acknowledgments

Not displayed for reasons of data protection

References

Anderson, H.-J., 1961. Gliederung und paläogeographische Entwicklung der Chattischen Stufe (Oberoligocän) im Nordseebecken. Meyniana 10, 118–146.

Anderson, T.F., Arthur, M.A., 1983. Stable isotopes of oxygen and carbon and their application to sedimentologic and paleoenvironmental problems. Society of Economic Paleontologists and Mineralogists (SEPM) Short Course 10, 1–151.

Bahlo, E., 1976. Gebißreste von Cricetiden und Theridomyiden (Rodentia) aus dem Mitteloligozän von Gabsheim bei Alzey (Rheinhessen). Mainzer Geowissenschaftliche Mitteilungen 5, 5–11.

Bahlo, E., Neuffer, F.O., 1978. Weitere Funde von Kleinsäugern aus Schleichsand und Cyrenen-Mergel in Rheinhessen (Oligozän, Tertiär, Mainzer Becken). Mainzer Geowissenschaftliche Mitteilungen 7, 5–25.

Bahlo, E., Tobien, H., 1982. Bestandsaufnahme der Säugetiere im „prä-aquitanen“ Tertiär des Mainzer Beckens. Mainzer Geowissenschaftliche Mitteilungen 10, 131–157.

Beerling, D.J., Royer, D.L., 2011. Convergent Cenozoic CO_2 history. Nature Geoscience 4, 418–420.

Berger, J.-P., Reichenbacher, B., Becker, D., Grimm, M.C., Grimm, K.I., Picot, L., Storni, A., Pirkenseer, C., Derer, C., Schaefer, A., 2005a. Paleogeography of the Upper Rhine Graben (URG) and the Swiss Molasse Basin (SMB) from Eocene to Pliocene. International Journal of Earth Sciences 94, 697–710.

Berger, J.-P., Reichenbacher, B., Becker, D., Grimm, M.C., Grimm, K.I., Picot, L., Storni, A., Pirkenseer, C., Schaefer, A., 2005b. Eocene-Pliocene time scale and stratigraphy of the Upper Rhine Graben (URG) and the Swiss Molasse Basin (SMB). International Journal of Earth Sciences 94, 711–731.

Boer, G.J., Yu, B., 2003. Climate sensitivity and climate state. Climate Dynamics 21, 167–176.

Bonfil, R., Meÿer, M., Scholl, M.C., Johnson, R., O'Brien, S., Oosthuizen, H., Swanson, S., Kotze, D., Paterson, M., 2005. Transoceanic migration, spatial dynamics, and population linkages of white sharks. Science 310, 100–103.

Brovkin, V., Raddatz, T., Reick, C.H., Claussen, M., Gayler, V., 2009. Global biogeophysical interactions between forest and climate. Geophys. Research Letters 36, L07405.

Bušelić, I., Peharda, M., Reynolds, D.J., Butler, P.G., González, A.R., Ezgeta-Balić, D., Vilibić, I., Grbec, B., Hollyman, P., Richardson, C.A., 2015. *Glycymeris bimaculata* (Poli, 1795) - a new sclerochronological archive for the Mediterranean? Journal of Sea Research 95, 139–148.

Cai, W., Chu, P.C., 1998. Oceanic responses to gradual transitions of equator-to-pole temperature-gradients. Quarterly Journal of the Royal Meteorological Society 124, 2817–2828.

Carpenter, K.E., Niem, V.H., 1998. FAO species identification guide for fishery purposes. The living marine resources of the Western Central Pacific. Volume 1. Seaweeds, corals, bivalves and gastropods. Food and Agriculture Organization of the United Nations, Rome, Italy, 686 pp.

Chauvaud, L., Thouzeau, G., Paulet, Y.M., 1998. Effects of environmental factors on the daily growth rate of *Pecten maximus* juveniles in the Bay of Brest (France). Journal of Experimental Marine Biology and Ecology 227, 83–111.

Chauvaud, L., Lorrain, A., Dunbar, R.B., Paulet, Y.M., Thouzeau, G., Jean, F., Guarini, J.M., Mucciarone, D., 2005. Shell of the Great Scallop *Pecten maximus* as a high-frequency archive of paleoenvironmental changes. Geochemistry, Geophysics, Geosystems 6, 1–15.

Chenery, C., Müldner, G., Evans, J., Eckardt, H., Lewis, M., 2010. Strontium and stable isotope evidence for diet and mobility in Roman Gloucester, UK. Journal of Archaeological Sciences 37, 150–163.

Collins, M., An, S.-I., Cai, W., Ganachaud, A., Guilyardi, E., Jin, F.-F., Jochum, M., Lengaigne, M., Power, S., Timmermann, A., Vecchi, G., Wittenberg, A., 2010. The impact of global warming on the tropical Pacific Ocean and El Niño. Nature Geosciences 3, 391–397.

Collins, M., Knutti, et al., 2013: Long-term climate change: projections, commitments and irreversibility. In: Stocker, T.F., Qin, D., et al., (Eds.), Climate Change 2013: The Physical Science Basis. Contribution of Working Group I to the Fifth Assessment Report of the Intergovernmental Panel on Climate Change. Cambridge University Press, Cambridge, United Kingdom and New York, NY, USA, pp. 1029-1136.

Cramer, B.S., Miller, K.G., Barrett, P.J., Wright, J.D., 2011. Late Cretaceous-Neogene trends in deep ocean temperature and continental ice volume: reconciling records of benthic foraminiferal geochemistry ($\delta^{18}O$ and Mg/Ca) with sea level history. Journal of Geophysical Research 116, 1–23.

Compagno, L.J.V., 2001. FAO species identification guide for fishery purposes. Sharks of the world. Volume 2. An annotated and illustrated catalogue of shark species known to date. Volume 2. Bullhead, mackerel and carpet sharks (Heterodontiformes, Lamniformes and Orectolobiformes). Food and Agriculture Organization of the United Nations, Rome, Italy, 269 pp.

Crnčević, M., Peharda, M., Ezgeta-Balić, D., Pećarević, M., 2013. Reproductive cycle of *Glycymeris nummaria* (Mollusca: Bivalvia) from Mali Ston Bay, Adriatic Sea, Croatia. Scientia Marina 77, 293–300.

De Man, E., Ivany, L.C., Vandenberghe, N., 2004. Stable oxygen isotope record of the Eocene-Oligocene transition in the southern North Sea Basin: positioning the Oi-1 event. Netherlands Journal of Geosciences 83, 193–197.

De Man, E., Van Simaeys, S., Vendenberghe, N., Harris, W.B., Wampler, J.M., 2010. On the nature and chronostratigraphic position of the Rupelian and Chattian stratotypes in the southern North Sea basin. Episodes 33, 3–14.

DeConto, R.M., Pollard, D., 2003. Rapid Cenozoic glaciation of Antarctica induced by declining atmospheric CO_2. Nature 421, 245–249.

DeConto, R.M., Pollard, D., Wilson, P. A, Pälike, H., Lear, C.H., Pagani, M., 2008. Thresholds for Cenozoic bipolar glaciation. Nature 455, 652–656.

Dèzes, P., Schmid, S.M., Ziegler, P.A., 2004. Evolution of the European Cenozoic Rift System: interaction of the Alpine and Pyrenean orogens with their foreland lithosphere. Tectonophysics 389, 1–33.

Dettman, D.L., Reische, A.K., Lohmann, K.C., 1999. Controls on the stable isotope composition of seasonal growth bands in aragonitic fresh-water bivalves (unionidae). Geochimica et Cosmochimica Acta 63, 1049–1057.

Dijkstra, H.H., 2013. Pectinoidea (Bivalvia: Propeamussiidae and Pectinidae) from the Panglao region, Philippine Islands. Vita Malacologica 10, 1–108.

Dijkstra, H.H., Warén, A., Gudmundsson, G., 2009. Pectinoidea (Mollusca: Bivalvia) from Iceland. Marine Biology Research 5, 207–243.

Domeier, M., Nasby-Lucas, N., 2008. Migration patterns of white sharks *Carcharodon carcharias* tagged at Guadalupe Island, Mexico, and identification of an eastern Pacific shared offshore foraging area. Marine Ecology Progress Series 370, 221–237.

Epstein, S., Buchsbaum, R., Lowenstam, H., Urey, H., 1953. Revisited carbonate-water isotopic temperature scale. Bulletin of the American Meteorological Society 64, 1315–1326.

Erdei, B., Utescher, T., Hably, L., Tamás, J., Roth-Nebelsick, A., Grein, M., 2012. Early Oligocene continental climate of the Palaeogene Basin (Hungary and Slovenia) and the surrounding area. Turkish Journal of Earth Sciences 21, 153–186.

Fischer, J., Schneider, J.W., Voigt, S., Joachimski, M.M., Tichomirowa, M., Tütken, T., Götze, J., Berner, U., 2013. Oxygen and strontium isotopes from fossil shark teeth: environmental and ecological implications for Late Palaeozoic European basins. Chemical Geology 342, 44–62.

Gilles, R., 1972. Osmoregulation in three molluscs: *Acanthochitona discrepans* (BROWN), *Glycymeris glycymeris* (L.) and *Mytilus edulis* (L.). Biological Bulletin 142, 25–35.

Gillikin, D.P., De Ridder, F., Ulens, H., Elskens, M., Keppens, E., Baeyens, W., Dehairs, F., 2005. Assessing the reproducibility and reliability of estuarine bivalve shells (*Saxidomus giganteus*)

for sea surface temperature reconstruction: implications for paleoclimate studies. Palaeogeography, Palaeoclimatology, Palaeoecology 228, 70–85.

Gong, X., Knorr, G., Lohmann, G., Zhang, X., 2013. Dependence of abrupt Atlantic meridional ocean circulation changes on climate background states. Geophyscial Research Letters 40, 3698–3704.

Gradstein, F.M., Ogg, J.G., Schmitz, M., Ogg, G., 2012. The Geologic Time Scale 2012. Elsevier Amsterdam, The Netherlands, 1144 pp.

Gramann, F., Harre, W., Kreuzer, H., 1980. A K-Ar glauconite age for Early Eochattian *Asterigerina* beds within the German Oligocene. Geologisches Jahrbuch A 54, 57–60.

Grimm, K.I., 1994. Paläoökologie, Paläogeographie und Stratigraphie im Mainzer Becken, im Oberrheingraben, in der Hessischen Senke und in der Leipziger Bucht während des Mittleren Rupeltons (Fischschiefer/Rupelium/Unteroligozän). Mitteilungen der Pollichia 81, 7–193.

Grimm, K.I., 1998. Correlation of Rupelian coastal and basin facies in the Mainz Basin (Oligocene, Germany). Neues Jahrbuch für Geologie und Paläontologie, Monatshefte 3, 146–156.

Grimm, K.I., 2002. Foraminiferal zonation of early Oligocene deposits (Selztal Group, Latdorfian, Rupelian) in the Mainz Basin, Germany. Journal of Micropalaeontology 21, 67–74.

Grimm, K.I., 2006. Meeresverbindungen im Rupelium Mitteleuropas - paläobiogeographische Untersuchungen anhand von Foraminiferen. Geologisches Jahrbuch Hessen 133, 19–27.

Grimm, K.I., Grimm, M.C., 2005. Die Alzey-Formation (Rupelium, Mainzer Becken) am Steigerberg bei Eckelsheim: sedimentologische, sequenzstratigraphische und biostratigraphische Untersuchungen eines transgressiven Küstensystems. Geologica et Palaeontologica 39, 79–108.

Grimm, K.I., Grimm, M.C., Schindler, T., 2000. Lithostratigraphische Gliederung im Rupelium/Chattium des Mainzer Beckens, Deutschland. Neues Jahrbuch für Geologie und Paläontologie, Abhandlungen 218, 343–397.

Grimm, K.I., Grimm, M.C., Neuffer, Lutz, H., 2003. Die fossilen Wirbellosendes Mainzer Tertiärbeckens Teil 1-1 Geologischer Führer durch das Mainzer Tertiärbecken. Mainzer Naturwissenschaftliches Archiv, Beihefte 26, 1–158.

Grimm, K.I., Grimm, M., Radtke, G., Kadolsky, D., Schäfer, P., Franzen, J.L., Schindler, T., Hottenrott Martin, 2011. Mainzer Becken. In: Deutsche Stratigraphische Kommission (Eds.), Stratigraphie von Deutschland IX. Tertiär, Teil 1. SDGG 75, 133–209.

Grossman, E.L., Ku, T.-L., 1986. Oxygen and carbon isotope fractionation in biogenic aragonite: temperature effects. Chemical Geology (Isotope Geoscience Section) 59, 59–74.

Hagemann, S., Dümenil, L., 1998. A parametrization of the lateral waterflow for the global scale. Climate Dynamics 14, 17–31.

Hall, J.G., 1985. The adaptation of enzymes to temperature: catalytic characterization of glucosephosphate isomerase homologues isolated from *Mytilus edulis* and *Isognomon alatus*, bivalve molluscs inhabiting different thermal environments. Molecular Biology and Evolution 2, 251–269.

Hallmann, N., Schöne, B.R., Irvine, G.V, Burchell, M., Cokelet, E.D., Hilton, M.R., 2011. An improved understanding of the Alaska Coastal Current: the application of a bivalve growth-temperature model to reconstruct freshwater-influenced paleoenvironments. Palaios 26, 346–363.

Hallmann, N., Schöne, B.R., Strom, A., Fiebig, J., 2008. An intractable climate archive - Sclerochronological and shell oxygen isotope analyses of the Pacific geoduck, *Panopea abrupta* (bivalve mollusk) from Protection Island (Washington State, USA). Palaeogeography, Palaeoclimatology, Palaeoecology 269, 115–126.

Hansen, B., Østerhus, S., Quadfasel, D., Turrel, W., 2004. Already the day after tomorrow? Science 305, 953–954.

Hansen, J., Sato, M., Kharecha, P., Beerling, D., Berner, R., Masson-Delmotte, V., Pagani, M., Raymo, M., Royer, D.L., Zachos, J.C., 2008. Target atmospheric CO_2: where should humanity aim? The Open Atmospheric Science Journal 2, 217–231

Haq, B.U., Hardenbol, J., Vail, P.R., 1988. Mesozoic and Cenozoic chronostratigraphy and cycles of sea-level change, in: Wilgus, C.K., Hasting, B.S., Posamentier, H., Van Wagoner, J., Ross, C.K., Kendall, C.G.S.C. (Eds.), Sea-Level Changes. Society of Economic Paleontologists and Mineralogists (SEPM) Special Publication 42, 71–108.

Hardenbol, J., Thierry, J., Farley, M.B., Jacquin, T., Graciansky, P.-C., Vail, P.R., 1998. Mesozoic and Cenozoic sequence chronostratigraphic framework of European basins. In: de Graciansky, P-C, Hardenbol, J, Jacquin, T, Vail, P. R. (Eds.), Mesozoic and Cenozoic Sequence Stratigraphy of European Basins, 3–14; Appendix 763–782 + 8 Charts.

Haywood, A.M., Hill, D.J., Dolan, A.M., Otto-Bliesner, B.L., Bragg, F., Chan, W.L., Chandler, M.A., Contoux, C., Dowsett, H.J., Jost, A., Kamae, Y., Lohmann, G., Lunt, D.J., Abe-Ouchi, A., Pickering, S.J., Ramstein, G., Rosenbloom, N.A., Salzmann, U., Sohl, L., Stepanek, C., Ueda, H., Yan, Q., Zhang, Z., 2013. Large-scale features of Pliocene climate: Results from the Pliocene Model Intercomparison Project. Climate of the Past 9, 191–209.

Henderiks, J., Pagani, M., 2008. Coccolithophore cell size and the Paleogene decline in atmospheric CO_2. Earth and Planetary Science Letters 269, 576–584.

Hendry, J.P., Perkins, W.T., Bane, T., 2001. Short-term environmental change in a Jurassic lagoon deduced from geochemical trends in aragonite bivalve shells. Geological Society of America Bulletin 113, 790–798.

Héran, M.-A., Lécuyer, C., Legendre, S., 2010. Cenozoic long-term terrestrial climatic evolution in Germany tracked by $\delta^{18}O$ of rodent tooth phosphate. Palaeogeography, Palaeoclimatology, Palaeoecology 285, 331-324.

Huber, M., 2010. Compendium of bivalves. A full-color guide to 3,300 of the World´s Marine Bivalves. A status on Bivalvia after 250 years of research. ConchBooks, Hackenheim, Germany, 904 pp.

Huyghe, D., Lartaud, F., Emmanuel, L., Merle, D., Renard, M., 2015. Palaeogene climate evolution in the Paris Basin from oxygen stable isotope ($\delta^{18}O$) compositions of marine molluscs. Journal of the Geolocial Society 172, 576–587.

Immenhauser, A., 2009. Estimating palaeo-water depth from the physical rock record. Earth-Science Reviews 96, 107–139.

Indans, J., 1965. Nachweis des Asterigerinen-Horizontes im Oberoligozän des Dobergs bei Bünde/Westfalen. Neues Jahrbuch für Geologie und Paläontologie, Abhandlungen 123, 20–24.

Jones, D.S., Quitmyer, I.R., 1996. Marking time with bivalve shells: oxygen isotopes and season of annual increment formation. Palaios 11, 340–346.

Jungclaus, J.H., Keenlyside, N., Botzet, M., Haak, H., Luo, J.J., Latif, M., Marotzke, J., Mikolajewicz, U., Roeckner, E., 2006. Ocean circulation and tropical variability in the coupled model ECHAM5/MPI-OM. Journal of Climate 19, 3952–3972.

Kim, S.-T., Mucci, A., Taylor, B.W., 2007. Phosphoric acid fractionation factors for calcite and aragonite between 25 and 75 °C: revisited. Chemical Geology 246, 135–146.

Knorr, G., Lohmann, G., 2014. Climate warming during Antarctic ice sheet expansion at the Middle Miocene transition. Nature Geoscience 7, 376–381.

Kocsis, L., Ozsvárt, P., Becker, D., Ziegler, R. Scherler, L., Codrea, V., 2014. Orogeny forced terrestrial climate variation during the late Eocene-early Oligocene in Europe. Geology 42, 727-730.

Körper, J., Höschel, I., Lowe, J. a., Hewitt, C.D., Salas y Melia, D., Roeckner, E., Huebener, H., Royer, J.-F., Dufresne, J.-L., Pardaens, A., Giorgetta, M. A., Sanderson, M.G., Otterå, O.H., Tjiputra, J., Denvil, S., 2012. The effects of aggressive mitigation on steric sea level rise and sea ice changes. Climate Dynamics 40, 531–550.

Kümmerle, E., 1963. Die Foraminiferenfauna des Kasseler Meeressandes (Oberoligozän) im Ahnetal bei Kassel (Bl. Nr. 4622 Kassel-West). Abhandlungen des Hessischen Landesamtes für Bodenforschung 45, 1–72.

Lear, C.H., H,E., Wilson, P.A., 2000. Cenozoic deep-sea temperatures and global ice volumes from Mg/Ca in benthic foraminiferal calcite. Science 287, 269–272.

Lécuyer, C., Grandjean, P., O'Neil, J.R., Cappetta, H., Martineau, F., 1993. Thermal excursions in the ocean at the Cretaceous-Tertiary boundary (northern Morocco): $\delta^{18}O$ record of phosphatic fish debris. Palaeogeography, Palaeoclimatology, Palaeoecology 105, 235–243.

Lécuyer, C., Hutzler, A., Amiot, R., Daux, V., Grosheny, D., Otero, O., Martineau, F., Fourel, F., Balter, V., Reynard, B., 2012. Carbon and oxygen isotope fractionations between aragonite and calcite of shells from modern molluscs. Chemical Geology 332-333, 92–101.

Liu, Z., Pagani, M., Zinniker, D., DeConto, R.M., Huber, M., Brinkhuis, H., Shah, S.R., Leckie, R.M., Pearson, A., 2009. Global cooling during the Eocene-Oligocene climate transition. Science 323, 1187–1190.

Lohmann, G., Pfeiffer, M., Laepple, T., Leduc, G., Kim, J.H., 2013. A model-data comparison of the Holocene global sea surface temperature evolution. Climate of the Past 9, 1807–1839.

Longinelli, A., Nuti, S., 1973. Revisited phosphate-water isotopic temperature scale. Earth and Planetary Science Letters 19, 373–376.

Lott, F., Miller, M.J., 1997. A new subgrid-scale orographic drag parametrization: its formulation and testing. Quarterly Journal of the Royal Meteorological Society 123, 101–127.

Markwick, P.J., 2007. The palaeogeographic and palaeoclimatic significance of climate proxies for data-model comparisons. In: Williams, A., Haywood, A.M., Gregory, F.J., Schmidt, D.N. (Eds.), Deep-Time Perspectives on Climate Change: Marrying the Signal from Computer Models and Biological Proxies. Geological Society London, London, 251-312.

Marshall, J., Kushnir, Y., Battisti, D., Chang, P., Czaja, A., Dickson, R., Hurrell, J.W., McCartney, M., Saravanan, R., Visbeck, M., 2001. North Atlantic climate variability: phenomena, impacts and mechanisms. International Journal of Climatology 21, 1863–1898.

Marsland, S.J., Haak, H., Jungclaus, J.H., Latif, M., Röske, F., 2003. The Max-Planck-Institute global ocean/sea ice model with orthogonal curvilinear coordinates. Ocean Modelling 5, 91–127.

Martini, E., 1982. Bestandsaufnahme des Nannoplankton im “prä-aquitanen” Tertiär des Mainzer Beckens. Mainzer Geowissenschaftliche Mitteilungen 10, 29–36.

Martini, E., Müller, C., 1971. Das marine Alttertiär in Deutschland und seine Einordnung in die Standard Nannoplankton Zonen. Erdöl und Kohle 24, 381–384.

McArthur, J.M., Howarth, R.J., Bailey, T.R., 2001. Strontium isotope stratigraphy: LOWESS version 3: best fit to the marine Sr-isotope curve for 0-509 Ma and accompanying look-up table for deriving numerical age. Journal of Geology 109, 155–170.

Miller, K.G., Wright, J.D., Fairbanks, R.G., 1991. Unlocking the ice house: Oligocene-Miocene oxygen isotopes, eustacy, and margin erosion. Journal of Geophysical Research 96, 6829–6848.

Mook, W.G., 1971. Paleotemperatures and chlorinities from stable carbon and oxygen isotopes in shell carbonate. Palaeogeography, Palaeoclimatology, Palaeoecology 9, 245–263.

Mosbrugger, V., Utescher, T., Dilcher, D.L., 2005. Cenozoic continental climatic evolution of Central Europe. Proceedings of the National Academy of Sciences USA 102, 14964–9.

Nerot, C., Lorrain, A., Grall, J., Gillikin, D.P., Munaron, J.-M., Le Bris, H., Paulet, Y.-M., 2012. Stable isotope variations in benthic filter feeders across a large depth gradient on the continental shelf. Estuarine, Coastal and Shelf Science 96, 228–235.

Otway, N.M., Ellis, M.T., 2011. Pop-up archival satellite tagging of *Carcharias taurus*: movements and depth/temperature-related use of south-eastern Australian waters. Marine and Freshwater Research 62, 607–620.

Owen, R., Richardson, C.A., Kennedy, H.A., 2002. The influence of shell growth rate on striae deposition in the scallop *Pecten maximus*. Journal of the Marine Biological Association of the United Kingdom 82, 621–623.

Pagani, M., Zachos, J.C., Freeman, K.H., Tipple, B., Bohaty, S., 2005. Marked decline in atmospheric carbon dioxide concentrations during the Paleogene. Science 309, 600–603.

PALAEOSENSE Project Members, 2012. Making sense of palaeoclimate sensitivity. Nature 491, 683–691.

Pälike, H., Norris, R.D., Herrle, J.O., Wilson, P.A., Coxall, H.K., Lear, C.H., Shackleton, N.J., Tripati, A.K., Wade, B.S., 2006. The heartbeat of the Oligocene climate system. Science 314, 1894–1898.

Pearson, P.N., Foster, G.L., Wade, B.S., 2009. Atmospheric carbon dioxide through the Eocene-Oligocene climate transition. Nature 461, 1110–1113.

Pekar, S.F., Christie-Blick, N., Kominz, M. A., Miller, K.G., 2002. Calibration between eustatic estimates from backstripping and oxygen isotopic records for the Oligocene. Geology 30, 903–906.

Picot, L., 2002. Le Paléogène des synclinaux du Jura et de la bordure sud-rhénane: paléontologie (Ostracodes), paléoécologie, biostratigraphie, paléogéographie. Geofocus 5, 1–240.

Pollard, D., DeConto, R.M., 2005. Hysteresis in Cenozoic Antarctic ice-sheet variations. Global Planetary Change 45, 9–21.

Pross, J., 2001. Biostratigraphie organisch-wandiger Dinoflagellatenzysten in der Rupel-Abfolge (Unter-Oligozän) des Mainzer Beckens. Mainzer Geowissenschaftliche Mitteilungen 30, 67–80.

Pross, J., Bruch, A., Kvaček, Z., 1998. Paläoklima-Rekonstruktionen für den Mittleren Rupelton (Unter-Oligozän) des Mainzer Beckens auf der Basis mikro-und makrobotanischer Befunde. Mainzer Geowissenschaftliche Mitteilungen 27, 79–92.

Pross, J., Bruch, A., Mosbrugger, V., Kvacek, Z., 2000. Paleogene pollen and spores as a tool for quantitative paleoclimate reconstructions: the Rupelian (Oligocene) of Central Europe. Proceedings of the Ninth International Palynological Congress, Texas, USA, 1996, 23–28 June 1996, American Association of Stratigraphic Palynologists Foundation, pp. 299–310.

Raitzsch, M., Honisch, B., 2013. Cenozoic boron isotope variations in benthic foraminifers. Geology 41, 591–594.

Retallack, G.J., 2001. A 300-million-year record of atmospheric carbon dioxide from fossil plant cuticles. Nature 411, 287–90.

Ritzkowski, S., 1965. Das marine Oligozän im nördlichen Hessen. Stratigraphie und Paläogeographie. Unpublished PhD thesis, University of Marburg, Germany, 194 pp.

Ritzkowski, S., 1967. Mittel-Oligozän, Ober-Oligozän und die Grenze Rupel/Chatt im nördlichen Hessen. Neues Jahrbuch für Geologie und Paläontologie, Abhandlungen 127, 293–336.

Ritzkowski, S., 2005. Das Tertiär der Hessischen Senke in der Stratigraphischen Tabelle von Deutschland 2002. Newsletters on Stratigraphy 41, 339–346.

Ritzkowski, S., Grimm, M.C., Hottenrott, M., 2011. Niederhessische Tertiärsenke. In: Deutsche Stratigraphische Kommission (Eds.), Stratigraphie von Deutschland IX. Tertiär, Teil 1. SDGG 75, pp. 303–375.

Roeckner, E., Brokopf, R., Esch, M., Giorgetta, M., Hagemann, S., Kornblueh, L., Manzini, E., Schlese, U., Schulzweida, U., 2006. Sensitivity of simulated climate to horizontal and vertical resolution in the ECHAM5 atmosphere model. Journal of Climate 19, 3771–3791.

Rögl, F., 1999. Mediterranean and Paratethys. Facts and hypotheses of an Oligocene to Miocene paleogeography (short overview). Geologica Carpathica 50, 339–349.

Roth, P.H., 1970. Oligocene calcareous nannoplankton biostratigraphy. Eclogae Geologicae Helvetiae 63, 799–881.

Roth-Nebelsick, A., Grein, M., Utescher, T., Konrad, W., 2012. Stomatal pore length change in leaves of *Eotrigonobalanus furcinervis* (Fagaceae) from the Late Eocene to the Latest Oligocene and its impact on gas exchange and CO_2 reconstruction. Review of Palaeobotany and Palynology174, 106–112.

Rousse, S., Duringer, P., Stapf, K.R.G., 2012. An exceptional rocky shore preserved during Oligocene (Late Rupelian) transgression in the Upper Rhine Graben (Mainz Basin, Germany). Geological Journal 47, 388–408.

Royer, C., Thébault, J., Chauvaud, L., Olivier, F., 2013. Structural analysis and paleoenvironmental potential of dog cockle shells (*Glycymeris glycymeris*) in Brittany, northwest France. Palaeogeography, Palaeoclimatology, Palaeoecology 373, 123–132.

Schindler, T., Poschmann, M., Wuttke, M., 2005. Chondrichthyan feeding depressions in a subtidal coastal environment from the Mainz Basin (Oligocene, SW Germany). Neues Jahrbuch für Geologie und Paläontologie, Abhandlungen 237, 29–39.

Schöne, B.R., 2013. *Arctica islandica* (Bivalvia): a unique paleoenvironmental archive of the northern North Atlantic Ocean. Global Planetary Change 111, 199–225.

Schöne, B.R., Pfeiffer, M., Pohlmann, T., Siegismund, F., 2005. A seasonally resolved bottom water temperature record for the period of AD 1866-2002 based on shells of *Arctica islandica* (Mollusca, North Sea). International Journal of Climatology 25, 947–962.

Schöne, B.R., Fiebig, J., 2008. Seasonality in the North Sea during the Allerød and Late Medieval Climate Optimum using bivalve sclerochronology. International Journal of Earth Sciences 98, 83–98.

Schöne, B.R., Freyre Castro, A.D., Fiebig, J., Houk, S.D., Oschmann, W., Kröncke, I., 2004. Sea surface water temperatures over the period 1884-1983 reconstructed from oxygen isotope ratios of a bivalve mollusk shell (*Arctica islandica*, southern North Sea). Palaeogeography, Palaeoclimatology, Palaeoecology 212, 215–232.

Scotese, C.R., Gahagan, L., Larson, R., 1988. Plate tectonic reconstructions of the Cretaceous and Cenozoic ocean basins. Tectonophysics 155, 27–48.

Scotese, C.R., 2014. Atlas of Paleogene paleogeographic maps (Mollweide projection), Maps 8-15, Volume 1, The Cenozoic, PALEOMAP Atlas for ArcGIS, PALEOMAP project, Evaston, IL, USA.

Shackleton, N.J., Kennett, J.P., 1975. Paleotemperature history of the Cenozoic and the initiation of Antarctic glaciation: oxygen and carbon isotope analyses in DSDP sites 277, 279, and 281. In: Kennett, J. P., Houtz, R. E. (Eds), Initial Reports of the Deep Sea Drilling Project, 743–755.

Sissingh, W., 2003. Tertiary paleogeographic and tectonostratigraphic evolution of the Rhenish Triple Junction. Palaeogeography, Palaeoclimatology, Palaeoecology 196, 229–263.

Siung, A.M., 1980. Studies on the biology of *Isognomon alatus* GMELIN (bivalvia : isognomonidae) with notes on its potential as a commercial species. Bulletin of Marine Science 30, 90–101.

Śliwińska, K.K., Clausen, O.R., Heilmann-Clausen, C., 2010. A mid-Oligocene cooling (Oi-2b) reflected in the dinoflagellate record and in depositional sequence architecture. An integrated study from the eastern North Sea Basin. Marine and Petroleum Geology 27, 1424–1430.

Solomon, S., Qin, D., Manning, M., Chen, Z., Marquis, M., Averyt, K.B., Tignor, M., Miller, H.L., 2007. Contribution of Working Group I to the Fourth Assessment Report of the Intergovernmental Panel on Climate Change, 2007, Cambridge University Press, Cambridge, UK and New York, NY, USA, 996 pp.

Spiegel, C., Kuhlemann, J., Frisch, W., 2007. Tracing sediment pathways by zircon fission track analysis: Oligocene marine connections in Central Europe. International Journal of Earth Sciences 96, 363–374.

Stepanek, C., Lohmann, G., 2012. Modelling mid-Pliocene climate with COSMOS. Geoscientific Model Development 5, 1221–1243.

Stocker, T.F., Qin, D., et al., 2013: Technical summary. In: Stocker, T.F., Qin, D., et al (Eds.), Climate Change 2013: The Physical Science Basis. Contribution of Working Group I to the Fifth Assessment Report of the Intergovernmental Panel on Climate Change. Cambridge University Press, Cambridge, United Kingdom and New York, NY, USA, pp. 33-115.

Trueman, E.R., Lowe, G. a., 1971. The effect of temperature and littoral exposure on the heart rate of a bivalve mollusc, *Isognomon alatus*, in tropical conditions. Comparative Biochemistry and Physiology A 38, 555–564.

Tütken, T., 2003. Die Bedeutung der Knochenfrühdiagenese für die Erhaltungsfähigkeit in vivo erworbener Element- und Isotopenzusammensetzungen in fossilen Knochen. Unpublished PhD thesis, Eberhard-Karls-Universität Tübingen, 331 pp.

Tütken, T., Vennemann, T.W., Janz, H., Heizmann, E.P.J., 2006. Palaeoenvironment and palaeoclimate of the Middle Miocene lake in the Steinheim basin, SW Germany: a reconstruction from C, O, and Sr isotopes of fossil remains. Palaeogeography, Palaeoclimatology, Palaeoecology 241, 457–491.

Van Simaeys, S., De Man, E., Vandenberghe, N., Brinkhuis, H., Steurbaut, E., 2004. Stratigraphic and palaeoenvironmental analysis of the Rupelian-Chattian transition in the type region: evidence from dinoflagellate cysts, foraminifera and calcareous nannofossils. Palaeogeography, Palaeoclimatology, Palaeoecology 208, 31–58.

Vandenberghe, N., Van Simaeys, S., Steurbaut, E., Jagt, J.W.M., Felder, P.J., 2004. Stratigraphic architecture of the Upper Cretaceous and Cenozoic along the southern border of the North Sea Basin in Belgium. Netherlands Journal of Geosciences 83, 155–171.

Vennemann, T.W., Hegner, E., Cliff, G., Benz, G.W., 2001. Isotopic composition of recent shark teeth as a proxy for environmental conditions. Geochimica et Cosmochimica Acta 65, 1583–1599.

Vennemann, T.W., Fricke, H.C., Blake, R.E., Neil, J.R.O., Colman, A., 2002. Oxygen isotope analysis of phosphates : a comparison of techniques for analysis of Ag_3PO_4. Chemical Geology 185, 321–336.

Wade, B.S., Pälike, H., 2004. Oligocene climate dynamics. Paleoceanography 19, 1–16.

Walliser, E.O., Schöne, B.R., Tütken, T., Zirkel, J., Grimm, K.I., Pross, J., 2015. The bivalve *Glycymeris planicostalis* as a high-resolution paleoclimate archive for the Rupelian (Early Oligocene) of central Europe. Climate of the Past 11, 653–668.

Wanamaker Jr., A.D., Kreutz, K.J., Schöne, B.R., Introne, D.S., 2011. Gulf of Maine shells reveal changes in seawater temperature seasonality during the medieval climate anomaly and the Little Ice Age. Palaeogeography, Palaeoclimatology, Palaeoecology 302, 43–51.

Weber, M.E., Clark, P.U., Kuhn, G., Timmermann, A., Sprenk, D., Gladstone, R., Zhang, X., Lohmann, G., Menviel, L., Chikamoto, M.O., Friedrich, T., Ohlwein, C., 2014. Millennial-

scale variability in Antarctic ice-sheet discharge during the last deglaciation. Nature 510, 134–138.

Wei, W., Lohmann, G., 2012. Simulated Atlantic Multidecadal Oscillation during the Holocene. Journal of Climate 25, 6989–7002.

Wei, W., Lohmann, G., Dima, M., 2012. Distinct modes of internal variability in the global meridional overturning circulation associated with the southern hemisphere westerly winds. Journal of Physical Oceanography 42, 785–801.

Weidman, C.R., Jones, G.A., Lohmann, K.C., 1994. The long-lived mollusk *Arctica islandica*: a new paleoceanographic tool for the reconstruction of bottom temperatures for the continental shelves of the northern North Atlantic Ocean. Journal of Geophysical Research, Oceans 99, 18305–18314.

Yan, L., Schöne, B.R., Arkhipkin, A., 2012. *Eurhomalea exalbida* (Bivalvia): a reliable recorder of climate in southern South America? Palaeogeography, Palaeoclimatology, Palaeoecology 350-352, 91–100.

Zachos, J.C., Pagani, M., Sloan, L., Thomas, E., Billups, K., 2001. Trends, rhythms, and aberrations in global climate 65 Ma to present. Science 292, 686–693.

Zachos, J.C., Dickens, G.R., Zeebe, R.E., 2008. An early Cenozoic perspective on greenhouse warming and carbon-cycle dynamics. Nature 451, 279–283.

Zhang, X., Lohmann, G., Knorr, G., Purcell, C., 2014. Abrupt glacial climate shifts controlled by ice sheet changes. Nature 512, 290–294.

Zhang, Y.G., Pagani, M., Liu, Z., Bohaty, S.M., DeConto, R.M., 2013. A 40-million-year history of atmospheric CO_2. Philosophical Transactions of the Royal Society A 371, 20130096.

MANUSCRIPT III

Inter-annual climate variability in Europe during the Oligocene Icehouse

Submitted to Nature Scientific Reports

Walliser, E.O.[1], Lohmann, G.[2], Niezgodzki I.[2, 3], & Schöne, B.R.[1]

[1] Institute of Geosciences, University of Mainz, Johann-Joachim-Becher-Weg 21, 55128 Mainz, Germany

[2] Alfred Wegener Institute Helmholtz Centre for Polar and Marine Research, Am Alten Hafen 26, 27568 Bremerhaven, Germany

[3] ING PAN - Institute Of Geological Sciences Polish Academy of Sciences, Research Center in Kraków, Senacka 1, 31-002, Kraków, Poland

Contribution:

Concept: EOW

Writing: EOW, BRS

Growth increment width analysis EOW

Numerical climate models: GL, IN

Walliser, E.O., Lohmann, G., Niezgodzki, T., Schöne, B.R, in review. Inter-annual climate variability in Europe during the Oligocene Icehouse. Nature Scientific Reports.

1. Introduction

The Eocence/Oligocene boundary marks the shift of global climate from the early Paleogene Greenhouse to the modern Icehouse state. Climate deterioration particularly affected the Northern Hemisphere, leading to the largest faunal turnover of the Cenozoic in Central Europe. Changes in atmospheric dynamics may have contributed to this extinction event. New sclerochronological data (stable carbon isotopes, annual shell growth) of long-lived marine bivalves and climate models suggest that a North Atlantic Oscillation (NAO)-like pattern dominated the inter-annual climate variability of Europe starting from the mid-Oligocene. Data revealed a distinct quasi-decadal climate variability of 3 - 7 years, which is coherent with simulated Oligocene NAO-like variability (2.5 - 6 years). However, the temporal variability of the NAO precursor differed from the modern NAO (biennial and 6 - 10 years), likely because of the different palaeogeography and elevated atmospheric pCO_2 during the Oligocene. Our results shed light on the climate dynamics behind the Eocene/Oligocene climate transition.

The inter-annual climate variability across Europe is well known for large parts of the Cenozoic[1-7]. As indicated by varved sediments, the atmospheric circulation across Europe was controlled by the El Niño-Southern Oscillation (ENSO) during the Paleogene Greenhouse[1,2]. As revealed by annually resolved archives of Miocene and younger age, however, a precursor of the NAO existed during the Neogene[3,4]. The oldest currently available evidence for such an NAO precursor comes from multi-decadal $\delta^{18}O$ records of late Miocene Mediterranean corals[3]. Due to the lack of specific studies, it is still unknown whether or not such conditions existed during the Oligocene as well. The Oligocene epoch (34 - 23 Ma) was an Icehouse interval characterised by large glaciation events[8]. Ocean and atmospheric circulation patterns were comparable to the present[9,10]. Very likely, the NAO established during this epoch, as westerlies from the North Atlantic became the major source of atmospheric moisture across Central Europe[9,11,12]. A promising approach to test this hypothesis is to study annual shell growth increment width chronologies of long-lived bivalves from shallow marine deposits of the Oligocene and compare their inherent frequencies to numerical climate models that are able to simulate the NAO variability in the past.

2. Results

Shells of long-lived bivalves, *Glycymeris planicostalis* (n = 8), *G. obovata* (n = 8) and *Arctica islandica* (n = 1) were collected from Oligocene shallow marine deposits of the southern North Sea Basin, Belgium (50°50'16.8"N, 5°25'40.8"E: Bilzen Formation), the Mainz Basin, Germany (49°44'24.2"N, 8°04'20.4"E and 49°44’49.4"N, 8°3’28.9"E: Alzey Formation; 49°48'46.4"N, W8°8'32.0"E: Stadecken Formation), and the Kassel Basin, Germany (51°19´11.04"N, 9°24´36.04"E: Kassel Formation) (supplementary Fig. S1 and Table S1).

To identify possible links between shell growth and environmental variables (temperature and food availability), the stable oxygen ($\delta^{18}O_{shell}$) and carbon isotope ($\delta^{13}C_{shell}$) signature of one *Glycymeris* sp. specimen was analysed (supplementary Fig. S2). Seasonal shell growth rates were reconstructed from $\delta^{18}O_{shell}$-derived temperature data that were fitted to sinusoidal temperature models (supplementary Fig. S3). The fossil material was pristinely preserved and therefore suitable for isotopic analysis[13]. Annual $\delta^{13}C_{shell}$ maxima occurred two months before the seasonal growth rate reached its maximum. On average, lowest and highest seasonal $\delta^{13}C_{shell}$ values occurred during spring (1.50 ± 0.39; average ± 1σ) and late autumn (1.78 ± 0.74) (Fig. 1a). Slowest shell accretion rates were observed during summer and autumn, i.e., before and after the annual growth line formation. On the contrary, growth rate maxima were attained during winter/spring (Fig. 1a). Shell growth data and stable carbon isotope data (lagged by two months) were significantly correlated to each other ($R^2 = 0.84$; $p = 0.004$) (Fig. 1b).

Annual growth increment widths were determined in the hinge plate and then converted into relative annual growth data (= standardised growth indices, SGI_{shell})[14] and analysed by means of continuous wavelets (CWT; Morlet wavelet, wave number = 6)[15] to identify their inherent spectral properties. The SGI_{shell} chronologies were between 42 and 155 years long (supplementary Figs. 4 - 6), and their CWT spectra displayed non-stationary signals, i.e., period length and intensity varied through time, between 2.1 and 11.7 year bands (Fig. 2a and b and supplementary Figs. S7-S8). Significant powers at frequencies corresponding to periods of 3 - 7 years occurred in all CWT spectra (e.g., Fig. 2a and b).

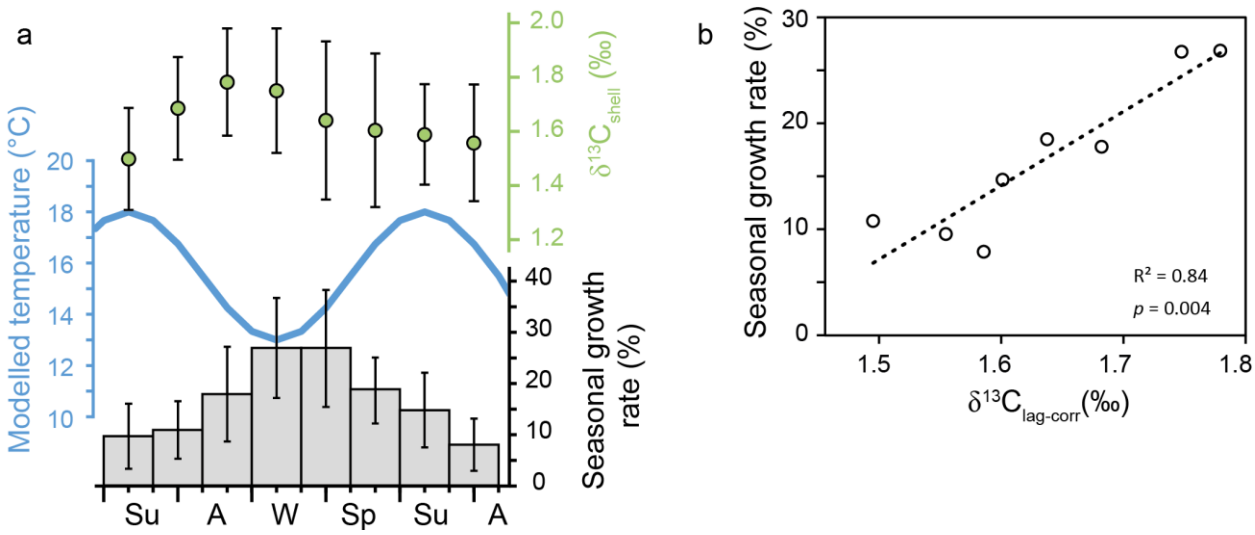

Figure 1. Reconstruction of seasonal shell growth rates of a *Glycymeris planicostalis* shell. (A) Bimonthly averaged seasonal growth rate (grey bars ± 1σ) and $\delta^{13}C_{shell}$ values (green circles ± 1σ). (B) When a two-month lag is applied to the $\delta^{13}C_{shell}$ data ($\delta^{13}C_{lag\text{-}corr}$), the time-series are strongly correlated to each other (dotted line; $R^2 = 0.84$; $p = 0.004$). In (A): blue line = average seasonal water temperature amplitude in the Mainz Basin during the Rupelian stage[18]. Su = summer, A = autumn, W = winter, Sp = spring.

Climate simulations were performed with the Earth System COSMOS using a coarse resolution for a preindustrial (PI_{sim}) scenario and two Oligocene scenarios with atmospheric pCO_2 set to 280 ($O\text{-}280_{sim}$) and 560 ppm ($O\text{-}560_{sim}$), respectively. Simulated data were used to compile correlation maps between winter (December-February) sea level pressure (wSLP) and precipitation rate (wPR). Across Central Europe, the wSLP vs. wPR correlation maps revealed a marked negative domain in both the PI_{sim} and $O\text{-}560_{sim}$ (Fig. 3a and b). However, this domain was larger in the $O\text{-}560_{sim}$ (Fig 3) than in the PI_{sim}, and the correlation value in the studied area was ca. -0.8. On the contrary, correlation between wSLP and surface temperature was relatively weak (R = 0.2 to 0.4) across Central Europe (supplementary Fig. S10).

The wSLP data also provided information on the spatial extent of the NAO in each simulation (NAO_{PI}, $NAO_{O\text{-}280}$ and $NAO_{O\text{-}560}$). For this purpose, we calculated the leading empirical orthogonal function (EOF) of the wSLP data across the North Atlantic (20-90 °N; 90-70 °E). The leading EOF of wSLP of the $O\text{-}560_{sim}$ (PC1 = 34 %) showed a NAO configuration comparable to the PI_{sim} control, i.e., positive and negative centres of action were located north of Iberia and near western Greenland, respectively; PC1 = 45 %) (Fig. 4a and b). However, the positive centre of action was located at higher latitudes (45° -55°N) than in the PI_{sim} control (40°-50°N), whereas the

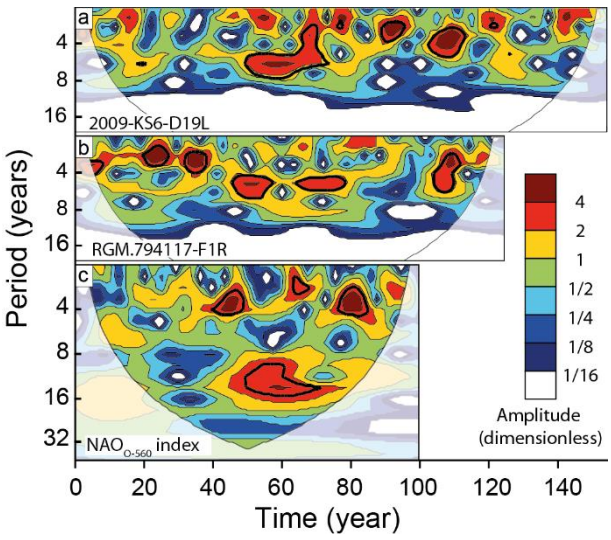

Figure 2. Continuous wavelet spectra (Morlet wavelet, wave number = 6) of SGI_{shell} (A, B) and simulated Oligocene NAO_{O-560} (C) index chronologies. In the studied bivalve shells, common significant spectral peaks (above 5 % significance level against red-noise spectrum) occur mostly between 3 and 7 years (see supplemental material).

negative centre of action was shifted by about 40° to the west (Fig. 4b). On the contrary, the EOF-wSLP pattern of the $O\text{-}280_{sim}$ (PC1 = 46 %) was shifted to the east, showing two distinct negative patterns at high latitudes over Greenland and Eurasia and a positive centre of action at mid latitudes (Fig. 4c).

The last 100 years of the principle component (PC1) series of the simulated wSLP data, were used to compute NAO-indices and successively analysed by mean of CWT. High-frequency periods similar to those observed in the SGI_{shell} chronologies occurred in numerical climate simulations, i.e., 3 - 5 years (NAO_{PI}), 2.5 - 5 years (NAO_{O-560}) and 2 - 6 years (NAO_{O-280}) (Fig. 2c and supplementary Fig. S9)

3. Discussion

Atmospheric circulation exerts a dominant influence on coastal environments by controlling seasonal temperatures, wind stress, and hydrological cycles on land[16,17]. As demonstrated by other studies of bivalves including modern representatives of the studied taxa[14,18], fluctuations of environmental conditions, in particular food supply, can influence shell growth rate[19]. Hence, it is very likely that the observed variations of growth increment widths reflect Oligocene climate dynamics. As demonstrated by previous studies, $\delta^{13}C_{shell}$ values of bivalve shells, including *Arctica islandica*[20], provide information on primary productivity[21], and ca. 10% of the carbon incorporated into the shells originates from metabolised food[22]. The high correlation between the average $\delta^{13}C_{shell}$ values and skeletal accretion rates (Fig. 2B) suggests that shell growth rates of the glycymerids were coupled to variations in food supply, i.e., primary productivity. As

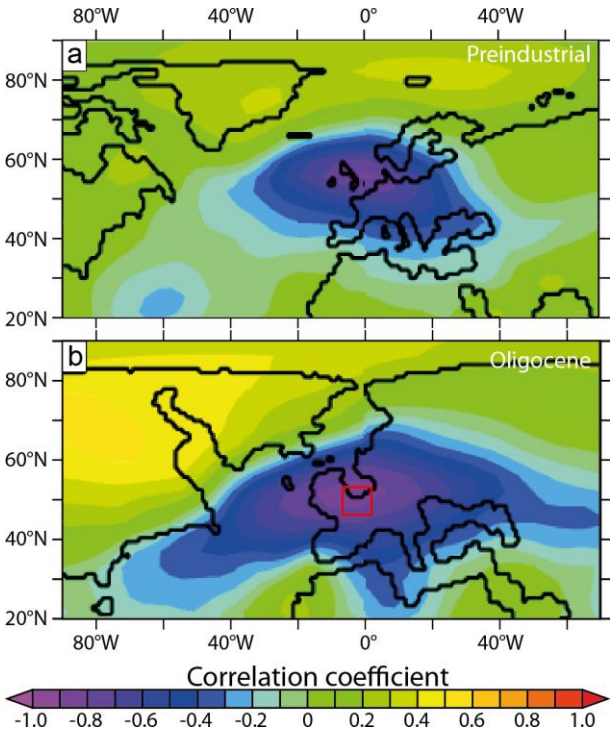

Figure 3. Correlation maps between modelled wSLP and local precipitation rate for preindustrial (A) and Oligocene (O-560) (B) simulations. A negative domain across Central Europe is visible in both correlation maps, suggesting that Oligocene North Atlantic wSLP dynamics governed the inter-annual variations in precipitation in a comparable manner as today. Red square in (B) shows the position of the studies area. Maps were generated using the GrADS software (Version 2.0.1; available at: http://cola.gmu.edu/grads/).

suggested earlier, changes in phytoplankton dynamics in the studied marine basins were primarily induced by variations in precipitation rate[23,24], which, according to our simulations, were controlled by atmospheric circulation, i.e., wSLP changes (Fig. 3 B). Most likely, the studied bivalves recorded such changes in their shells in the form of annual increment widths that fluctuated on NAO-like, quasi-decadal time-scales. Similar spectral peaks in the SGI_{shell} and the NAO_{O-560} time-series lend support to this hypothesis. Unfortunately, it is not possible to preclude that CWT spectra contain analytical artefacts (e.g., edge effects; see CWT spectra of specimen 2009-KS-D17L; supplementary Fig. S8). However, both longer (>70) and shorter (<70) SGI_{shell} chronologies displayed significant powers in the 3 to 7-year bands (Fig. 2A, B). According to this finding most of the high powers located between these periods are likely not the result of artefacts, but reflect oscillations of environmental variables to which the studied bivalves were exposed. Since the studied fossils cover a stratigraphic range of about 5 Ma (30 to 25 Ma) and originate from different marine basins located several hundreds of km from each other, the observed common spectral power is not merely the result of local environmental fluctuations but rather reflect a large-scale climate phenomenon. Accordingly, the CWT results suggest that the quasi-decadal atmospheric variability during the Oligocene (3 - 7 years) slightly deviated from the time-scales of the modern NAO (i.e., biennial and 6 - 10-year cycles)[7]. This is probably because of the different spatial distribution of the two patterns related to different palaeogeographical settings of the studied time intervals (Fig. 4). In this regard, the Oligocene atmospheric variability compares well to inter-annual oscillations observed in high-resolution records of Miocene age from Europe[3-

[5]. Similarly to the Oligocene, the Miocene was also an epoch characterised by narrower North Atlantic Basin than present and a reduced Greenland ice sheet [25].

The westward displacement of the $NAO_{O\text{-}560}$ pattern likely resulted from higher atmospheric pCO_2 levels during the Oligocene. In fact, the two Oligocene simulations yielded markedly different EOF-wSLP configurations. Stronger atmospheric forcing ($O\text{-}560_{sim}$) resulted in a counter-clockwise rotation of the EOF pattern (Fig. 4B). This is likely because higher global temperatures induce a northward migration of the sub-tropical jet streams which ultimately results in the contraction of the Northern Hemispheric atmospheric circulation patterns[26,27].

As demonstrated here, the North Atlantic variability gained control on the short-term climate fluctuations of Central Europe as early as during the Oligocene. Prior to that time, the climate of this region was influenced by the ENSO[1,2]. We hypothesize that the transition from an ENSO-dominated climate regime to an NAO-like regime contributed to the pervasive climate deterioration near the Eocene-Oligocene boundary[1,28,29] and possibly played a role in the late Paleogene terrestrial and marine faunal turnover[30].

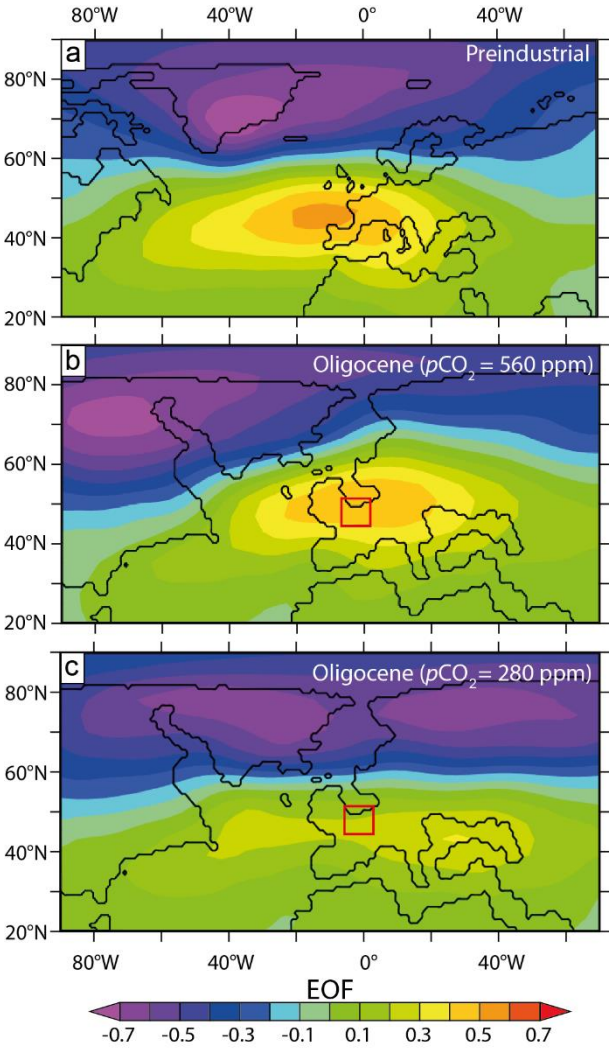

Figure 4. The empirical orthogonal Function (EOF) analysis of the modelled wSLP across the North Atlantic sector. NAO-like pattern (positive and a negative centres of action located at subpolar and European mid latitudes, respectively) are visible in both (A) preindustrial and (B) Oligocene (O-560) as well as (C) Oligocene (O-280) simulations. Red square in (B) shows the position of the studies area. Maps were generated using the GrADS software (Version 2.0.1; available at: http://cola.gmu.edu/grads/).

The spectral properties of the annual shell growth time-series of Oligocene bivalves from Central Europe closely resemble the variability of modern atmospheric circulation patterns.

According to numerical climate simulations, an NAO-like pattern existed across the North Atlantic, but its spatial distribution and internal variability differed from today, due to the peculiar palaeogeography and higher atmospheric pCO_2 concentrations during the Oligocene. Accordingly, the new data presented here show that an NAO-like atmospheric circulation pattern already existed during the middle Oligocene (31 - 25 Ma), about 20 Ma earlier than previously documented.

4. Methods

The geographical position and stratigraphic context of the studied deposits are illustrated in supplementary Fig. S1A, B. The deposits of the Bilzen Formation (Belgium) encompasses the lower part of the nanoplankton zone NP23[31]. The deposits of the Alzey Formation (Germany) comprise the upper part of the nanoplankton zone NP23 and the lower part of the NP24[32,33] and are slightly younger than the Bilzen Formation. The overlaying deposits of the Stadecken Formation (Germany) fall within the middle part of the nanoplankton zone NP24[33]. The deposits of the Kassel Formation and encompasses the upper part of the nanoplankton zone NP24 and the lower part of NP25[34-36]. $^{87}Sr/^{86}Sr$ dating performed on a well-preserved *Glycymeris obovata* shell from these deposits yielded an age of 25.5 ± 0.5 Ma[37].

The shell material (supplementary Fig. S1C) was mounted on Plexiglas cubes using Gluetec Multipower plastic welder and wrapped in a protective layer of WIKO metal epoxy resin to avoid breakage during sectioning. Sectioning was performed with a low-speed precision saw equipped with a 0.4 mm-thick diamond-coated blade. From each shell, two 3 mm-thick slabs were cut and successively attached to glass slides with the mirroring side facing up. The slabs were then repeatedly ground on glass plates using 320, 800, and 1200 grit SiC powder and finally polished with a 1 µm Al_2O_3 powder. Between each step, slabs were ultrasonically rinsed with water. One slab of each sample was immersed in Mutvei´s solution for 40 min at 37 - 40°C[38]. Thereafter, samples were carefully rinsed with deionised water and air-dried (supplementary Fig. S1D).

The stained samples were photographed under a binocular at 12X magnification. Growth increment widths were measured in the hinge plate (supplementary Fig. 1E) using the image processing software Panopea (©Peinl and Schöne) and used to construct age-detrended and

standardised annual shell growth data (= standardised growth indices, SGI)[15]. The ontogenetic trends of the shell accretion rates were estimated for each shell with a highly adaptive 4-year spline.

Carbonate powder samples (50 - 120 µg) for stable isotope analysis were collected (milling) from the outer shell layer of the valve of specimen MB-Wht-2. Stable oxygen and carbon analysis was performed at 72 °C using a Thermo Finnigan MAT 253 continuous flow isotope ratio mass spectrometer coupled to a GasBench II at the Institute of Geosciences, University of Mainz. Isotope data were calibrated against an NBS-19 calibrated Carrara marble ($\delta^{13}C$ = 2.01 ‰; $\delta^{18}O$ = -1.91 ‰) distributed by IVA-Analysentechnik e.K. (Germany). Internal precision (1σ) and accuracy were better than 0.05 ‰, respectively (for further details see[37]). Results of the analysis are expressed in ‰ (per mil) with respect to the VPDB (Vienna Pee Dee belemnite) standard.

Numerical climate simulations were performed with the Earth System Model COSMOS for pre-industrial[39] and Oligocene conditions including the atmosphere component ECHAM5 at T31 resolution (~3.75°) with 19 vertical layers[40]. The ocean component MPI-OM, including the dynamics of sea ice formulated using viscous-plastic rheology, has an average horizontal resolution of 3° × 1.8° with 40 uneven vertical layers[41]. Based on the palaeogeography compiled by GETECH company[42], we prepared boundary conditions necessary to run the model[43] including a global vegetation distribution, the set-up of the hydrological discharge model[44] and orography related parameters for the gravity wave drag parametrization[45]. Oligocene atmospheric carbon dioxide levels were set at 280 and 560 ppm. The coupled atmosphere - ocean configuration was integrated for 3500 years in order to achieve climate steady state. The last 100 years were taken for the (EOF) analysis[46] of modeled wSLP data. The NAO pattern was defined as the leading EOF (PC1) of the wSLP across the North Atlantic sector (20°N-90°N, 90°W-70°E)[47] and the 100-year long PC1 time-series were used to define the NAO-index in each simulation.

Acknowledgements

Not displayed for reasons of data protection

Author contributions

E.O.W. and B.R.S. designed the study, collected the samples and led the analysis of the fossil material. G.L. and I.N. led the numerical climate model analysis. E.O.W. and B.R.S. drafted the manuscript with comments from all authors.

Competing financial interest

The authors declare no competing financial interests.

Data availability

The datasets generated during and/or analysed during the current study are available from the corresponding author on reasonable request.

References

1 Mingram, J., 1998. Laminated Eocene maar-lake sediments from Eckfeld (Eifel region, Germany) and their short-term periodicities. Palaeogeography, Palaeoclimatology, Palaeoecology 140, 289–305.

2 Lenz, O.K., Wilde, V., Riegel, W., Harms, F.-J., 2010. A 600 k.y. record of El Niño-Southern Oscillation (ENSO): evidence for persisting teleconnections during the Middle Eocene greenhouse climate of Central Europe. Geology 38, 627–630.

3 Brachert, T.C., Reuter, M., Felis, T., Kroeger, K., Lohmann, G., Micheels, A., Fassoulas, C., 2006. *Porites* corals from Crete (Greece) open a window into Late Miocene (10 Ma) seasonal and interannual climate variability. Earth and Planetary Science Letters 245, 81–94.

4 Mertz-Kraus, R., Brachert, T.C., Reuter, M., Galer, S.J.G., Fassoulas, C., Iliopoulos, G., 2009. Late Miocene sea surface salinity variability and paleoclimate conditions in the Eastern Mediterranean inferred from coral aragonite $\delta^{18}O$. Chemical Geology 262, 202–216.

[5] Galeotti, S., von der Heydt, A., Huber, M., Bice, D., Dijkstra, H., Jilbert, T., Lanci, L., Reichart, G.J., 2010. Evidence for active El Niño Southern Oscillation variability in the Late Miocene greenhouse climate. Geology 38, 419–422.

[6] Scholz, D., Frisia, S., Borsato, A., Spötl, C., Fohlmeister, J., Mudelsee, M., Miorandi, R., Mangini, A., 2012. Holocene climate variability in north-eastern Italy: potential influence of the NAO and solar activity recorded by speleothem data. Climate of the Past 8, 1367–1383.

[7] Hurrell, J.W.,Van Loon, H., 1997. Decadal variations in climate associated with the North Atlantic Oscillation. Climatic Change 36, 301–326.

[8] Miller, K.G., Wright, J.D., Fairbanks, R.G., 1991. Unlocking the ice house: Oligocene-Miocene oxygen isotopes, eustacy, and margin erosion. Journal of Geophysical Research 96, 6829–6848.

[9] Kocsis, L., Ozsvárt, P., Becker, D., Ziegler, R. Scherler, L., Codrea, V., 2014. Orogeny forced terrestrial climate variation during the late Eocene-early Oligocene in Europe. Geology 42, 727–730.

[10] Scher, H.D., Martin, E.E., 2008. Oligocene deep water export from the North Atlantic and the development of the Antarctic Circumpolar Current examined with neodymium isotopes. Paleoceanography 23, PA1205.

[11] Bice, K.L., Scotese, C.R., Seidov, D., Barron, E.J., 2000. Quantifying the role of geographic change in Cenozoic ocean heat transport using uncoupled atmosphere and ocean models. Palaeogeography, Palaeoclimatology, Palaeoecology 161, 295–310.

[12] Héran, M.-A., Lécuyer, C., Legendre, S., 2010. Cenozoic long-term terrestrial climatic evolution in Germany tracked by $\delta^{18}O$ of rodent tooth phosphate. Palaeogeography, Palaeoclimatology, Palaeoecology 285, 331–324.

[13] Walliser, E.O., Schöne, B.R., Tütken, T., Zirkel, J., Grimm, K.I., Pross, J., 2015. The bivalve *Glycymeris planicostalis* as a high-resolution paleoclimate archive for the Rupelian (Early Oligocene) of central Europe. Climate of the Past 11, 653–668.

[14] Schöne, B.R., Oschmann, W., Houk, S.D., 2003. North Atlantic Oscillation dynamics recorded in shells of a long-lived bivalve mollusk. Geology 31, 1037–1040.

[15] Torrence, C., Compo, G.P., 1998. A practical guide to wavelet analysis. Bulletin of the American Meteorological Society 79, 61–78.

[16] Lindahl, O., Belgrano, A., Davidsson, L., Hernroth, B., 1998. Primary production, climatic oscillations, and physico-chemical processes: the Gullmar Fjord time-series data set (1985-1996). ICES Journal of Marince Science 55, 723–729.

[17] Hanna, E., Jónsson, T., Ólafsson, J., Valdimarsson, H., 2006. Icelandic coastal sea surface temperature records constructed: putting the pulse on air-sea-climate interactions in the northern North Atlantic. Part I: comparison with HadISST1 open-ocean surface temperatures and preliminary analysis of long-term pattern. Journal of Climate 19, 5652–5666.

[18] Brocas, W.M., Reynolds, D.J., Butler, P.G., Richardson, C.A., Scourse, J.D., Ridgway, I.D., Ramsay, K., 2013. The dog cockle, *Glycymeris glycymeris* (L.), a new annually-resolved sclerochronological archive for the Irish Sea. Palaeogeography, Palaeoclimatology, Palaeoecology 373, 133–140.

[19] Witbaard, R., Duineveld, G.C. A., De Wilde, P. a. W.J., 1997. A long-term growth record derived from *Arctica Islandica* (Mollusca, Bivalvia) from the Fladen Ground (Northern North Sea). Journal of the Marine Biological Association of the United Kingdom 77, 801.

[20] Schöne, B.R., Fiebig, J., Pfeiffer, M., Gleβ, R., Hickson, J., Johnson, A.L.A., Dreyer, W., Oschmann, W., 2005. Climate records from a bivalved Methuselah (Arctica islandica, Mollusca; Iceland). Palaeogeography, Palaeoclimatology, Palaeoecology 228, 130–148.

[21] Lorrain, A., Paulet, Y.-M., Chauvaud, L., Dunbar, R., Mucciarone, D., Fontugne, M., 2004. $\delta^{13}C$ variation in scallop shells: increasing metabolic carbon contribution with body size? Geochimica et Cosmochimica Acta 68, 3509–3519.

[22] McConnaughey, T.A., 2003. Sub-equilibrium oxygen-18 and carbon-13 levels in biological carbonates: carbonate and kinetic models. Coral Reefs 22, 316–327.

[23] Pross, J., 2001. Paleo-oxygenation in Tertiary epeiric seas: evidence from dinoflagellate cysts. Palaeogeography, Palaeoclimatology, Palaeoecology 166, 369–381.

[24] Pross, J., Schmiedl, G., 2002. Early Oligocene dinoflagellate cysts from the Upper Rhine Graben (SW Germany): paleoenvironmental and paleoclimatic implications. Marine Micropaleontology 45, 1–24.

[25] Markwick, P.J., 2007. The palaeogeographic and palaeoclimatic significance of climate proxies for data-model comparisons. In: Williams, A., Haywood, A.M., Gregory, F.J., Schmidt, D.N. (Eds.), Deep-Time Perspectives on Climate Change: Marrying the Signal from Computer Models and Biological Proxies. Geological Society London, London, 251-312.

[26] Archer, C.L., Caldeira, K., 2008. Historical trends in the jet streams. Geophysical Research Letters 35, L08803.

[27] Frauenfeld, O.W., Davis, R.E., 2003. Northern Hemisphere circumpolar vortex trends and climate change implications. Journal of Geophysical Research 108, 4423.

[28] Ivany, L.C., Patterson, W.P., Lohmann, K.C., 2000. Cooler winters as a possible cause of mass extinctions at the Eocene/Oligocene boundary. Nature 407, 887–890.

[29] Eldrett, J.S., Greenwood, D.R., Harding, I.C., Huber, M., 2009. Increased seasonality through the Eocene to Oligocene transition in northern high latitudes. Nature 459, 969–73.

[30] Prothero, D.R., 1994. The Eocene-Oligocene Transition. Paradise Lost. Columbia University Press, New York, 291 pp.

[31] Vandenberghe, N., Van Simaeys, S., Steurbaut, E., Jagt, J.W.M., Felder, P.J., 2004. Stratigraphic architecture of the Upper Cretaceous and Cenozoic along the southern border of the North Sea Basin in Belgium. Netherlands Journal of Geosciences 83, 155–171.

[32] Martini, E., 1982. Bestandsaufnahme des Nannoplankton im “prä-aquitanen” Tertiär des Mainzer Beckens. Mainzer Geowissenschaftliche Mitteilungen 10, 29–36.

[33] Grimm, K.I., Grimm, M., Radtke, G., Kadolsky, D., Schäfer, P., Franzen, J.L., Schindler, T., Hottenrott Martin, 2011. Mainzer Becken. In: Deutsche Stratigraphische Kommission (Eds.), Stratigraphie von Deutschland IX. Tertiär, Teil 1. SDGG 75, 133–209.

[34] Roth, P.H., 1970. Oligocene calcareous nannoplankton biostratigraphy. Eclogae Geologicae Helvetiae 63, 799–881.

[35] Martini, E., Müller, C., 1971. Das marine Alttertiär in Deutschland und seine Einordnung in die Standard Nannoplankton Zonen. Erdöl und Kohle 24, 381–384.

[36] Ritzkowski, S., Grimm, M.C., Hottenrott, M., 2011. Niederhessische Tertiärsenke. In: Deutsche Stratigraphische Kommission (Eds.), Stratigraphie von Deutschland IX. Tertiär, Teil 1. SDGG 75, 303–375.

[37] Walliser, E.O., Lohmann, G., Niezgodzki, I., Tütken, T., Schöne, B.R., 2016. Response of Central European SST to atmospheric pCO_2 forcing during the Oligocene - a combined proxy data and numerical climate model approach. Palaeogeography, Palaeoclimatology, Palaeoecology 459, 552–569.

[38] Schöne, B.R., Fiebig, J., Pfeiffer, M., Gleβ, R., Hickson, J., Johnson, A.L.A., Dreyer, W., Oschmann, W., 2005c. Climate records from a bivalved Methuselah (*Arctica islandica*, Mollusca; Iceland). Palaeogeography, Palaeoclimatology, Palaeoecology 228, 130–148.

[39] Wei, W., Lohmann, G., Dima, M., 2012. Distinct modes of internal variability in the global meridional overturning circulation associated with the southern hemisphere westerly winds. Journal of Physical Oceanography 42, 785–801.

[40] Roeckner, E., Brokopf, R., Esch, M., Giorgetta, M., Hagemann, S., Kornblueh, L., Manzini, E., Schlese, U., Schulzweida, U., 2006. Sensitivity of simulated climate to horizontal and vertical resolution in the ECHAM5 atmosphere model. Journal of Climate 19, 3771–3791.

[41] Marsland, S.J., Haak, H., Jungclaus, J.H., Latif, M., Röske, F., 2003. The Max-Planck-Institute global ocean/sea ice model with orthogonal curvilinear coordinates. Ocean Modelling 5, 91–127.

[42] Lunt, D.J., Farnsworth, A., Loptson, C., Foster, G.L., Markwick, P., O'Brien, C.L., Pancost, R.D., Robinson, S.A., Wrobel, N., 2015, Palaeogeographic controls on climate and proxy interpretation. Climate of the Past 11, 5683–5725.

[43] Stepanek, C., Lohmann, G., 2012. Modelling mid-Pliocene climate with COSMOS. Geoscientific Model Development 5, 1221–1243.

[44] Hagemann, S., Dümenil, L., 1998. A parametrization of the lateral waterflow for the global scale. Climate Dynamics 14, 17–31.

[45] Lott, F., Miller, M.J., 1997. A new subgrid-scale orographic drag parametrization: its formulation and testing. Quarterly Journal of the Royal Meteorological Society 123, 101–127.

[46] von Storch, H., Zwiers, F. W., 2001. Statistical analysis in climate research. Cambridge university press, Cambridge, UK, 384 pp.

[47] Hurrell, J.W., Deser, C., 2009. North Atlantic climate variability: the role of the North Atlantic Oscillation. Journal of Marine Systems 78, 28–41.

CHAPTER 3
SUMMARY AND OUTLOOK

3.1 Summary of the research

The results presented herein provided new information on short-term climate variability in shallow marine settings of Central Europe during the early phase of the global Icehouse climate of the Late Paleogene. The sclerochronlogical analysis of the fossil bivalve shells from middle Oligocene strata of Germany and adjacent countries allowed to reconstruct the seasonal sea water temperature amplitude and multi-decadal atmospheric variability over a stratigraphic range of 5 Ma, spanning from 30 to 25 Ma.

Glycymerid bivalves were in the focus of this study for three main reasons: (i) their extraordinary preservation, (ii) their large shells and (iii) their longevity. In fact, a series of extensive diagenesis screening tests (cathodoluminescence, immersion in Feigl´s solution, electron scanning microscopy) revealed a remarkably good preservation of the studied shells. They consisted of pristine aragonite and even microscopic features such as the microtubules and their inner organic walls were still preserved. Oligocene glycymerid shells from Europe are unusually thick when compared to the shells of their modern representatives. This provides a larger-than-usual amount of carbonate material for geochemical analysis, which in turn, allows to perform ultra-high-resolution seawater temperature reconstructions. Accordingly, sampling could be performed across several consecutive growth increments without experiencing significant biases related to time-averaging. In addition to this, the studied bivalves lived for several decades (usually > 50 years). This features make the shells of the Oligocene gylcymerids an extraordinary archive for sclerochronological paleoclimate reconstructions.

The detailed study of the $\delta^{18}O_{shell}$ record of the bivalve *G. planicostalis* from the strata of the Alzey Formation, Mainz Basin, corroborated the validity of this high-resolution proxy archive for seawater paleotemperature estimates. The combination of the highly resolved $\delta^{18}O_{shell}$ data with the annual growth patterns of three shells showed that this species grew its skeleton during both seasonal extremes, whereas the deposition of the annual growth line occurred during fall. Hence, $\delta^{18}O_{shell}$ data recorded the full seasonal temperature amplitude. The $\delta^{18}O$ values of tooth bioapatite of coeval sirenians from the Mainz Basin was used to reconstruct the regional $\delta^{18}O_{water}$ value that equaled -0.9 ± 0.3 ‰. Accordingly, the $\delta^{18}O_{water}$ signal of the Mainz Basin was ca. 0.5 ‰ lower than the global $\delta^{18}O_{water}$ average estimated from geochemical data of foraminiferan tests.

Surface water temperatures ranged between 12 and 22 °C, whereas the average (40 annual increments) winter and summer values were 13.6 ± 0.8 °C and 17.3 ± 1.2 °C, respectively. The results were in general agreement with previous estimates based on shark teeth and planktonic foraminiferan tests, confirming the validity of the reconstructions herein. However, the new data allowed to refine interpretations of the overall climate conditions in the Mainz Basin. According to the result of this study, prevailing water temperatures were colder than the subtropical conditions that were previously assumed for the Mainz Basin. In fact, the comparison of the new proxy-derived data and instrumental time-series revealed similarities between the seasonal SST fluctuations of the Mainz Basin during Rupelian and the modern northwestern Mediterranean realm.

Seasonal water temperatures in the German epicontinental seaway, however, varied greatly during the middle part of the Oligocene. The multitaxon-based SST reconstructions (five bivalve species: *G. planicostalis* and *G. obovata* as well as *Isognomon maxillata sandbergeri*, *Arctica islandica and Palliolum pictum*as; three shark species: *Carcharias cuspidata*, *C. acutissima* and *Physogaleus latus*) yielded information on the seasonal SST amplitude during four time intervals spanning from the middle Rupelian to the middle Chattian stages. By living in slightly different habitats (e.g., different water depths) and having different life styles (e.g., sessile vs. nektonic), each taxon provided complementary data about the environment. During the deposition of the lower Alzey Formation (ca. 31 - 30 Ma), seasonal SST ranged between 10 and 20 °C, whereas data from the upper Alzey Formation (ca. 30 Ma) show slightly higher temperatures ranging between 14 and 22 °C. This warming trend culminated in the latest Rupelian during the deposition of the Stadecken Formation (ca. 29 Ma) as seasonal SST fluctuated between 14 and 24 °C. During the Chattian stage, the climate cooled down, and by the time of sedimentation of the Kassel Formation (ca. 25.5 Ma) seasonal SST oscillated between 11 and 22 °C.

The trend of the proxy-derived temperatures generally compared well to those expected for the proxy-derived atmospheric pCO_2 estimates for the Oligocene, ranging between 400 and 560 ppm. According to numerical climate simulations of the SST, an increase of 160 ppm during the Oligocene did not fully justify the warming observed in the proxy-derived data. Hence, the atmospheric pCO_2 rise at the end of the Rupelian was likely larger than previously assumed, yet it did not reached the 3 x PAL (840 ppm) mark. According to the results, paleoclimate sensitivity (i.e., the change of surface temperatures following a doubling of atmospheric CO_2 levels) of Central

Europe during the Oligocene was higher than the estimated Cenozoic global average (2.2 and 4.8 °C).

The results showed that environmental conditions of the studied marine basins were directly linked to atmospheric climate dynamics both at inter-annual and decadal time-scales. The spectral analysis of the SGI_{shell} data of long-lived *Glycymeris spp.* and *A. islandica* shells from the strata of the Mainz and Kassel Basins as well as from the southern North Sea Basin strata from Belgium, revealed significant non-stationary signals at periods of around 3 - 7 years. As in many other modern bivalves, these periodic changes in shell growth were most likely related to changes in primary productivity, which in turn, were coupled to atmospheric circulation patterns and rainfall on land. Stable carbon isotope values of the shells further corroborated the link between shell growth and food availability. According to numerical climate models, precipitation rate across Central Europe during the Oligocene exhibited a pattern similar to the modern North Atlantic Oscillation (NAO). However, the inherent cyclicity of the SGI_{shell} chronologies diverged from the typical range of the modern NAO (biennial and 6 - 10 years), yet, was in good agreement with NAO variability simulated for the Oligocene by numerical climate models (2.5 - 6 years). Likely, the different paleogeography and elevated atmospheric CO_2 concentrations during the Oligocene not only influenced the spatial distribution of sea level pressure across the North Atlantic, but also the temporal variability of the NAO precursor.

The combined results of growth increments width data and climate model simulations show that an NAO-like pattern persisted already during the Oligocene, about 20 Ma earlier than previously documented. The results indicate that the Eocene/Oligocene transition likely corresponded to the shift from Pacific-dominated to North Atlantic-dominated climate across Central Europe. Infact, until the late Eocene the inter-annual climate variability of Central Europe was influenced by the El Niño - Southern Oscillation. The emergence of an NAO-like pattern during the Oligocene likely contributed to the overall climate deterioration in the Northern Hemisphere during the late Paleogene and possibly contributed to the largest mass extinction event of the Cenozoic Era, i.e., the *Grande Coupure*.

3.2 Outlook

Nearshore deposits have often been neglected in paleoclimate studies, because they usually cover less extended stratigraphic intervals than deep-sea sediments. Furthermore, coastal deposits are mainly composed of sands and gravels and contain fewer amounts of microfossils and nanofossils. Hence, it is more challenging to precisely determine their stratigraphic position. Despite that, the present research demonstrated that the macrofossil remains of nearshore deposits can provide information on past climate fluctuations with an unprecedented temporal resolution.

This thesis mainly focused on fossil bivalves, in particular *Glycymeris* spp. shells. The fossil history of the glycymerids dates back to the Aptian (Gillet, 1924; Casey, 1961) and besides some evolutionary innovations achieved during the Early Cenozoic, their fundamental *bauplan* remained largely invariant (Thomas, 1975, 1978; Squires, 2010). During evolution, glycymerids adapted to habitats in which strong hydrodynamic energy prevailed and sandy and gravelly sediments were deposited. The bivalves developed a strong tolerance against environmental instability (Thomas, 1975). This allowed the glycymerids to colonize shallow water habitats worldwide, from polar to equatorial latitudes, from the Late Cretaceous until present (Ansell and Trueman, 1967; Thomas, 1978; Squires, 2010; Nerot et al., 2012; OBIS, 2016). Because of their abundance and their large size, G*lycymeris* spp. shells are easy to collect in the field as they often occur in the form of accumulation beds (Cahuzac et al., 1993; Sivan et al., 2006; Gutierrez-Mas, 2011), and, for this very reason, they are abundant in the collections of most paleontological museums. Furthermore, fossil *Glycymeris* spp. shells are surprisingly resistant against diagenetic alteration, and their oxygen isotope signature as well as microstructures are often pristinely preserved (Tsuboi and Hirata, 1935; Dorman and Gill, 1959; Crippa, 2013; Böhm et al., 2016). Hence, *Glycymeris* spp. shells represent a unique proxy archive for paleoclimatological studies covering the past 120 Ma.

Such proxy archive opens new horizon towards a better understanding of past climate dynamics. In the present thesis, I concentrated on the Oligocene deposits of the Mainz and Kassel basin of Germany. However, Oligocene glycymerid-rich deposits are widely distributed in Europe (e.g., Paris Basin, Molasses Basin, Pannonian Basin) and the same approach used in this study can easily be applied to the material from other localities. Future studies should be expanded to other areas in order to construct a network of sclerochronological data. Shell $\delta^{18}O$ data could be used to construct seasonally resolved water temperature maps on continental scales. Such data sets would

facilitate the integration into numerical climate models which are usually too coarse to reproduce conditions on small spatial scales. Such an approach could then be conducted in other time intervals of Earth history and compared to global climate trends derived from other proxy archives. For example, as shown in the second manuscript, seasonally resolved $\delta^{18}O$-derived temperature data can be combined with the proxy-derived atmospheric pCO_2 estimates to better constrain the regional paleosensitivity of a selected region. Following the approach of the third manuscript, it is also possible to track the spatial evolution of large atmospheric circulation patterns such as the North Atlantic Oscillation back in time.

Future studies should also focus on the evaluation of other potential geochemical proxies in the shells of the Oligocene glycymerids. For example, preliminary shell strontium-to-calcium data displayed seasonal oscillations which appeared to be positively correlated to $\delta^{18}O_{shell}$ data (i.e., inversely correlated to water temperature) (Fig. 1). However, highest values always occurred at the growth line, suggesting a control of growth rates on the incorporation of Sr ions into the shell. Furthermore, the studied bivalve shells showed strong ontogenetic trends towards higher Sr/Ca, which may render the evaluation of such data challenging. However, if data from the growth lines are not taken into account, age-detrended data suggest that the temperature sensitivity of the shell Sr/Ca (ca. 0.05 mmol/mol per 1 °C) of Oligocene glycymerids may be higher than in other modern aragonite producing bivalve species.

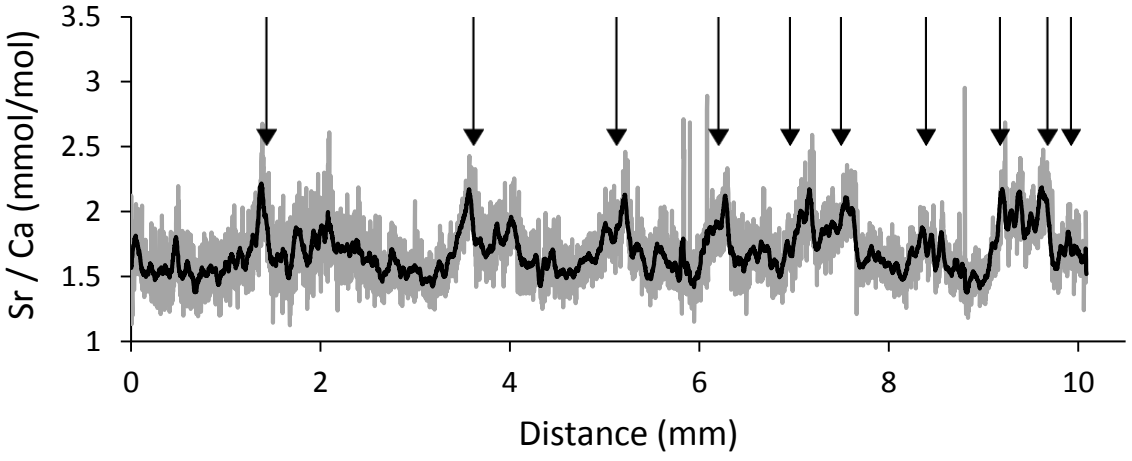

Figure 1. Sr/Ca_{shell} ratio measured with LA-ICP-MS (line scan mode) in the ventral shell portion of a *Glycymeris planicostalis* originating from the Oligocene deposits (Alzey Formation) of the Mainz Basin (Germany). Highest Sr/Ca_{shell} values were detected in corrispondence of annual growth lines (arrows), which were formed during fall.

Beside the opportunity to develop a new paleotemperature proxy, the Sr/Ca_{shell} data can possibly provide an insight into the geochemical composition of the Oligocene oceans. In fact, Sr/Ca_{shell} values from shell growth increments formed during early ontogeny were on average 0.6 to 0.8 mmol/mol higher than those measured in modern glycymerids (Fig. 2). These findings are in agreement with previous reports on aragonite secreting organisms form the Oligocene (Ivany et al., 2004). It is likely that these differences resulted from the elevated Sr levels in the oceans during the Late Paleogene, which is coherent with the transition from Calcite to the Aragonite Sea near the Eocene/Oligocene boundary.

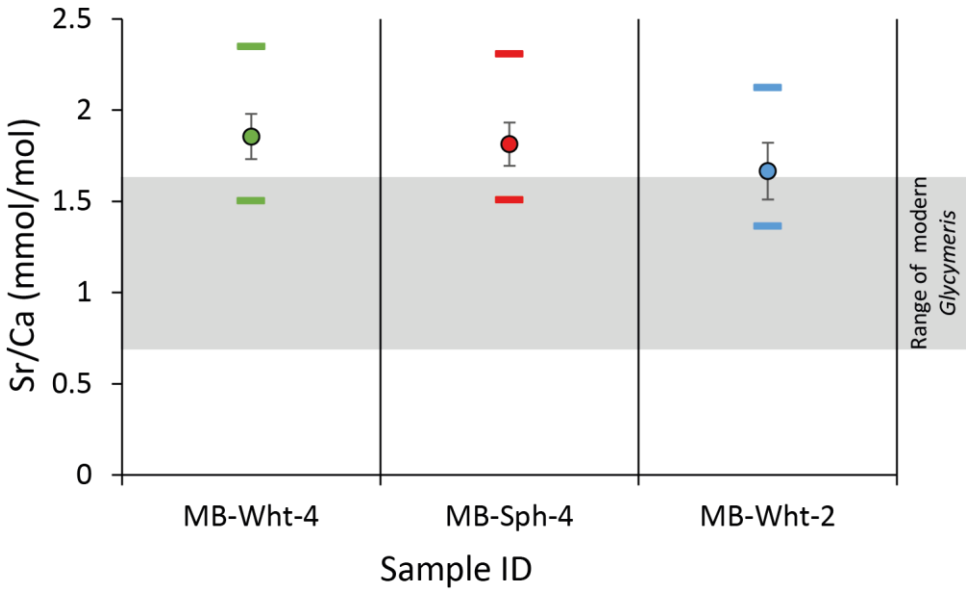

Figure 2. Average (± 1σ) Sr/Ca_{shell} ratio of fossil *Glycymeris planicostalis* shells from the Oligocene depositsof the Mainz Basin. Sr/Cas_{hell} values, measured in the hinge plate (MB-Wht-4 and MB-Sph-4) and the ventral shell portion (MB-Wht-2), are higher (ca. 0.8 and 0.6 mmol/mol, respectively) than the Sr/Ca_{shell} ratios of modern *G. glycymeris* from the North Atlantic. This is likely because of the higher Sr concentration in seawater during the Oligocene.

During the early phase of the Aragonite Sea, the number of organisms forming aragonite skeletons was relatively low and the rate of Sr sequestration into marine carbonates may have been lower than today (Ivany et al., 2004). Elevated Sr concentrations in the seawater likely enhanced the precipitation of skeletal material in those taxa secreting bioaragonite, e.g., corals (Kiessling, 2009). Similar processes may have occurred among glycymerid bivalves as well. In fact, shells of European Oligocene glycymerids are unusually thick in comparison to their Eocene, Miocene and modern relatives. A similar trend has also been observed in veronid bivalves (Lockwood, 2005). From this premise, the study of the life-history traits and the geochemical records of fossil and

modern glycamerids could open new avenues toward a better understanding of the mechanisms behind phenotypic evolution and phenotypic adaptation within bivalve mollusks.

3.3 References

Ansell, A.D., Trueman, E.R., 1967. Observations on burrowing in *Glycymeris glycymeris* (L.) (Bivalvia, Arcacea). Journal of Experimental Marine Biology and Ecology 1, 65–75.

Böhm, C.F., Demmert, B., Harris, J., Fey, T., Marin, F., Wolf, S.E., 2016. Structural commonalities and deviations in the hierarchical organization of crossed-lamellar shells: a case study on the shell of the bivalve *Glycymeris glycymeris*. Journal of Materials Research 31, 536–546.

Cahuzac, B., Cluzaud, A., Ringeade, M., 1993. Étude de populations de *Glycymeris* (Bivalvia, Glycymerididae) du Miocène d'Aquitaine, Sud-Ouest de la France. Ciências da Terra (UNL) 12, 91–109.

Casey, R., 1961. The stratigraphycal palaeontology of the Lower Greensand. Palaeontology 3, 487–621.

Crippa, G., 2013. The shell ultrastructure of the genus *Glycymeris* DA COSTA, 1778: a comparison between fossil and recent specimens. Rivista Italiana di Paleontologia e Stratigrafia 119, 387–399.

Dorman, F.H., Gill, E.D., 1959. Oxygen isotope paleotemperature determinations of Australian Cainozoic fossils. Science 130, 1576–1576.

Gillet, S., 1924. Études sur les lamellibranches néocomiens. Memoires de la Société Geologiqué de France, Nouvelle Serie 1, 1–324.

Gutierrez López, J.M., 2011. *Glycymeris* shell accumulations as indicators of recent sea-level changes and high-energy events in Cadiz Bay (SW Spain). Estuarine, Coastal and Shelf Science 92, 546–554.

Ivany, L.C., Peters, S.C., Wilkinson, B.H., Lohmann, K.C., Reimer, B. a., 2004. Composition of the early Oligocene ocean from coral stable isotope and elemental chemistry. Geobiology 2, 97–106.

Lockwood, R., 2005. Body Size, extinction events, and the Early Cenozoic record of veneroid bivalves: a new role for recoveries? Paleobiology 31, 578–590.

Nerot, C., Lorrain, A., Grall, J., Gillikin, D.P., Munaron, J.-M., Le Bris, H., Paulet, Y.-M., 2012. Stable isotope variations in benthic filter feeders across a large depth gradient on the continental shelf. Estuarine, Coastal and Shelf Science 96, 228–235.

OBIS (2016). Global biodiversity indices from the Ocean Biogeographic Information System. Intergovernmental Oceanographic Commission of UNESCO. Web. http://www.iobis.org (consulted on 2016/05/06)

Sivan, D., Potasman, M., Almogi-Labin, A., Bar-Yosef Mayer, D.E., Spanier, E., Boaretto, E., 2006. The *Glycymeris* query along the coast and shallow shelf of Israel, southeast Mediterranean. Palaeogeography, Palaeoclimatology, Palaeoecology 233, 134–148.

Squires, R.L., 2010. Northeast Pacific Upper Cretaceous and Paleocene glycymeridid bivalves. Journal of Paleontology 84, 895–917.

Thomas, R.D.K., 1975. Functional morphology, ecology, and evolutionary conservatism in the Glycymerididae (Bivalvia). Palaeontology 18, 217–254.

Thomas, R.D.K., 1978. Shell form and the ecological range of living and extinct Arcoida. Paleobiology 4, 181–194.

Tsuboi, C., Hirata, M., 1935. Arrangement of micro-crystals of calcium carbonate in some fossil shells, *Glycymeris yessoensis* SOWERBY. Tokyo Imperial University Bulletin of the Earthquake Research Institute 13, 660–664.

APPENDIX

The figures and tables presented in this appendix are original and were submitted to Nature Scientific reports as supplementary material to Walliser et al. (in review) (Chapter 2-III).

References

Walliser, E.O., Lohmann, G., Niezgodzki, T., Schöne, B.R., in review. Inter-annual climate variability in Europe during the Oligocene Icehouse. Nature Scientific Reports.

Supplementary material to MANUSCRIPT III

Reconstruction of seasonal growth rates

In order to reconstruct seasonal shell growth rates, incremental $T_{\delta 18O}$ values were aligned to modelled seasonal seawater temperature (T_{mod}) curves computed with a monthly resolution (12 data points) using a sinusoidal equation (Fig. S3). Since the studied *Glycymeris* spp. bivalves grew their shells over winter and summer[1,2] it was possible to extrapolate the full seasonal water temperature amplitude to which the animals were exposed. To account for the inter-annual variability of the seasonal seawater temperature amplitudes, each growth increment was treated separately. Accordingly, the minimum and maximum $T_{\delta 18O}$ values from each growth year were used to constrain the amplitude of the T_{mod} curve used for data alignment. To facilitate the arrangement of the $T_{\delta 18O}$ data on the T_{mod} curve, 3rd to 6th order polynomial functions were fitted to the $T_{\delta 18O}$ data (Fig. S3A). After the temporal alignment, seasonal shell growth rates were calculated as percentage of the respective year (Fig. S3B).

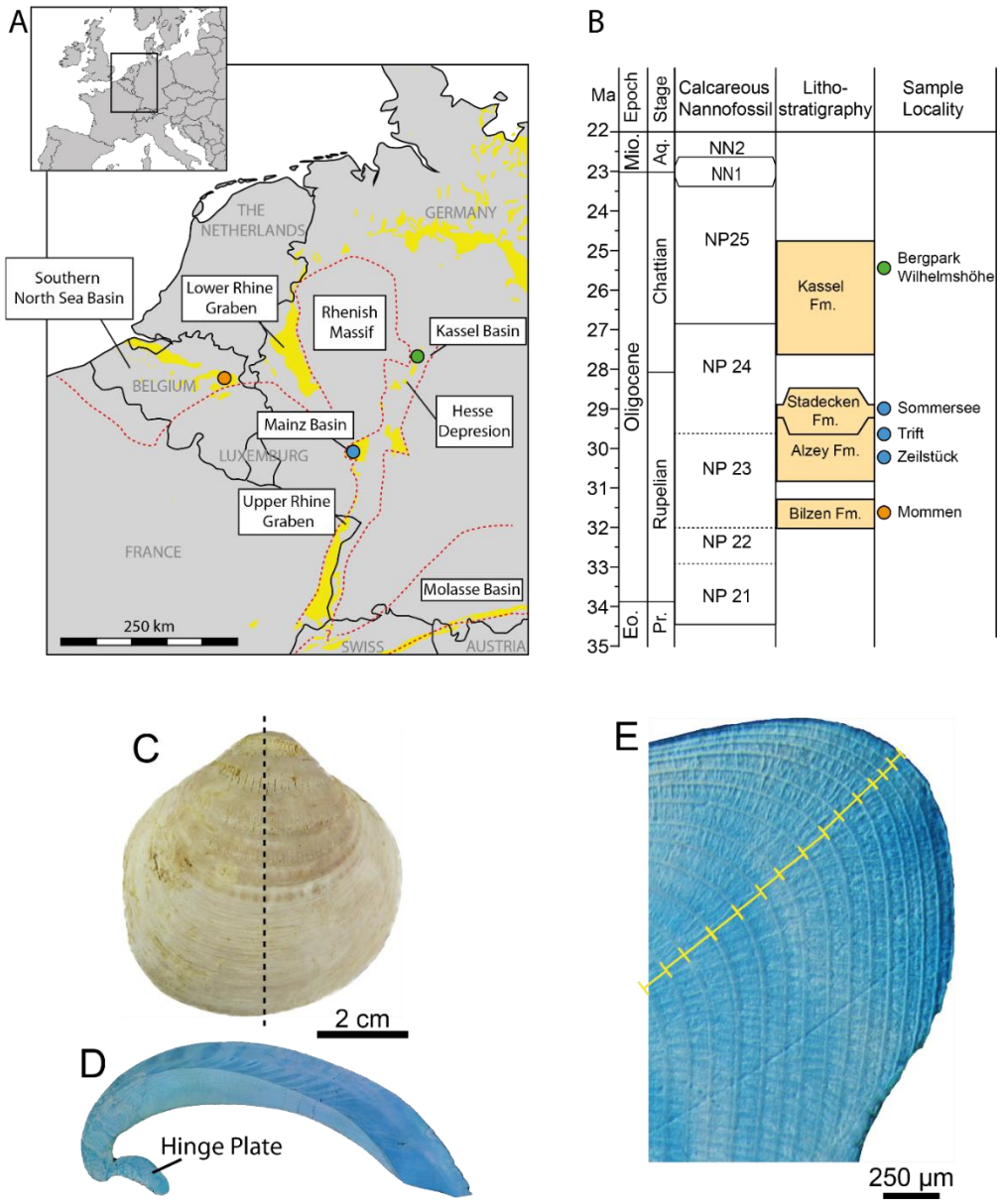

Figure S1. Geographical and stratigraphic position of the studied areas in Germany and Belgium and studied material. (A) Geographic position of the studied localities (Southern North Sea Basin = orange circle; Mainz Basin = blue circle; Kassel basin = green circle), the contour of the palaeocoast line (red dotted line) as well as the major occurrence of Oligocene strata in the area (yellow areas). (B) Chronostratigraphic position of the studied lithostratigraphic units and localities. (C) An example of *Glycymeris planicostalis* shell from the Mainz Basin. Dotted line indicates cutting axis. (D) Image of a *Glycymeris planicostalis* shell slab stained with Mutvei´s solution, and (E) magnification of the hinge plate where growth increment width were measured (yellow bars). Map in (A) was generated using the image processing software Adobe Illustrator (version CS5; http://www.adobe.com/it/products/illustrator.html) combining i) information from the geological map of Asch (2005)3, ii) paleocoastline reconstruction from Sissingh (2003)4 and iii) geographic map of Europe (freely available at: https://upload.wikimedia.org/wikipedia/commons/b/b3/Blank_map_of_Europe.svg; the map is licensed under the Creative Commons Attribution-Share Alike 2.5 Generic license; for further information about licensing conditions see: https://commons.wikimedia.org/wiki/File:Blank_map_of_Europe.svg).

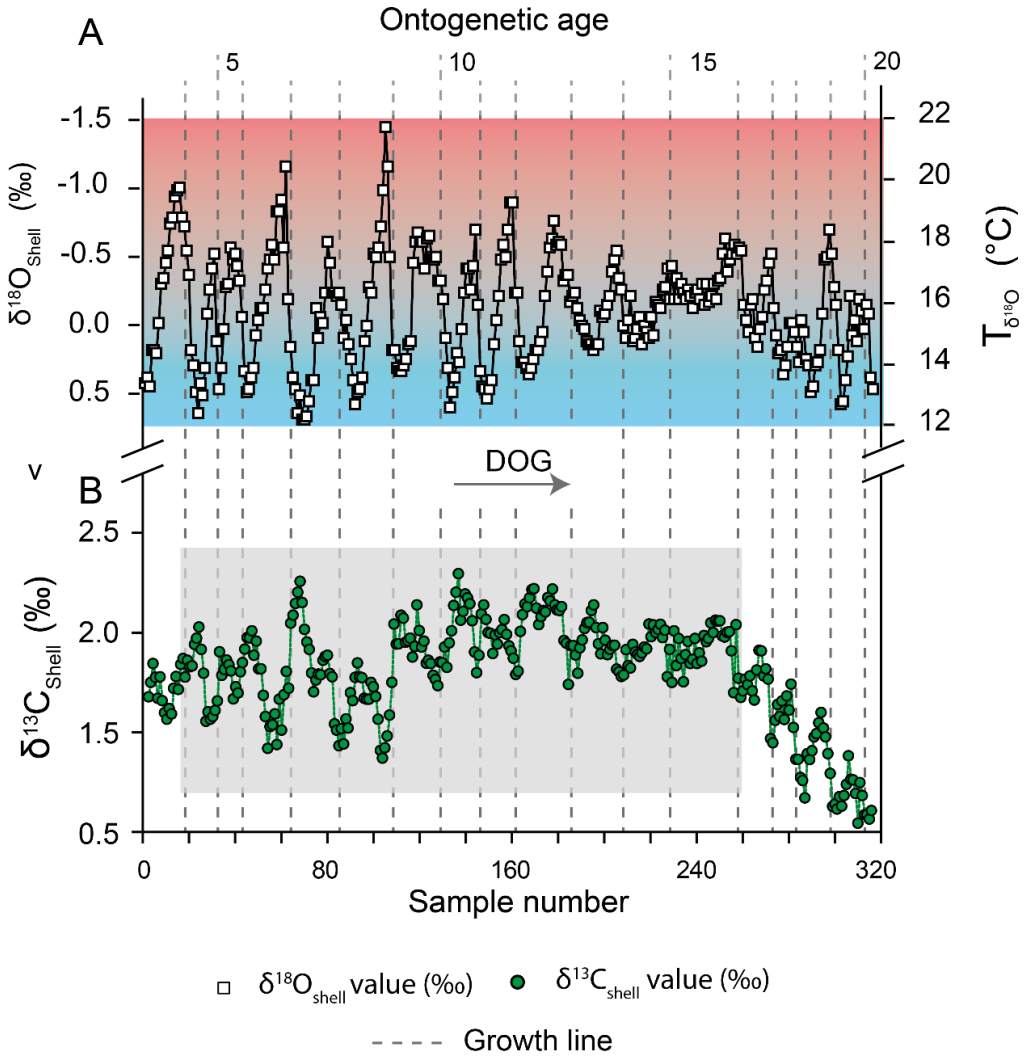

Figure S2. Stable isotope data from the studied *Glycymeris planicostalis* shell (MB-Wht-2) from the Rupelian deposits of the Mainz Basin. (A) Published stable oxygen isotope record and reconstructed water $T_{\delta 18O}$ values[1]. (B) Stable carbon isotope data presented in this study. The gray area shows the shell portion used for the reconstruction of seasonal growth rates, whereas the vertical bars represent the position of the growth lines. DOG = direction of growth.

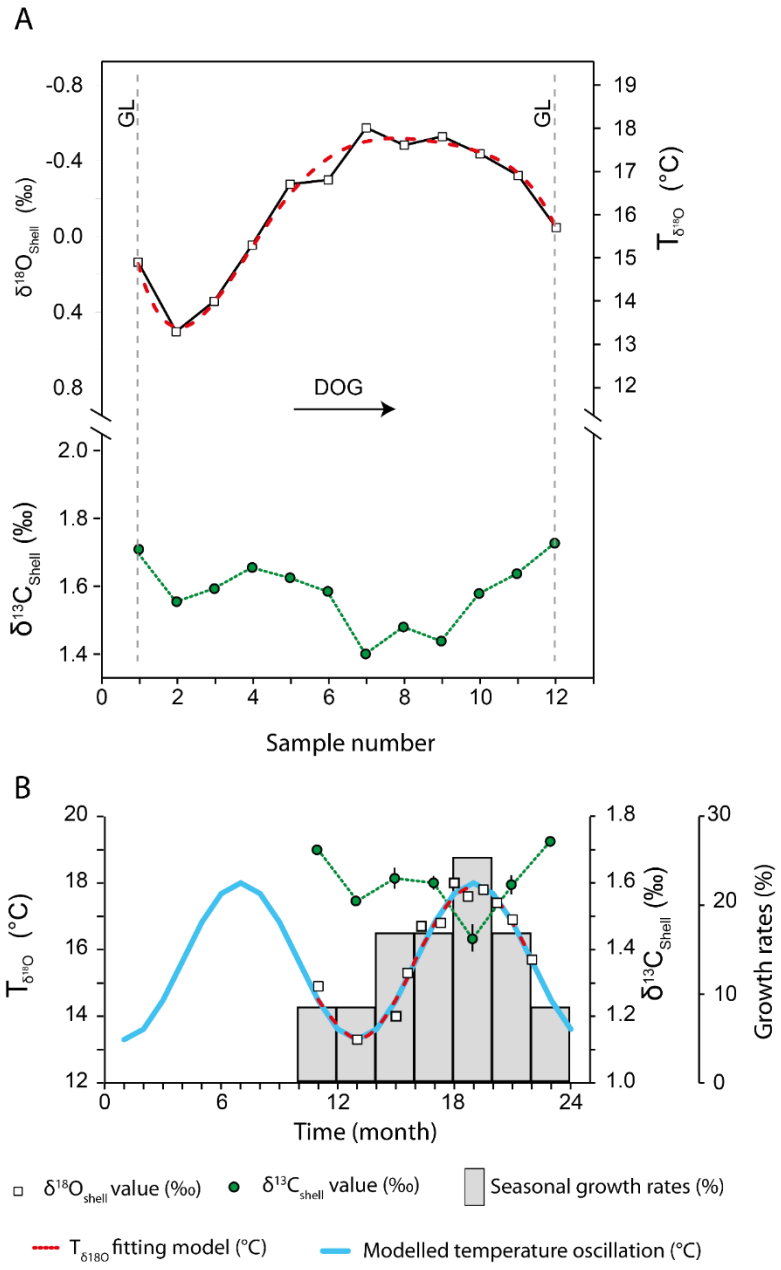

Figure S3. Average seasonal shell growth rates and the $\delta^{13}C_{shell}$ record reconstructed from the studied *Glycymeris planicostalis* shell. (A) Average seasonal growth rates (grey circles ± 1σ) and $\delta^{13}C_{shell}$ values (green circles ± 1σ) are plotted against the sinusoidal T_{mod} computed for the Rupelian of the Mainz Basin (Walliser et al., 2015); W = winter, Sp = spring, Su = summer, F = fall. (B - C) Relationship between uncorrected (B) and lag-corrected (C) seasonal growth rates and bi-monthly averaged $\delta^{13}C_{shell}$ values.

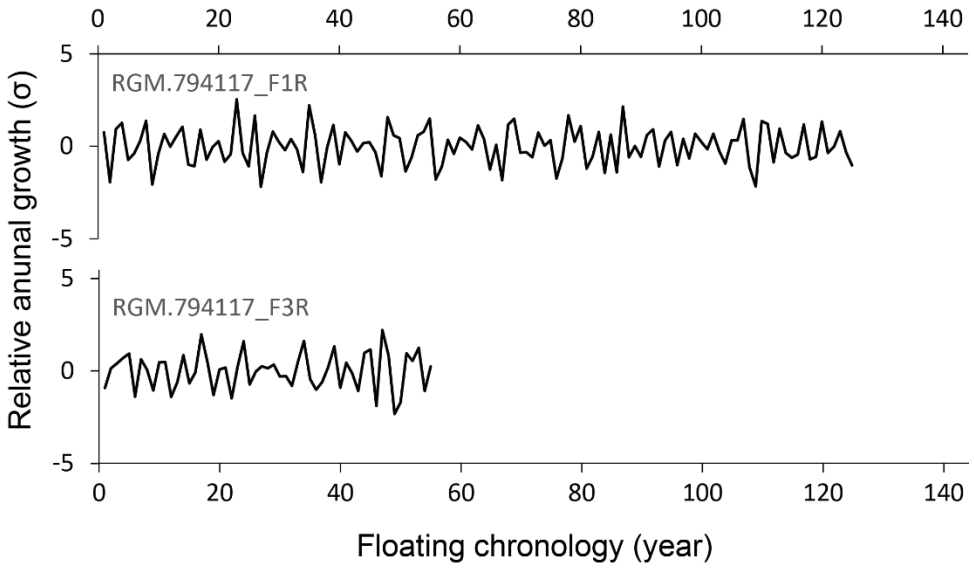

Figure S4. Age-detrended and standardised annual shell growth curves reconstructed from increment width chronologies of *Glycymeris obovata* shells from the Rupelian (Lower Oligocene) deposits of the Mommen sand pit near Vliermaal (Bilzen Formation, Belgium).

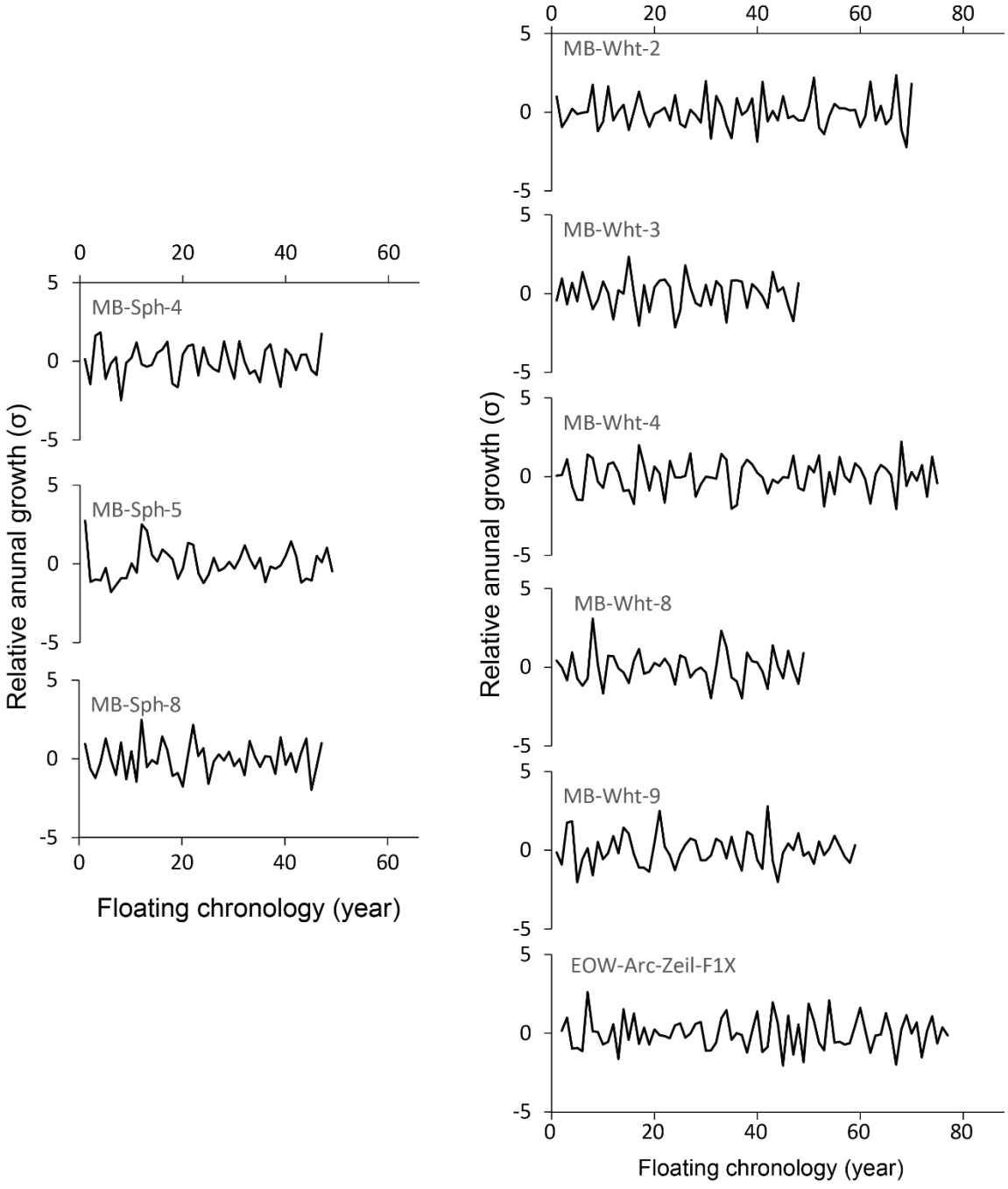

Figure S5. Age-detrended and standardised annual shell growth curves reconstructed from growth increment width chronologies of *Glycymeris planicostalis* (MB-WHT-*) and *Arctica islandica* (EOW-Arc-Zeil-F1X) shells from the Rupelian (Lower Oligocene) deposits of the outcrops Sommersee' near Spiesheim (Stadecken Formation, Germany; left panel), 'Trift' and 'Zeilstück' near Weinheim (Alzey Formation, Germany; right panel).

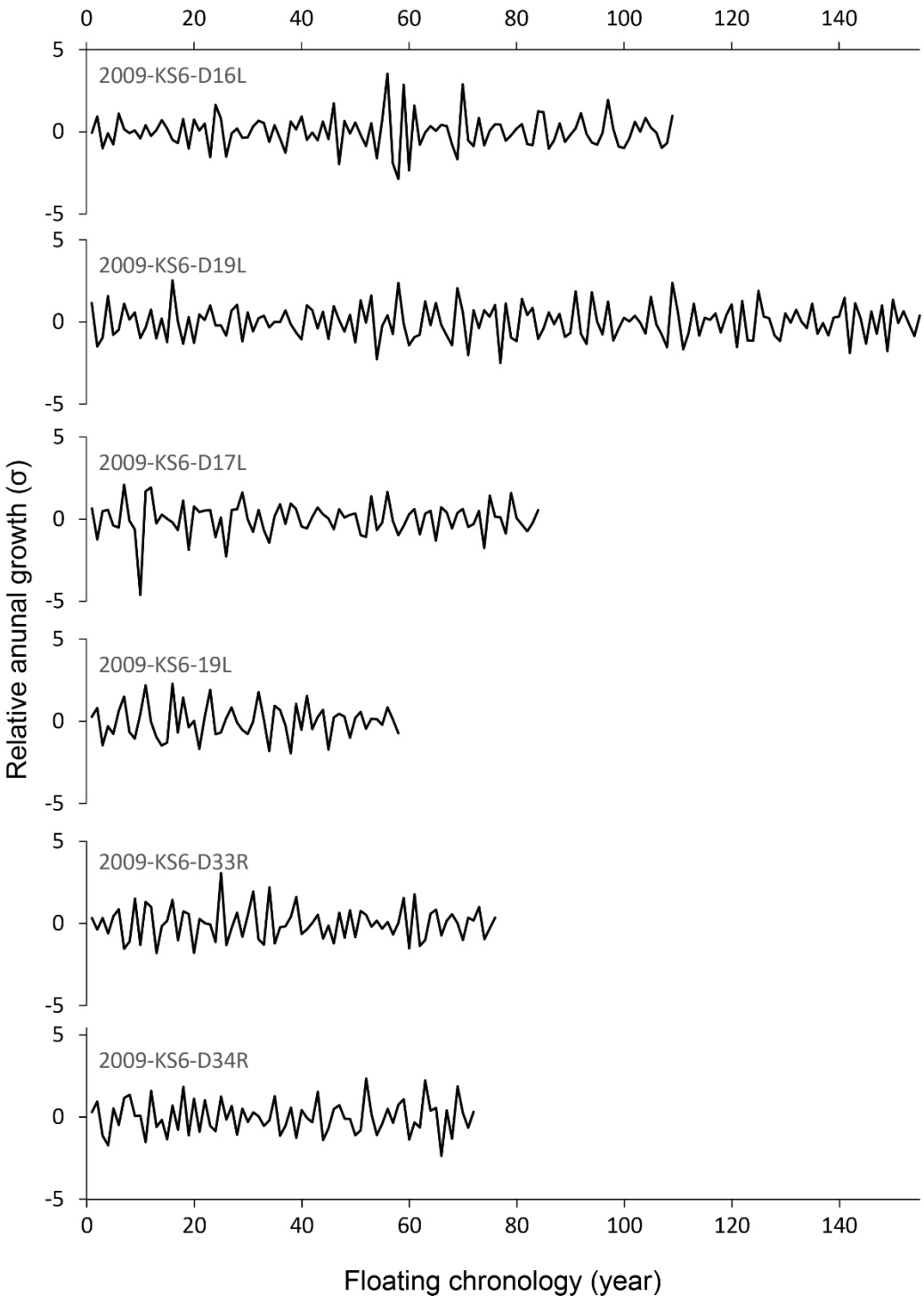

Figure S6. Age-detrended and standardised annual shell growth curves reconstructed from growth increment width chronologies of *Glycymeris obovata* shells from the Chattian (Upper Oligocene) deposit of the Bergpark Wilhelmshöhe, Kassel (Kassel Formation, Germany).

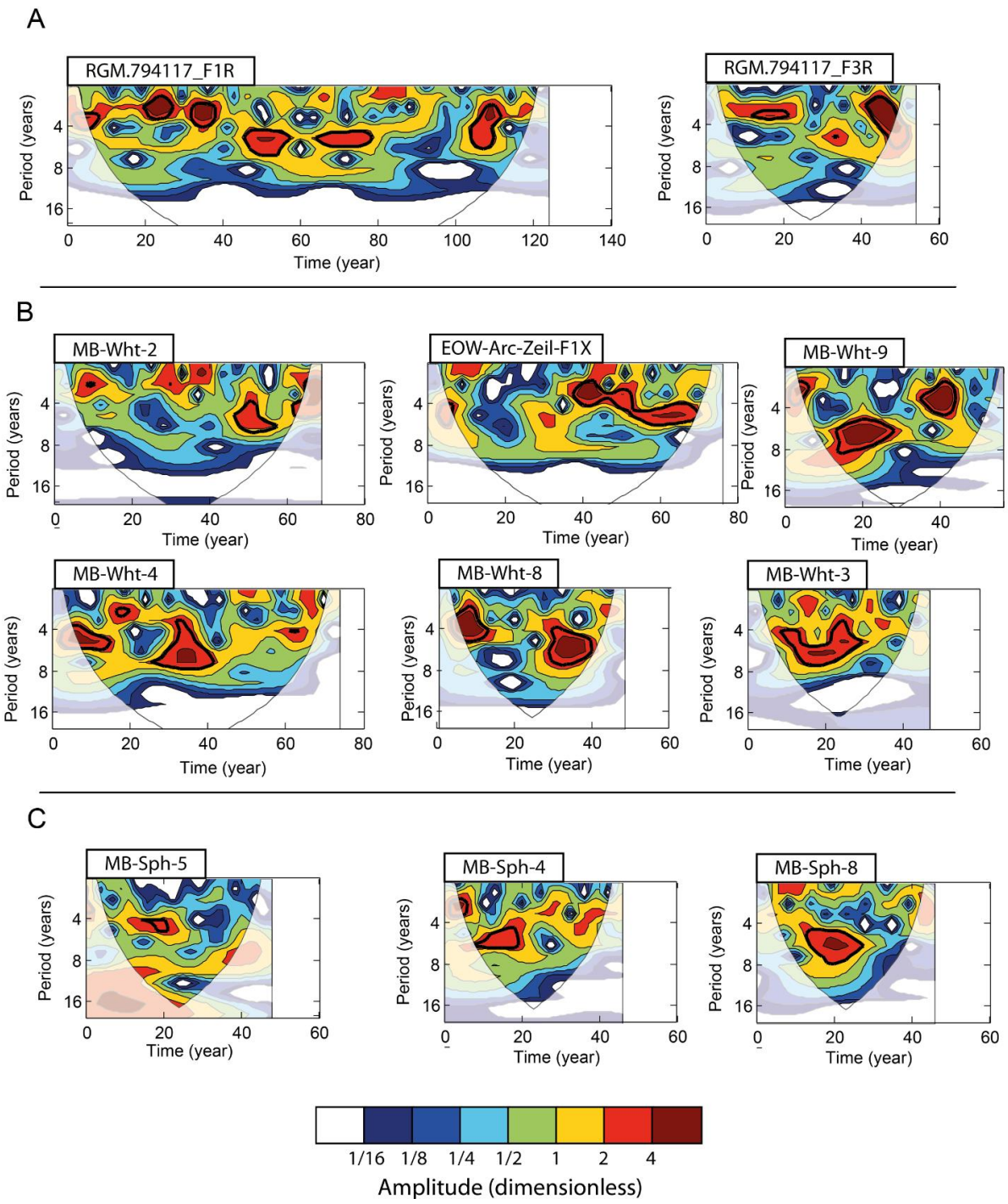

Figure S7. Continuous wavelet spectra of the SGI_{shell} chronologies of the studied bivalve shells (A) *Glycymeris obovata* shell from the Rupelian (Lower Oligocene) deposits of the Mommen sand pit near Vliermaal (Bilzen Formation, Belgium). (B) *Glycymeris planicostalis* (MB-WHT-*) and *Arctica islandica* (EOW-Arc-Zeil-F1X) shells from the Rupelian (Lower Oligocene) deposits of the outcrops 'Trift' and 'Zeilstück' near Weinheim (Alzey Formation, Germany). (C) *Glycymeris planicostalis* shells from the Rupelian (Lower Oligocene) deposits of the outcrop 'Sommersee' near Spiesheim (Stadecken Formation, Germany). Thick black contour lines display significant powers signals (above 5 % significance level against red-noise spectrum).

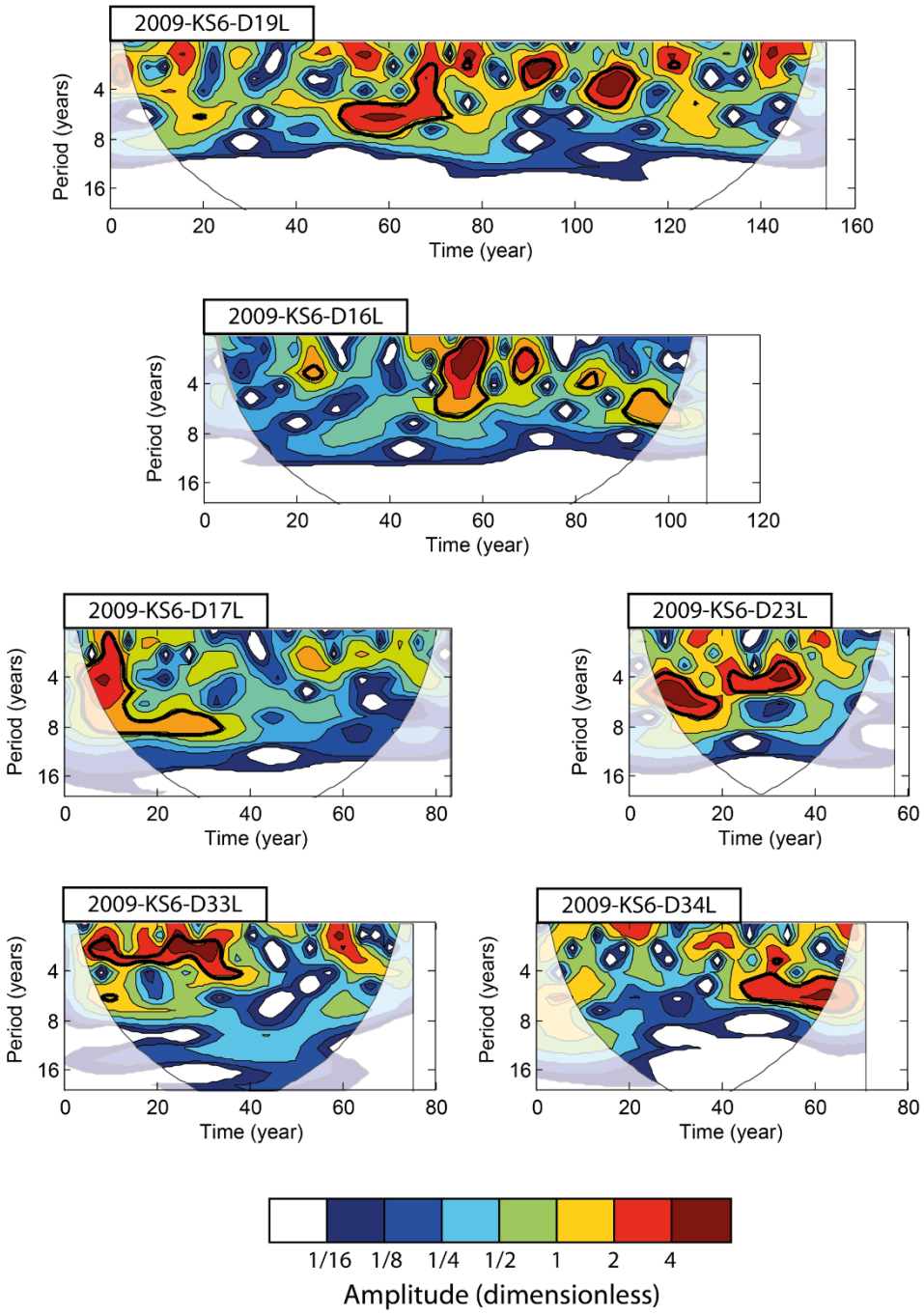

Figure S8. Continuous wavelet spectra of the SGI_{shell} chronologies of *Glycymeris obovata* shells from the Chattian (Upper Oligocene) deposit of the Bergpark Wilhelmshöhe, Kassel (Kassel Formation, Germany). Thick black contour lines display significant powers signals (above 5 % significance level against red-noise spectrum).

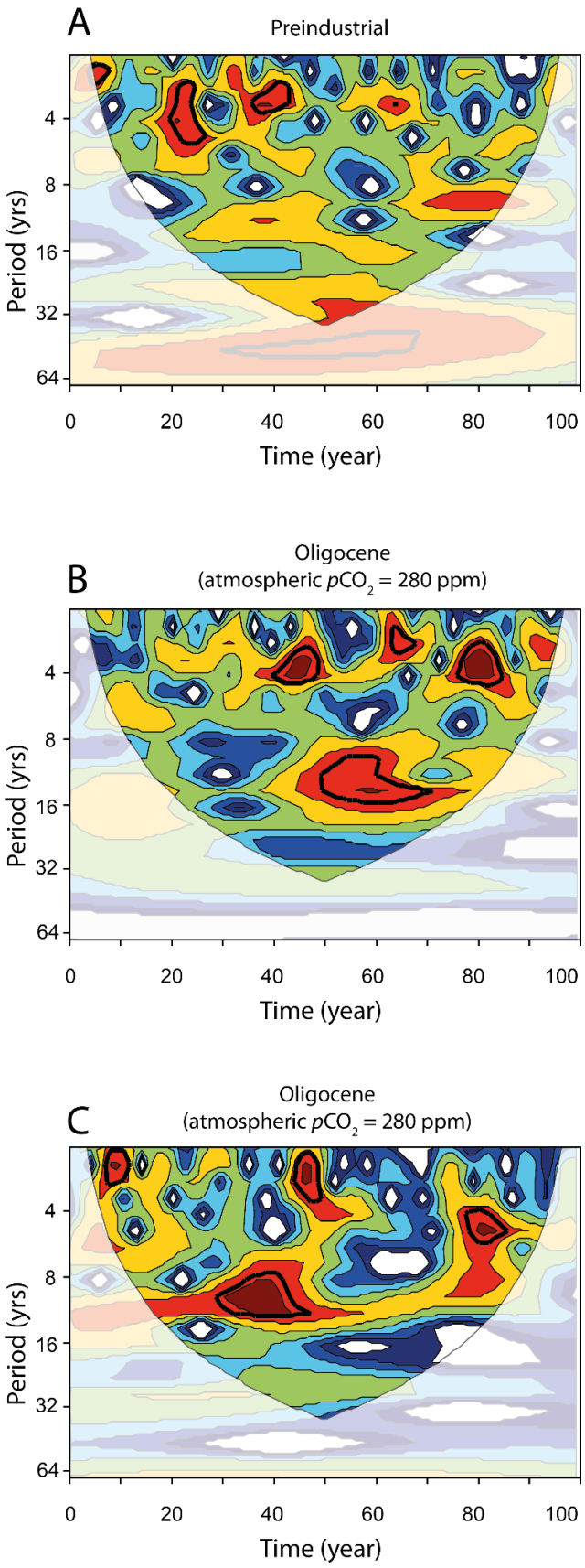

Figure S9. Continuous wavelet spectra of the NAO indices computed from the preindustrial (A), Oligocene O-560 (B) as well as O-280 (C) climate simulations. Thick black contour lines display significant powers signals (above 5 % significance level against red-noise spectrum). Oligocene O-560 (B) as well as O-280 (C) NAO indices display common a low frequencies component (around the 8-year band) that is not recognized in the NAO index of the preindustrial simulation.

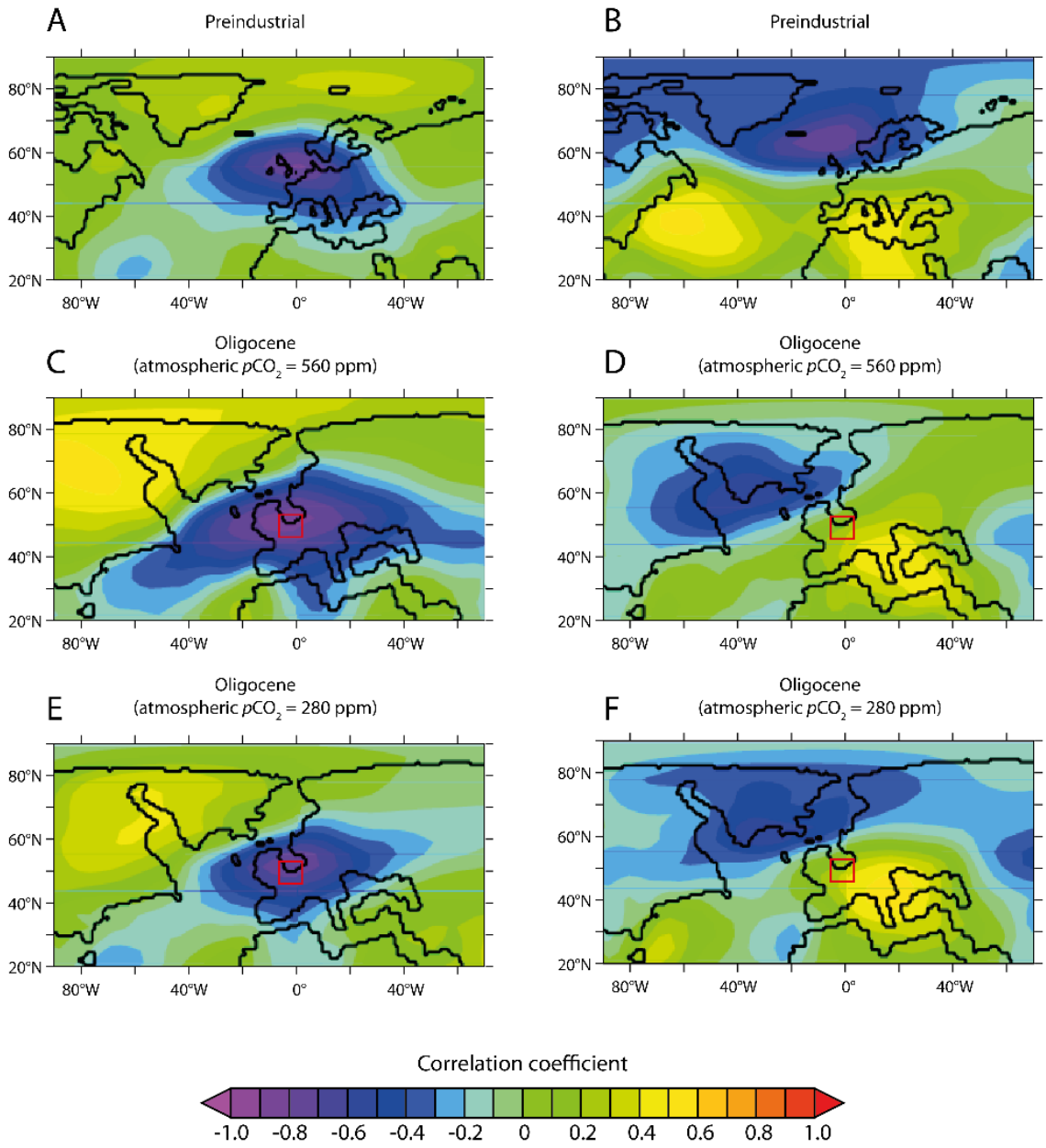

Figure S10. Correlation maps between SLP and local precipitation rates (A, C, D) as well as SLP and local surface temperatures (B, D, F). Preindustrial (A and B) and both Oligocene O-560 (C and D) and O-280 (E and F) correlation maps show a pattern suggestive of inter-annual precipitation rates and surface temperatures variability in the North Atlantic sector was controlled by SLP. Red square shows the geographical position of the studied area. Maps were generated using the GrADS software (Version 2.0.1; available at: http://cola.gmu.edu/grads/).

Table S1. Studied fossil taxa used for calculation of standardised growth indices (SGI_{shell}).

Taxon	Sampled locality	Stratigraphy	# of shells
Glycymeris obovata	Southern North Sea Basin (Belgium)	Bilzen Fm. (Rupelian)	2
	Kassel Basin (Germany)	Kassel Fm. (Chattian)	6
Glycymeris planicostalis	Mainz Basin (Germany)	Stadecken Fm. (Rupelian)	3
	Mainz Basin (Germany)	Alzey Fm. (Rupelian)	5
Arctica islandica	Mainz Basin (Germany)	Alzey Fm. (Rupelian)	1

References

1. Walliser, E.O., Schöne, B.R., Tütken, T., Zirkel, J., Grimm, K.I., Pross, J., 2015. The bivalve *Glycymeris planicostalis* as a high-resolution paleoclimate archive for the Rupelian (Early Oligocene) of central Europe. Climate of the Past 11, 653–668.

2. Walliser, E.O., Lohmann, G., Niezgodzki, I., Tütken, T., Schöne, B.R., 2016. Response of Central European SST to atmospheric pCO_2 forcing during the Oligocene - a combined proxy data and numerical climate model approach. Palaeogeography, Palaeoclimatology, Palaeoecology 459, 552–569.

3. Asch, K. 2005. IGME 5000: 1 : 5 Million International Geological Map of Europe and Adjacent Areas. BGR (Hannover).

4. Sissingh, W. 2003. Tertiary paleogeographic and tectonostratigraphic evolution of the Rhenish Triple Junction. Palaeogeography, Palaeoclimatology, Palaeoecology **196**, 229–263 (2003).

E quindi uscimmo a riveder le stelle.

-Dante Alighieri-